# An Experimental and Theoretical Investigation of Flow Measurement by Doppler Ultrasound

**Shaofeng Li**

Ph.D.
University of Edinburgh
1995

THE UNIVERSITY *of* EDINBURGH

# Declaration

I declare that the work contained in this thesis is my own and that the thesis has been composed by myself.

Shaofeng Li

6 April 1994

## Acknowledgments

I am very grateful to a number of people for their help and encouragement during the course of this project. Firstly, I would like to thank my supervisors, Professor Norman McDicken and Dr. Peter Hoskins, for their continued support and advice throughout this project and performing the proof-reading of this thesis and my other publications. I am also indebted to Mr. Tom Anderson Dr. Steve Pye, Dr. Duncan Potter and Mr. Mike Glabus for their valuable advices and help. For clinical trial, I would wish to thank Dr. Sarah Chamber for performing the patient measurements.

I am particularly thankful to Mr. Martin Connell for his generously help in computing, to Mr. Ali AlMejrad, with whom I shared the student lab for most of the duration of this project, for his friendship and help, and to Mr. Bob Borthwick for his the mechanical work and advice.

Finally, I am most thankful to my parents and my wife, Yiqun, for their continued encouragement and support.

# Abstract

Despite improvement in the performance of medical ultrasonic techniques in recent years, large errors in the volumetric flow measurement still remain. Many factors can affect volumetric flow measurement. It is therefore necessary to investigate individual and combined influences of these factors.

The aim of this thesis is to combine experimental and theoretical investigations of the sources of error in flow measurement techniques which use the Doppler principle and to look for possible ways to improve the accuracy.

Computer models were developed in this thesis to simulate the Doppler spectrum. Results from the computer models were carefully compared with the experimental data. The effect of factors including geometrical spectral broadening, type and size of the transducer, focusing, depth of the vessel, beam-vessel angle misalignment of the beam and vessel, reflection and refraction at vessel wall were analyzed using these models. Experiments showed that the errors in the diameter measurement were significant. Non-linear propagation has no significant effect on the Doppler measurement. It was confirmed experimentally that the mean velocity of pulsatile flow could be estimated by half of the maximum velocity averaged over an integral number of cardiac cycles. It was suggested that the geometrical spectral broadening and transit time spectral broadening were not the same effect as generally believed and should be treated separately. A detailed study of the flow phantom was also made prior to the investigation of the factors resulting in errors.

Possible improvements of the accuracy of volumetric flow measurement were sought during these studies. It was found that a half pulse length correction in the diameter measurement can significantly improve the accuracy of the cross-sectional area estimation. A new maximum frequency extraction method which is not sensitive to most of the measuring conditions was suggested and analyzed. The results of these investigations are also of direct relevance to velocity spectral analysis as well as volumetric blood flow measurement.

# Contents

# Chapter 1

# INTRODUCTION

## 1.1 Background

### 1.1.1 Medical ultrasound

One of the most important techniques for medical diagnosis employs ultrasound. The early use of ultrasound to obtain information about the structure of the body dates back to the late 1940s. Since then, over five decades, diagnostic ultrasonic instruments have developed from basic units for flaw detection to the present generation of sophisticated medical instruments. New techniques in ultrasound are continually being introduced, and routine ultrasound examinations are now performed in many medical disciplines, such as obstetrics gynaecology, neurology, cardiology, ophthalmology, urology and paediatrics. As a practical tool for medical investigation, ultrasound has become one of the most firmly established methods. It was estimated in 1986 that over 50 million ultrasonic examinations were performed worldwide every year and their number was increasing by about 20% annually (Hill, 1986).

The popularity of diagnostic ultrasound is largely thanks to the characteristics it offers.

- **Safety.** Although many investigations have been made into biological effects

of ultrasound, no evidence has suggested the occurrence of harmful effects to patients or operators at diagnostic levels. Most examinations are non-invasive and repeated investigations can be made.

- **Speed of examination.** Ultrasonic examinations can typically be completed in 20 minutes and introduce minimum patient inconvenience. It is an ideal method for routine examination.

- **Low cost.** Equipment and running costs for ultrasound are less than, for example, computerised tomography (CT) or magnetic resonance imaging (MRI) by 10 to 20 times.

- **Real-time display.** Ultrasonic scanners display real-time images or Doppler spectra that give information on moving structures.

- **Velocity information.** Ultrasonic units offer velocity information using the Doppler technique. Furthermore, the combination of imaging and colour Doppler flow mapping gives simultaneous visualization of blood flow and tissue structure.

Because of these characteristics, diagnostic ultrasound often presents unique information and has been a fast developing technique in recent years.

### 1.1.2 Doppler technique

Vascular diseases have become the most important cause of human death. In 1991 45.8% of deaths in the UK were caused by diseases of the circulatory system (Source : OPCS, main 5 causes 1991). The clinical situation requires an understanding of blood circulation in both normal and pathological circumstances.

The Doppler ultrasound technique is based on the principle that a moving reflector shifts the frequency of an ultrasonic signal. The velocity of the reflector $v$ can be measured from the Doppler frequency shift $\Delta F$ by

$$v = \frac{\Delta F \cdot c}{2F_0 \cos\theta} \tag{1.1}$$

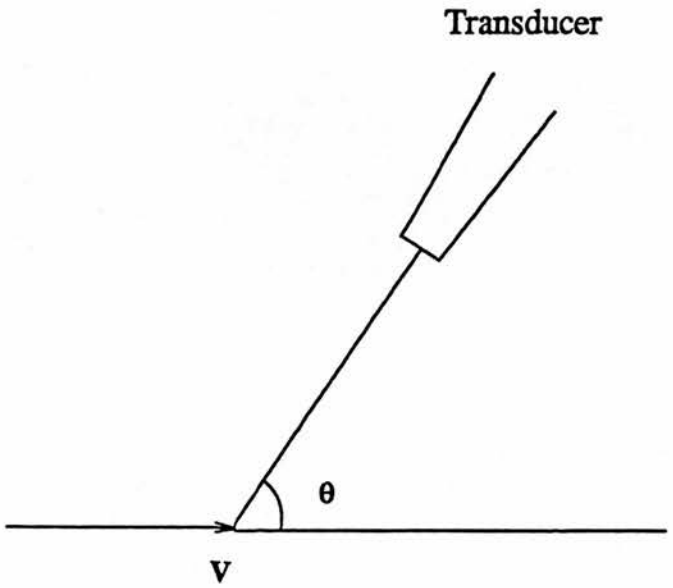


Figure 1.1: The frequency of ultrasonic waves shifts when it is reflected by a moving reflector or scatterer at an angle $\theta$ which is not 90°.

where $c$ is the speed of sound, $F_0$ is the frequency of the transmitted ultrasonic pulses and $\theta$ is the beam-vessel angle (Figure 1.1). Doppler devices give valuable information of the movement of structures, particularly the blood cells in the body. Almost without exception modern Doppler units display directional information of blood flow. Duplex scanners with pulsed wave (PW) Doppler devices allow operators to place the sample volume at a point of particular haemodynamic interest. Virtually all units now incorporate display of the Doppler information as a real time spectral display. Some units also provide real time calculation of waveform indices. This has greatly facilitated the interpretation of Doppler signals. In recent years, the development of Doppler colour flow mapping has added a new dimension to this technique by allowing simultaneous display of velocity information and surrounding tissue structure. The variety of information that Doppler ultrasound provides has greatly benefited the diagnosis of diseases in the circulatory system, finding its application in the lower limbs, cerebral circulation, obstetrics, nephrology, oncology and cardiology.

### 1.1.3 Volumetric flow measurement

The fundamental function of the circulatory system is to distribute blood to organs and regions of the body. Blood supply brings oxygen and nutrition to the whole body and carries carbon dioxide and wastes away. It is crucial to the physiological balance of the body. Shortage of blood supply results in disorders of the region and sometimes fatal consequences may occur.

Accurate measurement of blood flow to organs or tissue is necessary in many areas of medical and biological research. The clinical value of flow measurements, particularly in cardiology and in cardiac and vascular surgery, is well recognized. The ability to detect blood flow, even if it cannot be precisely measured, has also proved valuable.

Many methods for measuring blood flow are available. These include:

- venous occlusion plethysmography, whereby the rate of increase in volume of a part of the body is measured as blood flows into it while the outflow (venous return) is temporarily cut off;
- techniques using ultrasound and the Doppler effect in order to derive blood velocity;
- electromagnetic induction techniques, in which the blood flow is determined from the voltage induced when blood (an electrical conductor) flows through a magnetic field;
- indicator dilution methods, in which an indicator is added and its concentration is measured after thorough mixing with the flowing blood;
- indicator clearance methods, whereby blood flow is determined from the rate at which an indicator is carried away from the site of measurement by the flowing blood.

Electromagnetic induction techniques provide an accuracy better than 95%. A major advantage of this method is that the flowmeter is unaffected by changes

in the velocity profile across the vessel, provided that the blood velocity is symmetrical about the axis of the vessel (Shercliff 1962). As a uniform magnetic field perpendicular to the axis of the blood vessel must be provided, the probe (cannulation or cuff type) and a pair of electrodes must contact the vessel wall, this method is usually only used when the vessel is exposed during surgery or surgically implanted round a vessel.

Blood flow through the heart and major vessels can be measured by indicator dilution methods or indicator clearance methods. These methods require a catheter insert into the appropriate blood vessel. The available methods have been reviewed by Cobbold (1974), Woodcock (1975) and Mathie (1982). Many clinical applications have been described by Woodcock (1976).

Venous occlusion plethysmograph and Doppler ultrasonic measurements have the great advantage that they are noninvasive methods of blood-flow measurement. Venous occlusion plethysmography can yield highly accurate results (Barendsen 1980). However, it has the drawback of requiring the subject to remain still, in a suitable position, while measurement are made. It has the disadvantage that blood flow can only be measured in some of the vessels.

Compared to these methods, ultrasonic measurements of blood flow are noninvasive, fast and convenient, and can therefore be repeated at will so as to monitor the progress of a disease process or the effect of a therapy. Various blood vessels can be selected even if they are deep in the body, such as the fetal umbilical artery and common hepatic arteries. The disadvantage of the Doppler methods is that the accuracy of the measurement is often low. Typical errors in flow measurement are about 20%.

Many volumetric flow measurements have been made in various blood vessels, for example, carotid artery (Borodzinski, *et al.*, 1976); common femoral artery (Lewis *et al.*, 1986); superior mesenteric, splenic and common hepatic arteries (Nakamura, *et al.*, 1989); fetal descending aorta (Marsal, *et al.*, 1984), fetal cerebral arteries (Wladimiroff *et al.*, 1986; Wijngaard *et al.*, 1989) and umbilical vein (Gill *et al.*, 1984; Jouppila and Kirkinen, 1984). Several Doppler methods for measuring blood flow have been used. In general, they can be classified into four categories.

- **Uniform insonation method.** This method assumes the blood vessel is uniformly insonated. The Doppler spectrum is acquired from the entire cross section of the blood vessel and the mean velocity is estimated. The volumetric flow is then calculated by the multiplication of mean velocity and cross-sectional area (Gill, 1979; Eik-Nes *et al.*, 1984; Qamar *et al.*, 1985; Evans, D.H. 1986; Lewis *et al.*, 1986). The method is at its best for medium-sized vessels of between about 4 mm and 8 mm diameter. For smaller vessels it is difficult to make accurate measurement of vessel size, whereas for larger vessels it is difficult to obtain uniform insonation of the vessel.

- **Multigate system.** A multigate system produces a narrow beam passing through the centre of the vessel. The velocity of blood cells is measured in a large number of small elements and multiplied by the area of corresponding semi-annuli (Hoeks, *et al.*, 1981). This method gives errors when geometry changes disturb the symmetry of the flow profile or a very big vessel is examined while the sample volume is small compared with the vessel diameter. It also often suffers from low signal-to-noise ratio. A further practical problem is that the narrow beam has to be placed through the centre of the vessel.

- **Attenuation-compensated method.** This method combines Doppler power measurement and mean frequency measurement. A dual element annular array is used. First measurements of power and mean frequency are made using the small central transducer. This gives uniform insonation of the blood vessel. Secondly the combined dual element device is used to produce a narrow beam so that the sample volume is located entirely within the vessel. Combination of these power and mean frequency measurements results in volume flow without the need to measure the angle or the cross sectional area of the vessel (Hottinger and Meindl, 1979; Evans, J.M. *et al.*, 1986a, 1986b). The difficulty arises in producing two beams, one of which is uniform over the vessel and the other smaller than the lumen.

- **Assumed velocity profile.** This method measures the maximum velocity over an integral number of cardiac cycles and calculates the mean velocity according to the assumed velocity profile. Two distinct circumstances are of value, they are when the velocity profile is flat (Light and Cross 1972, Fisher

*et al.*, 1983, Huntsman *et al.*, 1983) or parabolic (Evans, D.H. 1985; Evans, D.H., *et al.*, 1989a). The maximum frequency is generally more reliable than the mean frequency because of its immunity to many effects such as non-uniform insonation, noise and filtering. However, when the flow profile is not fully established, this method is subject to errors.

The contents of this thesis have relevance for all of the above blood flow measurement techniques. The uniform insonation and the assumed velocity profile method have been investigated in detail. Some of the factors studied are also of interest in spectral analysis techniques.

### 1.1.4 The accuracy of the flow measurement

Accuracy is of central importance for the success of an ultrasonic examination. Despite the improvement in the performance of ultrasonic scanners in recent years, large errors in the volumetric flow measurement still remain. The reported errors in the flow measurement vary in the range of about 5% to 25%. This is partially due to limitations of ultrasonic machines and partially due to those effects that influence the propagation of ultrasound in tissue. A number of factors can affect volumetric flow measurement. They are listed as following:

- **Insonation.** Partial insonation can significantly change the spectrum and cause large errors in the mean velocity measurement. Many factors, such as type and size of the transducer, focusing, depth of the vessel, attenuation, misalignment of beam and vessel, reflection and refraction give rise to such an error.

- **Cross-sectional area.** Because of the relatively low resolution of ultrasonic images, the cross-sectional area is not accurately measured. The pulsatility and deformation of vessels also introduce errors.

- **Beam-vessel angle measurement.** Beam-vessel angles can be determined on duplex scanners to within about 3° (McDicken, 1991). This results in

errors in estimating velocity from the Doppler frequency shift, especially when large beam-vessel angles are used.

- **Flow disturbance.** The pulsatility of flow, curvature of vessel, stenosis, branches give rise to disturbance of the flow profile or even turbulence. This error is particularly important when the assumed flow profile method is used.
- **Electronic factors.** These are machine dependent factors including the filtering, method of signal processing and spectrum analysis, sensitivity, *etc.*.
- **Others.** Some errors arise from the characteristics of ultrasonic measurement. Intrinsic spectral broadening, non-linear propagation, angle dependent scattering and dispersive absorption of ultrasound can be included in this group.

Two reviews of the methods and errors of volumetric flow measurement have been made by Gill (1985) and Evans, D.H. (1986). Many errors can significantly affect the volumetric flow measurement. Therefore, to understand the results correctly, a thorough understanding of the sources of error is essential. The analyses of errors are undertaken for two reasons. The first obvious reason is to specify the source of error and determine the strength and limitation of each method, so that the correct operation and interpretation can be performed. The other reason is that through such studies, refinements and improvements of the current measuring methods may be discovered and therefore a higher accuracy of the measurement can be achieved.

## 1.2 Aims And Overview Of The Thesis

The aim of this thesis is to combine experimental and theoretical investigations of the sources of error in volumetric flow measurement using Doppler ultrasonic techniques and to look for possible improvements in the accuracy of such measurement.

Chapter 2 describes in some detail a flow phantom that was used in the project. It is highly desirable that experimental investigations are made in such a study.

Experiments on the human body are often difficult or impossible. Therefore artificial test objects, which simulate the conditions of the body, are usually used. However, test objects introduce artifacts that do not occur in the body. It is important that a thorough understanding of these artifacts is obtained before any measurements are performed. The setting and materials of the phantom were carefully considered. The effects of sedimentation of particles, wall reflection and refraction, which related to the use of the flow phantom, were experimentally and theoretically analyzed.

Chapter 3 describes a model of computer simulation of the generation of Doppler spectrum. As spectra can be affected by many factors simultaneously, difficulties are often found in interpreting the results from laboratory experiments or clinical measurements. Theoretical studies are of particular value in helping to find out the significance of the influence of each factor on the mean velocity measurement. The specific interests in this chapter are the effects of all the factors in the insonation category discussed previously on page 7, intrinsic spectral broadening and different laminar flow profiles. Efforts are made to reduce the computational intensity and to simulate spectra under different types of transducer and focusing. The theoretical results are carefully compared with experiments to verify the validity of such a simulation.

Chapter 4 investigates the spectra in various measuring conditions using the computer simulation model which is developed in Chapter 3. The objective of this chapter is to identify the significance of the effect of each factor on both mean frequency and maximum frequency measurement. Accordingly, errors due to these factors can be determined in the volumetric flow measurement. A method for, independent of intrinsic spectral broadening, extraction of maximum velocity is also suggested to improve the maximum velocity measurement. The errors in two typical clinical situations, which are the mean velocity measurements in carotid artery and umbilical vein, are analyzed.

In Chapter 5, the intrinsic spectral broadening is investigated. In recent years, electronic beam forming and dynamic focusing have improved the spatial resolution of ultrasonic images considerably. Linear arrays and phased arrays with large apertures are most widely used in modern ultrasound scanners. Many man-

ufacturers tend to use the same transducer for both B-mode imaging and Doppler examination. However, it is known that wide apertures and small sample volumes can give significant geometrical broadening and transit time spectral broadening. This reduces the accuracy of quantitative Doppler measurement. It had been suggested by a number of authors (Edwards, 1971; Newhouse *et al.*, 1980) that the geometrical spectral broadening and transit time spectral broadening were actually the same effect. In this chapter, it is suggested that the geometrical spectral broadening and transit time spectral broadening are independent effects and should be considered separately. The Doppler measurement, especially in the near field of a wide aperture transducer, is also investigated. Problems including the validity of estimating maximum frequency from extreme beam angles, and the error in measurement by using linear array are considered.

Chapter 6 investigates the accuracy of the inner diameter measurement. Volume flow is usually calculated by the multiplication of mean velocity in the vessel and cross-sectional area. The area is usually obtained by measuring the diameter of the vessel on a frozen B-mode image. However, the low resolution of ultrasonic images often results in uncertainty in the diameter measurement. The lack of literature on the accuracy of the diameter measurement makes this problem unclear. Chapter 6 describes an experimental study of the accuracy of such a measurement and a pulse length correction of the diameter, which may improve the measurement, is also suggested.

Chapter 7 examines the significance of non-linearity in pulsed wave Doppler and the consequences of this effect on Doppler spectra from commercial duplex scanners. It is well known that non-linear propagation results in distortion of pulse waveforms. The emphases of most research work in this area are usually on harmonic generation, attenuative losses and biological effects (Muir and Carstensen, 1980; Bacon, 1984; Duck *et al.*, 1985). In this chapter, it is shown experimentally that the non-linear propagation has no effect on Doppler measurement.

Chapter 8 deals with flow estimation for pulsatile velocity profiles. The objective of this chapter is to verify experimentally the use of time-averaged maximum frequency to estimate mean velocity when pulsatile flow is present. Some preliminary work is also made in spiral tubing and helical flow measurement.

Finally, Chapter 9 summarizes sources of errors and their significance. Further development and possible improvements are also discussed.

# Chapter 2

# STUDY OF THE FLOW PHANTOM

## 2.1 Introduction

For analysing errors in Doppler volumetric flow measurement, it is essential that experimental investigations are performed. However, as volumetric flow measurement often involves direct measurement of the flow rate, which usually means incision of the blood vessel, experiments on the human body are often difficult, destructive or impossible. Therefore, laboratory researches most often involve artificial test objects, such as flow phantoms, that simulate conditions in the body. However, test objects often introduce artifacts which do not occur in the human body. It is therefore important that a thorough understanding of these artifacts made before any measurements are performed.

Flow phantoms, which circulate artificial blood in a plastic tube to simulate blood flow in the human body, are often used to investigate flow in blood vessels *in vitro*. This approach is particularly useful in waveform analysis (Hoskins *et al.*, 1991a, 1991b), stenosis diagnosis (Douville *et al.*, 1983), flow measurement study (Evans, J.M. *et al.*, 1986b), calibration of equipment and quality assurance (Hoskins *et al.*, 1992). A number of different flow phantoms have been reported. Some flow phantoms use two reservoirs and the flow rate is controlled by changing

the height difference of the reservoirs (Wyatt *et al.*, 1971; Rasmussen, 1987). Only steady flow can be achieved using these devices. Kiyose *et al.* (1977) describe a mechanical piston pump system based on the principle that any given flow waveform can be synthesised from its component harmonics. However, it is difficult to set the adjustments and there are limitations in the types of waveforms that can be simulated. Roller pumps are used by several authors. Douville *et al.* (1983) use special backplate screws to adjust the degree of tube squeezing; the adjustment is empirical and therefore have a low reproducibility. Law *et al.*, (1987) control the motion of the roller by a computer and achieve physiological flow, which is similar to pulsatile flow in human blood vessels. However, this only allows the production of a limited number of waveforms and is not suited to produce steady flow. It is also difficult to program new waveforms or produce reverse flow using this pump. Furthermore, to obtain a high acceleration of the roller, an extremely powerful motor is necessary. The use of a gear pump seems to have solved these problems (Issartier *et al.*, 1978; McDicken *et al.*, 1986; Hoskins, *et al.*, 1989). The waveform and flow rate can be precisely controlled. The major difficulty with a gear pump is the damage of particles by the grinding action of the gears, for example for whole blood or particles such as sephadex. In most of the studies described in this thesis, a computer controlled physiological flow phantom with gear pump (Hoskins, *et al.*, 1989) was used.

The observed Doppler spectrum is considerably influenced by the physical characteristics of the phantom. For example, as the speed of sound and acoustic impedance in tubing material, surrounding fluid and artificial blood are usually different, reflection and refraction occur. As shown in Figure 2.9 (c), reflection causes a part of the incident energy to be sent back, the remaining energy propagating onwards at a different angle to the normal of the vessel–this is the refracted beam. The magnitude of the reflection is different at different positions due to the curvature of the vessel wall (Figure 2.9). This changes the beam intensity which insonates the moving scatterers and therefore distorts the Doppler spectrum.

Other factors such as sedimentation of particles, viscosity of the artificial blood, wall material, tubing thickness, possible air bubbles, wave reflection along the tubing, the distance to outlet and inlet and possible turbulence *etc.*, can also cause

distortions of the Doppler spectrum from a flow phantom. However, intensive studies on these effects have not been reported.

In general, the above factors can be divided into two categories; those whose influence can usually be avoided by careful experimental set up and measurement, and those which cannot. In this chapter, the flow phantom and its set up will be described. It will be shown that by careful choices of the setting up conditions, the effect of air bubbles, turbulence, inlet and outlet length can be minimised. The effects of sedimentation of particles, refraction and reflection at vessel walls, which may cause distortion of the Doppler spectrum, will be investigated both experimentally and theoretically. Their influence on the mean and maximum frequency measurement will be discussed.

## 2.2 Description Of The Flow Phantom

A detailed description of the physiological phantom is given in a publication by Hoskins *et al.* (1989). The phantom (Figure 2.1) is composed of 2 parts : a large tank with holders for the tubing and the transducer; a gear pump driven by a computer controlled stepping motor. A long section of the tubing is straight, and is held firmly in place in water by tubing holders, whose height can be adjusted. The probe holder has an arm which keeps the distance between transducer and sampling site unchanged when the angle is altered (Figure 2.2). A protractor is fixed on the holder so that accurate setting of angles can be achieved. The speed of the motor is controlled by a micro-computer and therefore pulsatile waveforms of different shapes and velocities can be produced.

For artificial blood, a suspension of Sephadex G 25 superfine particles in a mixture of 42% glycerol to 58% water was used. The swollen particles have dimensions of approximately 20 to 70 $\mu m$. These are large compared to red cells which have linear dimensions of 2.4 by 8.5 $\mu m$. However, they are convenient and relatively inexpensive to use. The glycerol and water mixture has a viscosity of 0.004 $kg/ms$ at 20 $^{\circ}C$ which corresponds to that of blood at 37 $^{\circ}C$ according the acoustic properties listed in Table 2.1. To avoid the distortion due to refraction,

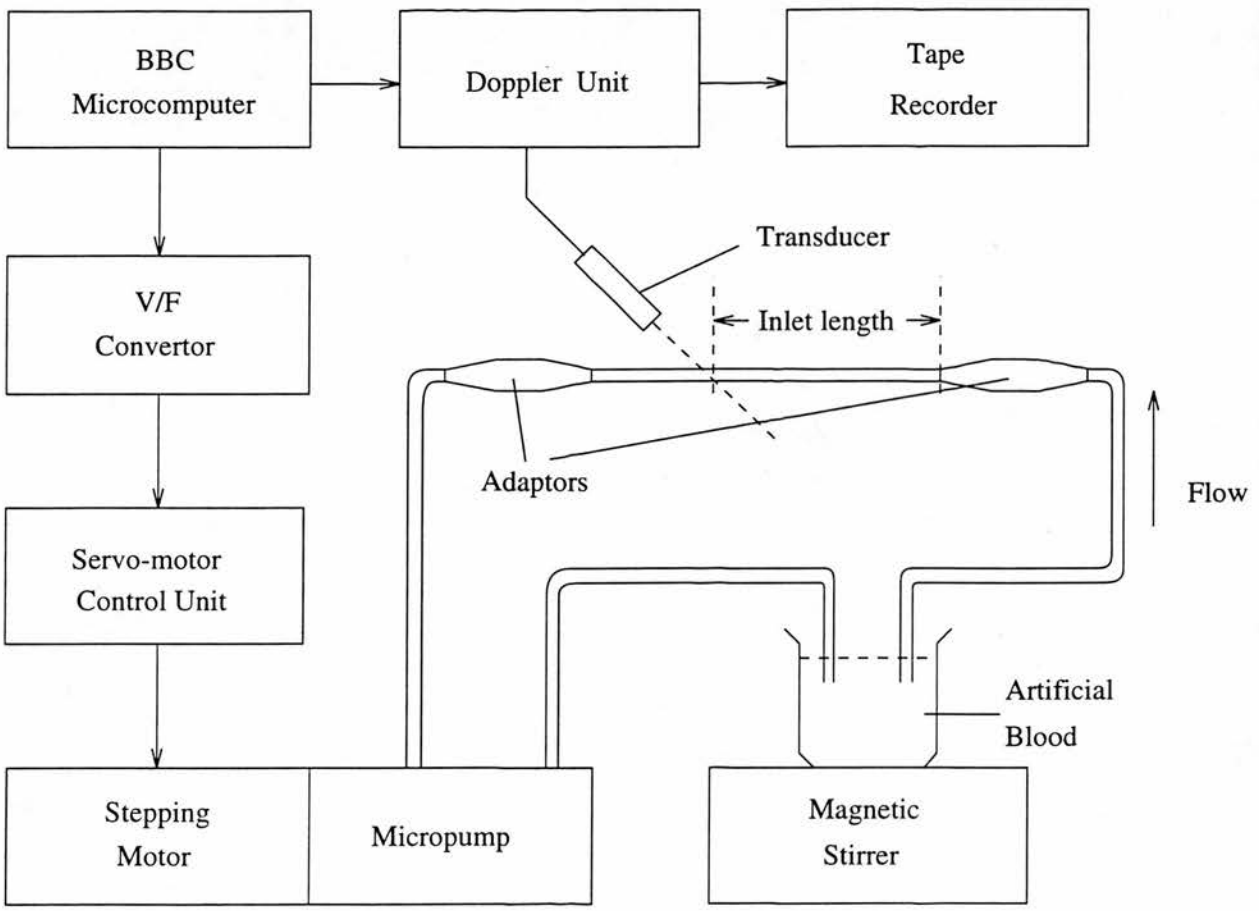


Figure 2.1: The block diagram of the flow phantom. A computer controlled stepping motor and a micropump circulate the artificial blood in plastic tubes. The Doppler spectrum is acquired and recorded by the Doppler unit and tape recorder. The inlet length is measured by the distance between sample volume and the adaptor.

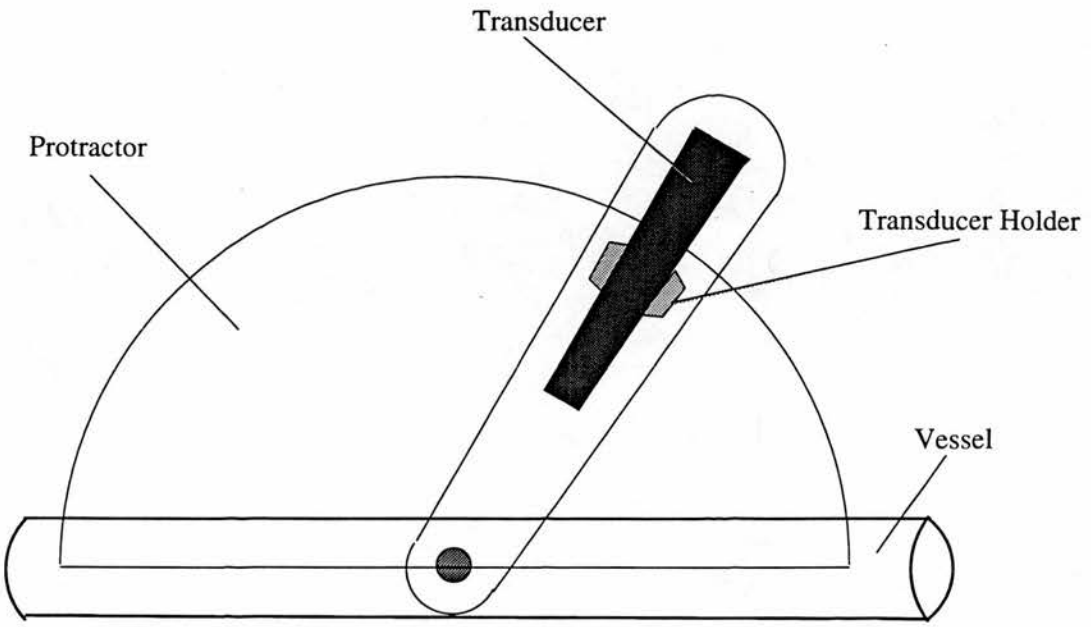


Figure 2.2: The transducer holder keeps the sampling site and distance between the transducer and sample volume unchanged when angle is altered.

degassed water and sephadex mixture was also used in some studies to match the sound speed inside and outside the tube. The spectra from blood and sephadex are very similar in terms of their first and second order statistical properties (Hoskins *et al.*, 1990b).

The vessels were constructed from heat-shrinkable material which was moulded around rods of known diameter (McDicken, 1986). Some acoustic properties of the heat-shrinkable material are listed in Table 2.1.

A Doptek 4 MHz continuous wave unit was usually used for waveform acquisition. A continuous wave unit was used in most of our experiments. It was intended to avoid the distortion in the Doppler spectrum due to the short transmitted pulse associated with a pulsed wave unit so that a clear observation could be made on the factor investigated. All the spectra were recorded on magnetic tapes so they could be replayed afterwards. The spectra could also be transferred to the micro-computer for further analysis.

Simultaneous to the Doppler acquisition, measurements of absolute flow were made using a measuring cylinder and a stop watch. This was compared with flow rate measured from the Doppler spectrum.

## 2.3 Materials And Set Up Of The Flow Phantom

In this section, some factors, such as dissolved air bubbles, accuracy of the tube construction, turbulence, *etc.*, which may affect the Doppler measurement are discussed. Careful set up of the flow phantom, which may minimise the effect of these factors, is described.

### 2.3.1 Tubing materials

Two kinds of material are often used in constructing tubes for flow phantoms. The first kind is stiff materials including glass (Eik-Nes, 1980), PVC, polythene, heat-shrinkable material, *etc.*. The diameter of these tubes usually does not change during simulated cardiac cycles so an accurate diameter measurement can be made. However, as the speed of sound in these materials is usually significantly higher than surrounding liquid (usually water) (Table 2.1), there may be relatively strong reflection and refraction at the tubing wall. This can distort the beam profile, and therefore cause distortion of the Doppler spectrum. The second kind of material is soft and elastic, such as silicon rubber, latex *etc.* (Table 2.1). The diameter of this kind of tube usually changes during the cardiac cycles. It can be used to simulate the pulsatility of a real blood vessel. Latex rubber, in particular, has similar speed of sound to soft tissue. However, the diameter of the tube is often difficult to measure as it changes when the pressure in the vessel changes. Large changes in waveform shape along the length of elastic tube, which are due to reflected pressure waves from the end of the tube, can be often observed. Kinking may also occur, especially when large flow reversal is present.

In most of our studies, heat-shrinkable material was used in the construction

| Material | Density ($kgm^{-3}$) | Speed of sound ($ms^{-1}$) | Acoustic resistance ($kgm^{-2}s^{-1} \times 10^{-6}$) |
|---|---|---|---|
| Heat shrink | 960 | 1979 | 1.90 |
| Latex rubber | 921 | 1566 | 1.44 |
| Silicon rubber | 1140 | 1005 | 1.15 |
| C-flex | 886 | 1556 | 1.38 |
| Norprene | 975 | 1571 | 1.53 |
| Glycerol-water mixture | 1025 | 1690 | 1.86 |
| Water | 1000 | 1480 | 1.48 |

Table 2.1: Some acoustic properties of tubing materials and artificial blood measured by National Physics Laboratory.

of tubes to give an accurate diameter. The heat-shrinkable tubing is also the best thin wall tubing we can find which gives the least wall reflection.

### 2.3.2 Tubing diameter

Artificial vessels were constructed by moulding the heat-shrinkable material around metal rods of known diameter. The diameter of the tubing was examined by using a microscope and compared with the diameter of the rods. It was found that the accuracy of the construction of tubing diameter was better than 0.05 mm.

### 2.3.3 Water in waterbath

Water in the waterbath needs to be preserved for at least two days to allow the dissolved air to be released. Tap water always releases micro-air bubbles, particularly around the tubing. Air bubbles can give very strong back scattered signals. This signal may be too strong to be completely filtered out by the high pass filter and may give rise to low frequency artifacts. Experiments were made repeatedly to compare the spectra with and without surrounding air bubbles. Figure 2.3 gives an example spectrum with micro-air bubbles surrounding the tubing and also after wiping off the bubbles. It is found constantly that a small peak appeared when the air bubbles are present due to strong scattering from the bubbles.

### 2.3.4 Angle measurement

Accurate angle measurement is always crucial to the Doppler measurement. To obtain accurate readings of the beam-vessel angle, a protractor was fixed to the transducer holder (Figure 2.2). The angle was always determined by the following way. First the transducer was oriented to allow equivalent spectra on both forward and reverse channels of the Doptek to find the 90° angle position. The accuracy for obtaining 90° was better than 0.5° since 0.5° was enough to give significant difference between spectra in the two channels. The required angle was then positioned relative to the 90° position. As the reading was very accurate, it was estimated that the accuracy of the angle setting was better than 1°.

### 2.3.5 Artificial blood and air bubbles

The artificial blood was made in such a manner as to remove air bubbles. Water was boiled several times to remove the dissolved air and then added to the glycerol carefully. The sephadex was then prepared by adding an amount of dry sephadex to the glycerol-water solution and heating for 1 to 2 hours at about 85 $°C$. This swells the particles to their final volume and removes dissolved air.

The flow phantom was flushed with water, which had been degassed by boiling, for several minutes. Special care was taken to remove air trapped within the gear pump and tube by inverting the gear pump and running it at high speeds. The presence of microbubbles was monitored using the Doptek unit. Flushing was repeated until no recirculating bubbles were observed. The flow phantom was further flushed with glycerol-water solution while monitoring using the Doptek unit. The sephadex suspension was then introduced.

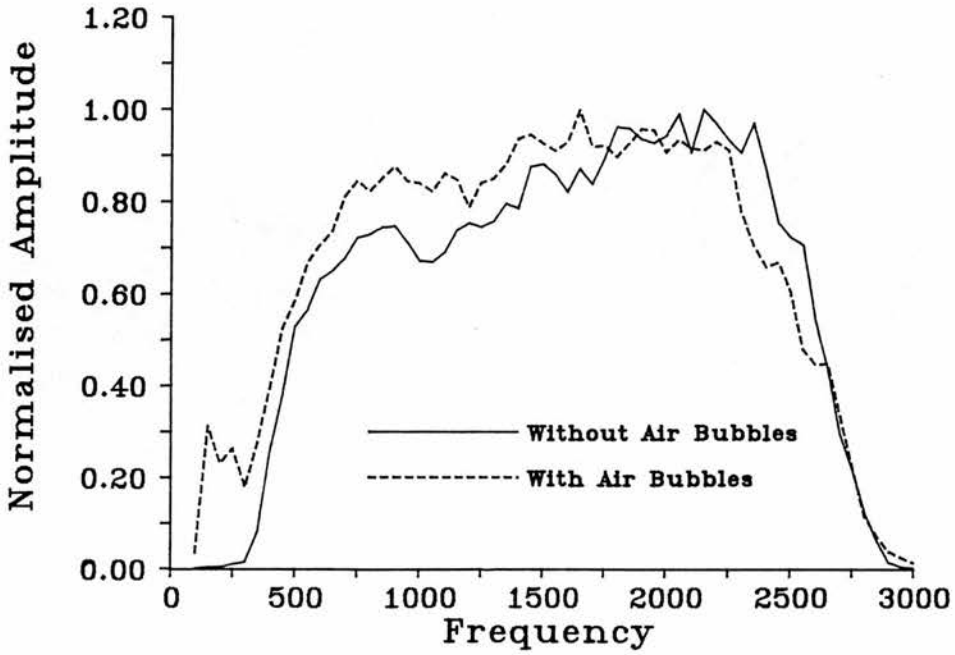


Figure 2.3: The spectra acquired with air bubbles settled outside the vessel wall and while air bubbles were wiped out. The small peak in the low frequency is caused by the scattering of these air bubbles.

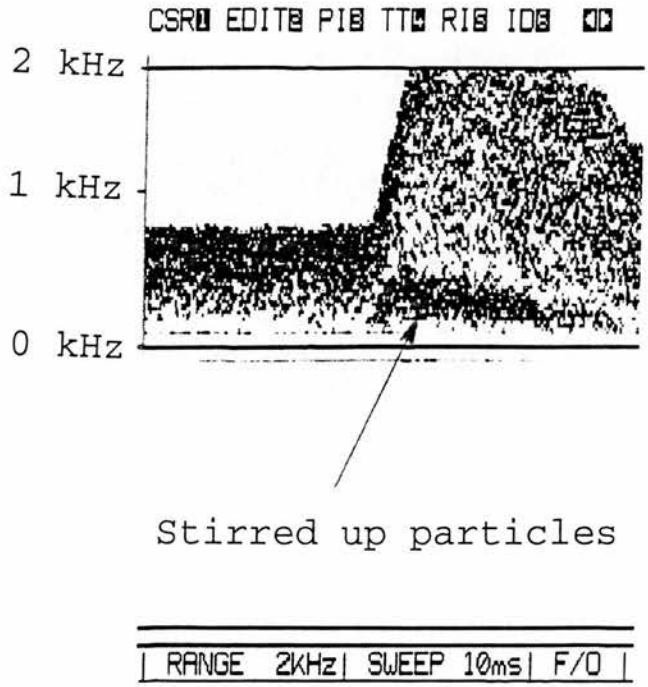


Figure 2.4: When the flow rate was suddenly increased, the settled particles were stirred up.

### 2.3.6 Inlet and outlet length

The length of tubes was made large enough to produce stable flow conditions at the point of insonation. The inlet length $L$ is quoted as (McDonald, 1974)

$$L = 0.04DRe \tag{2.1}$$

where $D$ is the tubing diameter and $Re$ is the Reynolds number given by

$$Re = \frac{\overline{V}D\rho}{\mu} \tag{2.2}$$

where $\overline{V}$ is the average velocity of flow across the pipe, $\rho$ is the density of the liquid and $\mu$ its viscosity.

The exit of the tube usually does not affect the flow profile unless it is too near to the exit (within 2 cm for a 5 mm tube, see Chapter 8 about stenosis).

### 2.3.7 Viscosity changes

For continuous use over 9 hours it was observed that the viscosity of the artificial blood increased. This might be because the water content decreases due to evaporation. Destruction of particles by the gear pump might also give rise to viscosity changes. In the experiments of this thesis the artificial blood was freshly made; this ensured that the viscosity was correct, that the particles remain relatively unbroken, and that air did not enter the solution from the atmosphere.

### 2.3.8 Flow rate

The flow rate was always adjusted to ensure that the Reynolds number, $Re$, was less than 2000 in order to avoid turbulence in the tube, unless of course this was specifically required. The appearance of turbulence was also monitored on the Doppler unit by observing the presence of high frequency spikes. It was also found that when the pump ran at a speed above a critical level, a large amount of air bubbles occurred. This may be because the gears of the pump produced

very low pressure in the pump which may expand the micro-air bubbles dissolved in the artificial blood and also cause cavitation. In our experiments, the pump speed was kept below this level.

### 2.3.9 Particle breaking

As a gear pump was used, the particles were broken up by the grinding action of the gears. This reduces the particle size and makes the shape and size of the particle irregular. However, according to acoustic theory, when particles are much smaller than the wavelength, the scattering characteristics are not dependent on the shape of the particles (Morse and Ingard, 1964) except for backscattered power. As shown in Section 2.4, the major part of the spectrum does not change significantly when the particles are substantially broken, though the sedimentation may be different.

## 2.4 Sedimentation

The effect of sedimentation of particles is investigated experimentally in this section.

### 2.4.1 Distribution of particles in the vessel

In the blood vessel, the scatterers (mainly red cells) can be considered to be uniformly distributed (McDonald, 1974). However, in the flow phantoms, the sephadex particles have a higher density than the suspending fluid (which can be observed by the fact that the particles always settled at the bottom in the fluid), and sedimentation may occur. In a study of drug injection into a vessel through which a fluid is flowing, Najib *et al.* (1985) described the effect as four situations:

1. The particles migrate to the tube wall and remain stationary.
2. The particles migrate to the tube wall and slide or roll along the tube.

3. Some of the particles start to suspend and flow at a lower rate than the fluid (heterogeneous flow).

4. The particles remain suspended and flow at the same rate as the fluid (homogeneous flow).

Each of these situations is associated with a different range of fluid velocity. For low flow rate, drag and lift effects are too small to overcome the buoyancy effect so particles are stationary at the bottom of the tubing. For a higher flow rate, particles start rolling, being lifted and becoming suspended in the fluid. At relatively high speed, the particles become fully suspended and homogeneous flow occurs. The velocity range of each situation is determined by particle size, particle density, fluid viscosity and tubing diameter.

In a long, straight and non-branching tubing, the flow profile of a steady flow is parabolic. The velocity varies from almost zero near the wall to the maximum at the centre of the tubing. Inevitably, different situations happen in the tubing. Near the wall, particles are settled and rolling or sliding along the tubing. At regions a bit farther to the wall, situation (3) occurs. In this region, particles are not homogeneously distributed; particles are settling so there is a relatively low concentration of particles compared to the central stream. At the central region, as the speed is enough to drag and lift particles, situation (4) may occur. Particles are suspended more uniformly and travel at the same speed as the fluid.

Based on the discussion above, all four situations described by Najib *et al.* may happen in flow phantoms at the same time. This will probably lead to distortions in the Doppler spectra acquired from flow phantoms, especially for low frequency components which are from particles with low velocities in the region near the vessel wall. In an experiment using water and sephadex particles, when the flow rate was abruptly increased, the spectrum (Figure 2.4) clearly showed that the particles which were originally settled were suddenly stirred up to produce a large increase in the amplitude of low frequency components. This is consistent with the explanation that sedimentation of particles occurs in the flow phantom.

The critical velocity of the fluid required to start stationary particles rolling along the wall was studied by Najib. This velocity is usually a few centimetres per second in most of the common set ups of the flow phantom. The particle rolling and heterogeneous flow is more important to Doppler measurement. However, no report about the effect of sedimentation on Doppler spectra has been found in the literature. A more detailed study of this effect is necessary, as presented in the next section.

### 2.4.2 Experiment

To investigate the effect of sedimentation on the Doppler spectrum, experiments were made on the flow phantom. A 5 mm heat-shrinkable tube was connected to the pump. Both water and glycerol-water solutions were used in the investigation.

The Doppler spectra were acquired using a Doptek 4 MHz continuous wave unit. The beam-vessel angle was 50° and the distance between the transducer and vessel was 5 cm. The sample volume was first placed at 40 cm from the entrance where the adaptor was placed. Seven different flow rates were used. The Doppler spectra were transferred to a BBC master micro-computer, analyzed and the averaged spectrum of 240 lines was calculated and plotted. The flow phantom then was kept running for 9 hours to enable particles to be sufficiently broken up by gears of the pump. The same experiment was repeated. The particles were observed under a microscope.

The transducer then was placed at different distances to the entrance. The distances ranged from 10 cm to 70 cm in 10 cm steps. The spectra again were calculated and plotted.

### 2.4.3 Results

Figure 2.5 shows the spectrum acquired at 40 cm from the entrance using water as the suspending fluid. At extremely low frequency, no signal is observed. This may be due to the fact that the high pass filter (300 Hz for the Doptek unit)

eliminating components in that frequency range. A sharp peak, which is from the particles rolling along the tubing wall, is present at low frequency. The high frequency components change smoothly. However, there is a sharp dip at the frequency just higher than the peak frequency range. This may result from the heterogenous flow described previously. Therefore, it seems all the four situations described before can be observed. The frequency range of the spectrum which is affected by sedimentation can be considered as 0 to the end of the dip.

Figure 2.6 shows spectra at different distances to the entrance with water as the artificial blood. The central frequency of the dips in these spectra is very similar. However, the low frequency peaks become higher in amplitude when the sampling site is far away from the entrance. This is possibly because when it is far from the entrance, where turbulence occurs and particles are well mixed with the fluid, the flow profile is more well established, more stable and laminar, therefore, more particles settle and roll at the bottom of the vessel.

When the flow rate was increased, the frequency of the low frequency peaks and the frequency of the dips had small changes (Figure 2.7). The dependence of frequency of the dip on the flow rate or velocity may be due to the fact that for higher velocity, more local small disturbance of the flow was created and it took longer distance for flow profile to establish.

After 9 hours running, it was observed with a microscope that the particles were substantially broken up. So there were fewer particles settled. Compared to the spectrum with original particles, the height of the peak at low frequency was much lower. However, the frequency of the dip was still the same (Figure 2.8). This suggests that reducing particle size may only reduce the number of particles which settle. However, particles still settle below the same velocity as the frequency of the dip remains the same.

With the water-glycerol artificial blood, the low frequency peak can still be observed (Figure 2.5). However, the amplitude of the peak is not as high as that with water and the frequency of the dip is lower than that with water. This is probably because the density of glycerol-water mixture (1.10 $g/cm^3$) is higher than water (1.0 $g/cm^3$) and the viscosity is 4 times that of water, which makes

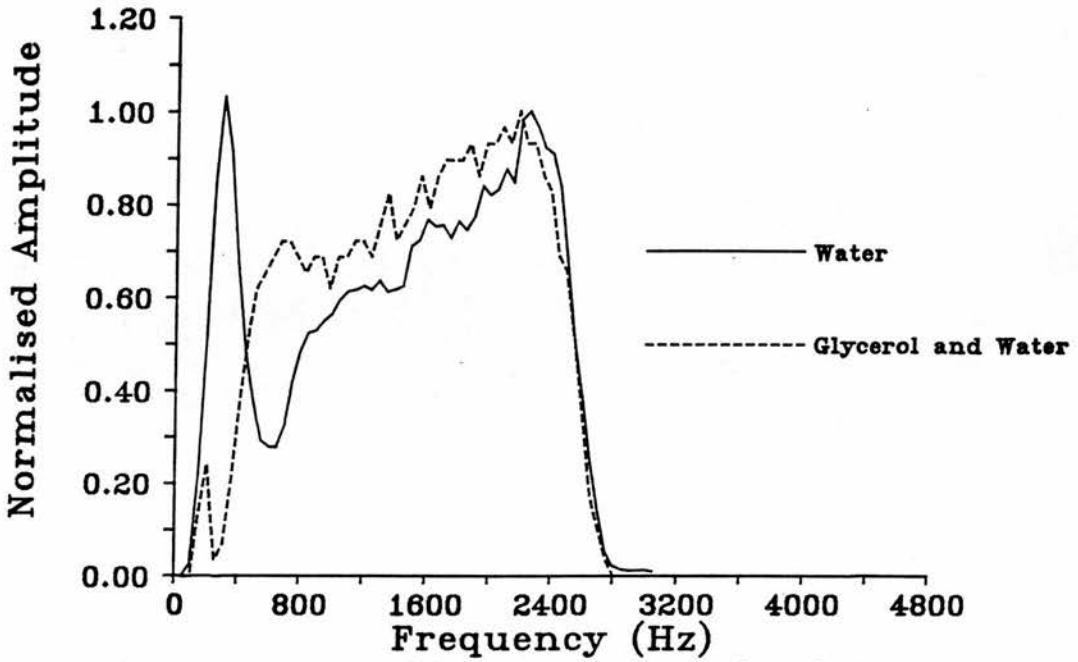


Figure 2.5: The spectrum acquired from water and sephadex solution at 40 cm to the entrance from original particles. The water-glycerol solution with sephadex gives much smaller low frequency peak and the dip appears at lower frequency. This is consistent with the assumption that the dip and small peak result from sedimentation of particles.

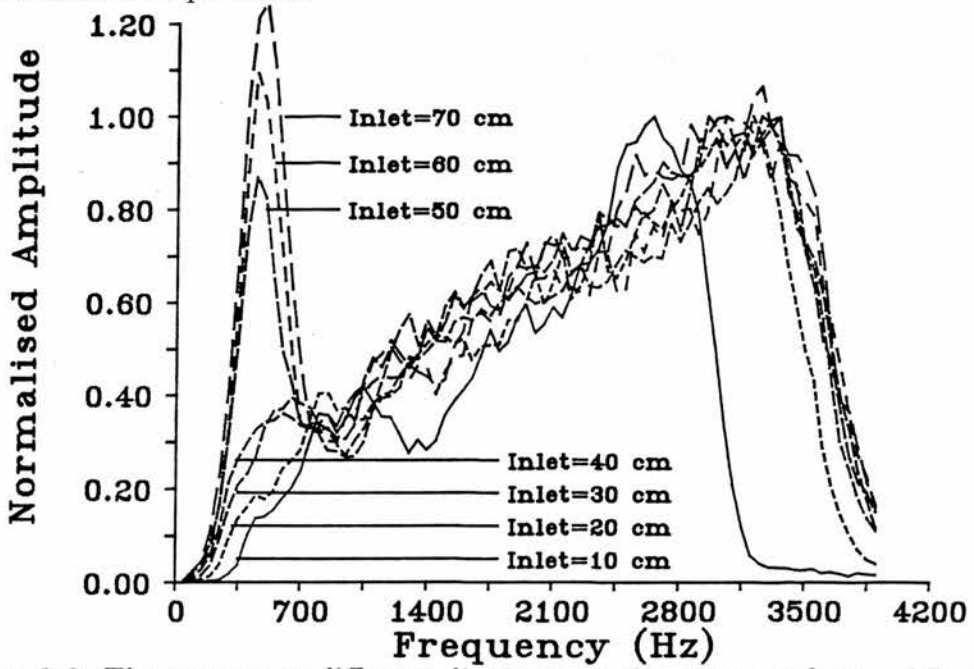


Figure 2.6: The spectra at different distances to the entrance from original particles. The peaks became higher when the inlet distances increase. This is possibly due to the fact that at positions far from the entrance, laminar flow is more well established so more particles are likely to settle down to the bottom of the vessel.

sedimentation less significant. The reduction of the sedimentation suggests that making the densities of the fluid and particles as close as possible should be a solution to the sedimentation.

## 2.5 Refraction

In flow phantoms, as the speed of sound in surrounding fluid, tubing wall material and artificial blood is usually different, refraction occurs at the vessel wall. Reflection and refraction change the intensity distribution in the beam and the direction of propagating waves, and consequently distort the Doppler spectrum. It was suggested that the change on the Doppler angle at the tissue-vessel-blood boundary can cause as much as 7% error (Kremkau, 1991) in Doppler shift. In this section, the refraction at vessel wall boundaries will be discussed. The study of reflection will be given in section 2.6.

### 2.5.1 Theory

When ultrasonic waves meet a boundary between two media with different sound speed at an angle, the direction of the propagation will change. This is known as refraction. As a vessel is a cylindrical tubing, different incident angles occur at different positions across the vessel. In general, the refraction at a tubing wall can be considered along two directions; that is along the vessel axis and across the vessel (Figure 2.9).

For the refraction along the vessel, first we consider the boundary of the surrounding media and vessel. As shown in Figure 2.9 (b), the waves are refracted and the direction of the refracted wave is given by

$$\sin\theta_2 = \frac{c_2}{c_1}\sin\theta_1 \tag{2.3}$$

where $\theta_1$ is the incident angle, $\theta_2$ is the refracted angle, $c_1$ and $c_2$ are sound speeds in the surrounding media and vessel wall. Similarly, at the second boundary of

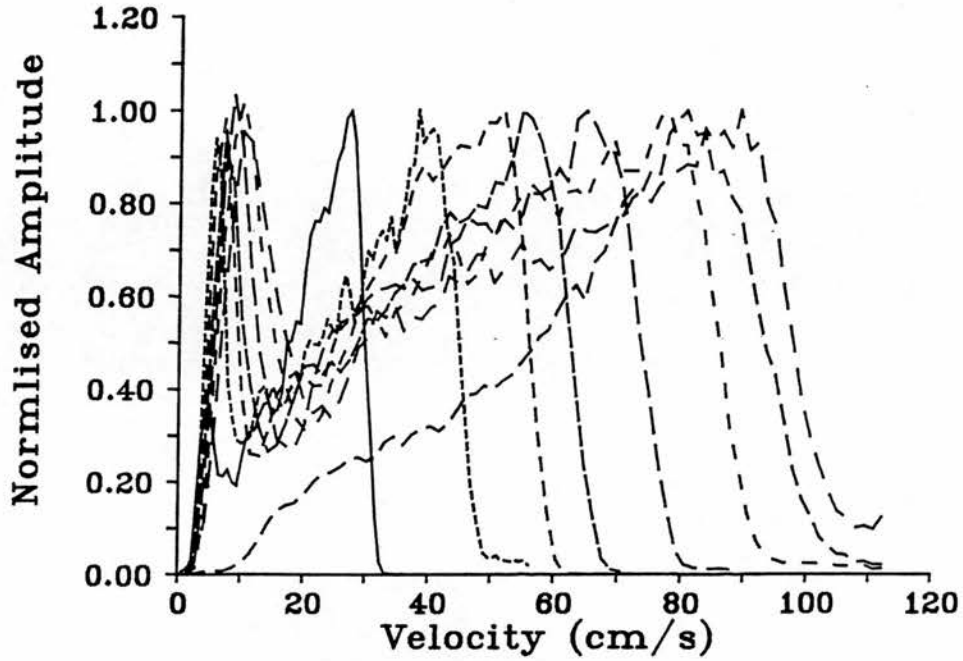


Figure 2.7: Sedimentation for original particles at different flow rates. It is noticed that when the flow rate was increased, the frequency of the peaks in low frequency has no significant change.

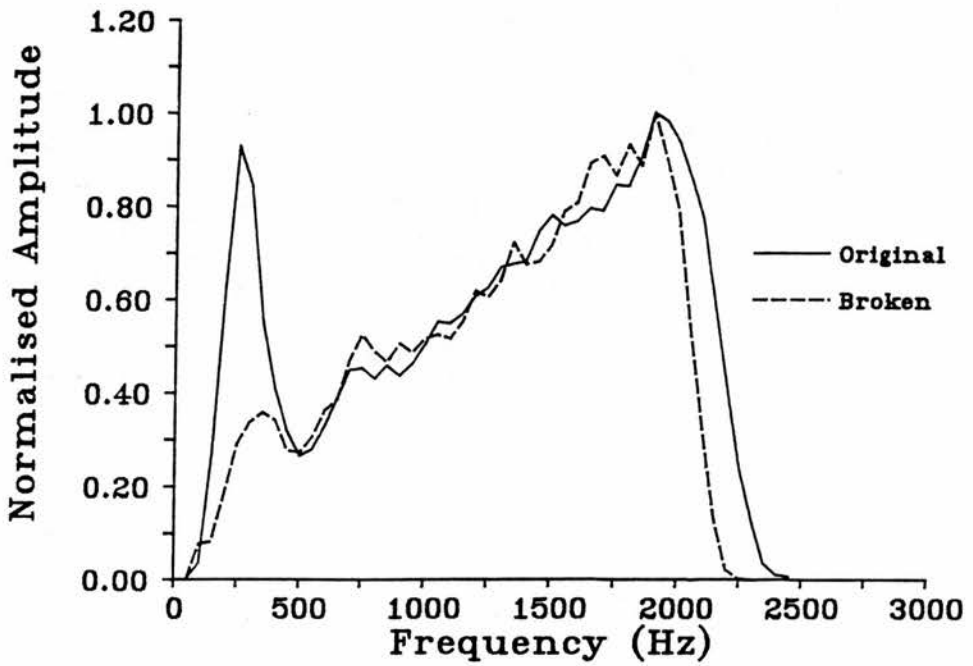


Figure 2.8: Spectra with original particles and broken particles. The peak in low frequency of broken particles is smaller than the peak of original particles. This is possibly because the broken particles are smaller and easier to be lifted. So there is less particle sedimentation for broken particles.

the wall and the artificial blood, the direction can be expressed as,

$$\sin\theta_3 = \frac{c_3}{c_2}\sin\theta_2 \tag{2.4}$$

where $c_3$ is the sound speed in the artificial blood. Substitute Equation ( 2.4) to ( 2.3), the following equation can be obtained.

$$\sin\theta_3 = \frac{c_3}{c_1}\sin\theta_1 \tag{2.5}$$

Assuming backscattered ultrasound waves received by the transducer travel along the same path as that of transmission, the Doppler formula becomes,

$$\begin{aligned} F_d &= \frac{2VF_0}{c_3}\sin\theta_3 \\ &= \frac{2VF_0}{c_1}\sin\theta_1 \end{aligned} \tag{2.6}$$

where $V$ is the velocity of the particles, $F_d$ is the Doppler frequency shift and $F_0$ the frequency of transmitted ultrasound. It is noted that Equation ( 2.6) is the Doppler shift formula without considering the refraction and vessel wall. In other words, refraction along the vessel axis has no effect on the Doppler shift and therefore the Doppler spectrum, provided that the interfaces are parallel (Li *et al.*, 1993).

An extension of this theory for parallel layers of medium is that no matter how many parallel layers of medium separate tissue and blood, unless total reflection occurs, the Doppler shift will not change. This is because for each layer, the refraction angles can be written as

$$\frac{\sin\theta_1}{c_1} = \frac{\sin\theta_2}{c_2} = \frac{\sin\theta_3}{c_3} = \cdots \tag{2.7}$$

As a consequence of this, the Doppler formula Equation ( 2.6) remains unchanged. Therefore, it is not necessary to consider changes in Doppler angle at each boundary and detailed structure of the vessel wall.

The refraction across the vessel, however, is different. Because of changes in the direction of propagation, the beam tends to converge or diverge behind the vessel wall (Figure 2.9 (c)). In the experimental set up used in this thesis, as

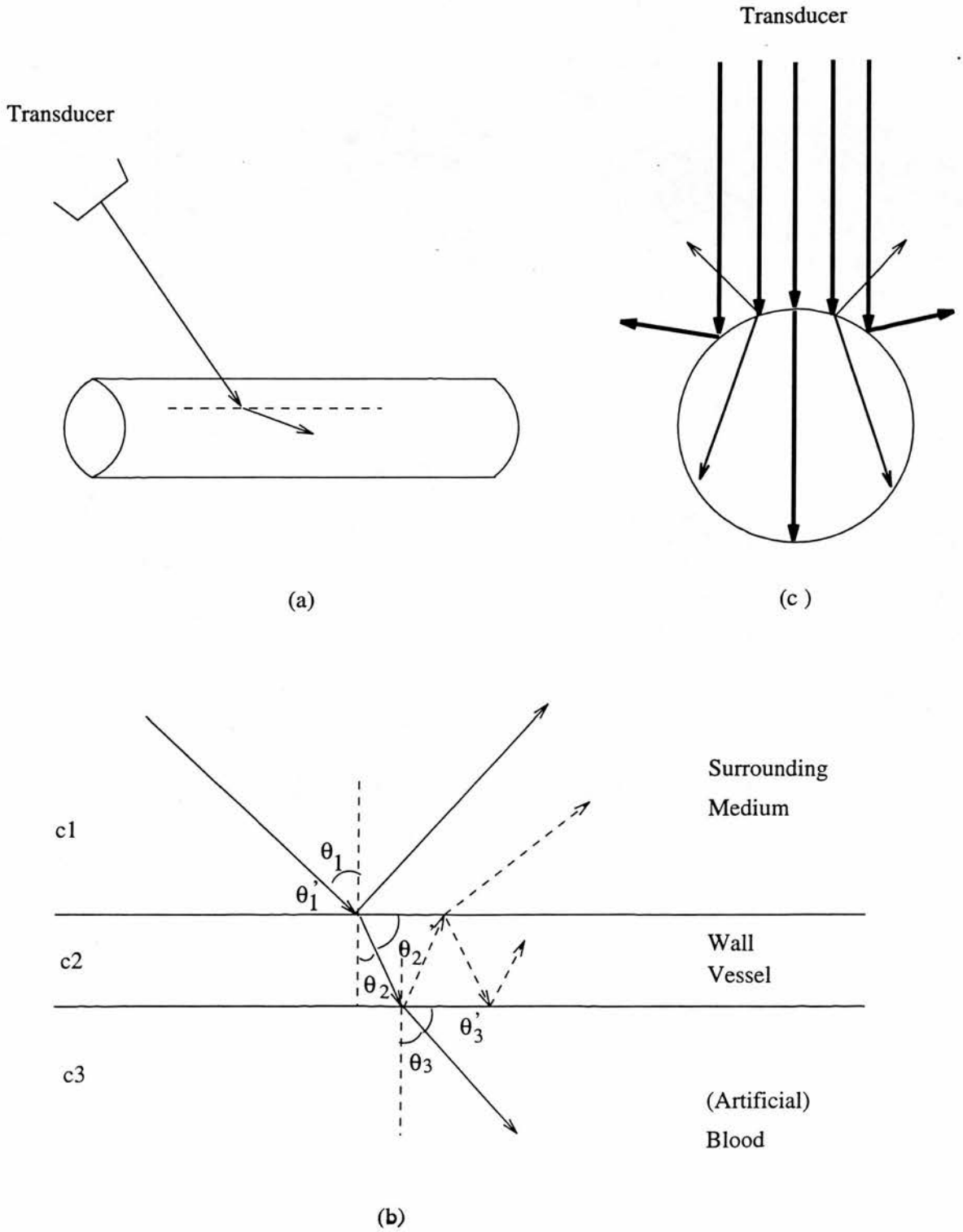


Figure 2.9: The refraction on the vessel wall (a) can be considered along two directions; that is (b) along the vessel axis and (c) across the vessel.

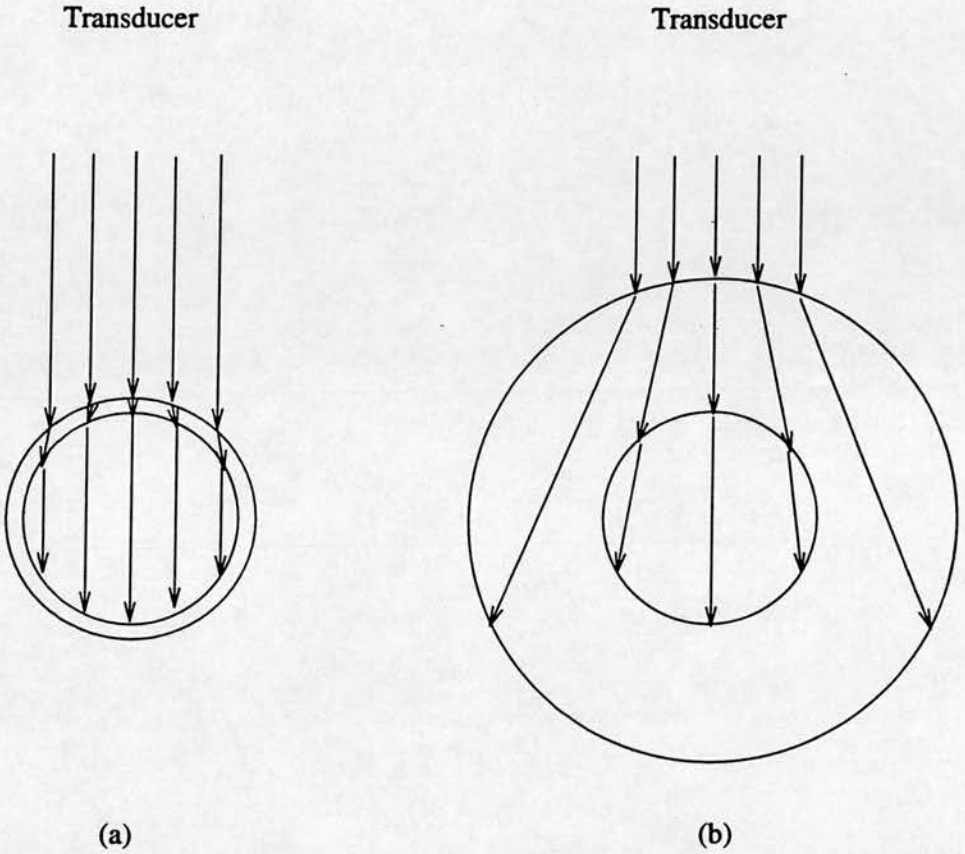


Figure 2.10: Thick wall tubing may give an underestimation of the maximum velocity compared to thin wall tubing as refraction may divert the beam more significantly than for the thin wall tubing.

the speed of sound in the artificial blood (1850 m/s) is higher than that in water (1480 m/s), the beam diverges. This gives a more uniform beam pattern and larger amplitude low frequency components of the Doppler spectrum compared to the case without refraction. However, as the maximum Doppler frequency is obtained from the central stream of the flow, it should not be affected by refraction.

One special case, however, remains; that is with thin wall tubing and with water and sephadex as artificial blood. As the sound speeds inside and outside the vessel are the same, the direction of propagation does not change (Equation 2.6). So refraction at the wall in both directions has no effect on the Doppler spectrum. As will be seen in the next section, we will use this method to examine reflection at the vessel wall.

Finally, I want to briefly discuss the use of thick walled tubing. When thick walled tubing is made of material with a high speed of sound, strong refraction occurs at the boundary. As the tube is thick, ultrasonic waves travel a relatively long distance within the wall. When the wave passes the boundary of wall and (artificial) blood, the incident angle is significantly different to the reflected angle at the boundary between the surrounding material and the wall (Figure 2.10). Therefore, the ultrasonic waves are not in the plane parallel to the transducer axis and vessel axis. Equation ( 2.6) does not hold in this situation. Furthermore, the position shift of each ultrasonic wave may significantly reduce the insonation in the central region of the vessel, so that the high frequency components are weakened. Therefore, the maximum frequency can be changed.

### 2.5.2 Experiment

Based on the discussion in Section 2.5 the effect of refraction on the Doppler spectrum can be examined by using water and a glycerol-water mixture as artificial blood. The refraction along the vessel axis can be detected by changes in the maximum frequency shift, which is mainly from the centre of the vessel. The refraction across the vessel should manifest itself by the changes in the whole spectrum, especially the low frequency components of the spectrum.

Experiments were made on the flow phantom. A 5 mm heat-shrinkable tubing was constructed. Both water and the standard glycerol-water mixture were used as artificial blood. Water gave little refraction as the sound speed inside and outside the tubing was the same while glycerol-water mixture gave a higher degree of refraction.

The tubing was fixed at 5.0 mm to the 4 MHz CW transducer of the Doptek unit. Doppler waveforms were acquired during steady flow at angles from 85° to 40° in 5° steps. All the spectra were recorded on magnetic tapes. Simultaneous measurements of absolute flow rate were made using a measuring cylinder and a stop watch. Assuming parabolic flow, in which the maximum velocity is double

the mean velocity, the real maximum velocity $V_{real}$ was then calculated by

$$V_{real} = \frac{Volume\ in\ measuring\ cylinder}{Time\ of\ collecting} \cdot \frac{2}{\pi r^2} \tag{2.8}$$

where $r$ is the internal radius of the tubing.

The recorded spectra were analyzed by the Doptek spectrum analyzer. The maximum frequency was extracted automatically using the 15/16 percentile method. In the percentile method the total value T of pixel values (voltage amplitude) of a single spectral line was calculated. The maximum frequency was then calculated as the point where the sum of pixel values below that frequency just exceeds a specified percentage of T. In this case this was 15/16 expressed in percentage terms. The maximum velocity $V_{meas}$ was then estimated using the Doppler shift formula ( 2.6) and the percentage error $E$ was calculated by

$$E = \frac{V_{meas} - V_{real}}{V_{real}} \times 100\% \tag{2.9}$$

The whole spectra were also plotted. Comparisons between the averaged spectra of water and glycerol-water solution were made.

To examine the effect of wall thickness on the received Doppler spectrum, the same experiment was made on 4.0 mm heat shrinkable tubing and 4.0 mm thick wall perspex tubing. The thicknesses of the tube wall were 0.3 mm and 3.1 mm respectively.

### 2.5.3 Results

First the effect of refraction along the vessel axis is considered. Figure 2.11 gives the error $E$ of maximum frequency at different beam-vessel angles. The degrees of the refraction were quite different between the water and water + glycerol solutions. For example, at beam-vessel angle ($\theta_1'$ in Figure 2.9) of 50°, the real incident angle $\theta_2$ for glycerol + water solution is 36.5° because of refraction and for water it remains at 50°. However, there is no significant difference in the maximum frequencies between spectra from the two types of artificial blood, although the degrees of the refraction were different. The overestimation of the $V_{meas}$, especially

at large beam-vessel angles, is due to geometrical spectral broadening which will be discussed in Chapter 3. It is noted that even the overestimation are very similar. Therefore, it can be concluded that the refraction has no effect on the maximum velocity measurement when thin walled heat shrink tubes are used. It also suggests the refraction along the vessel axis does not change the Doppler frequency.

If we observe the spectrum from the water and glycerol-water solutions (Figure 2.5) in detail, it is found that the high frequency components of the spectra are almost the same. However, as refraction widened the beam, the spectrum from water-glycerol solution shows a flatter curve at low frequency. The spectrum with water-glycerol is very similar to the ideal square shape, which should only happen when both a parabolic flow profile and uniform insonation occur. This indicates the region near the edge of the vessel, which is not oblique to the ultrasound because of the wall reflection (see Section 2.6), is also insonated due to refraction (see Figure 2.9 (b)).

When a thick wall tubing was used, the maximum frequency was underestimated by about 10% compared with the thin wall tubing (Figure 2.12). The refraction may be a reason for the effect. However, the magnitude of the underestimation of the maximum frequency is not fully understood. It is therefore necessary to consider in more detail the effect of wall thickness on detected maximum frequency. In general, the use of thick-walled tubing is not recommended on flow phantoms.

### 2.5.4 Discussion

This study has shown that refraction at wall boundaries can change the beam profile and consequently affects the Doppler spectrum. Refraction along the vessel axis has no effect on the Doppler shift and therefore the Doppler spectrum provided that the interfaces are parallel. The refraction in general does not affect the maximum frequency measurement, unless thick walled tubing is used.

There has been discussion in the literature concerning value for the appropriate

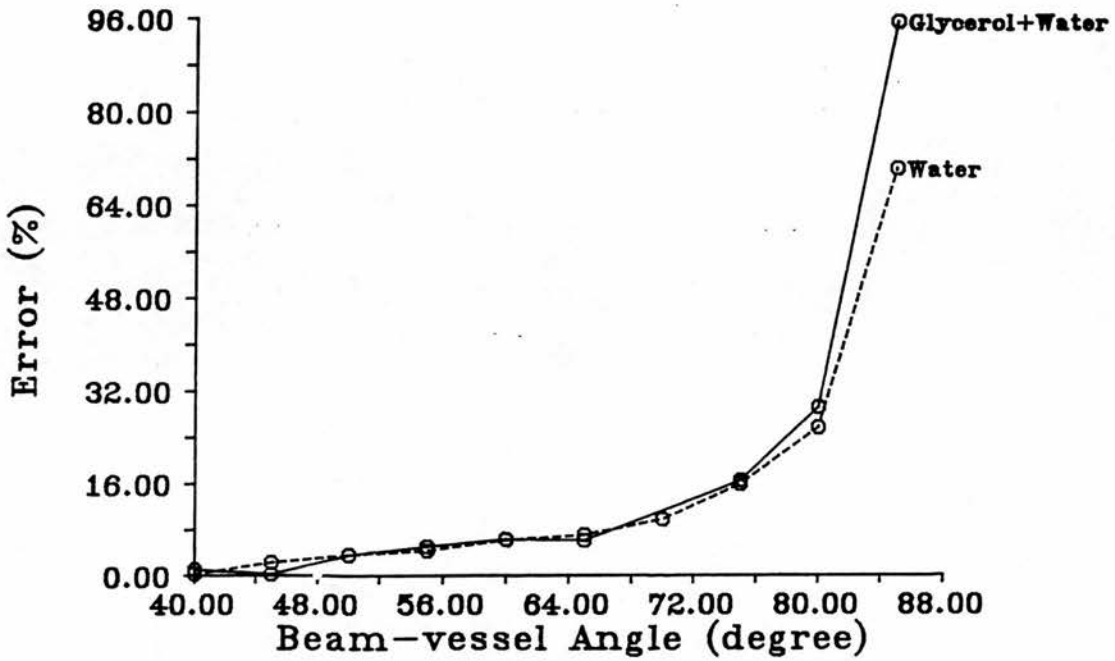


Figure 2.11: The maximum frequency measured from both glycerol-water and water solution at different beam-vessel angles. No significant difference was found. This indicates that refraction along vessel axis has no significant effect on the Doppler spectrum.

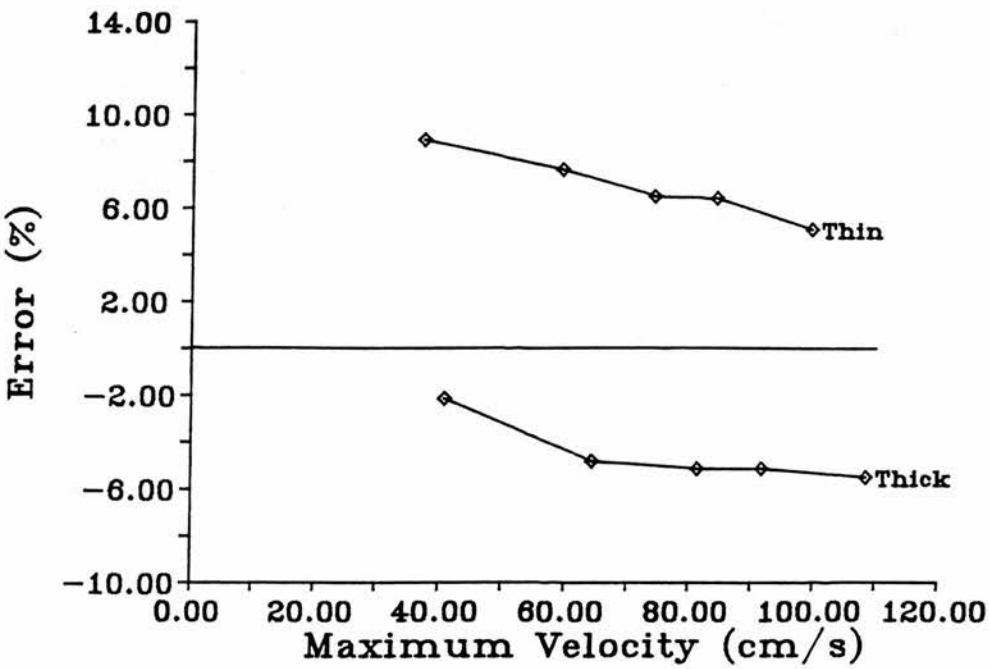


Figure 2.12: Compared with the thin wall tubing, the flow rates with the thick wall tubing were underestimated by about 10%.

speed of sound for blood that should be used in Doppler ultrasound. Oates (1990) claimed that by using the sound speed in tissue (1540 m/s) rather than that in blood (1570 m/s), the velocity could be underestimated. On the other hand, by considering the angle change at the vessel/blood boundary, Kremkau (1991) found the change in Doppler angle could cause overestimation of the velocity. However, refraction caused by differing sound speeds across an interface changes the Doppler angle in the two media. So the two factors cannot be treated separately. It is concluded that the appropriate sound speed for calculation of blood velocity using the Doppler equation is the speed in tissue (1540 cm/s) rather that in blood (1570 cm/s).

## 2.6 Reflection

For various flow phantoms, because the acoustic properties of the vessel material are usually not identical to that of the surrounding medium, reflection and refraction occur at the boundaries. By considering total reflection, Thompson *et al.* (1990) showed that there was a severe distortion of the Doppler spectrum, especially for the low frequency components from flow in plastic tubes. However, partial reflection was not taken into account. It will also be shown that the experimental results of this paper may have problems. In this section, a theory and a computer model to simulate the partial reflection at the vessel wall will be developed and the results of the simulation will be compared with the experimental results. The effect of the partial reflection on the mean and maximum Doppler frequency shift will be discussed. The interpretation of the results of Thompson *et al.* will be reconsidered in the light of the effects of partial reflection.

### 2.6.1 Theory

#### Doppler spectrum

It is known that the backscattered signal from a single particle, which is smaller than the wave length, is a spherical wave and can be written by

$$e_s(t) = e_0 e^{-j\omega_0 t + j2\mathbf{k}\cdot\mathbf{R}} \tag{2.10}$$

where

$$\mathbf{k} = \frac{\omega_0}{c}\mathbf{k_0} \tag{2.11}$$

is the wavenumber vector, $\mathbf{R}$ is the position vector of the particle and $\omega_0$ is the transmitted frequency. If the particle moves at velocity $\mathbf{v}$, we have

$$\mathbf{R} = \mathbf{R_0} + \mathbf{v}t \tag{2.12}$$

Consequently, Equation ( 2.10) can be rewritten as

$$\begin{aligned} e_s(t) &= e_0 e^{-j\omega_0 t} e^{j2kR_0} e^{j2\mathbf{k}\cdot\mathbf{v}t} \\ &= e_1 e^{-j\omega_0 t} e^{j2\mathbf{k}\cdot\mathbf{v}t} \end{aligned} \tag{2.13}$$

where $e_1$ is a constant. It is noted that the Doppler shift is given by

$$2\mathbf{k}\cdot\mathbf{v} = \frac{2\omega_0 v}{c}\cos\theta \tag{2.14}$$

where $\theta$ is the angle between the beam and the direction of particle motion and $c$ is the sound speed[1]

Therefore, the spectrum from a single scatterer is given by the Fourier transform of $e_s$,

$$E_s(\omega) = e_1\delta(\omega_0 - 2\mathbf{k}\cdot\mathbf{v}) \tag{2.15}$$

If it is assumed that scatterers have random uncorrelated positions within the sample volume and therefore produce uncorrected signals which have random phases, the total received power spectrum is obtained by adding up all the intensity (rather than amplitude) contributions from each scatterer. The intensity of the

[1]A more detailed derivation can be found in Section 3.2.

backscattered signal is proportional to the number of scatterers and therefore is proportional to the volume of the region where the signal comes from, and also to the incident power to the region. The power spectrum is therefore given by

$$G(\omega) = \int_{Vol} I_0(r)\delta(\omega_0 - 2\mathbf{k}\cdot\mathbf{v})\sigma(r)ds \tag{2.16}$$

where $I_0(r)$ is the incident power density, $\sigma(r)$ is the local concentration of particles and $Vol$ is the sample volume. As it is generally accepted that particles are uniformly distributed, $\sigma(r)$ can be set to unity. [2]

The beam intensity at position $r$, $I_0(r)$, can be set to unity when uniform insonation is assumed. In practice, because of the cylindrical shape of the vessel (Figure 2.9), the incident ultrasound waves strike the vessel wall at various incident angles. As the acoustic properties of the wall material and surrounding medium are usually different, a part of the energy is reflected at the boundaries. Furthermore, when the angle between the beam and the normal to the vessel surface is greater than the critical angle $\theta_c$, total reflection occurs. This results in a lack of insonation in the regions near to the edge of the vessel wall. So when a vessel is insonated, the ultrasonic field is re-shaped by the vessel wall. The spectrum therefore is distorted by total and partial reflection. This distortion may be significant for flow phantoms (Thompson *et al.*, 1990).

Hence, considering the reflection at a vessel wall, Equation ( 2.16) can be rewritten by

$$G(\omega) = \int_{Vol} I_0(r)W(r_i)\delta(\omega_0 - 2\mathbf{k}\cdot\mathbf{v})d\sigma \tag{2.17}$$

where $W(r_i)$ is the weighting function of the vessel wall and $I_0(r)$ is the beam intensity profile, which would be present if there was no reflection.

### Weighting function

According to acoustic theory (Morse and Ingard, 1968), when a plane wave meets the interface between different media, it may be partially reflected (Figure 2.9

[2] On flow phantoms, as discussed in Section 2.5, the sedimentation may change the uniform insonation.

(c)). By assuming that both media do not support shear waves, the transmission coefficient $\alpha_t$ can be written

$$\alpha_t = \frac{I_t}{I_0} = \frac{4Z_1 Z_2 \cos\theta_1 \cos\theta_2}{(Z_1 \cos\theta_2 + Z_2 \cos\theta_1)^2} \tag{2.18}$$

where $I_0$ and $I_t$ are the incident intensity and transmitted intensity respectively. $Z_1$ and $Z_2$ are the acoustic resistance of the first and second media given by

$$Z = \rho c \tag{2.19}$$

where $\rho$ is the density of the medium. The angle $\theta_1$ is the incident angle and $\theta_2$ is given by

$$\sin\theta_2 = \frac{c_1}{c_2}\sin\theta_1 \tag{2.20}$$

where $c_1$ and $c_2$ are the sound speed in medium 1 and medium 2 respectively. In particular, when $c_2 > c_1$, the critical angle $\theta_c$ for a total internal reflection arises at

$$\sin\theta_c = \frac{c_2}{c_1} \tag{2.21}$$

If a wave propagates through three media separated by plane parallel surfaces (Figure 2.9 (c)), partial reflection may occur at each interface. This leads to the establishment of standing waves in the first and second media. The standing wave in the second medium controls the reflection into the first medium and transmission to the third medium. In general, it is necessary to consider the standing wave in the calculation of transmission coefficient. However, the laws governing transmission at oblique incidence are very complicated so that the complete calculation of the transmitted intensity is difficult.

However, when $Z_1 \simeq Z_2 \simeq Z_3$, the reflected waves at the boundaries between medium 2 and medium 3 are weak and less important. In this case the interference of the transmitted pulses and the reflected pulses from the first and second boundaries may be ignored. In other words, we may ignore the standing wave in medium 2 and medium 3. The transmission coefficient can then be written as

$$\begin{aligned} \alpha(r_i) &= \alpha_{t2}\alpha_{t2} \\ &= \frac{4Z_1 Z_2 \cos\theta_1 \cos\theta_2}{(Z_1 \cos\theta_2 + Z_2 \cos\theta_1)^2} \cdot \frac{4Z_3 Z_2 \cos\theta_3 \cos\theta_2}{(Z_3 \cos\theta_2 + Z_2 \cos\theta_3)^2} \end{aligned} \tag{2.22}$$

where $\theta_3$ can be calculated by

$$\sin\theta_3 = \frac{c_3}{c_1}\sin\theta_1 \tag{2.23}$$

where $c_3$ is the sound speed in medium 3. As the ultrasound wave needs to pass the wall twice, first for the transmitted pulse and then for the backscattered pulse, the weighting function $W(r_i)$ is given by

$$W(r_i) = \alpha^2(r_i) \tag{2.24}$$

### 2.6.2 The validity of ignoring of the reflected wave assumption

In Section 2.6.1, it is assumed that the interference of the reflected wave in the vessel wall is weak and can be ignored. However, due to the curvature of the vessel wall, in the region near the edge of the vessel, the incident angle to the normal of the vessel wall is large (Figure 2.13). The reflection in that region can be significant so the its effect may be strong. Therefore, the validity of the ignoring such an effect has to be examined.

At normal incidence, it is possible to calculate the transmission coefficient of a wave passing through three media by (Kinsler and Frey, 1962),

$$\alpha_t = \frac{4Z_3Z_1}{(Z_3+Z_1)^2\cos^2(k_2l_2) + (Z_2 + Z_3Z_1/Z_2)^2\sin^2(k_2l_2)} \tag{2.25}$$

where $k_2$ and $l_2$ are the wave number and the thickness of the intervening medium.

By using acoustic properties of heat shrinkable materials (Table 2.1), it is found that the maximum difference in the transmission coefficient estimated by Equation ( 2.22) is less than 1.6% from that using Equation ( 2.25). This indicates that standing waves give very small error at normal incidence.

However, the reflection increases when the incident angle to the normal of vessel wall is increased. As shown in Figure 2.13 the curvature of the vessel wall results in a large incident angle. So in the area near the edge of the vessel, the reflection will be considerably stronger. Inevitably, a part of the vessel, especially

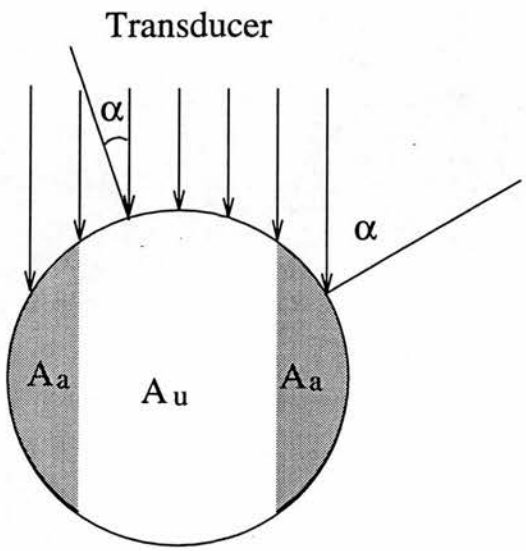


Figure 2.13: The vessel can be divided into two parts. In region $A_u$, as the incident angle $\alpha$ is smaller than a threshold, the reflected wave is weak and can be ignored. In region $A_a$, however, the reflected waves are strong and can not be ignored.

near the edge, has insonation which may not follow Equation ( 2.22). Therefore, it is necessary to estimate if the standing wave is small enough to be ignored.

To make such an estimation, two regions are defined. In Figure 2.13, $A_u$ is an area where the reflection is small so that the transmission power is not affected by the interference of the incident wave and reflected wave. $A_a$ is the area in which the effect of the interference causing standing waves cannot be ignored and therefore the application of Equation ( 2.22) is not reliable in this region. Obviously, if the backscattered power from region $A_a$ is small compared to the total backscattered power received by the transducer, then the inaccuracy caused by the interference between incident wave and reflected wave may be ignored. In other words, we can use Equation( 2.22) in the simulation. If the backscattered power from region $A_a$ is too strong to be ignored, the whole simulation is not reliable. It must be noted that the size of region $A_a$ also depends on the beam-vessel angle.

To obtain an idea of at what beam-vessel angle the simulation would be valid,

| Beam vessel angle | 50° | 55° | 60° | 70° | 90° |
|---|---|---|---|---|---|
| E | 23.6% | 8.40% | 4.95% | 2.83% | 2.04% |

Table 2.2: When the reflection coefficient is larger than a 10%, it is considered that the reflected wave cannot be ignored so an affected region $A_a$ can be defined. The table shows the ratio E of the backscattered power from the affected region $A_a$ and total power from the whole vessel at different thresholds. When this ratio is small enough, the simulation description in this section can be considered to be valid. If E smaller than 5% is acceptable, it can be found that model is valid for beam-vessel angle larger than 60°.

it is assumed that if the reflection coefficient is larger than 10%, the standing wave cannot be ignored. For using heat-shrinkable tubes, the ratios (E) of the backscattered power from $A_a$ and the total backscattered power at different beam-vessel angles are listed in Table ( 2.2). When this ratio is small enough, the simulation description in this section can be considered to be valid. For example, it is found that at 60°, about 5% of backscattered power is from the area $A_a$. If it is considered that in this situation the effect of the interference between incident and reflected waves can be ignored, then the model is valid at beam-vessel angles larger than 60°. For smaller beam-vessel angles, the use of Equation ( 2.22) may cause significant errors. Experiment evidence of this effect will be shown in Section 2.6.5.

### 2.6.3 Computer model of wall reflection

A computer model was written in Fortran on a university mainframe computer. The realization of this simulation will be briefly described in this section.

#### Incident angle

First the incident angle is considered. As indicated before, because of the curvature of the vessel wall, the incident angle is not the beam-vessel angle $\theta_0$. At different distance off the centre of the vessel, the incident angle is different.

The coordinate system used to calculate the incident angle is illustrated in

Figure 2.14. The radius of the vessel is $\rho_0$. At a distance $d$ from the vessel centre, the angle between the $z-axis$ and $r_0$, which is the normal of the cylindrical vessel wall at incident point, is $\alpha$. $\mathbf{r_0}$ is the unit vector normal to the vessel wall and $\mathbf{r_s}$ is the unit vector with opposite direction to the incidence.

As shown in Figure 2.14, it is not difficult to obtain $\mathbf{r_0}$ and $\mathbf{r_s}$,

$$\mathbf{r_0} = -\mathbf{j}\sin\alpha + \mathbf{k}\cos\alpha \tag{2.26}$$

$$\mathbf{r_s} = -\mathbf{i}\cos\theta_0 + \mathbf{k}\sin\theta_0 \tag{2.27}$$

where $\mathbf{i}$, $\mathbf{j}$, $\mathbf{k}$ are the unit vector along $x-axis$, $y-axis$ and $z-axis$ respectively. Therefore, the incident angle is given by

$$\cos\theta = \mathbf{r_0}\cdot\mathbf{r_s} = \cos\alpha\sin\theta_0 \tag{2.28}$$

Supposing that total reflection happens at distance $d_c$ off the vessel centre, we obtain,

$$\cos\alpha = \frac{\cos\theta_c}{\sin\theta_0} \tag{2.29}$$

$$d_c = \rho_0\sqrt{1-\frac{\cos^2\theta_c}{\sin^2\theta_0}} \tag{2.30}$$

Only the region that falls within $d_c$ from the vessel centre is insonated by the ultrasound beam. The region beyond is not insonated due to total reflection.

### Division of the vessel

To calculate the spectrum with a computer, it is usually necessary to divide the vessel into small sections and then sum up all the contributions from each section. In the literature, the whole vessel is broken into shells with equal thickness (Bascom *et al.*, 1986). However, there are several drawbacks to this method. First of all, the velocity of scatterers in the vessel as a function of the distance to the centre of the vessel is non-linear. The local velocity $v(r)$ can usually be given by

$$v(r) = v(0)\left[1-\left(\frac{r}{R}\right)^{\mu}\right] \tag{2.31}$$

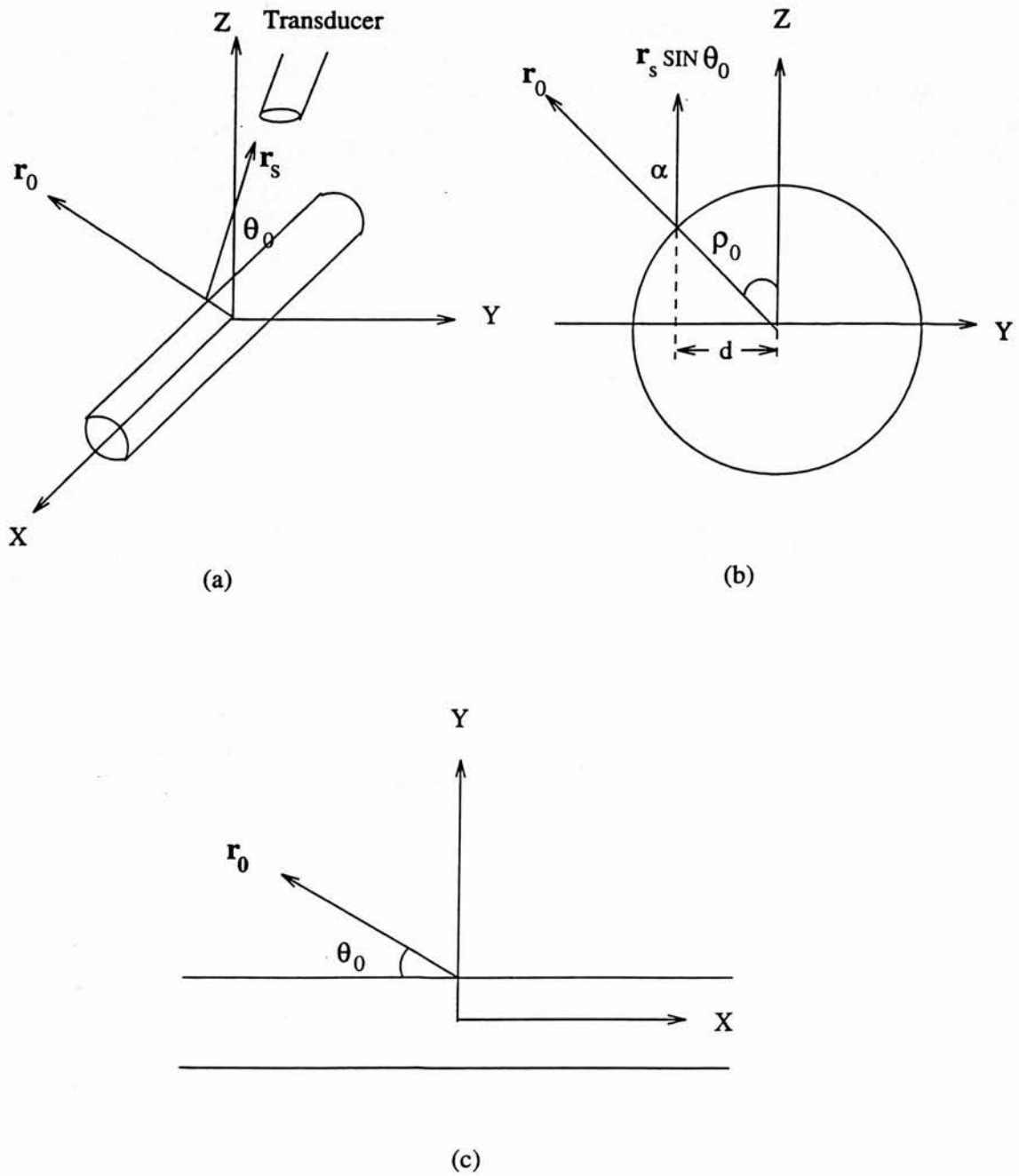


Figure 2.14: The coordinate system to calculate the incident angle and reflection. In the figure, $\mathbf{r}_s$ is a unit vector along the transducer axis and $\mathbf{r}_0$ is a unit vector normal to the vessel wall surface.

where $v(0)$ is the maximum velocity in the vessel centre and $\mu$ is a constant to describe the profile. $\mu$ equals 2 when the profile is parabolic and $\mu$ is $\infty$ when the profile is flat. If the vessel is divided into shells with equal thickness, each shell will contain a different range of velocity. Shells near the central stream, which have higher velocities, contain a much smaller range of velocity than those shells near the vessel wall. To obtain the whole spectrum, it is usually necessary to divide the whole spectrum into a number of frequency bins and calculate the contribution of every shell to these bins. Therefore each high frequency bin obtains contributions from many shells, often more than the number which is necessary to obtain a smooth section of the Doppler spectrum, near the central stream. This makes the calculation very inefficient. On the other hand, shells near the wall can often have a velocity (or frequency) range similar or even larger than the frequency range of bins (frequency resolution). This leads to inaccuracy of the simulation. In order to have a satisfactory result, a considerable number of shells is required for obtaining a smooth the low frequency section of the Doppler spectrum. This results in a large amount of calculation (Bascom, *et al.* 1986) which can be avoided if an appropriate method of dividing the vessel can be found.

To reduce the computation time and raise accuracy, the vessel is divided non-linearly in the model. As shown in Figure 2.15, the radius of each shell is given by

$$r_i = r_0 \left[1 - \frac{v(r_i)}{v(0)}\right]^{\frac{1}{\mu}} \tag{2.32}$$

where

$$v(r_i) = \frac{v(0)}{N} i \qquad i = 0, 1, \cdots, N-1 \tag{2.33}$$

where $N$ is the number of shells.

So each shell contains the velocity range in

$$\frac{v(0)}{N} i \leq v(r_i) < \frac{v_0}{N}(i+1) \tag{2.34}$$

and therefore gives the Doppler shift

$$\Delta f \cdot i \leq f_{d_i} < \Delta f(i+1) \tag{2.35}$$

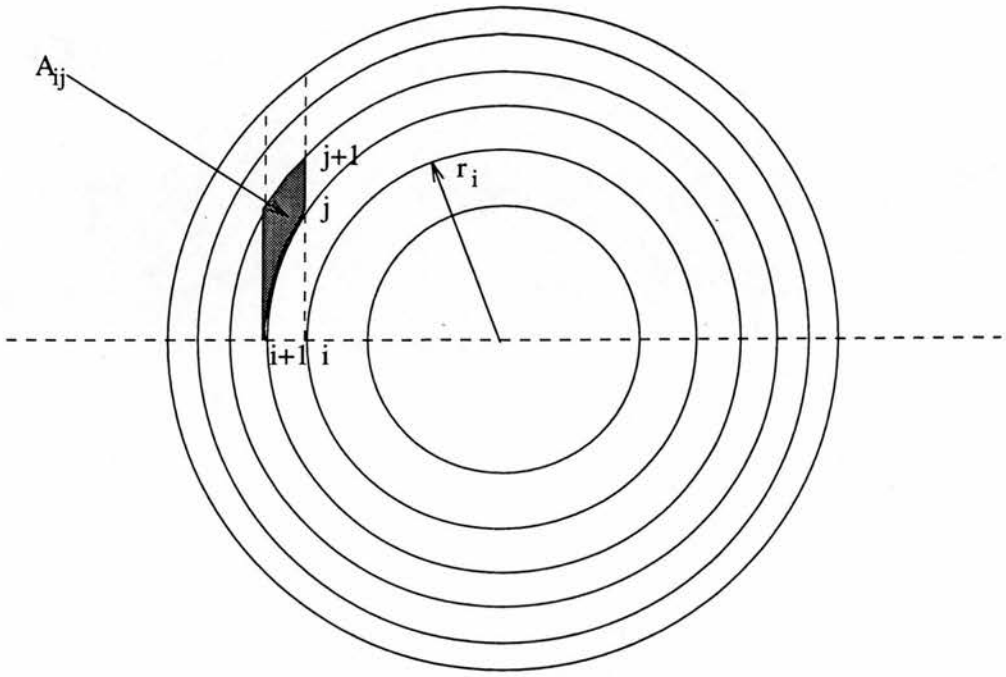


Figure 2.15: The vessel is divided into shells and further broken up into sections.

where

$$\Delta f = \frac{2 f_0 v_0 \cos\theta}{c} \frac{1}{N} \tag{2.36}$$

where $N$ is the frequency resolution and $f_0$ is the frequency of the transmitted pulses. It is noted that with such a division each shell corresponds to the same range of frequencies.

Each shell is further broken up into small sections (Figure 2.15). The area of each section is given by

$$\begin{aligned} A_{ij} = & \frac{r_{j+1}^2}{2}\left[\arcsin\left(\frac{r_{i+1}}{r_{j+1}}\right) + \left(\frac{r_{i+1}}{r_{j+1}}\right)\sqrt{1-\left(\frac{r_{i+1}}{r_{j+1}}\right)^2}\right] \\ & -\frac{r_{j+1}^2}{2}\left[\arcsin\left(\frac{r_i}{r_{j+1}}\right) + \left(\frac{r_i}{r_{j+1}}\right)\sqrt{1-\left(\frac{r_i}{r_{j+1}}\right)^2}\right] \\ & -\frac{r_j^2}{2}\left[\arcsin\left(\frac{r_{i+1}}{r_j}\right) + \left(\frac{r_{i+1}}{r_j}\right)\sqrt{1-\left(\frac{r_{i+1}}{r_j}\right)^2}\right] \end{aligned}$$

$$+\frac{r_j^2}{2}\left[\arcsin\left(\frac{r_i}{r_j}\right)+\left(\frac{r_i}{r_j}\right)\sqrt{1-\left(\frac{r_i}{r_j}\right)^2}\right] \qquad (2.37)$$

$$i \neq j$$

$$A_{ii} = \frac{r_{i+1}^2}{2}\left[\frac{\pi}{2}-\arcsin\left(\frac{r_i}{r_{i+1}}\right)-\left(\frac{r_i}{r_{i+1}}\right)\sqrt{1-\left(\frac{r_i}{r_{i+1}}\right)^2}\right] \qquad (2.38)$$

where

$$\begin{aligned} i &= 0,1,\cdots,N-1 \\ j &= i+1,i+2,\cdots,N-1 \end{aligned}$$

**Spectrum**

The spectrum can be calculated on a computer by

$$G(\omega)=\sum_{i=0}^{N-1}\sum_{j=i}^{N-1}A_{ij}B(r_i)^2W(r_i)\delta(\omega-\omega_j) \qquad (2.39)$$

where $B(r_i)$ is the beam amplitude and

$$\omega_j=\frac{2\pi f_0 v(0)}{c}\cos\theta\left[1-\frac{2i+1}{2N}\right] \qquad (2.40)$$

$$i=0,1,\cdots,N-1$$

### 2.6.4 Experiment

To measure the beam profile of the 4 MHz CW transducer, a bilaminar polyvinylidene fluoride (PVDF) membrane hydrophone was used (GEC-Marconi Ltd). The hydrophone is made from a membrane stretched over an annular frame and has an active element of 0.5 mm diameter in the centre. The thin membrane introduces little acoustic perturbation and so senses the free field acoustic pressure at the element. The bandwidth of the hydrophone is 10 MHz.

A measuring tank was used to measure the beam profile. The Doptek 4 MHz continuous wave transducer was rigidly fixed on a platform above the water level which could move in two orthogonal directions. The platform was attached to a micrometer so that accurate movements could be achieved. Waveforms were then displayed on an oscilloscope (HP 4540 A 500 MHz digital oscilloscope) connected to the preamplifier of the hydrophone. The peak-to-peak amplitude was measured in 0.5 mm steps in both directions and recorded. The data was normalised and plotted, and used in the simulation.

Doppler spectra were acquired using the 4 MHz CW transducer from the flow phantom. Tubing of 3.0 mm in diameter was used in the experiment. Steady flow was used in the study. Spectra with beam-vessel angles ranging from 40° to 85° in 5° steps were acquired. The distance between the transducer face and centre of the vessel was 5 cm. All the spectra were recorded on magnetic tapes. Simultaneously absolute flow measurements were made by using a measuring cylinder and a stop watch. The true maximum velocity was then calculated and used in the theoretical simulation.

The spectra then were transferred to the micro-computer and the average of 240 lines was calculated and compared with the theoretical data.

### 2.6.5 Results

The beam amplitude in two directions is shown in Figure 2.16. The beam width across the crystal gap is slightly narrower than along the gap. Within 1.5 mm of the beam centre, which was the radius of the tubing used in experiments, the beam is reasonably uniform.

Figure 2.17 gives the simulated Doppler power spectrum from a uniformly insonated tube. A parabolic velocity profile is assumed for the flow. The square box is the spectrum without wall reflection. It is shown that the spectra are considerably distorted and the influence of the wall reflection becomes larger as the beam-vessel angle increases. Figure 2.18 gives the theoretical percentage error in the intensity averaged mean velocity estimation due to the wall reflection at

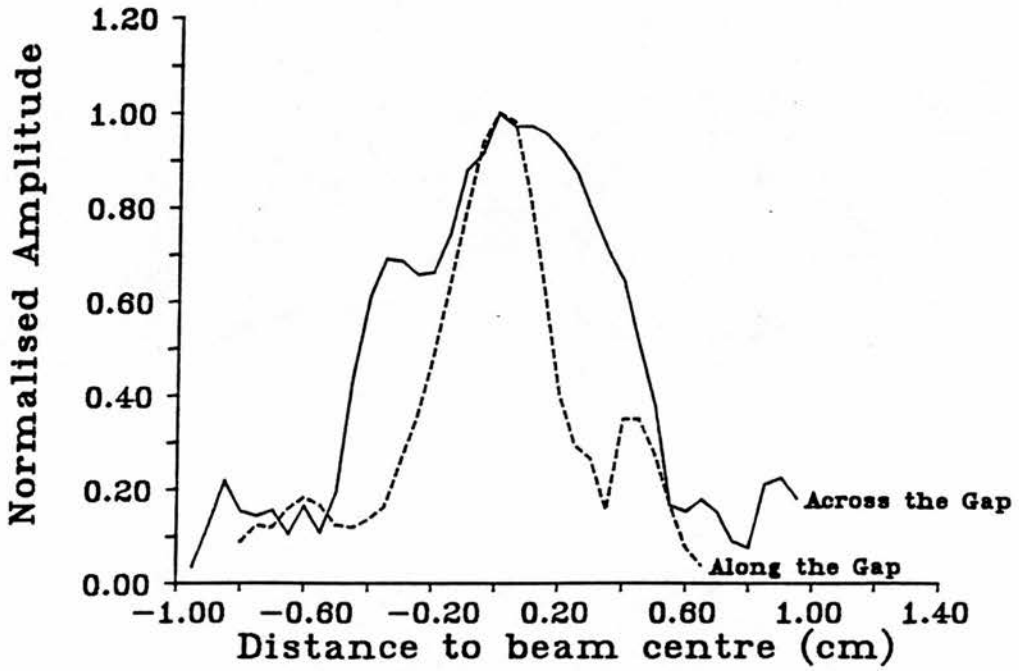


Figure 2.16: Beam amplitude along and across the gap between the two crystals of a Doptek 4 MHz continuous wave transducer.

different beam-vessel angles.

Figure 2.19 shows the Doppler spectra acquired from the flow phantom and theoretical simulation for identical conditions. In the simulation, the real beam measured by the hydrophone (Figure 2.16) was fed into the computer model. For beam-vessel angles which are larger than 55°, the agreement is good. The discrepancy at high frequency is due to geometrical spectral broadening (Censor *et al.* 1988) which is not considered in the computer model. The disagreement in the low frequency is because of the sedimentation of particles discussed in Section 2.4. For beam-vessel angles smaller than 50°, where the standing wave is too large to be ignored as discussed previously, the agreement is very poor as expected. The peak at low frequency is due to the sedimentation of the sephadex in the tube.

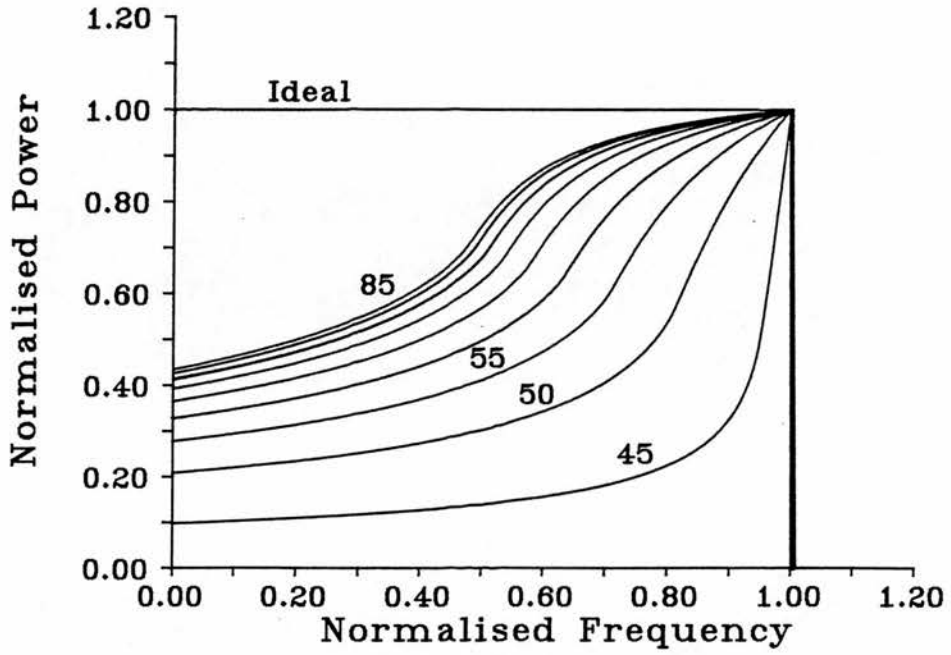


Figure 2.17: The simulated Doppler spectra at different angles with a uniform insonation. Heat shrinkable tubing is used. Large distortions due to reflection are observed, especially in low frequency components.

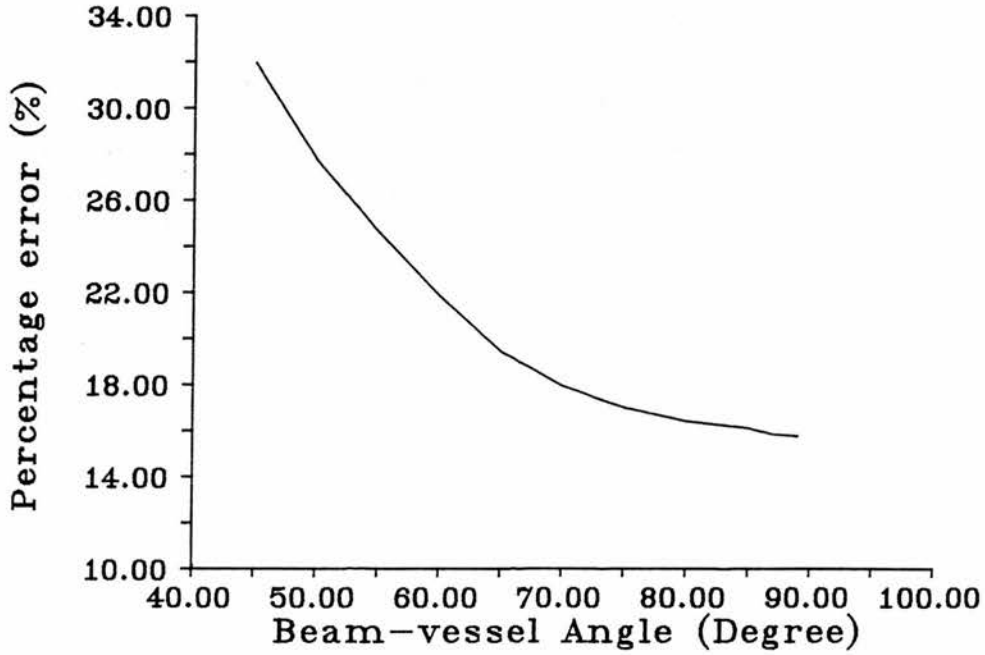


Figure 2.18: The theoretical percentage errors in mean frequency estimation due to wall reflection.

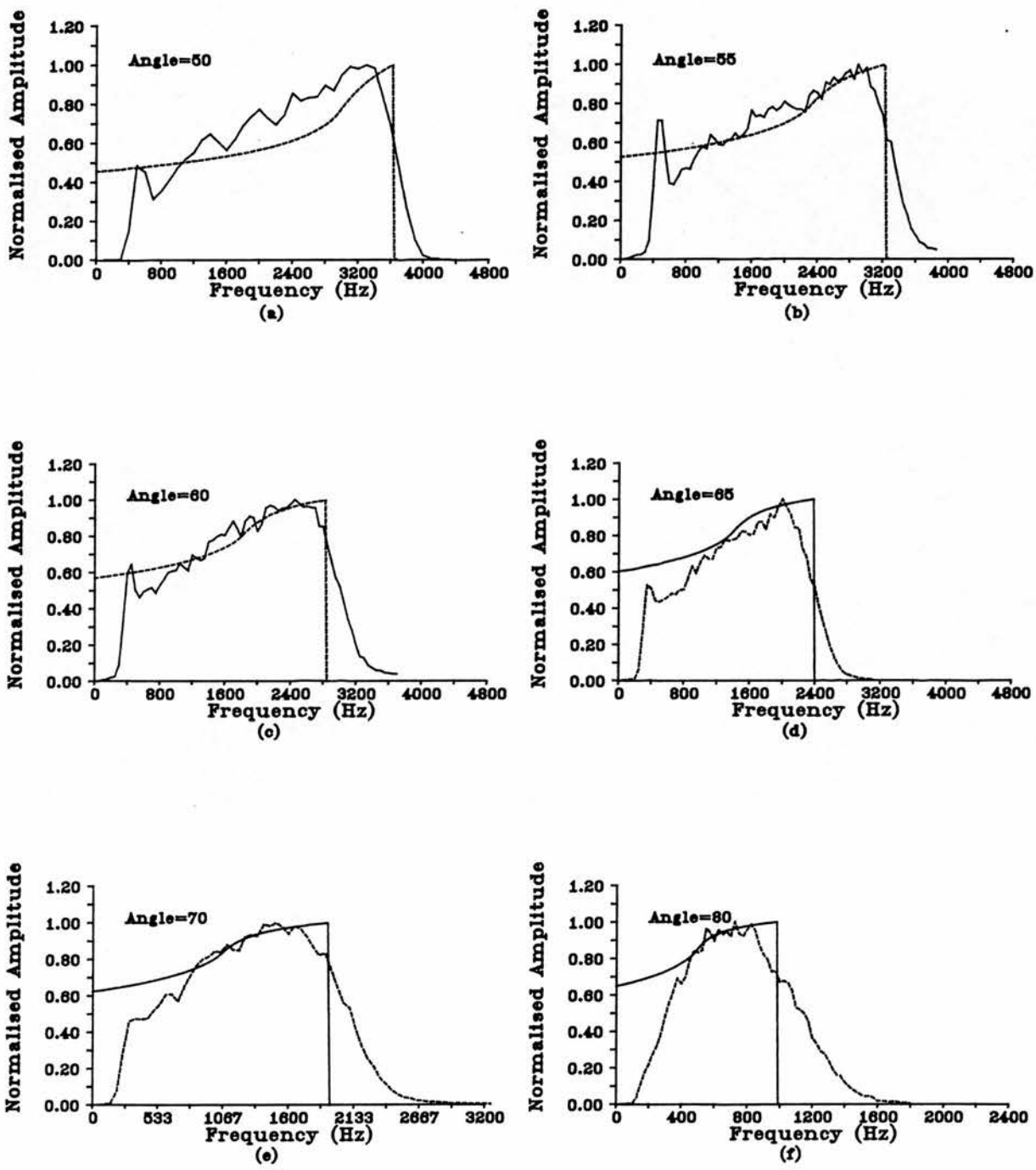


Figure 2.19: Theoretical and experimental results using the flow phantom. The agreement was good. However, as expected, when the angle is near the critical angle, the standing wave resulted in a significant discrepancy between experiment and theory.

### 2.6.6 Discussion

The results have shown that the wall reflection can cause significant distortion of the spectrum acquired from the flow phantom. The agreement with the theoretical simulation is good when the beam-vessel angle is larger than 55° which is not near to the critical angle (46.6°) for a total reflection.

It is also found that the experimental results are different to those of Thompson *et al.*, (1990) in which only total reflection was considered. The results of this simulation show a good agreement with experimental data when both total and partial reflection are considered. When only total reflection is taken into account, the agreement is poor (Figure 2.20(b)). However, a good agreement was obtained in Thompson's paper when only total reflection is calculated (Figure 2.20(a)). It is noticed that in Thompson's results (Figure 2.20 (a)), the overestimation of the maximum frequency due to geometrical spectral broadening at larger beam-vessel angle is less than that at smaller beam-vessel angle. These certainly conflict with other studies of geometrical spectral broadening (Newhouse *et al.*, 1980; Censor *et al.*, 1988). One possible explanation of this discrepancy may be due to the fact that Thompson *et al.* used thick wall tubing. For example, the internal and external diameters of their PVC tubing were 2.8 and 5.0 mm respectively. As discussed before, thick tubing may cause some unknown effects and the maximum frequency can therefore decrease.

## 2.7 Conclusion

This study has shown that by careful choice of materials and setting up of the system, distortions in the Doppler spectrum from air bubbles, turbulence, viscosity change, inlet and outlet length, *etc.*, can be avoided. The accuracy of the beam-vessel angle measurement and vessel diameter are better than 1° and 0.5 mm respectively. The distortion of the Doppler spectrum is mainly from the sedimentation of particles, refraction and reflection of ultrasonic waves at vessel wall boundaries.

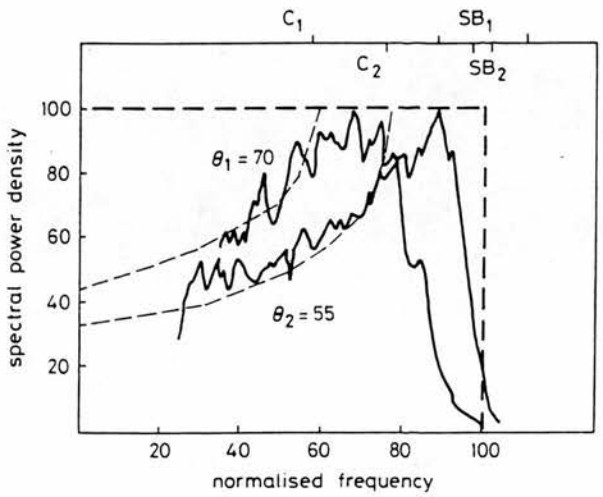


(a)

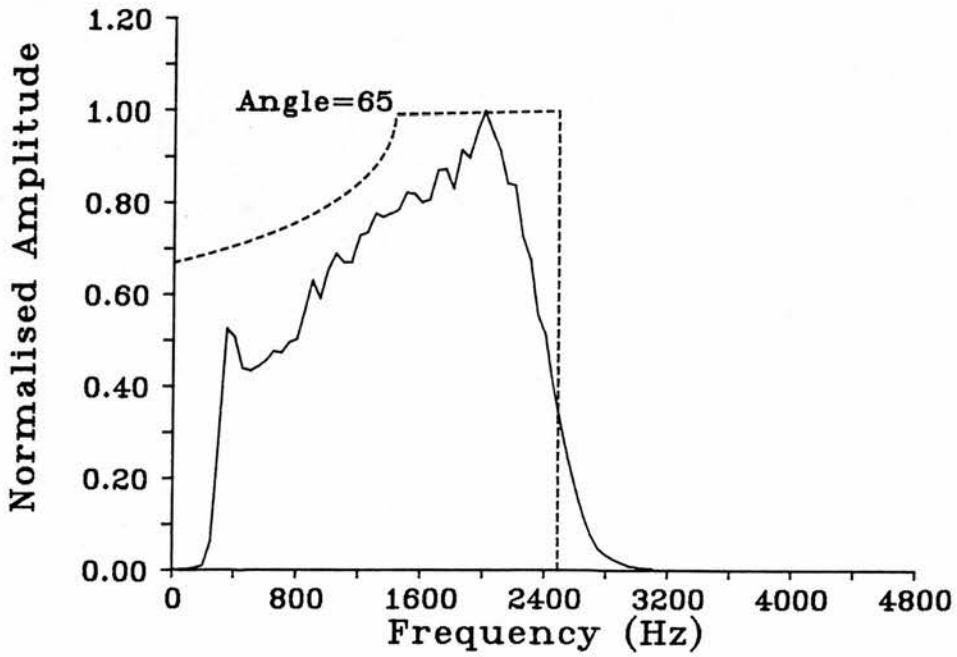


(b)

Figure 2.20: Without considering partial reflection, (a) Thompson's model has a good agreement with the experiment. But (b) our experiment shows a discrepancy.

Sedimentation causes particles to roll along the bottom of the tubing and produces a non-uniform distribution of particles in the vessel. This results in a significant loss, which can be observed as a dip, in low frequency components of the Doppler spectrum. The rest of the spectrum remains unaffected. Therefore, the maximum frequency is not affected.

The refraction in the direction along the vessel axis does not affect the Doppler spectrum. The speed of sound used in calculation of Doppler shift is the speed of sound in tissue in the body or in the surrounding medium in phantoms rather than speed of sound in (artificial) blood. The refraction in the direction across the vessel axis changes the beam profile and therefore distorts the Doppler spectrum. When a thin wall tubing is used, refraction does not affect the maximum frequency measurement. Thick walled tubing may cause about 10% underestimation of the maximum frequency. Therefore it is not recommended that thick walled tubing should be used in flow phantoms. The mechanism of the underestimation by using thick walled tubing is not fully understood and more investigation needs to be performed.

A computer simulation of the effect of the reflection at a wall was made in this study. Good agreement was obtained between experiment and theory. A significant loss in low frequency components in the Doppler spectrum was found due to the reflection at vessel wall. This causes 16% to 32% over-estimation of the mean frequency at beam-vessel angles from 50° to 90° when heat shrinkable tubing is used.

In conclusion, maximum frequency can be measured well on the flow phantom when a careful choice of materials and setting up of the system is made. The sedimentation of the particles, refraction and reflection at the vessel wall do not affect maximum frequency measurement. When the mean frequency is of interest, the effects of sedimentation, refraction and reflection should be considered.

# Chapter 3

# SIMULATION OF THE DOPPLER SPECTRUM

## 3.1 Introduction

Volumetric flow is usually calculated by multiplication of the mean velocity in a vessel by the cross-sectional area of the vessel. The mean velocity is estimated from either the mean frequency or maximum frequency envelope. Therefore the accuracy of the mean and maximum Doppler frequency shift is very important to volumetric flow estimation.

Many factors (Chapter 1) can affect the accuracy of the mean and maximum frequency measurement. Some of these factors, such as partial insonation (Evans, D.H. 1985; Bascom *et al.*, 1990), relative size of transducer and vessel (Cobbold *et al*, 1983), misalignment (Evans, D.H. 1985), geometrical spectral broadening (Newhouse *et al.*, 1977), *etc.* have been theoretically or experimentally investigated separately by a number of authors. Most of these studies used idealised conditions such as a uniform beam and did not consider the effect of intrinsic spectral broadening. However, in clinical measurements the situation is much more complex, and numerical models for simulating the Doppler spectrum are needed to investigate in more detail the accuracy of the Doppler measurement.

Two simulations of the Doppler spectrum have been made in the literature.

Bascom *et al.* (1986) developed a numerical model to simulate geometrical spectral broadening. However, it was assumed in the model that the transmitter and receiver transducer are coincidental. The model also suffered from a long computational time. It will be suggested later in this chapter that there are deficiencies in the model of Bascom. Censor *et al.* (1988) also made a simulation of spectral broadening. Typical transducer types, such as unfocused circular transducer and long strip rectangular transducer were simulated. It was, however, wrongly assumed in this simulation that the intensity of backscattered signal was proportional to the velocity of particles. Therefore it is doubtful that the results from these two models are reliable. There has been no comparison between simulation and experiment of the Doppler spectrum to date.

It is the aim of this chapter to develop a more sophisticated computer model to simulate the Doppler spectrum. Improvements to previous models are made; the model described in this chapter can simulate different types of focused and unfocused transducer; the computational time for a simulation is significantly reduced and the wall reflection model described in Chapter 2 is incorporated. The theory of the simulation and the realization of the simulation on the computer are described in detail. The validity of the model will be examined by comparing simulated and experimental results for beam patterns and Doppler spectra.

## 3.2 Theory

The mathematical formula for the Doppler spectrum is derived in this section. The details of the computer realization will be described in Section 3.3 and 3.4.

### 3.2.1 Geometrical spectral broadening

The Doppler shift $\Delta F_d$ is usually expressed by

$$\Delta F_d = \frac{2vF_0}{c}\cos\theta \tag{3.1}$$

where $F_0$ is the frequency of transmitted ultrasonic signals, $\theta$ is the angle between the beam axis and the direction of the particle movement, $c$ is the speed of sound

in the medium and $v$ is the velocity of the moving target. However, in practice, since any real beam has a finite cross section and any transducer has a limited area, the field produced by a transducer at any observation point is not a plane wave. The ultrasonic waves can be transmitted and received in many direction so that the angle $\theta$ has a range of value. Therefore, a scatterer in the ultrasonic field of a transducer produces a spectrum with a range of frequency rather than a monotonic signal. This effect is known as geometrical spectral broadening. Thus to calculate the spectrum using a realistic transducer, a non-plane-wave ultrasonic field has to be considered.

### 3.2.2 Transmission field

The transmission field of a transducer can be calculated by summing up the contribution from each point on the transducer face. Suppose the transducer is broken into a number of small sectors. Each sector has the same area and the size of the sectors is smaller than the wavelength. It is known that in the far field, each sector can be considered as a point source. On a CW transducer or a PW transducer transmitting long pulses, it can be further considered as a periodic simple source, which is a point source emitting sine waves evenly in all directions. Hence, the ultrasonic excitation field produced by one sector can be written as (Morse and Ingard, 1964)

$$e_s(t) = e_0 \frac{1}{R_p} e^{i\mathbf{k}\cdot\mathbf{R_p} - i\omega_0 t} \tag{3.2}$$

where $\mathbf{k} = k \cdot \mathbf{k_0}$, $k = \omega_0/c$ is the wavenumber vector in the transmission field; $e_0$ is a constant and can be set to unity; $\mathbf{R_p}$ is the vector from each sector source to observer and its value $R_p$ equals the distance between each sector and observation point. To make the problem simple, it is assumed that the transducer face vibrates like a rigid disc so the phase and amplitude of each section are the same. Thus by summing up contribution from all sectors on the transducer face, the excitation field produced by the whole transmitter is given by

$$e_T(t) = e^{-i\omega_0 t} \int_{A_t} \frac{1}{R_p} e^{i\mathbf{k}\cdot\mathbf{R_p}} ds_T \tag{3.3}$$

where $A_t$ indicates the area of transmitter.

### 3.2.3 Doppler effect

The Doppler effect manifests itself by the change of the phase of $e_T(t)$ in Equation ( 3.3). For a single particle moving at velocity $\mathbf{v}$ in an ultrasonic field of a simple source described by Equation ( 3.2), the position of the particle $\mathbf{R_p}$ is given by

$$\mathbf{R_p} = \mathbf{R} + \mathbf{v}t \tag{3.4}$$

The sound pressure received by the moving particle in such an ultrasonic field is given by (Morse and Ingard, 1964)

$$p = \frac{1}{4\pi}\frac{q'[t-(R/c)]}{R(1-M\cos\theta)^2} + \frac{q}{4\pi}\frac{(\cos\theta - M)v}{R^2(1-M\cos\theta)^2} \tag{3.5}$$

where $q$ is the strength of the source, $M = v/c$ is the Mach number. For a simple harmonic source, $q$ can be written by

$$q = q_0 e^{-j\omega_0 t} \tag{3.6}$$

where $\omega_0$ is the frequency of transmitted pulses. Combining Equation ( 3.5) and ( 3.6), we obtain

$$p = \frac{1}{4\pi R}\frac{q_0 e^{-j\omega_0(t-R/c)}}{(1-M\cos\theta)^2}\left[-j\omega + \frac{v(\cos\theta - M)}{R}\right] \tag{3.7}$$

In medical ultrasound use the second term is much smaller than the first and $M \ll 1$, Equation ( 3.7) can therefore be written as

$$p = \frac{p_0}{R}e^{-j\omega_0(t-R/c)} \tag{3.8}$$

where

$$p_0 = \frac{-j\omega}{4\pi}$$

The frequency is now considered. The pressure field has the phase

$$\phi = \omega_0\left(t - \frac{R}{c}\right) \tag{3.9}$$

which is no longer simply proportional to time since $R$ now is a function of time. Thus the concept of frequency is not so well defined in this case. If we generalise

the concept of frequency and define it as the time derivative of the phase, we obtain[1]

$$\begin{aligned} \omega &= \frac{d\phi}{dt} = \frac{\omega_0}{1 - M\cos\theta} \\ &\simeq \omega_0(1 + M\cos\theta) \end{aligned} \tag{3.10}$$

It is noted that this is the general Doppler formula.

### 3.2.4 The signal received by scatterers in the transmission field

Due to the Doppler effect, the frequency of the signal received by the moving particles is shifted. However, as the Doppler shift is a function of time, it is difficult to calculate the received signal by a particle from Equation ( 3.3). If the instantaneous frequency described by Equation ( 3.10) is considered then by combining Equation ( 3.3), ( 3.10) and ( 3.8), Equation ( 3.8) can be re-written as

$$p = \frac{p_0}{R} e^{-j\omega_0 t} e^{j\omega_0 M t\cos\theta} e^{jkR} \tag{3.11}$$

where $kR$ is the time delay from source to scatterers.

For a particle in the transmission field of a transducer, every section on the transducer surface needs to be considered. The received signal by scatterers in position $\mathbf{R}$, which may be derived in a similar manner to the method used in Section 3.2.2, is given by

$$g_T(t) = e^{-j\omega_0 t} \int_{A_1} \frac{p_0}{R} e^{j\omega_0 M t\cos\theta} e^{jkR} ds_T \tag{3.12}$$

It should be noted that $\theta$ and $R$ in Equation ( 3.12) is time-dependent for each particle. Therefore, Equation ( 3.12) is an expression of the instantaneous signal received by the receiver if $R$ and $\theta$ are fixed.

Equation ( 3.8) gives the sound pressure received by a particle in the field produced by a simple harmonic source. It is noted that its instantaneous frequency (Equation 3.10) is time-dependent. For a single particle moving in a real

[1]For details of the derivation see Morse and Ingard, 1964.

ultrasound field produced by a transducer, along its path, the sound pressure also changes. Considering the complex sound field produced by transducers of different shapes and different focusing, it is generally fairly difficult to calculate the frequency spectrum by Fourier Transform.

Fortunately, in Doppler ultrasound, it is almost always the case that a large number of particles rather than only several single particles are dealt with. For a group of particles, the (backscattering) events happening in the sample volume at any time interval are statistically the same. A signal typically lasts several transmitted cycles (0.2 $\mu s$ for one cycle of 5 MHz ultrasonic waves). In such a short time, each particle does not move very much. For each particle, the ultrasound field and the Doppler angle $\theta$ do not change appreciably. In the next cycle, some particles move into the sample volume and the same number of particles move out. The number of particles and the position of each particle are statistically the same. Therefore, as only the summation of the backscattered signals from all the particles in the sample volume is of interest, the backscattered signal is statistically the same as the previous cycle.

For each small region in the sample volume, the situation would be the same although there may be less particles in that region. Therefore the contribution from each small region can be calculated. The received signal would be the summation of all the contributions from every small region in the sample volume.

Bascom *et al.* (1986) used Equation ( 3.12) to calculate the received spectrum from particles at the observation point. However, there is a problem in this approach. As indicated previously, Equation ( 3.12) is only the expression of the instantaneous signal received at, or near, the observation point. It is incorrect to assume that it can be used as an expression for continuous signals at that point. A very important assumption here is being made, and this is that a very short piece of signal repeats itself in the following time intervals, from a restricted region. But if Equation ( 3.12) is inspected carefully, it actually describes the signal from a particle (or a group of particles) travelling through a whole ultrasound field which is composed of a number of plane waves (when $\theta$ and $R$ is fixed) from each section on the transducer surface to the observation point. It is questionable that the spectrum of this signal equals the spectrum of the piece of signal which was

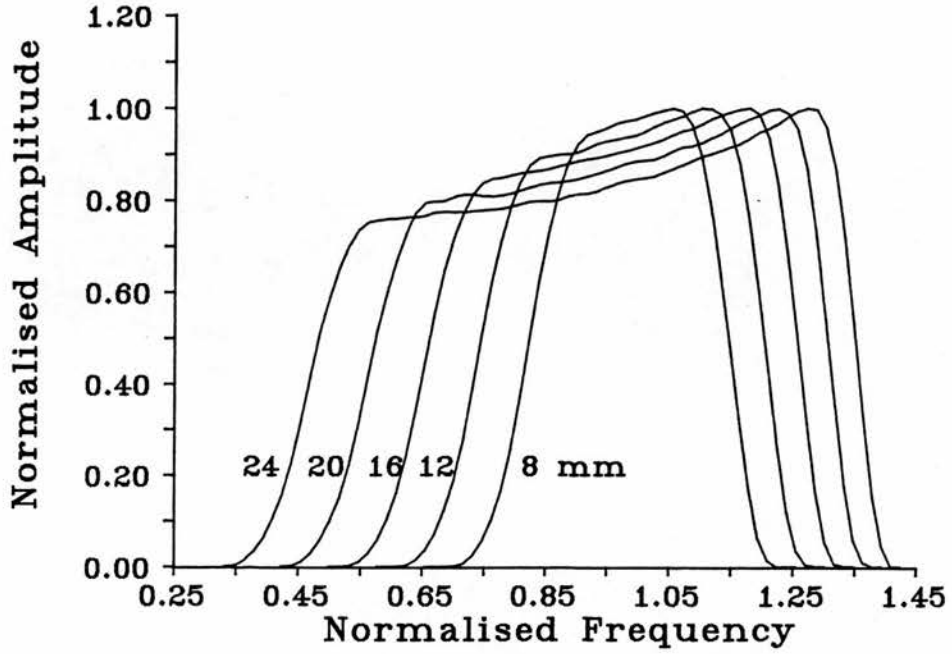


Figure 3.1: A simulation using Bascom's model shows that bandwidth of the spectra increases when the size of the calculated area increases, indicating the model obtains intensity contributions from outside of beam which is un-physical.

described above.

To confirm that such an approach has problems, the simulation model made by Bascom *et al.* (1986) was repeated. A streamline of particles moving at a constant velocity was simulated for different calculated area. As all backscattered signals come from the sample volume, if the calculated area is already larger than the beam width, further increase of the calculated area should make little difference. However, the result shows (Figure 3.1) that the spectrum changes when the calculated width increases, even when the width is much larger than the beam width. This indicates that the model obtains significant contributions from outside the beam, which in a real situation of course should never happen.

It is fairly difficult to calculate the spectrum of the signal from an observation point. This is because in order to calculate the spectrum, it is necessary to calculate the spectrum from a restricted region. This means the signal has to be truncated. Truncation of the signal causes large spectral leakage (Lynn and

Fuerst, 1990) and therefore distorts the simulated Doppler spectrum.

To solve this problem, it is assumed that every sector on the transducer has the same intensity contribution to the received spectrum by particles at, or more strictly around, the observation point. This is certainly true in the far field of the transducer. Within a small interval near the observation point, particles always produce the same frequency contributions determined by $R$, $\theta$ and beam intensity at that position. Therefore, the received signal at the observation point can be considered as a signal with beam intensity and corresponding frequency shift, which can be described by,

$$e_T(t) = e^{-j\omega_0 t}\frac{B(R)}{A_T}\int_{A_T}\frac{1}{R}e^{j\omega_0 tM\cos\theta}ds_T \tag{3.13}$$

where $A_T$ is the area of the transmitter and $B_T(R)$ is the beam intensity at point $R$ which is given by

$$B_T(R) = \int_{A_T}\frac{1}{R}e^{jkR}ds_T \tag{3.14}$$

If it is assumed that $G_T$ is the spectrum of

$$g_T = \int_{A_T}\frac{1}{R}e^{j\omega_0 tM\cos\theta}ds_T \tag{3.15}$$

The frequency spectrum at observation point can be written by

$$G_T(\omega) = \delta(\omega-\omega_0)B_T(R)G_T(\omega) \tag{3.16}$$

### 3.2.5 Contribution from particles at position R

The Doppler effect actually occurs twice in a Doppler velocity measurement. Firstly when the particle receives the signal from a transducer, because the particle is moving, the frequency of the received signal shifts. Secondly the moving particle scatters the signal back and the backscattered ultrasonic wave is received by a stationary transducer. This results in a frequency shift for the second time.

The mechanism of the second frequency shift is very similar to the first, which has been described in Section 3.2.4. According to acoustic theory (Morse and Ingard, 1964), in response to an excitation at frequency $\omega'$, the scattered wave

from a scatterer, whose size is small compared to the wavelength, can be written as,

$$e_q(t) = e'_0 \frac{1}{R'} e^{i\mathbf{k}'\cdot\mathbf{R}'} \Phi(\varphi) \tag{3.17}$$

where $e'_0$ is the amplitude of the excitation wave, $\mathbf{k}'$ is the wavenumber vector, $\mathbf{R}'$ is the vector from scatterer to observer and $\Phi(\varphi)$ is the angle distribution function (Shung *et al.*, 1977). Because the Doppler signal is a narrowbanded signal, we assume that frequency dependent scattering can be ignored. The angle distribution should be very small due to the fact that the transmitter and receiver are the same crystal or are mounted very closely. Therefore $\Phi(\varphi)$ can be set to be unity. Thus, Equation ( 3.17) becomes

$$e_q(t) = e'_0 \frac{1}{R'} e^{i\mathbf{k}'\cdot\mathbf{R}'} \tag{3.18}$$

According to the principle of reciprocity, the field from a simple source is symmetric with respect to interchange of the source and observer. In other words, if the source acts as observer, and the observer acts as source, the received signal would be the same. Therefore, we can consider the receiver as a transmitter and the scatterers at the observation point as a receiver, which is the same as Section 3.2.4. Hence, the received signal can be written by

$$e_R(t) = e^{-j\omega'_0 t} \frac{B_R(R')}{A_R} \int_{A_R} \frac{1}{R'} e^{j\omega'_0 t M\cos\theta'} ds_R \tag{3.19}$$

$$B_R(R') = \int_{A_R} \frac{1}{R'} e^{jk'R'} ds_R \tag{3.20}$$

where $B_R(R')$ is the sensitivity of the receiver at position $R$ and $A_R$ is area of the receiver.

Equation ( 3.19) describes the received signal from particles insonated by a harmonic source. However, as discussed in the last section, the signal received by particles $e_T(t)$ has a range of frequency. In a multi-frequency excitation, Equation ( 3.19) can be written by

$$e_R(t) = \int_{A_R} \frac{B_T(R)}{A_R} \left( \int_{A_T} \frac{1}{R} e^{j\omega_0 t M\cos\theta} e^{j\omega_0 t} ds_T \right) \frac{B_R(R')}{A_R} \frac{1}{R'} e^{j\omega'_0 t M\cos\theta'} ds_R \tag{3.21}$$

where $\omega_0'$ is the excitation frequency which is given by

$$\omega_0' = \omega(1 + M\cos\theta) \tag{3.22}$$

As $v \ll c$, it can be considered that $\omega_0' = \omega_0$. Hence, Equation ( 3.21) can be re-written by

$$e_R(t) = e^{j\omega_0 t}\int_{A_T}\frac{1}{R}e^{j\omega_0 tM\cos\theta}ds_T\int_{A_R}\frac{B_T(R)}{A_T}\frac{B_R(R')}{A_R}\frac{1}{R'}e^{j\omega_0 M\cos\theta'}ds_R \tag{3.23}$$

If it is assumed $G_R(\omega)$ is the spectrum of

$$g_{R'} = \int_{A_R}\frac{1}{R'}e^{j\omega_0 M\cos\theta'}ds_R \tag{3.24}$$

and transducer sensitivity of both transmitting and receiving $B_{RT}(R, R')$ as

$$B_{RT}(R, R') = B_T(R)B_R(R') \tag{3.25}$$

The received signal is given by

$$e_R(t) = \frac{B_T(R)}{A_T}\frac{B_R(R')}{A_R}g_T(t)g_R(t) \tag{3.26}$$

Therefore, the received spectrum from observation point by transducer is given by

$$G_{RT}(\omega) = \frac{B_{RT}(R, R')}{A_T A_R}\delta(\omega - \omega_0)G_T(\omega) * G_R(\omega) \tag{3.27}$$

where $*$ denotes convolution.[2]

### 3.2.6 Spectrum from a vessel

Up to now the spectrum produced by a group of particles at an observation point has been derived. To obtain the whole spectrum from a vessel, it is necessary to sum up all the contributions from each point in the sample volume. It is known that the probability of N scattering particles contained in a volume $dv$ is a Poisson process which is given by

$$P(N) = \frac{(\sigma dv)^N e^{-\sigma dv}}{N!} \tag{3.28}$$

[2]Bascom *et al.* (1986) used autocorrelation by mistake, convolution and autocorrelation are the same only when the spectrum is symmetrical.

where $\sigma$ is population density of particle. The expected number of scatterers in volume $dv$ is $\sigma dv$ (Papoulis, 1958).

As the power of the backscattered signal is proportional to the number of scatterers, assuming the contribution from a position $(x, y, z)$ is $G_{RT}(x, y, z, \omega)$, we obtain the power spectrum by

$$P(\omega) = \int\int\int_{\mathbf{Vol}} |G_{RT}(x, y, z, \omega)|^2 \sigma(x, y, z) dx dy dz \tag{3.29}$$

where **Vol** denotes the sample volume. $\sigma(x, y, z) = 1$ when the particles are uniformly distributed in blood vessels.[3]

## 3.3 Computer Model

In this section and Section 3.4 the details of the realization of the simulation on computer are described. This section mainly deals with the basic problem of realising the problem while Section 3.4 will show the characteristics of the model which is new to the previous simulations described in Chapter 2. To make the text simple, in most parts of this section, only the $2D$ continuous wave transducer has been discussed in detail. The details about circular and rectangular transducer can be derived easily in similar ways.

### 3.3.1 Division of the transducer face

To calculate the Doppler spectrum, it is necessary to divide both the transducer face and vessel into small sections. For a circular or semi-circular transducer, the method used in this model is illustrated in Figure 3.2. The whole transducer is broken up into $N$ rings of width $\Delta r$. Each ring is further divided into $8i$ sectors where

$$i = 1, 2, \cdots, N-1 \tag{3.30}$$

[3]Censor *et al* (1988) thought the backscattered signal is proportional to the density and velocity as "the larger the velocity, the higher the number of uncorrelated events created in the sampling volume". This is a mistake. For theoretical and experimental proofs please see Mo *et al.*, 1992 and Shung *et al.*, 1992.

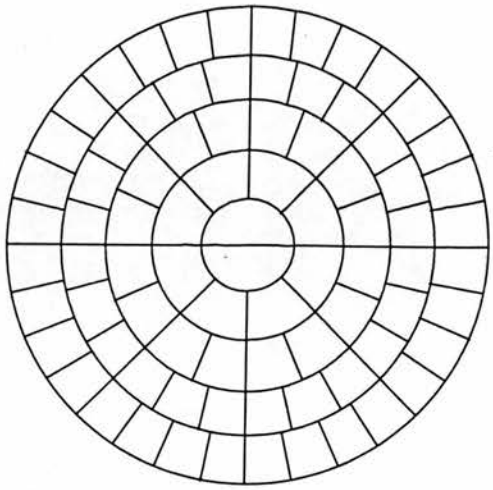

Figure 3.2: The method for breaking the transducer into sections. It is noted that the area of each section is the same.

For the central sector, $i = 0$ and the radius is chosen as $\Delta r/2$. This method, which was first introduced by Cobbold *et al.* (1983) to sub-divide vessels, has a very good characteristic that each sector has equal area which is given by

$$S = \pi(\Delta r)^2/4 \tag{3.31}$$

Using this dub-division, the energy transmitted or received by each sector is equal. The central position of each sector is

$$\begin{aligned} r_i &= i\Delta \\ \Phi_{ij} &= \pi(2j+1)/8i \\ \Delta r &= \frac{R_b}{N-0.5} \end{aligned} \tag{3.32}$$

$$\begin{aligned} i &= 1, 2, \cdots, N-1 \\ j &= -2i, -2i+1, \cdots, 6i-1 \end{aligned} \tag{3.33}$$

where $R_b$ is the radius of the transducer and $N$ is the number of rings.

For a $2D$ shaped (for continuous wave) transducer, the central sector is divided into two semicircular discs for the transmitter and receiver respectively. Assuming

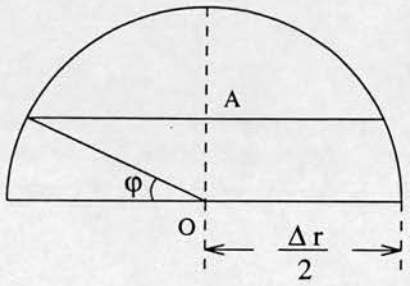


Figure 3.3: The model to divide the central sector for a CW transducer.

that the central point A of the sector divides the disc into two part as illustrated in Figure 3.3. Each part has the same area. Thus we obtain

$$\frac{\varphi}{2\pi}\pi\left(\frac{\Delta r}{2}\right)^2+\frac{1}{2}\left(\frac{\Delta r}{2}\right)^2\sin\varphi\cos\varphi=\frac{\pi}{8}\left(\frac{\Delta r}{2}\right)^2 \tag{3.34}$$

Hence, $\varphi \simeq 0.416\ rad$ and consequently

$$AO = 0.202\ \Delta r \tag{3.35}$$

A rectangular transducer was divided into small rectangular sections.

### 3.3.2 Division of the vessel

Bascom *et al* (1986) used the method described in Section 3.3.1 to sub-divide vessels. However, as discussed in Chapter 2, this method is very inefficient. Furthermore, using this method, the results of the simulation at low frequency have high variability because of binning problems that occur in this region. This problem is the result of the small bandwidth of the spectra in this region; small changes

in Doppler shift cause large changes in amplitude. To solve this problem, the frequency quantisation has to be very small and that often produces a very long computing time.

The method of division of the vessel used in this model has been described in Chapter 2. As each shell corresponds to a frequency bin, this model does not have the "small bandwidth of spectra" problem. The spectrum for low frequencies is as smooth as that at high frequency.

To calculate the spectrum, each streamline is further broken into small sections. The length of each section will be described later.

### 3.3.3 Transducer-vessel geometry

The coordinate systems used to describe the transducer-vessel geometry is depicted in Figure 3.4. A primary Cartesian coordinate system ($x$, $y$, $z$) is used with the origin at the intercept of the vessel and transducer axes. A point on the transducer face is described by ($x'$, $y'$). The transducer-vessel angle is $\theta_0$ and the distance of the centre of the transducer from the origin of the system is denoted as $D_0$.

On the transducer surface, the central point of the sector $S_{kl}$ is given by

$$\begin{aligned} x'_{kl} &= r_k \cos \Phi_{kl} \\ y'_{kl} &= r_k \sin \Phi_{kl} \end{aligned} \tag{3.36}$$

where $r$ and $\Phi$ are described by Equation ( 3.32). Similarly, a point $N_{ij}$ in the vessel can be written as (see Chapter 2 for details)

$$\begin{aligned} y_{ij} &= \rho_i \\ z_{ij} &= \sqrt{\rho_j^2 - \rho_i^2} \end{aligned} \tag{3.37}$$

where $\rho_i$ is the radius of $i$th shell of the vessel. Therefore, it is not very difficult to derive from Figure 3.4 that projections of $MN$ on $x - axis$, $y - axis$, $z - axis$ are given by

$$D_x = -D_0 \cos \theta_0 + r_k \cos \Phi_{kl} \sin \theta_0 - x$$

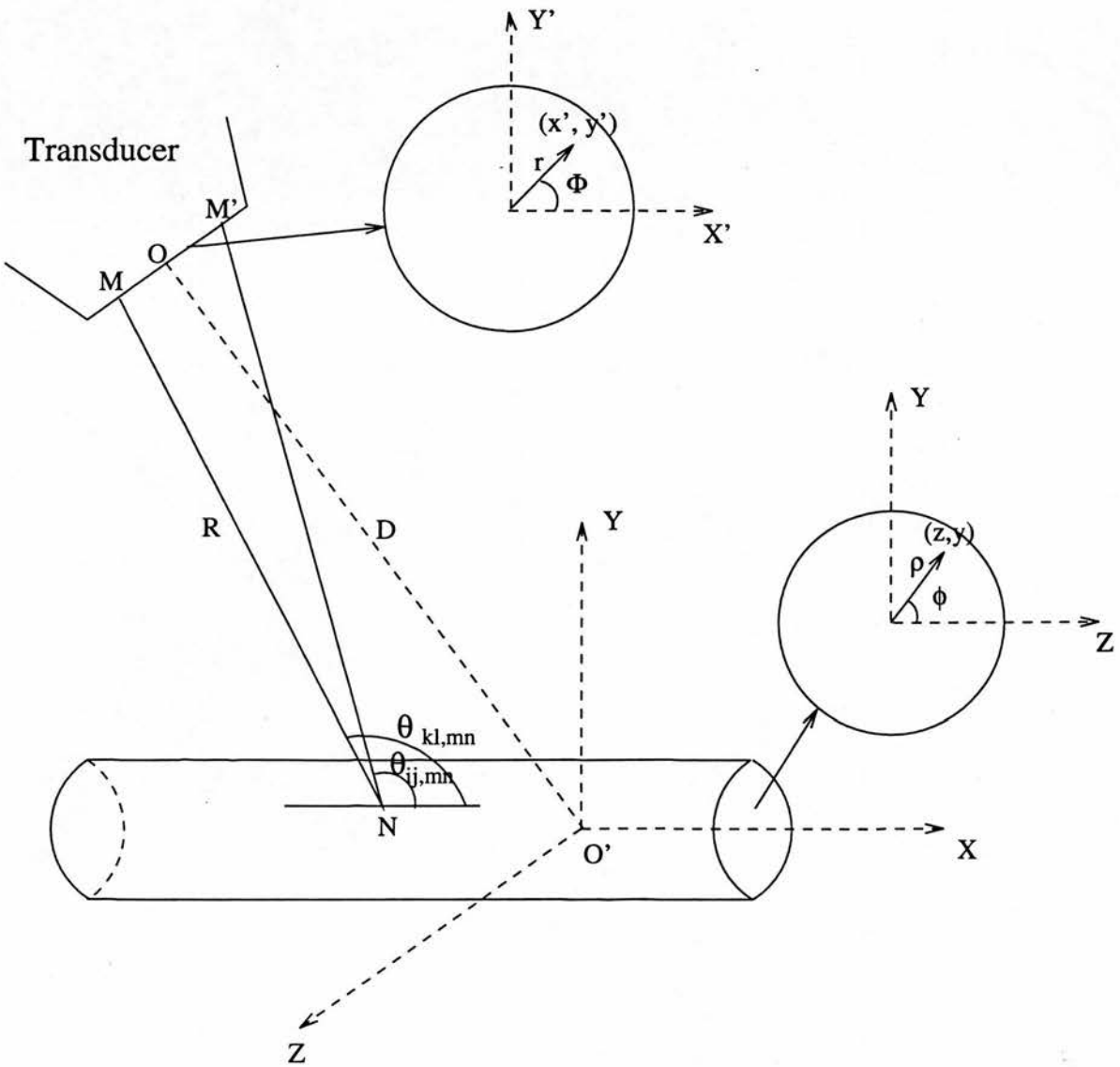


Figure 3.4: The coordinate systems used to describe the transducer-vessel geometry.

$$\begin{aligned} D_y &= r_k \sin\Phi_{kl} - \rho_i \\ D_z &= D_0 \sin\theta_0 + r_k \cos\Phi_{kl} \cos\theta_0 - \sqrt{\rho_j^2 - \rho_i^2} \end{aligned} \tag{3.38}$$

Consequently, the cosine of the incident angle is

$$\cos\theta = \frac{-D_x}{(D_x^2 + D_y^2 + D_z^2)^{1/2}} \tag{3.39}$$

and the distance between the source and observation point is given by

$$|R| = (D_x^2 + D_y^2 + D_z^2)^{1/2} \tag{3.40}$$

Therefore, if the scattered wave received by sector $K_{mn}$ on the transducer surface, the Doppler shift can be written as

$$\Delta F_{kl,ij,mn} = \frac{f_0 v}{c}(\cos\theta_{kl,ij} + \cos\theta_{ij,mn}) \tag{3.41}$$

where $kl$ corresponds to transmitters and $mn$ refers to receivers.

For linear arrays and phased arrays, the geometry is slightly different. The transducer face is assumed parallel to the vessel[4] (Figure 3.5) as the position and focus of the beam can be decided by activating different elements on the transducer face and setting a delay for each element. It is easy to derive that;

$$\begin{aligned} D_x &= -D_0 \cos\theta_0 + x_k - x \\ D_y &= y_l - \rho_i \\ D_z &= D_0 \sin\theta_0 - \sqrt{\rho_j^2 - \rho_i^2} \end{aligned} \tag{3.42}$$

where $x_k$ and $y_l$ are the distance between an element and short or long axis of the transducer.

### 3.3.4 Length of each streamline section

To obtain the spectrum, it is necessary to break each streamline (along the $x - axis$) into small sections. The length of the section is chosen to achieve a given

[4]It may not be parallel in practice but this assumption makes the model simple.

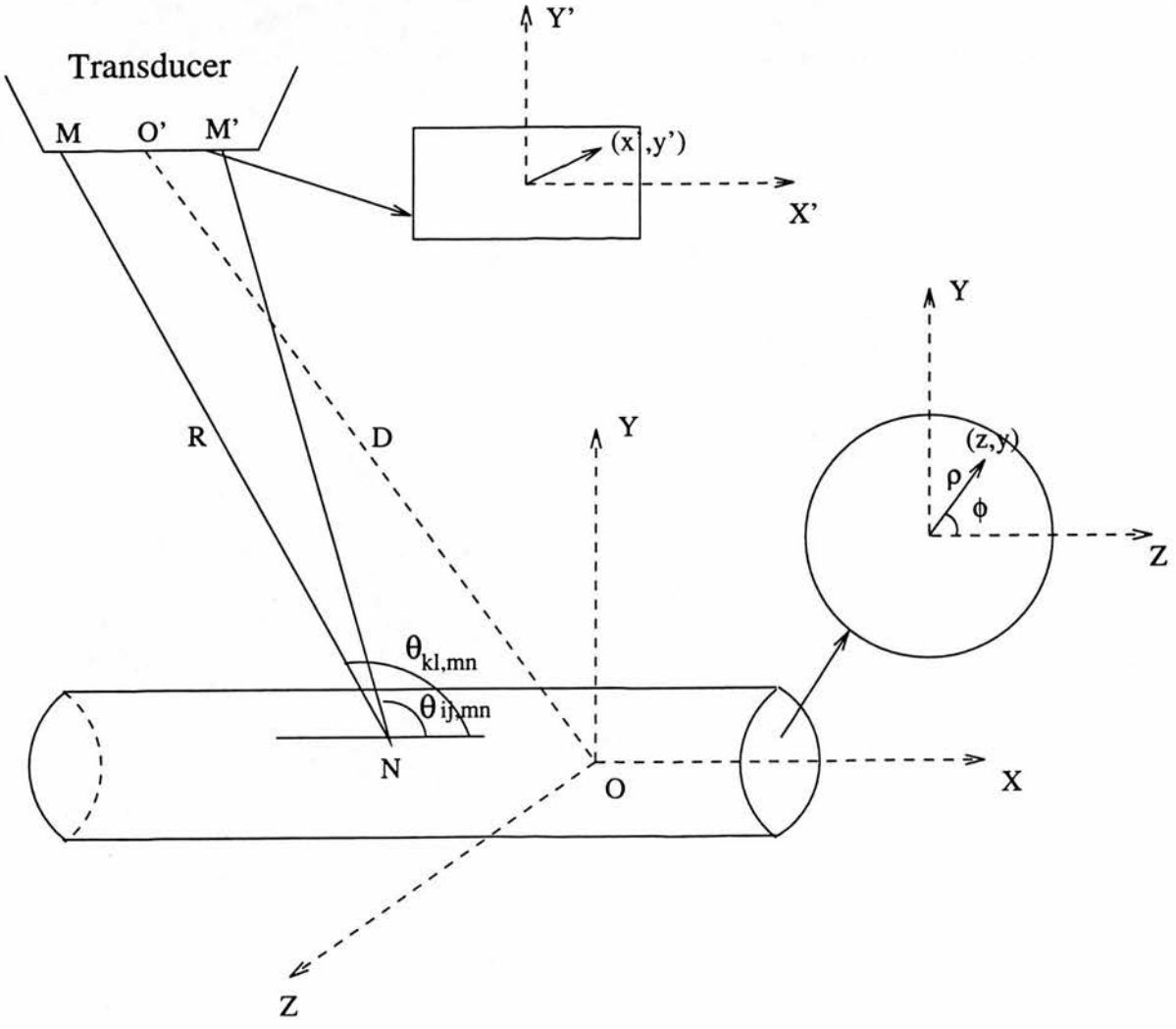


Figure 3.5: The coordinate systems for the linear array. The transducer face is parallel to the vessel axis.

frequency resolution for a specific geometry. If we differentiate both side of the basic Doppler function, we obtain

$$\frac{\Delta F}{dx} = \frac{2f_0 v}{c} \sin\theta \frac{d\theta}{dx} \tag{3.43}$$

For a bandwidth of each frequency bin of $\Delta F_{bin}$, and for a position $x$, to ensure that a change $\Delta x$ gives rise to a corresponding change in Doppler shift less than $\Delta F_{bin}$, Equation ( 3.44) must be satisfied.

$$\Delta F_{bin} \leq \frac{\Delta F}{dx} \Delta x \tag{3.44}$$

It is known that for a small change in $\theta$ (Figure 3.6), we have

$$d\theta \simeq \sin d\theta \simeq \frac{dx \sin\theta}{R_{ij}} \tag{3.45}$$

Rearrangement of both sides of the equation gives

$$\frac{d\theta}{dx} = \frac{\sin\theta}{R_{ij}} \tag{3.46}$$

In order to make Equation ( 3.44) always valid, the largest $\sin\theta$ and smallest $R_{ij}$ should be chosen. In the far field of the transducer, $d\theta/dx$ is a much faster varying function of $\sin\theta$ than $R_{ij}$, so that the change of $R_{ij}$ in the beam can be ignored and the largest value of $\sin\theta$ is chosen.

Two situations are illustrated in Figure 3.7. In Figure 3.7 (a), $D_0 \cos\theta_0 \leq R_b / \sin\theta_0$. In the beam, ultrasonic waves can propagate perpendicular to the velocity vector of particles. The angle $\theta$ is therefore chosen to be 90° and the largest length is given by

$$\Delta x = \frac{c}{2f_0 v} D_0 \sin\theta_0 \Delta F_{bin} \tag{3.47}$$

The other situation is depicted in Figure 3.7 (b) where $D_0 \cos\theta_0 > R_b / \sin\theta_0$. In this case, we can only use the extreme angle instead of a right angle. It can be derived from Equation ( 3.38), ( 3.44), ( 3.46) that

$$-\frac{d\cos\theta}{dx} = \frac{D_0^2 + x^2 + 2xD_0\cos\theta_0 - (D_0\cos\theta_0 + x)^2}{D_0^2 + x^2 + 2D_0\cos\theta_0)^{3/2}} \tag{3.48}$$

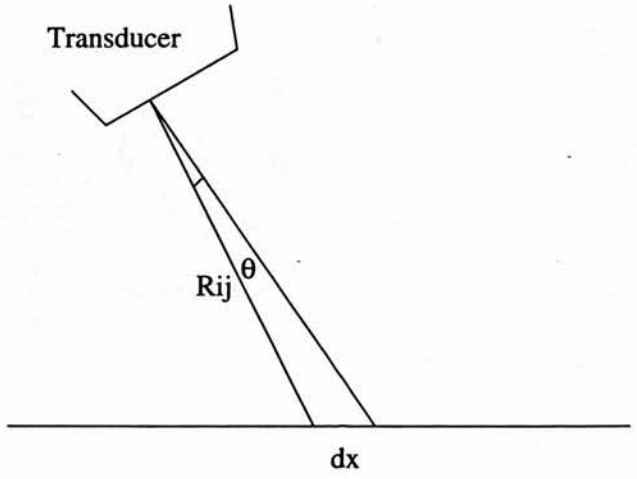


Figure 3.6: For a small change in $\theta$, $d\theta \simeq \sin d\theta$.

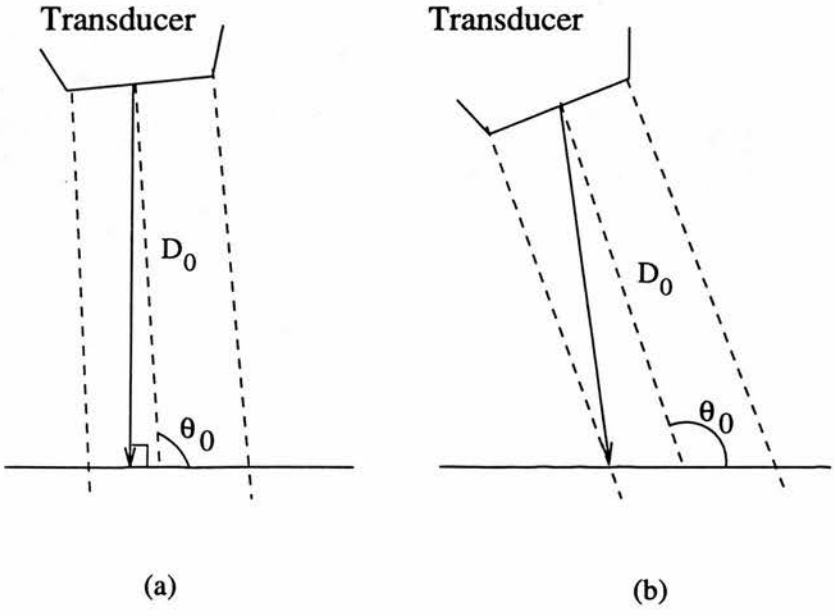


Figure 3.7: The maximum length of streamline section is calculated to achieve a given frequency resolution in which (a) a right angle is possible and (b) a right angle is not possible.

The following expression is derived

$$\Delta x = \frac{c}{2f_0 v} \frac{AN^{3/2}}{AN - (AM + x)^2} \Delta F_{bin} \tag{3.49}$$

where $x$ is chosen as $x = -R_b / \sin\theta_0$ to get the extreme angle, and

$$\begin{aligned} AM &= D_0 \cos\theta_0 \\ AN &= D_0^2 + x^2 + 2xAM \end{aligned} \tag{3.50}$$

### 3.3.5 Width of rings on the transducer face

In a similar manner to 3.3.4, if $D_0 \cos\theta_0 \leq R_b / \sin\theta_0$, the right angle is achievable. The largest width is given by

$$\Delta r = \frac{c}{2f_0 v} D_0 \Delta F_{bin} \tag{3.51}$$

If $D_0 \cos\theta_0 > R_b / \sin\theta_0$, the largest angle is chosen. Therefore, $\Delta x$ is given by

$$\begin{aligned} \Delta r &= \frac{c}{2f_0 v} D_0 \left( \frac{d\cos\theta}{dr} \right) \\ &= \frac{c}{2f_0 v} \frac{\sin\theta_0 D_0 (D_0 + x\cos\theta_0)}{(D^2 + x^2 + 2xD_0\cos\theta_0)^{3/2}} \Delta F_{bin} \end{aligned} \tag{3.52}$$

It is assumed for the discussion in Section 3.2 that the size of each section on the transducer face should be smaller than the wavelength. The width of each ring is therefore given by

$$\Delta r_f = min(\Delta x,\ \lambda) \tag{3.53}$$

where $\lambda$ is the wavelength and $min(\Delta x,\ \lambda)$ gives the smaller value of $\Delta x$ and $\lambda$.

The choice of size of sections on a rectangular transducer is more complex and it is not described here.

## 3.4 Other Characteristics

### 3.4.1 Reducing computation

Although the new vessel dividing method smooths the spectrum so that a smaller number of shells can be used, the computation of this simulation is still fairly extensive. A simulation with 80 shells usually needs about 2 hours CPU time on the university mainframe computer. In the day time, it means we have to wait for at least 10 hours to obtain each spectrum. To make the calculation more realistic, a method to increase the speed must be provided.

It is generally known that although ultrasound intensity changes considerably across the beam, it does not vary much along the beam in the far field of the transducer (Evans and Parton, 1981; Evans, D.H. *et al.*, 1989b). Therefore, as an approximation, it may be assumed that the intensity of the ultrasound field does not change along the beam axis within the vessel. This transfers a 3-dimensional problem to a 2-dimensional one and consequently greatly reduces the computation. In a test run on the mainframe computer, the CPU time dropped from 2 hours to about 1 minute when 80 shells were chosen.

### 3.4.2 Focusing

For each kind of transducer, the mechanism of focusing is different. Therefore the simulation of focusing of $2D$ CW transducer, circular transducer and rectangular transducer will be described separately.

For a $2D$ shaped transducer, the schematic diagram of the transducer is shown in Figure 3.8. Two semi-circular discs are mounted with their faces at an angle to each other. The half discs are separated by acoustic insulator. In operation, one element generates a transmission field which overlaps the reception zone of the other element and that gives the focusing.

To make the problem simple, it is assumed that the gap is positioned per-

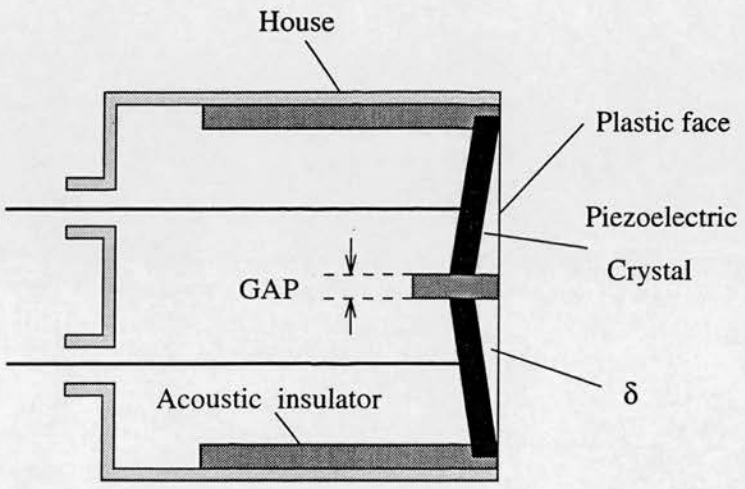


Figure 3.8: The schematic diagram for a CW double crystal transducer.

pendicular to the vessel axis, or in other words, in a direction across the vessel. Therefore, it can be derived that in this case, Equation ( 3.38) becomes

$$\begin{aligned} D_x &= -D_0 \cos\theta_0 + r_k \cos\Phi_{kl} \sin(\theta_0 \mp \delta) - x \mp \frac{1}{2} GAP \sin\theta_0 \\ D_y &= r \sin\Phi_{kl} - \rho_i \\ D_z &= D_0 \sin\theta_0 + r_k \cos\Phi_{kl} \cos(\theta_0 \mp \delta) \sqrt{\rho_j^2 - \rho_i^2} \pm \frac{1}{2} GAP \cos\theta_0 \end{aligned} \tag{3.54}$$

where $\delta$ is the angle between the discs and transducer face, $GAP$ is the gap between the two discs and $\mp$ for transmitter and receiver respectively.

A single-element transducer, as found in PW Doppler devices, is shown schematically in Figure 3.9. Focusing at a fixed range is achieved by using a lens (Tarnoczy 1965) or a concave piezoelectric element. In the latter case, to provide a flat face on the transducer and hence easier coupling to the skin a weaker convex lens is placed in front of the concave element.

Theoretically, all the focusing is achieved by delays in the phase of ultrasonic rays. To obtain the maximum focusing, all the ultrasound waves from the transducer should arrive the focal point at the same phase so that the largest intensity

at the focal point and the narrowest beam is produced at the focal length. For an annular array or single crystal transducer, as shown in Figure 3.9, the focusing can be achieved by correcting the phase difference between $MD$ and $OD$ where $OD$ is the focal length. We can calculate the delay of each ring on the transducer by

$$\begin{aligned} \tau_k &= 2\pi f_0 \Delta t \\ &\simeq \frac{2\pi f_0}{c}\left(\sqrt{OD^2 + r_k^2} - OD\right) \\ &\qquad k = 1, 2, \cdots, N-1 \end{aligned} \tag{3.55}$$

where $N$ is the number of rings on the transducer used in the simulation. Hence, the ultrasound intensity $B_T(R)$ and receiving sensitivity $B_R(R)$ in Equation ( 3.14) and ( 3.20) become

$$\begin{aligned} B_T(R) &= \int_{A_T} \frac{1}{R} e^{jkR-\tau_k} ds_T \\ B_R(R) &= \int_{A_R} \frac{1}{R} e^{jkR-\tau_k} ds_R \end{aligned} \tag{3.56}$$

The principle of focusing of rectangular single crystal is the same. It can be described by Equation ( 3.56) and $r_k$ in this case is also the distance between the section and centre of the transducer.

In practice, single crystal transducers are often not fully focused as described in Equation ( 3.55) and ( 3.56). Weak and medium focusing are used instead to obtain an appropriate size of sample volume. Therefore, three levels of focusing $FL$ are defined in this model. The delay $\tau$ is set to be

$$\tau = FL \cdot \tau_{ij} \tag{3.57}$$

where $FL = 1$, $FL = 2/3$ and $FL = 1/3$ indicates weak, medium and strong focusing.

Linear array and phased array transducers are usually rectangular. These transducers are constructed from a number of piezoelectric-element strips. A group of elements on a linear array, or all the element on a phased array, are used

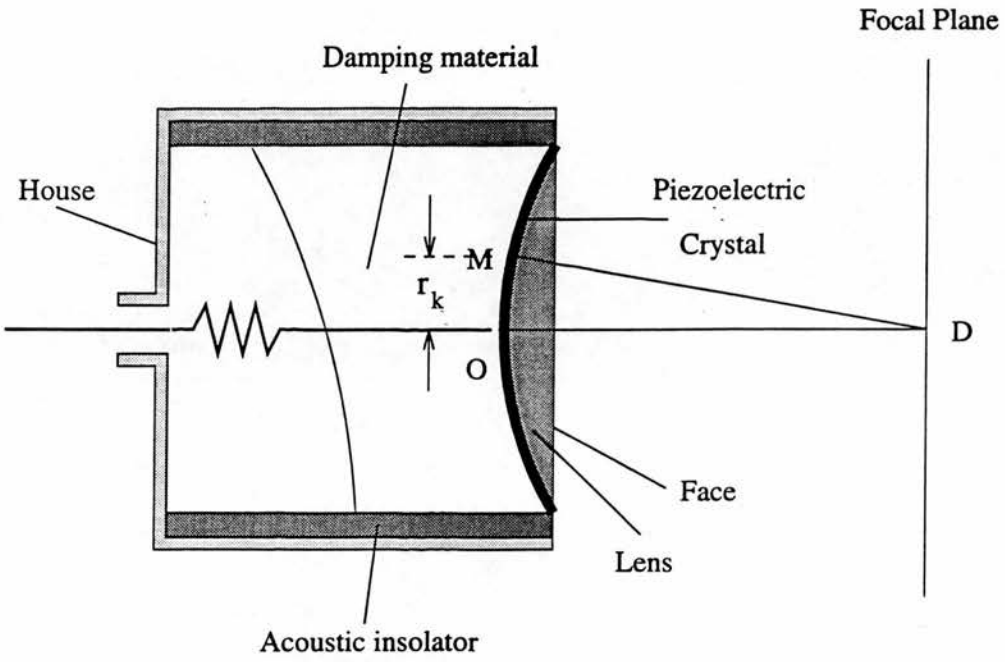


Figure 3.9: The geometry for a single element transducer. Focusing is achieved by correcting the phase difference between ultrasonic rays from the transducer to its focus.

to move the beam along the array, alter the angle of the beam, focus or de-focus the beam.

The focusing of these transducers is different from the single element transducer. In the direction parallel to the plane of scan, the electronic focusing is utilised. This focusing results from selecting the optimum number of elements and appropriate time delays in the transmission and reception electronics (Figure 3.10). Some linear arrays may have a curved face to achieve a wider field of view. However, the basic mechanism of focusing is the same. To assist in making the beam narrower in the direction at right angles to the plane of scan, curved elements or cylindrical lens may be employed. This is very similar to that on single crystal transducers.

Therefore, two focal lengths need to be considered. In the direction parallel to the plane of scan, we obtain the delay $\tau_i$ by

$$\tau_i = \frac{2\pi f_0}{C}(F_x - \sqrt{(F_x - r_i \cos\theta_0)^2 + (r_i \sin\theta_0)^2}$$

$$\tau_i = \frac{2\pi f_0}{C}(F_x - \sqrt{(F_x \cos\theta_0 - r_i)^2 + (F_x \sin\theta_0)^2} \quad \begin{matrix} r_i > 0 \\ r_i < 0 \end{matrix} \tag{3.58}$$

where $F_x$ is focal length electronically controlled and $r_i$ is the distance between the element and the short axis of the transducer. In the direction normal to the plane of scan, the delay $\tau_{0j}$ is given by

$$\tau_j = \frac{2\pi f_0}{C}\sqrt{(F_y + r_j)^2 - F_y^2)} \tag{3.59}$$

where $F_y$ is the fixed focal length and $r_j$ is the distance between an element and long axis of the transducer. Hence we obtain the delay $\tau_{ij}$ for each element on the transducer by adding the delay alone each direction by

$$\tau_{ij} = \tau_i + \tau_j \tag{3.60}$$

### 3.4.3 Wall reflection

Wall reflection has been discussed in Chapter 2 assuming a known (uniform or experimentally measured) beam profile. It was noted that there was a disagreement at high frequency components between experiment and theory as geometrical spectral broadening was not considered in that model. To investigate how wall reflection affects the Doppler spectrum, especially the high frequency components of the spectrum, the wall reflection model is combined with the spectral broadening model in this simulation.

It is highly expensive in computation time if the incident angle for each ultrasound ray is considered. Therefore, only the average effect is considered in this model. As illustrated in Figure 3.11 (b), if point $C$ is insonated by the transducer, the average angle is approximately given by $\alpha + \beta$.

Now we calculate the incident angle to the vessel. The coordinate system is illustrated in Figure 3.11. The radius of the vessel is $\rho_0$. At distance $x_r$ off the vessel centre, the angle between the $z-axis$ and $\mathbf{r_0}$, which is the unit vector normal

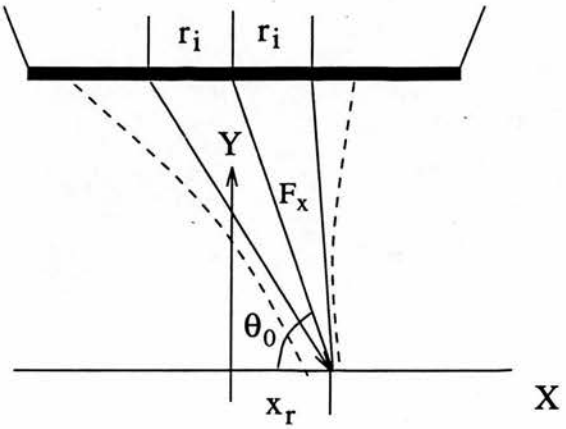


(a)

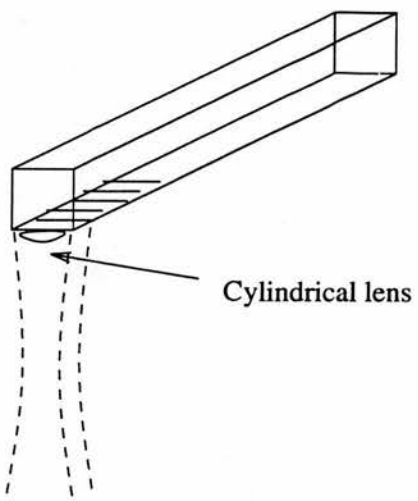


(b)

Figure 3.10: The focusing for a multi-element transducer. The focusing is achieved by both electronic delay (a) and mechanical focusing (b).

to cylindrical vessel wall at the incident point, is $\alpha$. The angle between the $z-axis$ and the incident ultrasound wave on $yz-plain$ is $\beta$ and the distance between the incident point and $z-axis$ is $x_r$. The beam-vessel angle is $\theta_0$. Supposing $\mathbf{r_s}$ is the unit vector of the incident wave with opposite direction, it can easily be derived from Figure 3.11 that,

$$\mathbf{r_0} = -\mathbf{j}\sin\alpha + \mathbf{k}\cos\alpha \tag{3.61}$$

$$\mathbf{r_s} = -\mathbf{i}\cos\theta_0\cos\alpha + \mathbf{j}\sin\beta + \mathbf{k}\cos\beta\sin\theta_0 \tag{3.62}$$

Therefore, we obtain the incident angle as

$$\cos\theta = \mathbf{r_0}\cdot\mathbf{r_s} = \cos\alpha\cos\beta\sin\theta_0 \tag{3.63}$$

From Figure 3.11 it can be derived that

$$\cos\alpha = \sqrt{1-\left(\frac{x_r}{p_0}\right)^2} \tag{3.64}$$

$$\cos\beta = \frac{D_0\sin\theta_0 - \sqrt{p_0^2-x_r^2}}{\sqrt{x_r^2+(D_0\sin\theta_0-\sqrt{p_0^2-x_r^2})^2}} \tag{3.65}$$

As in general $D_0\sin\theta_0 \gg p_0$ and $D_0\sin\theta_0 \gg x_r$, Equation ( 3.65) can be rewritten as

$$\cos\beta \simeq \frac{D_0\sin\theta_0}{\sqrt{x_r^2+D_0\sin\theta_0^2}} \tag{3.66}$$

Therefore, the cosine of incident angle is given by

$$\begin{aligned}\cos\theta &= \cos\theta\cos\beta\sin\theta_0 \\ &= \sqrt{\frac{p_0^2-x_r^2}{D_0\sin\theta_0^2+x_r^2}}\frac{D_0\sin\theta_0}{p_0}\end{aligned} \tag{3.67}$$

It is assumed that the complete reflection occurs at distance beyond $x_r$ to the vessel axis. Therefore, the region from $x_r$ to the vessel edge is not insonated. From Figure 3.11 (b), we obtain

$$\frac{D_0\sin\theta_0}{D_0\sin\theta_0-(p_0-\sqrt{p_0^2-x_r^2})} = \frac{x_r}{x} \tag{3.68}$$

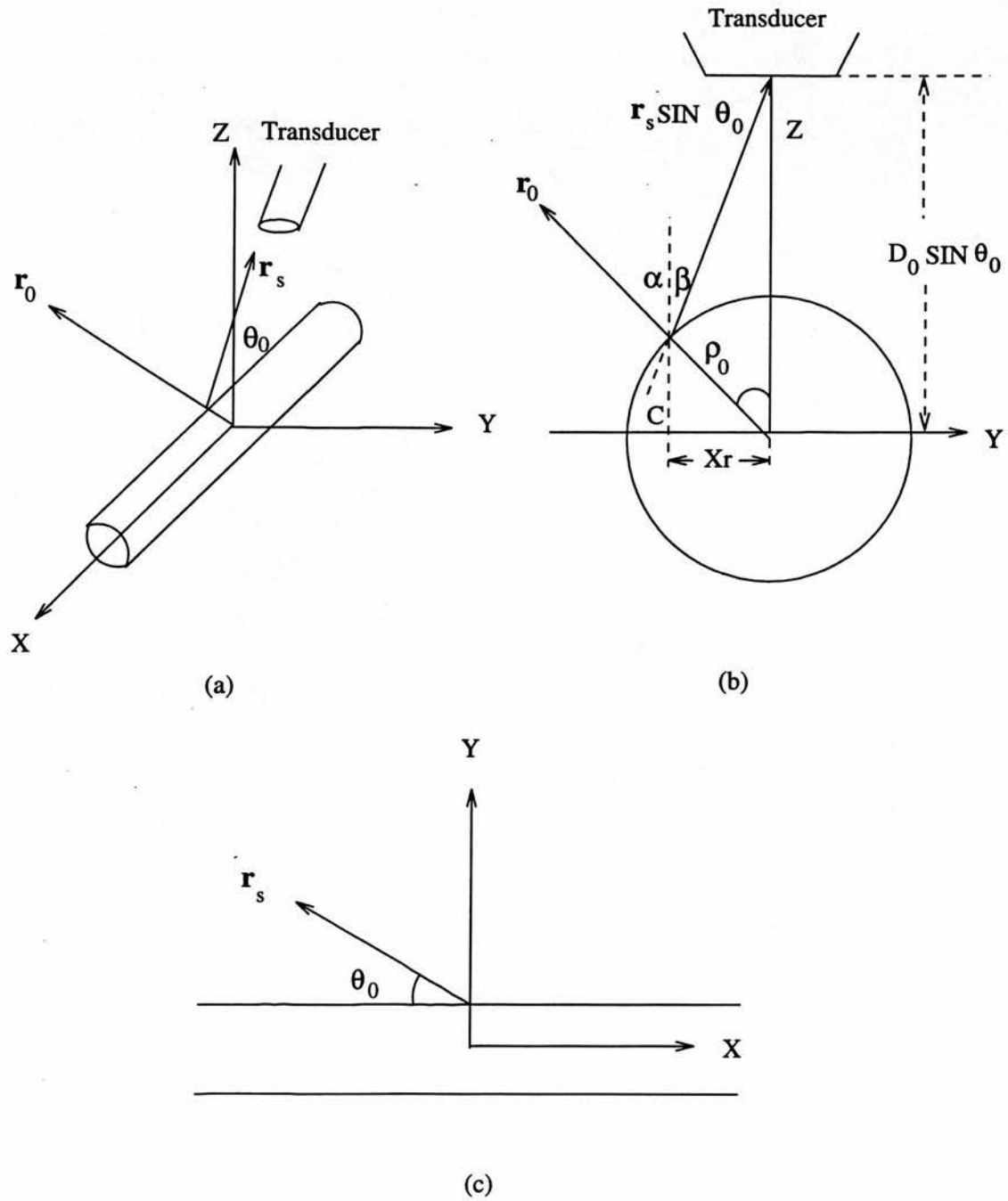


Figure 3.11: The geometry for calculating the wall reflection.

It is difficult to calculate $x_r$ for a given $x$ from this Equation ( 3.68). However, as $D_0 \sin\theta_0 \gg p_0$, $x_r$ and total reflection usually occurs when $x$ is large, Equation ( 3.68) can be simplified by

$$x_r \simeq \frac{D_0 \sin\theta_0}{D_0 \sin\theta_0 + p_0} x \tag{3.69}$$

It is not difficult to derive from Equation ( 3.69) that total reflection occurs when

$$x_r \geq \frac{p_0 D_0 \sqrt{\sin^2\theta_0 - \cos^2\theta_c}}{\sqrt{D_0^2 \sin^2\theta_0 + p_0^2 \cos^2\theta_c}} \tag{3.70}$$

where $\theta_c$ is the critical angle for total reflection.

The rest of the model has been described in Chapter 2. Wall reflection is an option in the simulation.

### 3.4.4 Beam simulation

Partial insonation is an important source of error in Doppler ultrasound, particularly where mean velocity is concerned. It is often necessary to compare the realistic beam with the theoretical beam used in the simulation, especially when different degrees of focusing are taken into account. It is also very useful in the simulation itself to define the edge and consequently the area of calculation. An appropriately chosen area of calculation can save computation time and achieve a good accuracy at the same time. Therefore, as an option, the beam along three lines, which are two orthogonal lines across the beam through the vessel centre and the axis of the vessel, can be plotted.

Two kinds of beam can be plotted. One is the transmitting field $B_T(R)$ described by Equation ( 3.14), which can be compared with the beam amplitude measured by a hydrophone. The other is the sensitivity of both transmitting and receiving field $B_{RT}(R)$ illustrated in Equation ( 3.25), ( 3.14) and ( 3.20). $B_{RT}(R)$ shows where the backscattered signal comes from and the size of the real beam width (both transmitting and receiving).

## 3.5 Experiment

To prove the validity of this numerical model, it is necessary to compare the results of the simulation with the Doppler spectra acquired from experiments. This was performed on the flow phantom described in Chapter 2 using a Doptek CW Doppler unit. This involves two experiments; firstly to obtain the parameters for theoretical simulation and to investigate the details of the transducer and beam; and secondly Doppler spectra were acquired from the flow phantom and compared with the simulated spectra in identical conditions.

### 3.5.1 Beam and transducer

A 2D shaped double crystal transducer was used on the Doptek device. Because the gap between the crystals was not marked on the transducer face, a needle, which was linked to a piezoelectric crystal, was used to detect the orientation of the gap. The needle point was made to contact the transducer face. The vibration of the transducer was transmitted to the needle crystal and the detected signal was displayed by an oscilloscope. The appearance of the signal indicated contact on the transmitting crystal. The orientation of the gap was determined by the positions of vibrating and non-vibrating points. The orientation of the gap is needed for further X-ray examination to detect the convergence angle and the size of the gap between the two crystal, as the picture has to be taken in the direction along the gap.

The transducer then was pictured by using X-ray in the direction parallel to the gap. The gap and convergence angle between two crystals were measured. The accuracy of the convergence angle is estimated to be better than 1°. These data were used in the theoretical simulation.

The beam profile was measured on the hydrophone measuring system described in Chapter 1. Peak-to-peak amplitudes were examined along two directions, that is along and across the gap between the two crystals. The distance between transducer face and the hydrophone was 5 cm which is identical to the depth in

the Doppler spectrum acquisition.

### 3.5.2 Doppler spectrum

Doppler spectra were acquired on the flow phantom. A 5.0 mm diameter heat-shrinkable tubing was constructed as the artificial vessel. To avoid the strong refraction at the vessel wall, a mixture of degased water and sephadex was used as artificial blood.

Steady flow was used in the experiment. Doppler spectra were acquired at beam-vessel angles ranging from 50° to 90°. The transducer was placed so that the gap between the two crystals was perpendicular to the vessel axis. Simultaneous measurements of absolute flow were made using a measuring cylinder and a stop watch. All the spectra were transferred to micro-computer. Averaged spectra from 240 lines were calculated and compared with experimental results.

## 3.6 Results

### 3.6.1 Transducer

The angle between the two crystals was measured as 176°. The gap between the two crystals was 1 mm.

### 3.6.2 Beam

The experimental and theoretical beam profiles along and across the gap of two crystal is given in Figure 3.12. The experimental beam is slightly wider than the real beam in both direction along and across the vessel. This is because the rigid disc assumption is used (Evans and Parton, 1981).

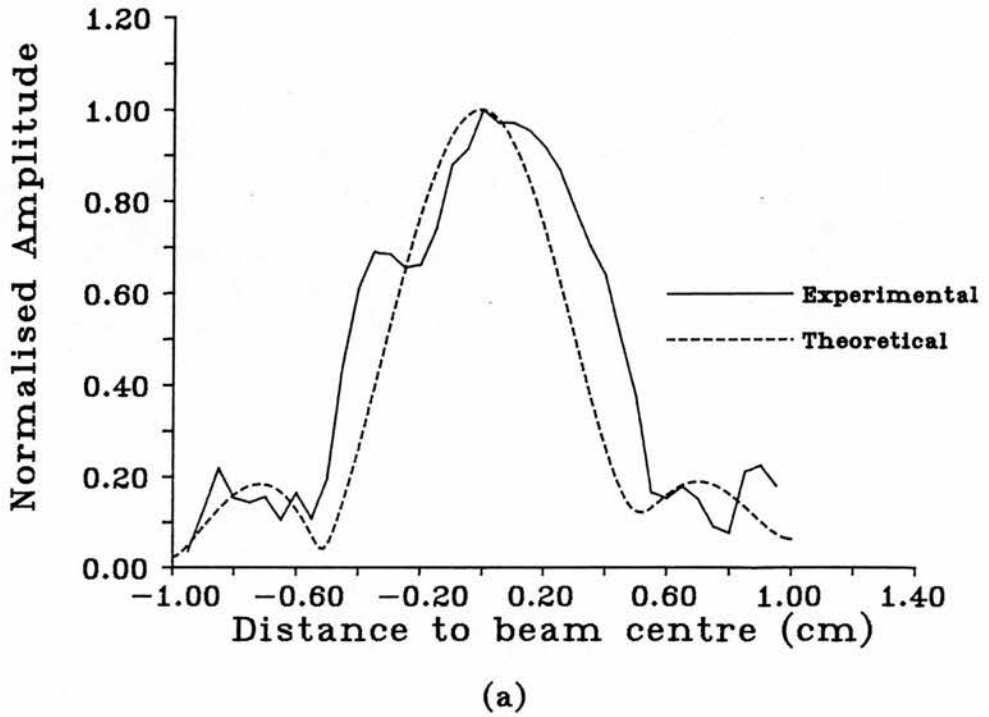


(a)

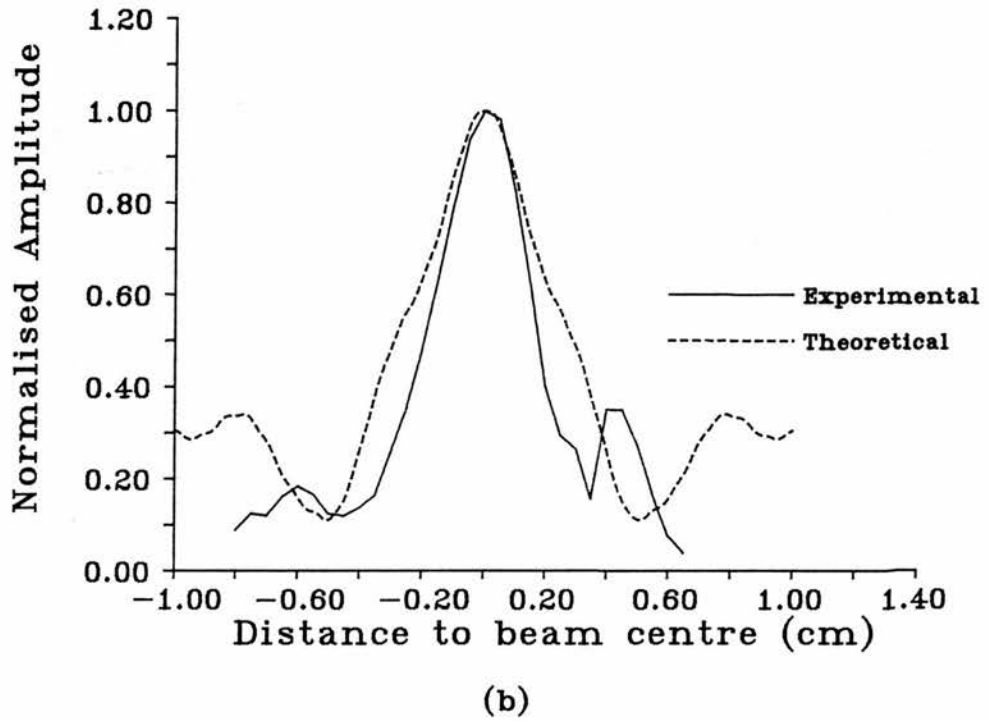


(b)

Figure 3.12: Comparison between simulated beam (linked lines) and experimentally measured beam (broken lines) profiles. (a) Beam across the gap. (b) Beam along the gap.

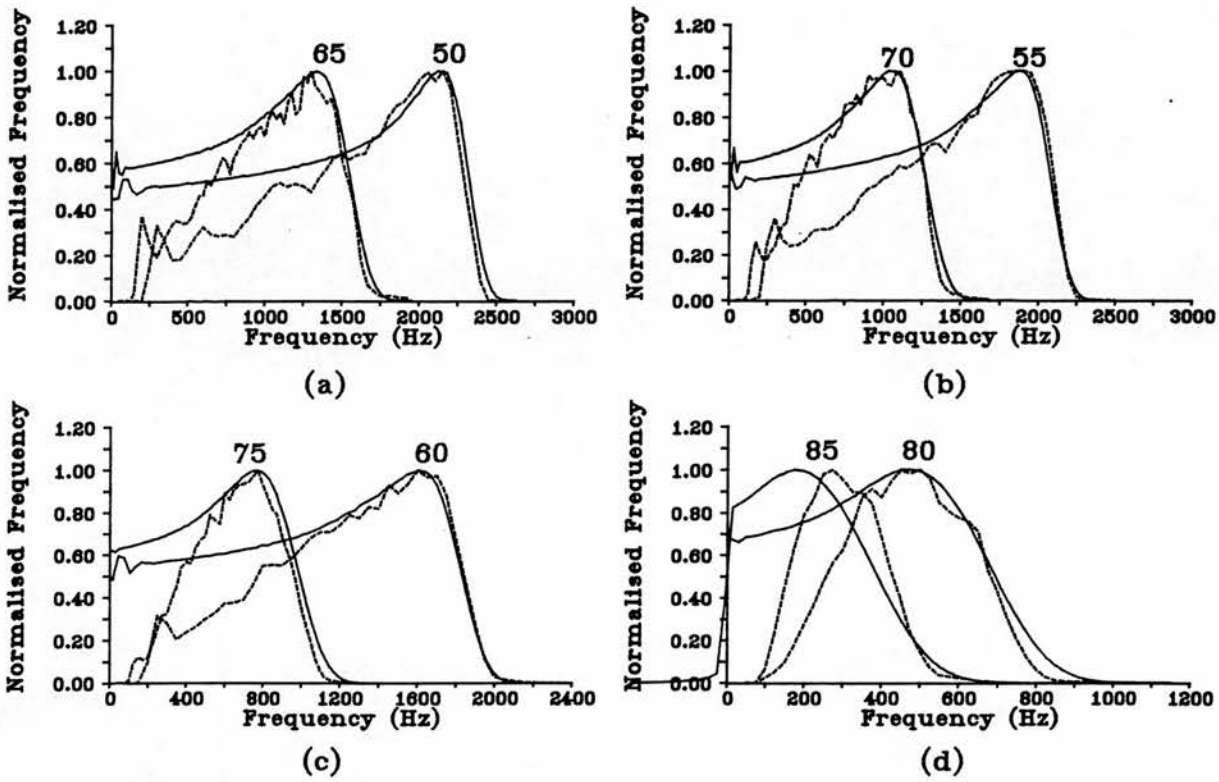


Figure 3.13: Comparison between simulated spectra by the computer model and experimentally measured spectra by Doptek CW unit. The beam-vessel angles are (a) 50° and 65°, (b) 55° and 70°, (c) 60° and 75°, (d) 80° and 85°.

### 3.6.3 Spectrum

Figure 3.13 gives spectra at different beam-vessel angles from both theoretical simulation and experiments. It is shown that the high frequency components of these spectra agree well, while the discrepancy in low frequency is because the simulated beam is slightly wider than the beam measured experimentally. The sedimentation also increased the difference (Chapter 2).

## 3.7 Conclusion

A computer model was developed in this chapter to simulate Doppler spectra. The computational time has been significantly reduced. A wide range of physical conditions, particularly different types of focused or unfocused transducer and

reflection at vessel walls can be simulated. A good agreement has been obtained between the experiment and the simulation except at low frequency. It is believed that the model presented provides a more detailed understanding of the Doppler spectrum and can be used to investigate the accuracy of the Doppler velocity measurement.

# Chapter 4

# MEAN AND MAXIMUM FREQUENCY ESTIMATION

## 4.1 Introduction

The mean velocity is estimated from either the mean frequency or maximum frequency envelope. Therefore the accuracy of the mean and maximum Doppler frequency shift is important to velocity estimation using Doppler techniques.

The mean frequency envelope is affected by a number of physical factors, especially nonuniform insonation. Evans, D.H. (1982) indicated that the true mean velocity can only be measured by uniform insonation over the whole area of the vessel. It was shown that partial insonation can give an error up to 50% in the mean velocity estimation (Evans, D.H. 1985). Bascom *et al* 1990 further estimated the error by using a uniform beam profile with a circular cross-section as well as a Gaussian beam profile for various conditions. Cobbold *et al.*, (1983) established a numerical model and calculated the effect of misalignment between the beam and vessel using square beam and Gaussian beam profile. Large errors were found when the conditions were not ideal. Obviously, other factors such as flow profile, type of transducer and focusing can also significantly change the Doppler spectrum and consequently the mean frequency.

The maximum frequency, on the other hand, is considered to be more immune

to most of the physical factors. Therefore, it is more often used in clinical measurements. Among the factors affecting the maximum frequency, the geometrical spectrum broadening is of the most interest. Geometrical spectral broadening is dependent on the geometry of transducer and vessel, such as beam-vessel angle, size and distance of transducer and vessel, size of sample volume, etc. Early studies in geometrical spectral broadening concentrated on the bandwidth of the spectrum from a uniform velocity flow. Newhouse *et al* (1977) made a simple approach by calculating the bandwidth from the two angles from the centre of the transducer to the edges of the beam. Later, in 1980, Newhouse *et al.* theoretically and experimentally investigated the use of extreme angles in estimating the bandwidth. More recent studies in geometrical spectral broadening have focused on the simulation of the whole Doppler spectrum. Bascom *et al.* (1986) developed a numerical model for the spectral broadening. Censor *et al.* (1988) also made a simulation of spectral broadening. It was found that the Doppler frequency shift does not follow its normal Equation (1.1) when the beam-flow angle is bigger than 60°. However, as explained in Chapter 3, both existing techniques for simulating the Doppler spectrum may have problems. It is questionable that the results from the two models are reliable. Furthermore, there have been no comparison between simulation and experiment to date.

The objective of this chapter is to examine the effect of a number of factors on the spectrum using the model described in Chapter 3. A possible method for extraction of the maximum frequency, which is independent of the geometrical spectral broadening, is suggested. The results are carefully compared to quantify the importance of each factor which affects the measurement of the mean and maximum frequency shift. Two typical clinical situations, which are the mean velocity estimation in the umbilical vein and carotid artery, will be analyzed. Relevant review materials will be given in each section.

## 4.2 Development Of A New Method For Extraction Of The Maximum Frequency.

There are several algorithms for maximum frequency estimation in Doppler spectral analyzers. The maximum frequency was obtained by a threshold (Light, 1970; Johnston *et al.*, 1978;) or a phase-locked loop (Sainz *et al.*, 1976) or a voltage-controlled high pass filter (Skidmore and Follet, 1978). Digital methods have been described such as the zero-crossing time-interval histogram method (Baker *et al.*, 1974; Nowicki *et al.*, 1985) and the "objective" algorithm (D'Alessio, 1985). It is know that the method of extracting of maximum frequency can affect the accuracy of the measurement. Mo *et al.* (1988) examined four digital maximum frequency estimators. The study concentrated on their performance in a noisy background.

However, there have been few studies on the accuracy of maximum frequency estimation when geometrical spectral broadening is present. Experiments (Figure 2.11) showed that the error of the maximum velocity estimation was from 0.1% at 50° to 18.6% at 80° using a Doptek CW unit. To correct this error, Newhouse indicated that the maximum frequency can be estimated by using extreme angles. Censor *et al.* (1988) also suggested that at beam-vessel angles larger than 60°, the maximum frequency can be estimated by

$$\Delta(F_d)_{max} = \frac{2v_{max}W}{cF}\sin\theta \tag{4.1}$$

where $v_{max}$ is the maximum velocity, $W$ is the width of the transducer, $F$ is the focal length and $c$ is the sound speed. However, as focusing and beam patterns are complicated in practice, these methods are not likely to be accurate or easy to achieve.

As errors due to the geometrical spectral broadening increase significantly at large beam-vessel angles, corrections are necessary. Ideally, the maximum frequency estimation should be independent of the geometrical spectral broadening (GSB) or beam-vessel angle. Figure 4.1 (a) gives the normalized spectra simulated by computer (see Chapter 3) using the Doptek 4 MHz, 8 mm double crystal CW transducer at different beam-vessel angles. It is noted that all the spectra

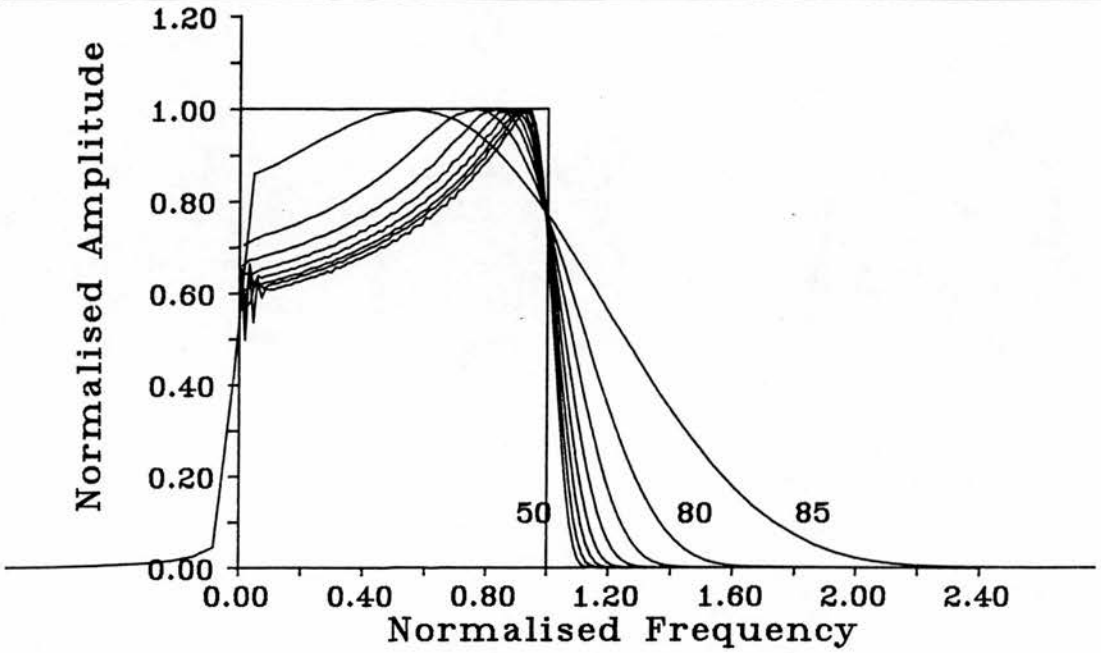


(a)

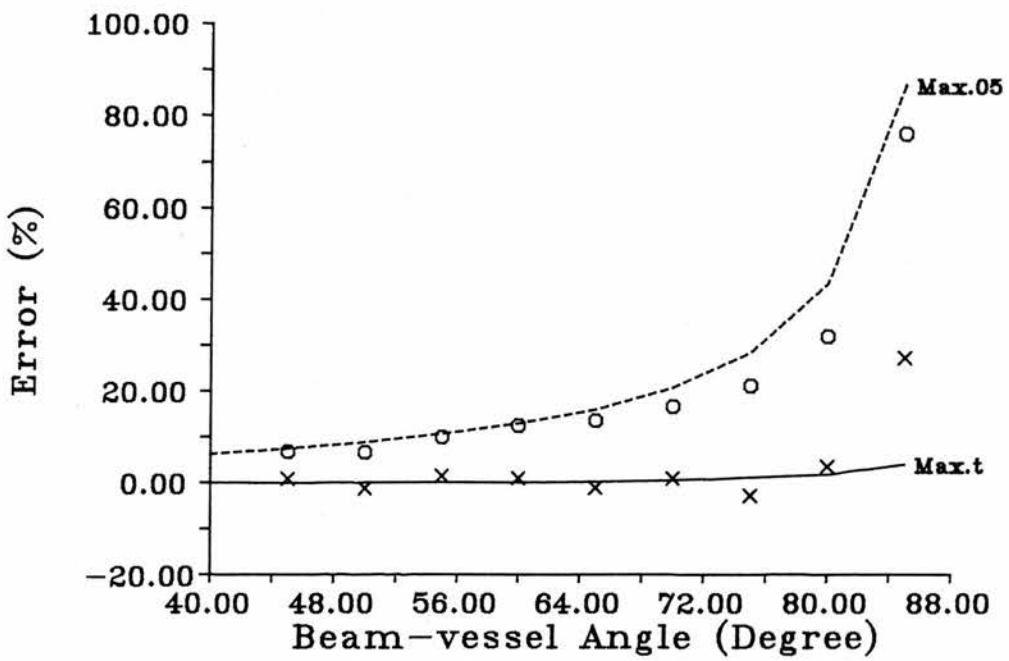


(b)

Figure 4.1: CW double crystal transducer (4 MHz 8 mm) (a) Doppler spectra at different beam-vessel angles. It is noted that spectra pass the true maximum frequency at the same point. (b) Errors in 5% threshold (max.05) and GSB independent threshold maximum frequency (max.t) estimation. Symbol o and × are errors in maximum frequency measured by 15/16 threshold method and GSB independent threshold method.

pass the true maximum frequency at almost the same (normalised) amplitude. If this amplitude is used as a threshold, which in this case is 0.74 of the maximum amplitude, for maximum frequency estimation, the errors in the maximum frequency was less than 1.7% from 40° to 80° (Figure 4.1 (b)). Using the same method, the maximum frequencies are estimated from the spectra obtained by experiments in Chapter 3. Again the errors in the maximum frequency were less than 3.4 % when the beam-vessel angle is smaller than 80° and independent of the beam-vessel angle (Figure 4.1 (b)). This suggests that it is possible to use a higher threshold to give an estimation of the maximum frequency which is independent of the beam-vessel angle. The effect of other factors on this new threshold will be examined in Section 4.3.

## 4.3 Effects Of Factors

In this section, the effect of a number of factors on the mean frequency, 5% maximum frequency and new GSB independent maximum frequency are examined. These factors include the type of transducer, distance and misalignment between transducer and vessel, focusing, size of transducer, size of vessel, reflection at the vessel wall and velocity profile. The 5% maximum frequency is defined as the frequency at which the amplitude is 5% of the maximum amplitude.

Flow measurements are most often performed using an offset circular probe or a linear array. The number and position of active elements on a linear array depends on the depth of the vessel, beam-vessel angle and position of the sample volume. Different manufactures also have different configurations. It is more difficult to simulate a linear array than a circular transducer. Therefore a circular transducer will be used in most parts of this section.

The standard conditions for the simulation in this section are listed in Table 4.1. The conditions used in simulations in the rest of the chapter are the same as listed in this table unless stated. For simplicity of the text, the details of the conditions may not be repeated in this section. The effect of each factor is examined by changing that particular factor with other factors fixed.

| Type of transducer | Misalignment | Focusing |
|---|---|---|
| Circular | 0 mm | Unfocused |
| Distance | Diameter of Vessel | Reflection |
| 5 cm | 5 mm | None |
| Diameter of Transducer | Velocity Profile | Beam-vessel Angle |
| 8 mm | Parabolic | 60° |

Table 4.1: The standard conditions for the simulation.

### 4.3.1 Effect of transducer type

There are many types of transducer used in Doppler ultrasound. These transducers includes circular single crystal transducer, rectangular single crystal transducer (hardly used), CW double crystal transducer, linear array, phased array, annular array. The type of transducer affects the Doppler spectrum by means of its beam-vessel geometry and beam patterns. The geometrical spectral broadening and insonation of the vessel varies for different transducers. Therefore, both the mean frequency and maximum frequency are affected.

The spectra from a circular transducer (4 MHz, 8mm) with uniform insonation, a circular transducer (4 MHz, 8 mm, unfocused) and a linear array (3.5 MHz, 20 mm$\times$10 mm, focused) at different beam-vessel angles are shown in Figure 4.2 (a), Figure 4.3 (a) and Figure 4.4 (a). The distance of between the transducer and the sample volume is 5 cm for each simulation and the diameter of the vessel is 5 mm. It is noticed that the spectral broadening is more significant when the beam-vessel angle increases. Consequently the errors in the maximum frequency estimation using the 5% threshold method increases significantly when the beam-vessel angle is enlarged. This error can be larger than 30% at large beam-vessel angles such as 70°. Different transducers show different degrees of spectral broadening and give different overestimation of the true maximum frequency.

However, for each transducer, except for those at beam-vessel angles larger than 75°, almost all the spectra pass the true maximum frequency at one amplitude. Therefore, a threshold for the GSB independent maximum frequency extraction can be found for all these transducers. It should be noted that the threshold for each transducer is different. For uniform insonation, circular trans-

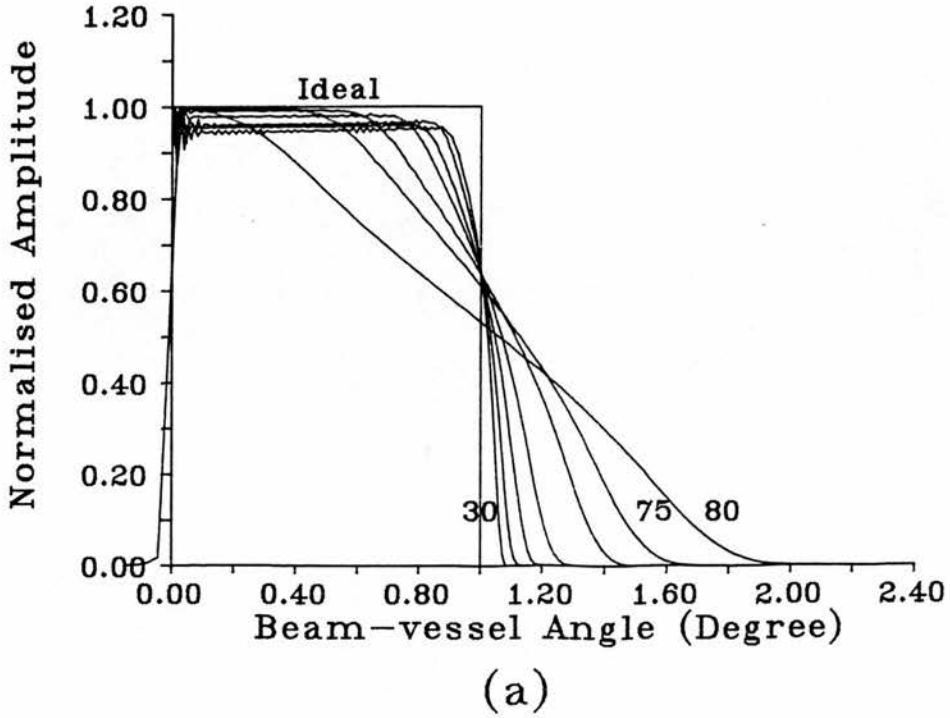


(a)

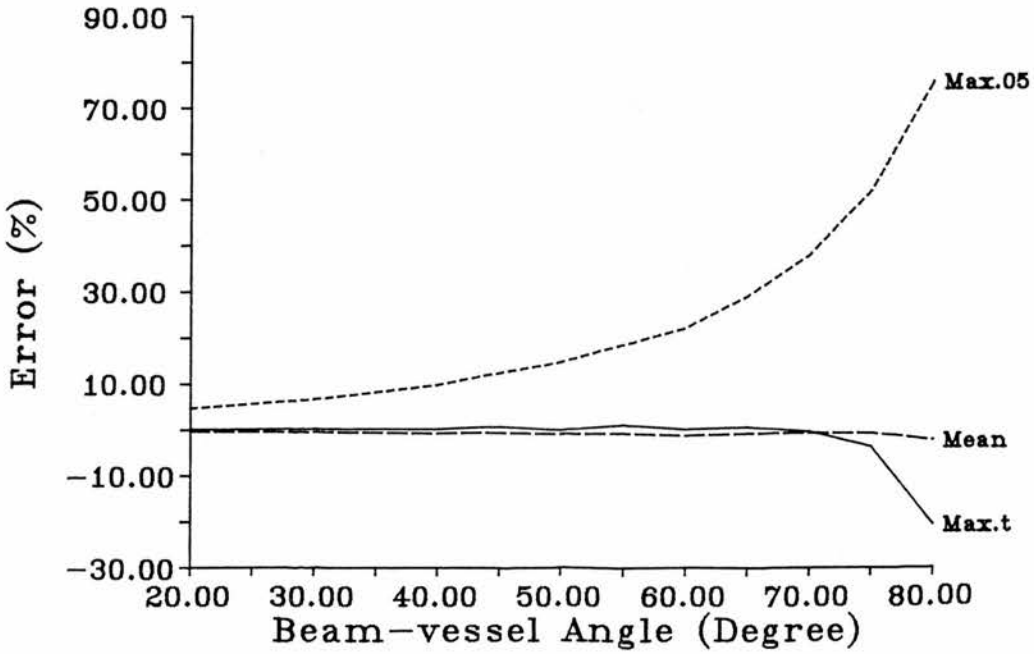


(b)

Figure 4.2: Uniform insonation (a) Doppler spectra for different beam-vessel angles. Most spectra cross the true maximum velocity at the same point. (b) Errors in the mean (mean), 5% threshold (max.05) and GSB independent maximum frequency (max.t) estimation. The GSB independent estimation shows very low errors.

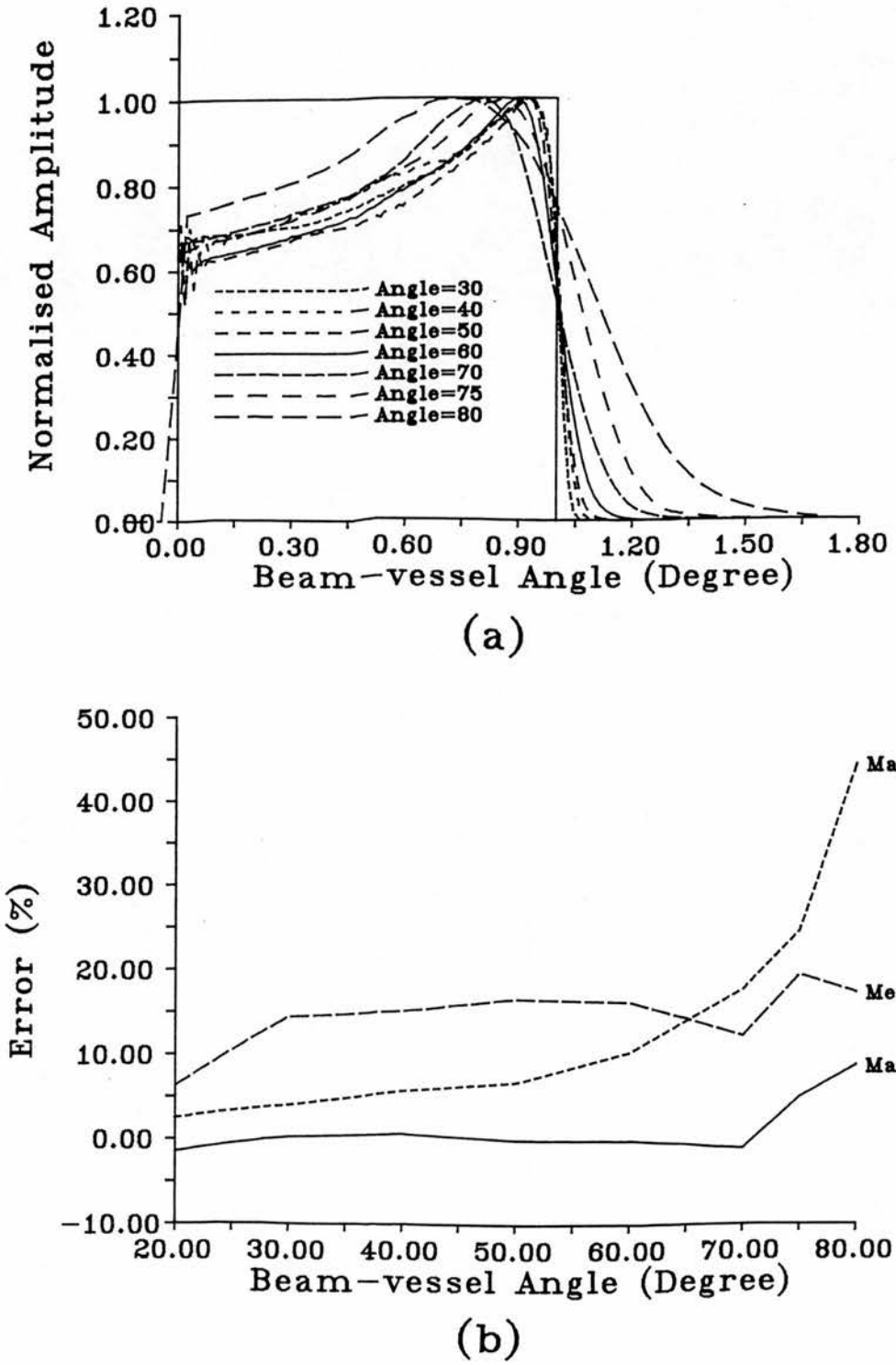


Figure 4.3: Circular transducer (4 MHz, 8 mm diameter, unfocused) (a) Doppler spectra for different beam-vessel angles. Most spectra cross the true velocity at the same point. (b) Errors in the mean (mean), 5% threshold (max.05) and GSB independent maximum frequency (max.t) estimation. Again GSB independent estimation shows low errors.

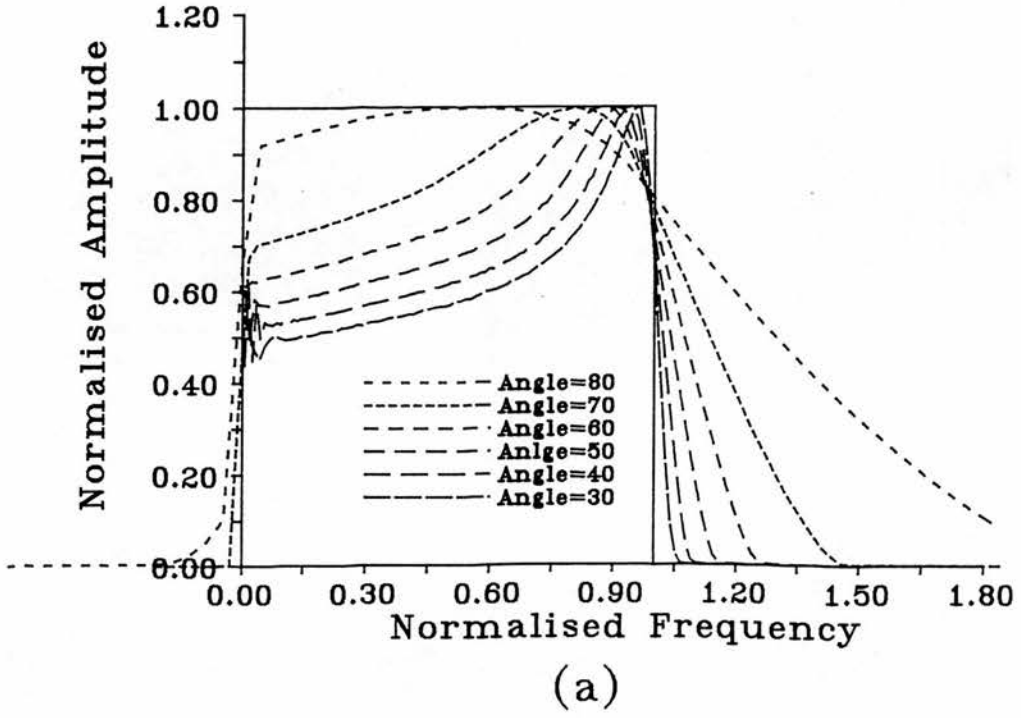


(a)

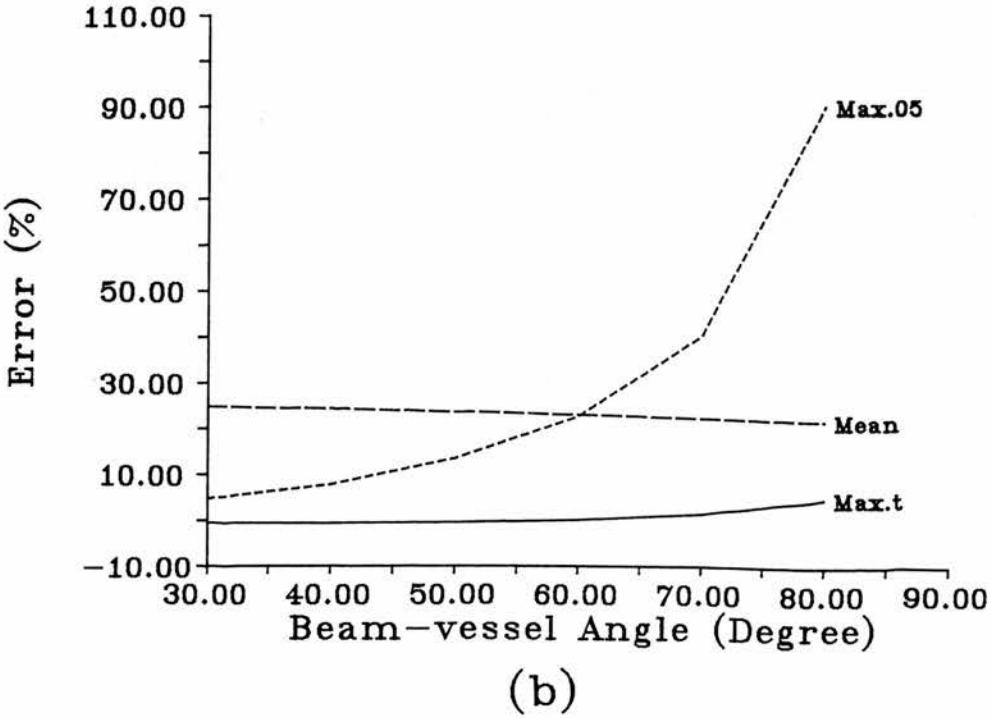


(b)

Figure 4.4: Linear array (5 MHz, 2 cm × 1 cm, focused at 5 cm) (a) Doppler spectra for different beam-vessel angles. (b) Errors in the mean (mean), 5% threshold (max.05) and GSB independent maximum frequency (max.t) estimation. Again GSB independent estimation shows low errors.

ducer and linear array, the thresholds are 0.64, 0.56 and 0.75 respectively, and the maximum errors of the estimated maximum frequencies are 1.59%, 1.49 %, 1.43% respectively for beam-vessel angles not larger than 70° (Figure 4.2 (b), Figure 4.3 (b) and Figure 4.4 (b). This suggests that all the transducers have a cross point threshold. However, the threshold may be different for different type of transducer.

For mean frequency estimation, the errors are relatively independent of the beam-vessel angle. This is consistent with the suggestion by Bascom *et al.* (1991) that geometrical spectral broadening has no significant effect on the mean frequency estimation. However, due to different uniformity of insonation associated with each transducer, the error in the mean frequency estimation varies. For a transducer with uniform insonation, a circular transducer and a simulated linear array, errors are about 0.5%, 16% and 25% respectively.

### 4.3.2 Distance between transducer and vessel

The distance between transducer and vessel affects the Doppler spectrum by two mechanisms. First, when the distance changes, the blood vessel intercepts a different region of the beam so the uniformity of insonation over the vessel changes. Many transducers focus at their focal length. For an unfocused transducer, the focal length $F$ is given by

$$F = \frac{a^2}{\lambda} \tag{4.2}$$

where $a$ is the diameter of the transducer and $\lambda$ is the wavelength of ultrasonic waves. The beam is narrowest at the focal plane. At distances larger or smaller than $F$, the beam is wider and therefore more uniform insonation occurs. Second, the distance between transducer and vessel changes the angles available for transmitting and receiving ultrasonic waves. At short distances, a scatterer in the beam can both receive waves from the transducer and backscatter them to the transducer over a larger range of angles, so the spectral broadening is more significant and the spectrum is wider.

The spectra using an 8.0 mm circular unfocused transducer at distances from

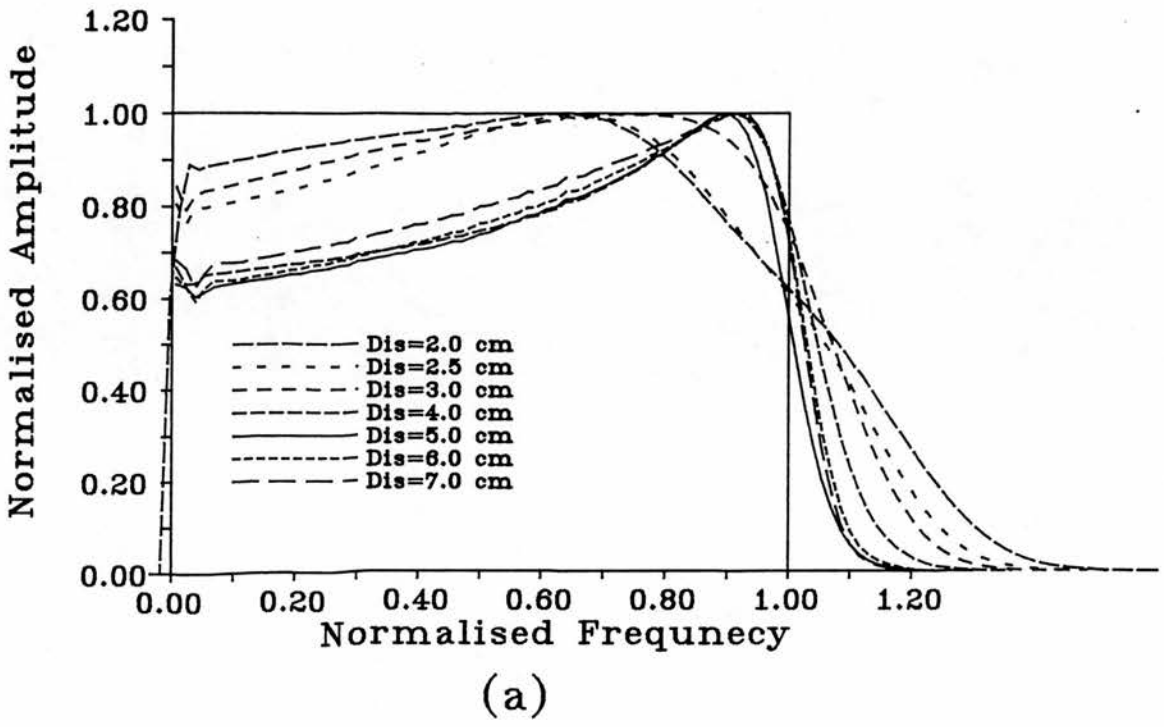


(a)

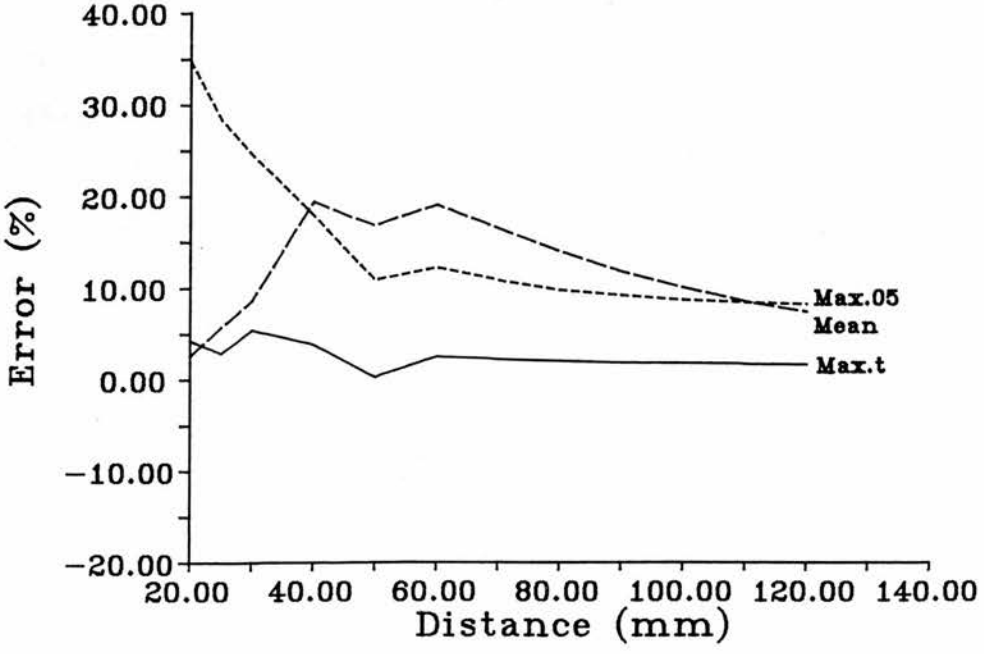


(b)

Figure 4.5: Effect of distance between transducer and vessel. The transducer is 5 MHz 8mm single crystal circular transducer. Beam-vessel angle is 60°. (a) Spectra at different distances. (b) Errors in the mean (mean), 5% threshold (max.05) and GSB independent maximum frequency (max.t) at different distances. The GSB independent estimation shows low errors.

2.0 cm to 7.0 cm are illustrated in Figure 4.5. The beam-vessel angle is 60°. Apart from short distances (less than 3.0 cm), the spectra seem to be not particularly sensitive to the distance.

The mean frequency for these spectra changes significantly for different distances (Figure 4.5). The overestimation is largest at a distance near 5 cm. This corresponds to the focus of the transducer. The errors in the mean frequency estimation are from 2.5% to 19.3% at distance from 2 cm to 12 cm. In other words, the mean frequency cannot be well estimated over a wider range of distance or vessel depth.

The error for the 5% threshold maximum frequency is about 34.8% at a distance of 2.0 cm due to the large geometrical spectral broadening. It falls to about 10% when the distance is larger than 5 cm. For the GSB independent maximum frequency, errors in the maximum frequency are less than 5.4% in the near field which is within 5 cm from the transducer. At distances which are greater than 5 cm, the GSB independent maximum frequency can be estimated to better than 2.3%. This shows that this method is the best for the maximum frequency estimation over a range of distance.

### 4.3.3 Focusing

In Doppler ultrasound, focusing is used to obtain the signal from the region of interest. However, in some cases, focusing causes partial insonation of the vessel. For volumetric flow measurement, a uniform insonation over the whole vessel is required if the mean frequency is measured. Although it was suggested that an electronically controlled annular array can be used to achieve uniform insonation (Evans, J.M. *et al.*, 1986a, 1986b), the focused or unfocused single crystal transducer, linear array and phased array are most often used in duplex scanners. The non-uniform beam profile of these transducers will in general distort the Doppler spectrum.

As an example, Figure 4.6 shows the spectrum from a 4 MHz single crystal transducer. The diameter of the transducer was 1.0 cm and the vessel was placed

at the focal length; 5 cm from the transducer. The low frequency components differ for different levels of focusing. However, the high frequency components are very similar. If the vessel is placed out of the focal plane, the difference among the spectra would be even less significant.

The errors of mean frequency of these spectra again vary due to partial insonation. The 5% threshold maximum frequency has errors above 10%. For the GSB independent maximum frequency, apart from the uniform insonation, which is only a theoretical beam, the errors are less than 1.6%.

### 4.3.4 Misalignment

It is in general assumed in Doppler ultrasound measurement that the beam is centrally placed on the blood vessel. However, in practice, the alignment between the axis of blood vessel and the transducer is not always perfect. Slight offset often occurs.

The effect of misalignment has been studied by a number of authors. By using an idealised square beam, Evans, D.H. (1985) concluded that mean frequency can be under estimated by up to 50% by a small off-set. With consideration of attenuation and beam profile (square beam and Gaussian beam), the spectra with misalignment were simulated and it was shown that the error in the mean frequency was from +10% to -$\infty$ (Cobbold *et al.*, 1983; Bascom and Cobbold, 1990). Both papers used highly idealised beams, *i.e.*, square beam or Gaussian beam. The beam width was assumed to be the same as the diameter of the transducer. No consideration of realistic beam and spectral broadening have been made. For the maximum frequency, Hoskins (1991a) experimentally showed on a flow phantom that the misalignment had little effect on the maximum frequency. The reason for this result was not explained.

Misalignment affects the Doppler spectrum mainly by means of changing the insonation of the vessel. Most ultrasonic beams are Gaussian-like. When the beam is moved off the axis of the vessel, the beam centre which gives the strongest insonation is placed not in the vessel axis which has maximum velocity but in a

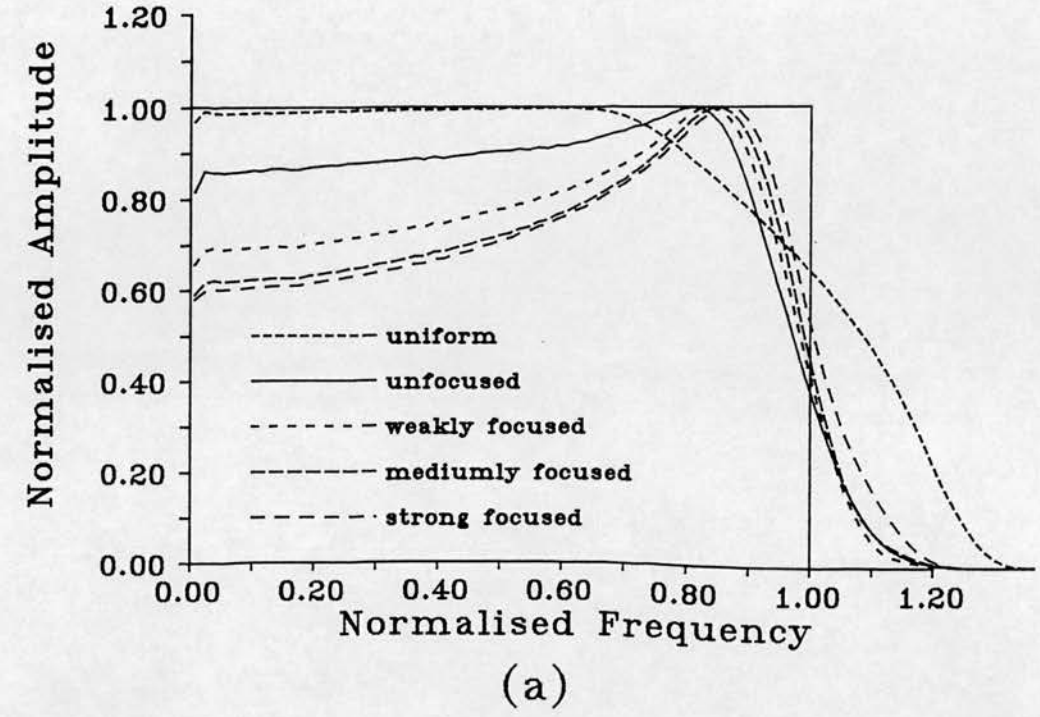


(a)

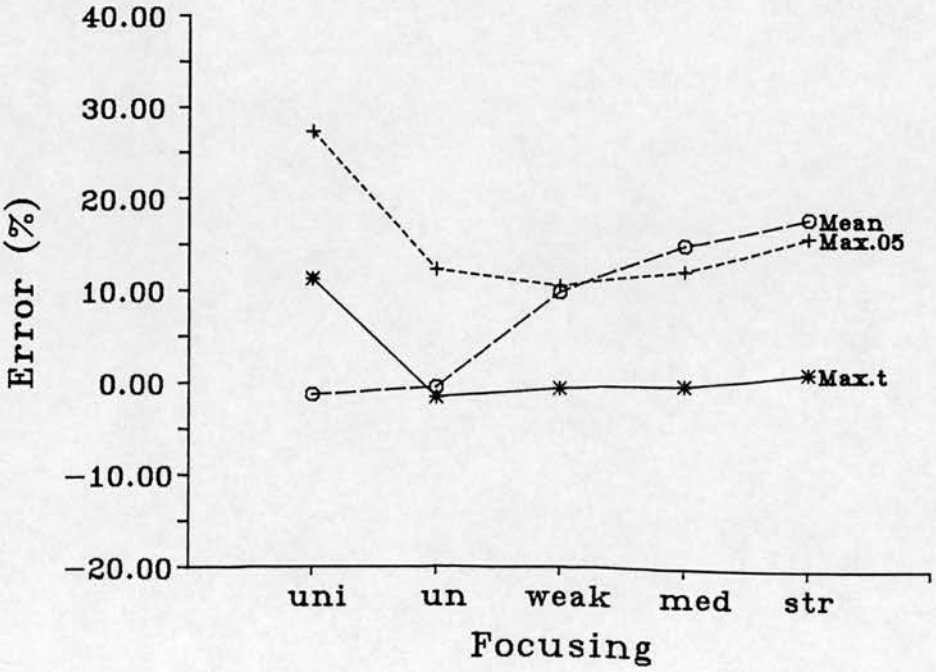


(b)

Figure 4.6: Effect of focusing. (a) Spectra from an 5 MHz 8 mm circular transducer with uniform insonation and different focusing levels at 60° (b) Errors in the mean (mean), 5% threshold (max.05) and GSB independent maximum frequency (max.t). The x-axis is the focusing level which includes uniform insonation (Uni), unfocused beam (un), weakly focused beam (weak), medium focused beam (med) and strong focused beam (str).

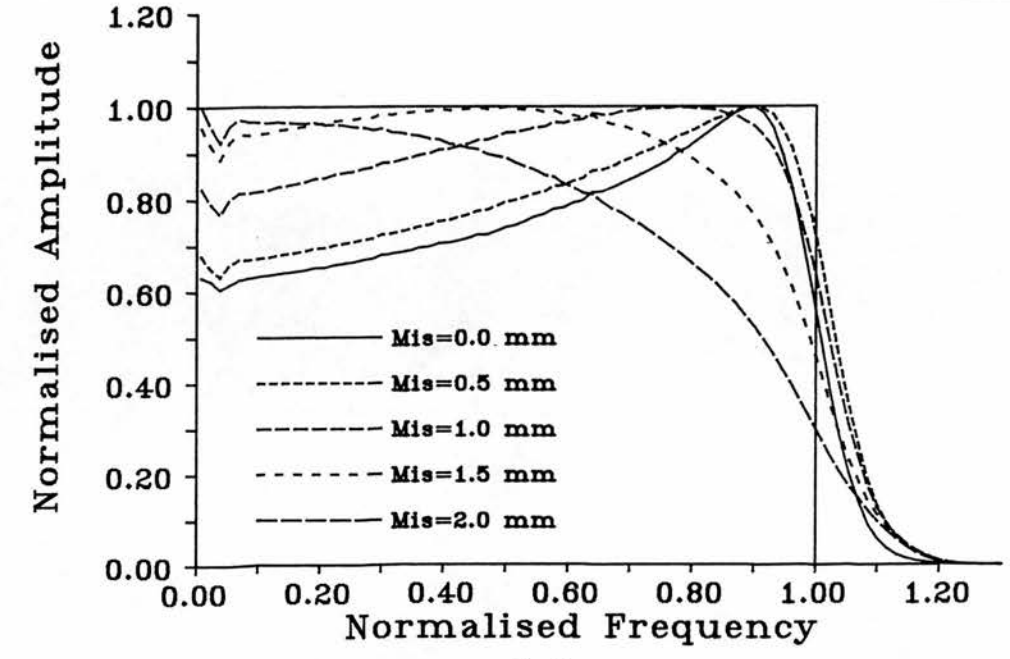


(a)

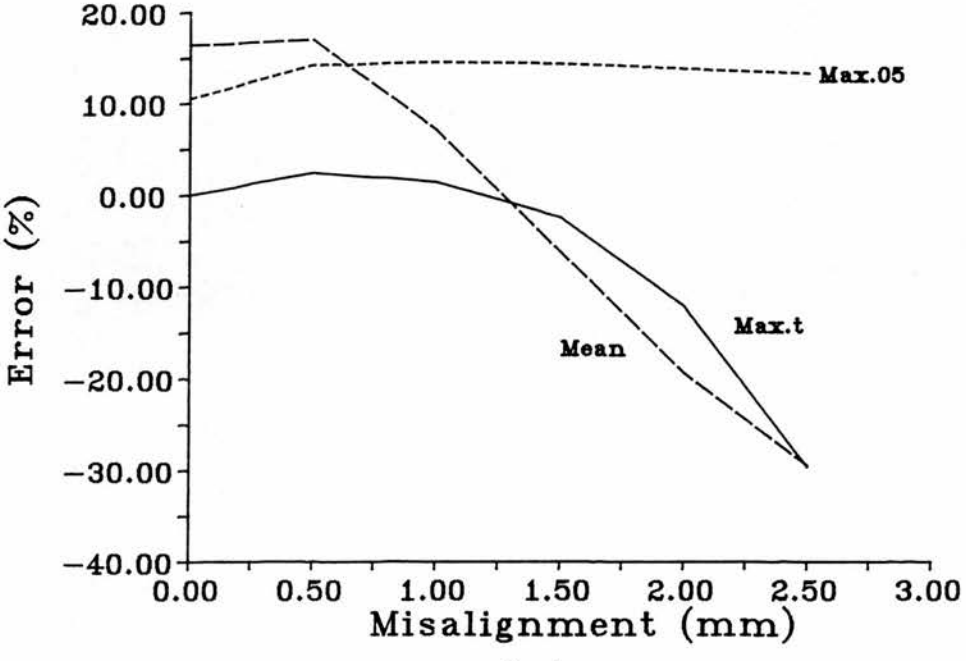


(b)

Figure 4.7: Effect of misalignment between transducer and vessel axis. The transducer is a 8 mm 5MHz circular transducer. The diameter of the vessel is 5.0 mm and beam-vessel angle is 60°. (a) Spectra with different misalignment. (b) Errors in the mean (mean), 5% threshold (max.05) and GSB maximum frequency (max.t) with different misalignment. Again GSB independent estimation shows low errors when the misalignment is smaller than ±1.5 mm. 5% threshold method give more than 10% error but it is not sensitive to misalignment.

region which has relatively low velocity. This reduces high frequency components and increases low frequency components. Therefore, both mean frequency and maximum frequency decrease.

Figure 4.7 (a) shows spectra from tubing of 5.0 mm in diameter. The transducer is an 8 mm unfocused circular transducer as described before. When the beam moves off axis, the low frequency components increase significantly. This causes the errors in the mean frequency to drop from 16.5% to -29.5% at an offset of 2.5 mm (Figure 4.7 (b)).

The high frequency components changes not as significantly as the low frequency components. Consequently, the overestimation of the maximum frequency using the 5% threshold method are constantly about 13%. The GSB independent maximum frequency estimation has errors less than 2.5% if the misalignment is less than 1.5 mm. When the misalignment is larger, the underestimation increases considerably to above 10%.

### 4.3.5 Size of transducer

Studies on the effect of the size of transducer on the mean frequency in the literature (Evans, D.H. 1985; Cobbold *et al.*, 1983) assumed a square, cylindrical or Gaussian beam profile; which is idealised. Under such an assumption, the effect of the size of the transducer is determined by the relative size of transducer and vessel.

However, in practice, the situation is not so simple. The transducer size and the ultrasound wavelength determine the beam profile. In general, a very small transducer of relatively low frequency, say 2 mm diameter and 5 MHz, produces a very wide beam rather than a narrow beam. This gives a uniform insonation of the vessel. However, the geometrical spectral broadening may be significant due to the wide range of angle available. The beam width of a medium transducer may be similar to its diameter. This results in non-uniform insonation at the edge of the vessel which is similar to the findings described by Evans, D.H. (1985) and Bascom and Cobbold (1990). An even larger transducer insonated the vessel in

its near field which is highly complicated. The spectrum in the near field may not be easily predicted.

Figure 4.8 (a) illustrates a typical example. The transducers used are 5 MHz unfocused circular transducers of different diameter. A small transducer of 2 mm in diameter gives a near-ideal spectrum. Transducers of 4 mm to 8 mm in diameter produce spectra with losses in low frequency components because of the circular beam shape. A large 10 mm transducer gives again a near-ideal spectrum, and 12 mm and 16 mm transducers cause some loss in high frequency components which is due to the irregular beam patterns. The changes in the spectra result in a large variation in errors of the mean frequency. The mean frequency can be overestimated by 16.5% or underestimated by about 19.5%.

On the other hand, the high frequency components do not change very much. Apart from 12 mm and 16 mm transducers which are very large, the maximum frequency are very similar. The 5% threshold maximum frequency has errors from 8.0% to 19.2%. The errors in GSB independent maximum frequency are only -1.2% to 0.6% when the diameter of the transducer is smaller than 10 mm.

### 4.3.6 Vessel size

Vessel size determines the region of a vessel insonated by an ultrasonic beam. A small vessel is more likely to be uniformly insonated. For large vessels, only a part of the vessel, which is usually the central area, is strongly insonated. The region near the edges of the vessel, which contains flow with low velocity may not be uniformly insonated and this results in loss in low frequency components. By using a square beam, Evans, D.H. (1985) concluded that when the ratio of beam width and vessel diameter ($\tau$) decreases, the error in mean frequency at first rapidly increases and then levels off. For small vessels ($\tau < 0.25$), the mean frequency is overestimated by a more or less constant amount of 30%-33%.

The spectra from vessels of different size are shown in Figure 4.9 (a) and Figure 4.9 (b). An 8 mm unfocused circular transducer was used in the simulation. Small vessels obtain almost uniform insonation so the spectra are near to ideal. The low

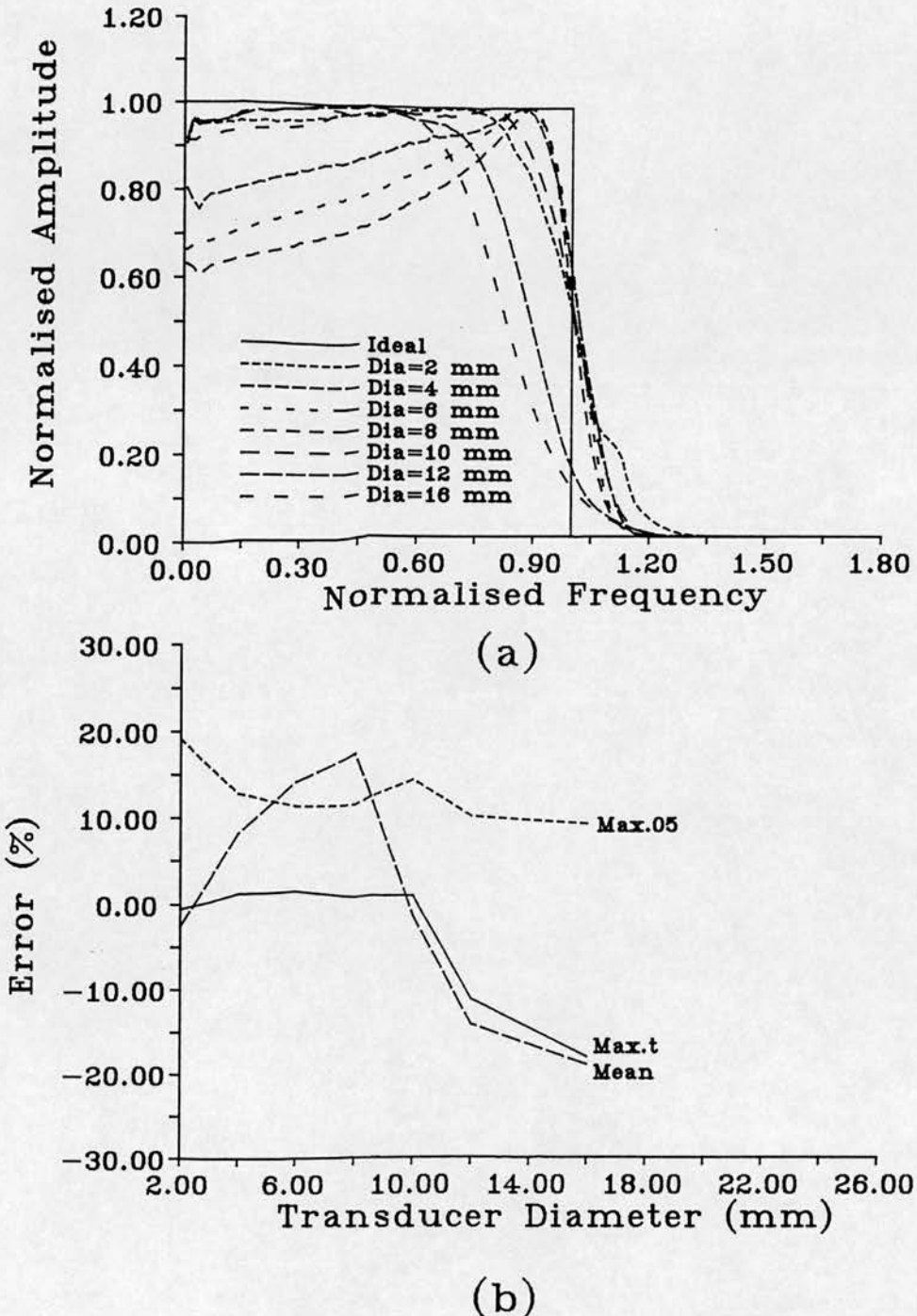


Figure 4.8: Effect of transducer size. Transducers are 5 MHz circular transducers with different diameters and the distance between transducers and vessel is 5 cm. The beam-vessel angle is 60°. (a) Spectra from transducers of different sizes. (b) Errors in mean (mean), 5% threshold (max.05) and GSB independent maximum frequency (max.t) with transducers of different size. When diameter of a transducer is larger than 12 mm, the vessel is in the complex near field of the transducer and the shape of the spectra become more difficult to predict. Again GSB independent estimation shows low errors in far field.

frequency components decrease with vessel size. The mean frequencies of these spectra are illustrated in Figure 4.9. The error is only -1.3% when a 1 mm small vessel is used. This error increases with the size of the vessel and levels off at about 27% when the diameter of the vessel is larger than 13 mm. Therefore, for a realistic beam, the conclusion drawn by Evans, D.H. (1985) is still valid, although the error is about 27% rather than 33%. This may have some practical value for very large vessels despite the fact that there may be difficulties in finding the vessel centre.

The maximum frequency is not dependent on the vessel size. This is because for a well aligned vessel, the centre part of the vessel is always strongly insonated. The errors for the 5% threshold maximum frequency stays constant at about 11%. The GSB independent maximum frequency again has very small errors (less than 1.75%).

### 4.3.7 Reflection at the vessel wall

In Chapter 2 and Chapter 3, the reflection at artificial vessel walls has been discussed. It is shown that the reflection can cause significant distortion to the spectra from flow phantoms. However, In humans, the acoustic properties of the surrounding tissues, blood vessel and blood are very similar. The sound speed of a blood vessel is lower than the surrounding tissue so that no total reflection occurs. Therefore, the influence of the wall reflection could be very small.

In clinical situations, the real blood vessel may be more complicated than the three media model described previously. Histological studies have shown that the arterial wall is composed of intima, internal elastic lamina, media, external elastic lamina and adventitia. Veins are usually less echoic than the muscular arteries. Therefore the acoustic properties of aorta was used in this study to give an approximate limit to the distortion of Doppler spectrum. To simplify the problem, the reflection at the inner boundaries of blood vessel, such as intima, internal elastic lamina, external elastic laminal and adventitia are ignored as they are very small.

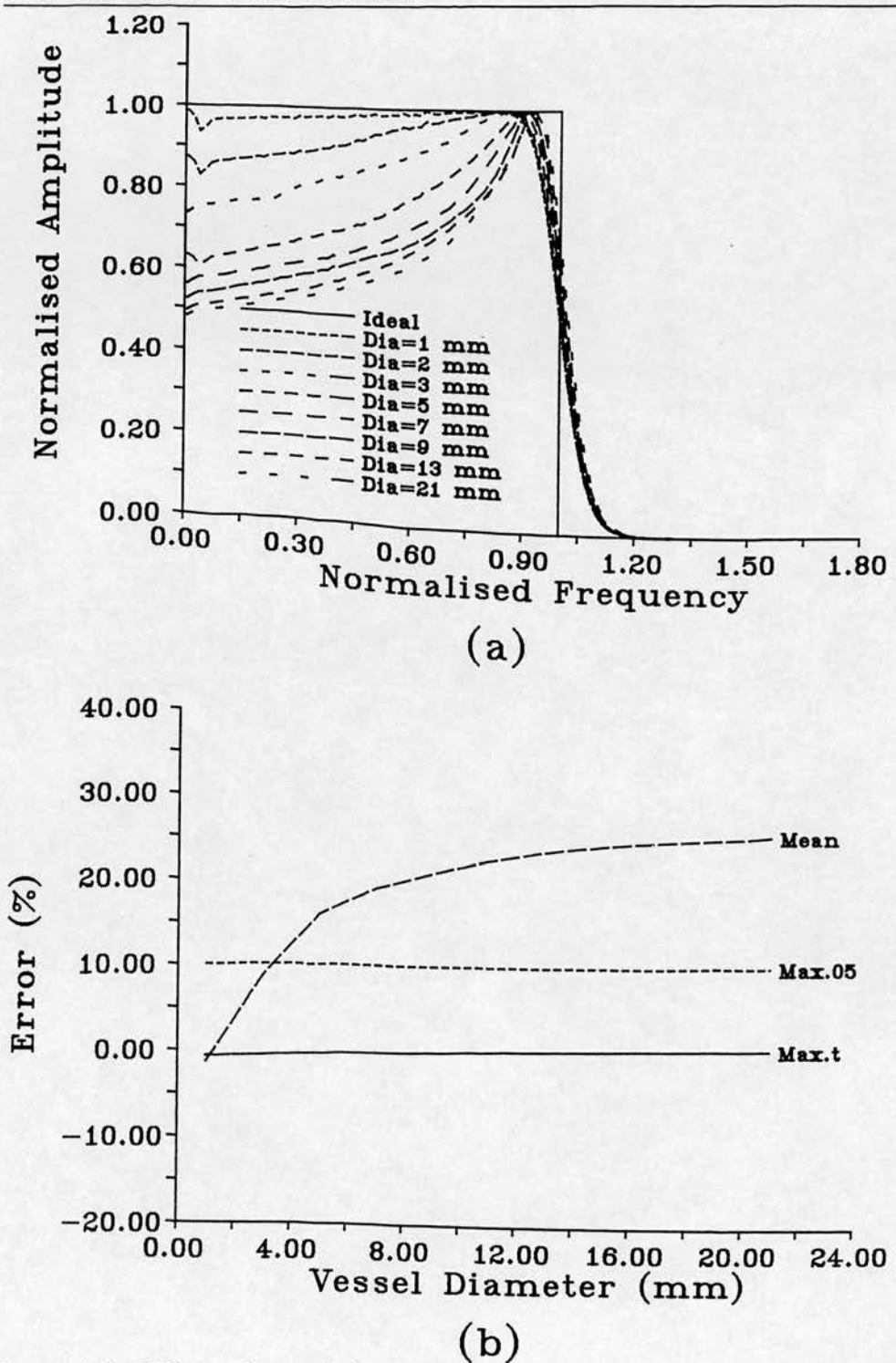


Figure 4.9: Effect of vessel size. The transducer is 5 MHz 8 mm transducer and the beam-vessel angle is 60°. (a) Spectra from vessels of different diameters. (b) Errors in the mean (mean), 5% threshold (max.05) and GSB independent maximum frequencies (max.t). It is shown that the error in mean velocity estimation increases with the size of the vessel but become flat around 27%. The GSB independent estimation shows low errors.

| Tube | Density ($kg/m^3$) | C ($m/s$) | Z ($kg/s/m^2$) |
|---|---|---|---|
| Surrounding Tissue | 1091 | 1540 | $1.68 \times 10^6$ |
| Blood Vessel (aorta) | 1039 | 1501 | $1.56 \times 10^6$ |
| Blood | 1064 | 1560 | $1.66 \times 10^6$ |

Table 4.2: Some acoustic properties of surrounding tissue, blood vessel and blood used in the simulation.

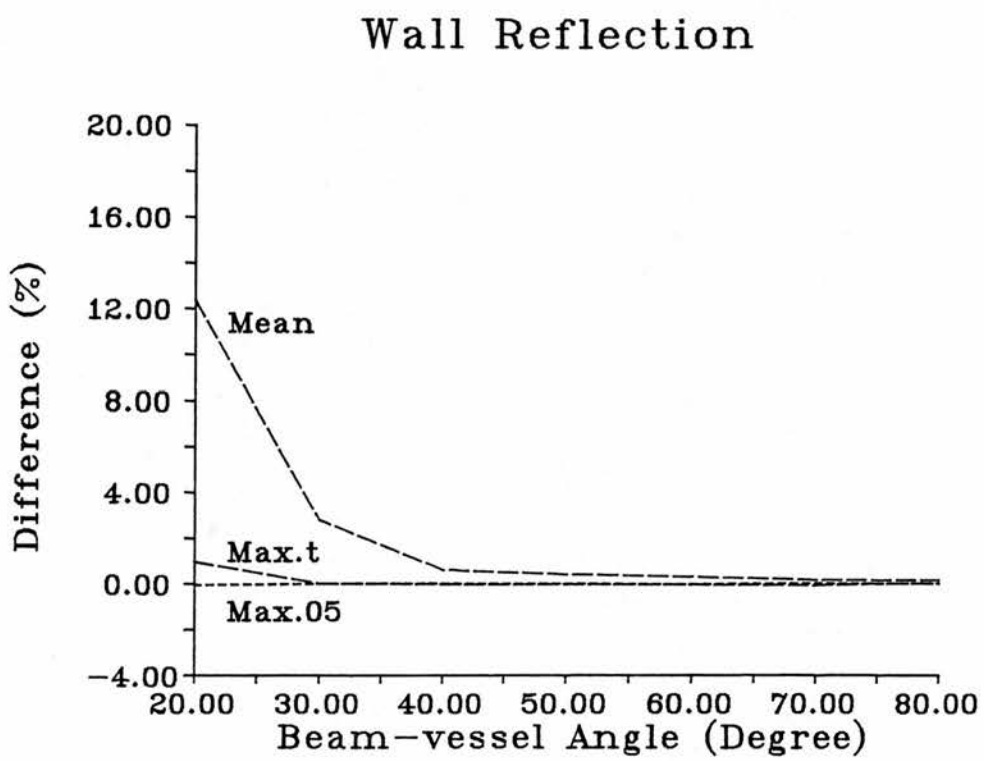


Figure 4.10: The reflection at the vessel wall gives less than 3% error in mean frequency measurement at angles larger than 30°. The effect of the reflection at the wall on the 5% threshold (max.05) and GSB independent maximum frequency (max.t) is smaller than 1%.

The transducer used is an 8 mm unfocused 4 MHz circular transducer. The acoustic properties of tissue, blood vessel and blood are listed in Table 4.2. Figure 4.10 gives the percentage difference between spectra with and without the reflection at wall in the mean, 5% maximum and GSB independent maximum frequency. For the maximum frequencies, the reflection at wall boundaries have almost no effect. For the mean frequency, except at angles smaller than 30°, the effect of the reflection is smaller than 3%.

The multi-layer structure of blood vessels may give slightly more reflection than estimated. However, as the acoustic properties of these layer are very similar and the reflectivity of these structures on ultrasonic images are much lower than the media of the vessel, these structures should introduce little difference. Therefore it can be concluded that the reflection on a real blood vessel does not have a significant effect on Doppler measurement as long as the beam-vessel angle is larger than 30°.

### 4.3.8 Velocity profile

In the above discussion, it is assumed that the velocity profile is parabolic. To establish a parabolic profile, a long straight and non-branching vessel is required. In practice, this condition is often not satisfied. In general, the time averaged velocity profiles fall somewhere between parabolic and flat. The velocity of particles $v(t)$ at distance $r$ to the vessel axis can be described by

$$v(r) = v(0)\left[1 - \left(\frac{r}{R}\right)^{\mu}\right] \tag{4.3}$$

where $v(0)$ is the maximum velocity at the centre of a vessel, $R$ the is diameter of the vessel and $\mu$ is the profile parameter. The flow profile is parabolic when $\mu = 2$. The profile is more flat when $\mu$ is larger so there are more particles moving at high velocity.

Figure 4.11 (a) gives spectra with different velocity profiles obtained from an 8 mm circular transducer. As expected, the spectra move towards high frequency when $\mu$ is larger. However, the falling slopes are very similar among these spectra.

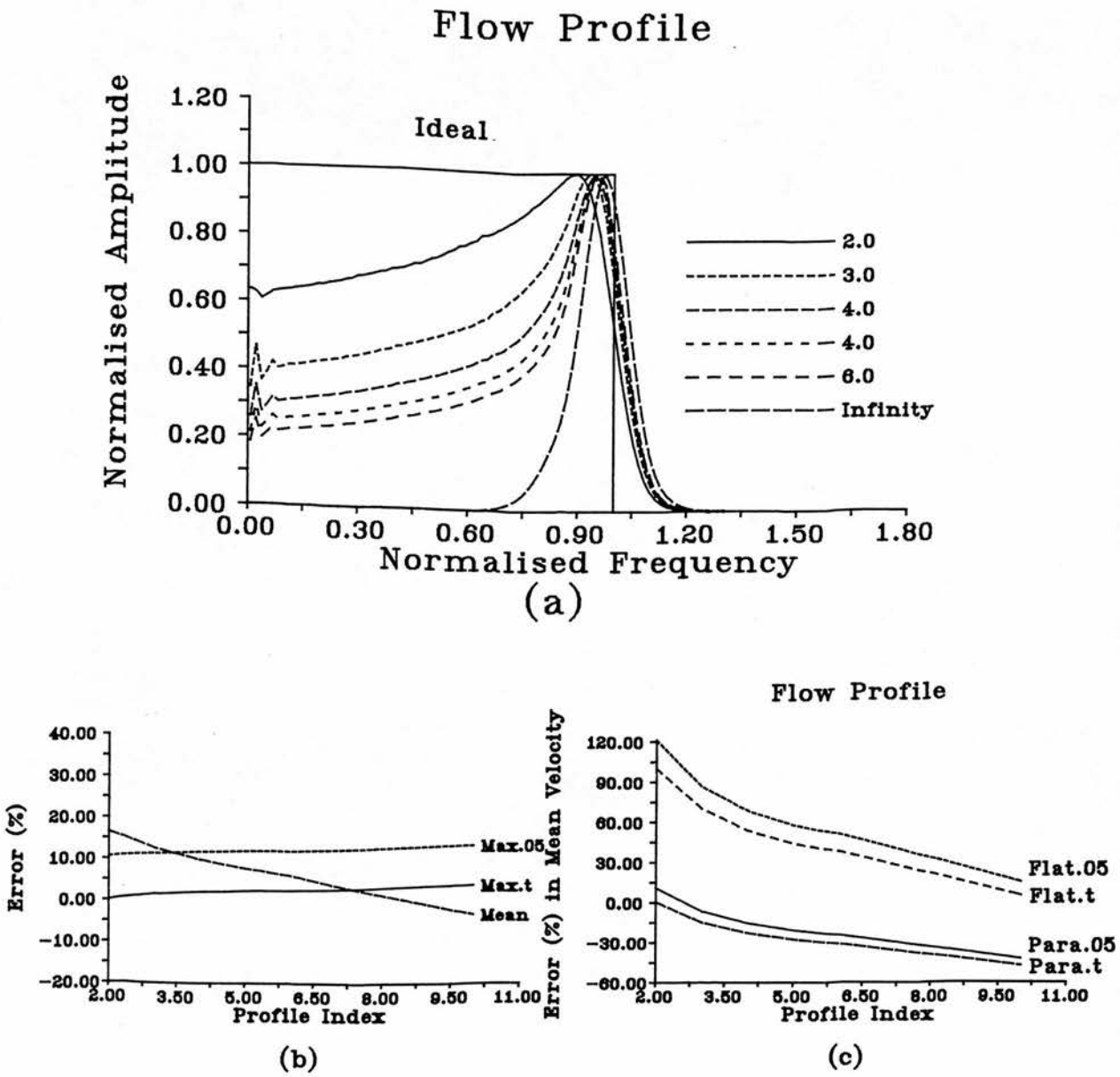


Figure 4.11: Effect of flow profile. (a) Spectra from flow with different flow profile parameters. (b) Errors in mean and maximum frequencies. (c) Errors in the estimated mean velocity using 5% threshold frequency (max.05) and GSB independent threshold frequency (max.t) when the flow profile is assumed as flat or parabolic but actually in between.

The ideal mean frequency of the spectrum from flow with profile parameter $\mu$ can be estimated by

$$\begin{aligned} V_{mean} &= \frac{\int_0^R 2\pi r v(0)\,[1-(\frac{r}{R})^{\mu}]\,dr}{\pi r^2} \\ &= \frac{\mu}{\mu+2} \end{aligned} \tag{4.4}$$

Comparing with the simulation, the mean errors decline for larger value of $\mu$ (Figure 4.11 (b)). This can be explained by the fact that the velocity is more uniform for a higher value of $\mu$, so partial insonation results in less overestimation of the mean frequency when the velocity is flatter. For maximum frequency, both the 5% and GSB independent threshold maximum frequency are not sensitive to the velocity profile. The errors in 5% maximum frequency are about 12% while in GSB independent frequency are around only 2%.

In clinical practice, it is often assumed that the flow profile is flat (for example in the aorta) or parabolic (in veins and some arteries). If the maximum frequency is used in the estimation of mean velocity, errors are introduced. Figure 4.11 (c) gives the errors of mean velocity estimation when a parabolic or a flat profile is assumed while the true profile is in between. It can be seen that the errors can be very large indeed.

## 4.4 Two Clinical Situations

In this section, two clinical situations are simulated and analyzed. The vessels were chosen to be umbilical vein and common carotid artery, where volume flow measurements are often made clinically. Both a single crystal circular transducer and a linear array are used. The circular transducer is a 10 mm 3.5 MHz focused transducer. The linear array is a 5.0 MHz probe. The size of the region of active elements on the transducer face is assumed to be 2.0×1.0 cm.

The measuring conditions are listed in Table 4.3. These conditions are selected from experience in clinical measurements of these vessels. It is noted that different focal lengths are chosen for each situation.

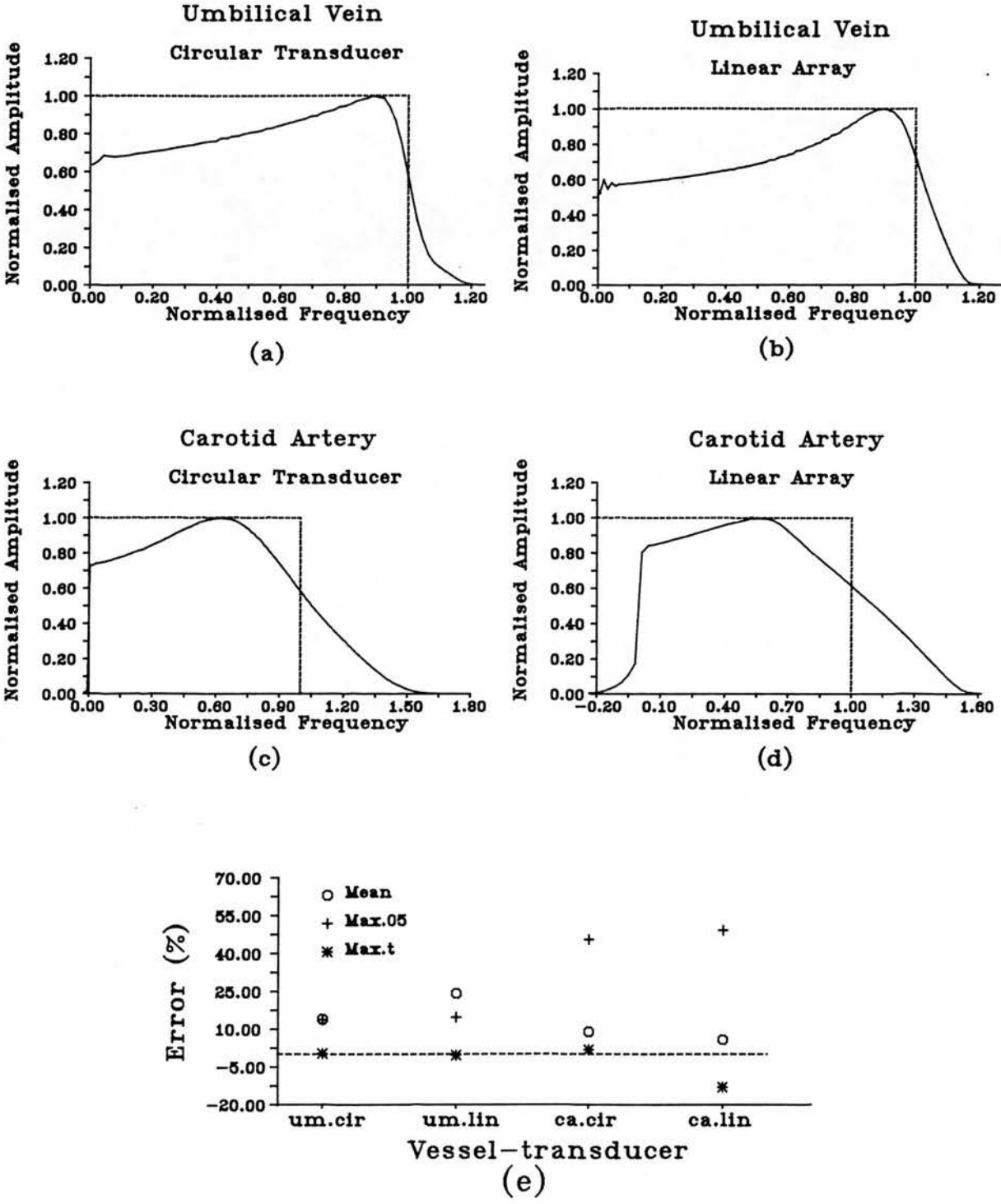


Figure 4.12: Clinical situations. (a) Spectrum from umbilical vein measured by a circular transducer (5 MHz, 8 mm). (b) Spectrum from umbilical vein measured by a linear array (5 MHz, 2 cm × 1 cm). (c) Spectrum from carotid artery measured by a circular transducer (d) Spectrum from carotid artery measured by a linear array. (e) Errors in the mean, 5% and GSB independent maximum frequency.

| Vessel and Transducer | Umbilical Vein Circular | Umbilical Vein Linear Array | Carotid Artery Circular | Carotid Artery Linear Array |
|---|---|---|---|---|
| Vessel Size (mm) | 5.0 | 5.0 | 8.0 | 8.0 |
| Depth (cm) | 8.0 | 8.0 | 1.7 | 1.7 |
| Angle (degree) | 60 | 60 | 60 | 60 |
| Focal Length (cm) | 8.0 | 3.0 | 8.0 (L), 7.0 (S) | 1.7 (L) 3.0 (S) |

Table 4.3: Measuring Conditions of the umbilical vein and carotid artery. (L) and (S) denote the focal length along the long and short axis of the transducer.

The results are shown in Figure 4.12. For the mean velocity measurement, the error varies from 5% to 24%. The measurements on the carotid artery, which is near to the transducers, gives relatively small error of 5% and 8%. In the measurement on the carotid artery, as the vessel is near to transducers, the geometrical spectral broadening gives over 45% of error in the 5% maximum frequency. The GSB independent maximum frequency gives the best overall accuracy. The carotid artery measurement using the linear array gives 13% error. Errors in the GSB independent maximum frequency in the other 3 situations are less than 2%.

## 4.5 Discussion

The errors using mean, maximum frequency and a high GSB threshold maximum frequency were estimated in this chapter. The GSB threshold maximum frequency showed very small errors under a range of conditions and can possibly be used to reduce errors in the maximum frequency estimation. However, it must be noted that this is achieved by analysing underlying spectra. In practice, Doppler spectra have fluctuations due to scattering processes and it is difficult to obtain an underlying spectrum. When the flow rate is constant, it is possible to calculate the underlying spectrum by averaging a number of spectra. If the flow is pulsatile, this becomes more difficult. One possible method is to average spectra at the same phase in the cardiac cycle. Another possible way to do it is using filtering techniques (Hoskins *et al.*, 1990) which use image processing methods to reduce speckle in Doppler spectra. None of these methods are examined and therefore further work is necessary before this new threshold can be applied. However, this

shows that the error in maximum velocity estimation can be reduced by moving to a higher amplitude threshold than those currently being used. For example, in practice, the 7/8 percentile method, which has higher amplitude threshold, may give lower error than the 15/16 percentile method.

## 4.6 Conclusion

In this chapter, spectra and errors in both the mean and maximum frequency in various measuring conditions have been studied. The effect of each parameter has been demonstrated and it is felt that such a numerical simulation can help to reduce the error in clinical measurement. In general, it is found that the mean frequency is particularly sensitive to the variation of these conditions. As conditions in clinical measurement are usually not well known, an accurate estimation of the mean frequency could be difficult unless the device is specifically designed for volume flow measurement. The maximum frequency is much less sensitive to the conditions. The major factor to affect maximum frequency estimation is geometrical spectral broadening.

A new method which is called as the GSB independent threshold method, was suggested in this chapter to make the estimation of maximum frequency independent of the geometrical spectral broadening. It is found this new estimator gives very small errors for different conditions and is particularly insensitive to most of the factors. However, further work is necessary before this method can be applied to clinical measurement.

The errors in the mean and maximum velocity measurement in two clinical situations were analyzed. It is demonstrated that significant error in the velocity measurement can be found in clinical situations. The numerical analysis of the spectrum may be used to reduce the errors.

# Chapter 5

# INTRINSIC SPECTRAL BROADENING

## 5.1 Introduction

Many modern duplex systems use the same transducer for both imaging and Doppler. For imaging, the transducer needs to have a wide aperture to make the beam highly focused to increase the resolution. However, it is known that a wide transducer aperture and narrow beam, especially when the sample volume is in the near field, can give very significant geometrical spectral broadening and transit time spectral broadening. It was found that when the beam is moved across the face of a linear array, the measured maximum frequency can change up to about 40% due to the spectral broadening (Hoskins *et al.*, 1992). It was estimated that the transit time spectral broadening is of the order of the inverse of the time taken for the scatterer to pass across the beam but more precise calculation is difficult. It was suggested that the geometrical spectral broadening and transit time spectral broadening are the same effect and should not be added to obtain the total broadening (Newhouse *et al.*, 1980). This implies that the maximum frequency can be always estimated by the extreme angles through the beam. However, as will be explained in this chapter, a wider beam has wider extreme angles than a narrower beam, so it should produce more significant geometrical spectral broadening but less significant transit time spectral broadening than the narrower beam.

This conflicts with the conclusion that the geometrical and transit time spectral broadening are the same effect. Therefore, it is necessary to reconsider whether geometrical and transit time spectral broadening are actually the same.

In this chapter, three problems associated with the spectral broadening will be considered. They are:

- Are the geometrical spectral broadening and transit time spectral broadening identical?
- Can we always use extreme angle (Newhouse *et al.*, 1980) to calculate the maximum frequency?
- How reliable is it to use a linear array to measure Doppler maximum frequency?

## 5.2 Intrinsic Spectral Broadening

### 5.2.1 Background

In the ultrasound literature, the effect of beam geometry on the output spectrum has been attributed to two effects. The first relates the output signal bandwidth to the transit time of a scatterer crossing the beam (Varner *et al.*, 1975; Griffith *et al.*, 1976)). When the scatterer passes through a beam, the strength of the backscattered signal is modulated by the beam intensity. Therefore, the signal has a broadened bandwidth. The bandwidth is inversely proportional to $t_r$, which is the time taken for the scatterer to pass across the beam. The second is called geometrical spectral broadening based on the fact that a scatterer in the beam can both receive rays from the transducer and backscatter them to the transducer over a range of angles (Newhouse *et al.*, 1977, 1980, Censor *et al.* 1988; Bascom *et al.*, 1986).

It was found that transit time broadening and geometrical broadening were already known in the laser flow measurement literature as "Doppler radar ambi-

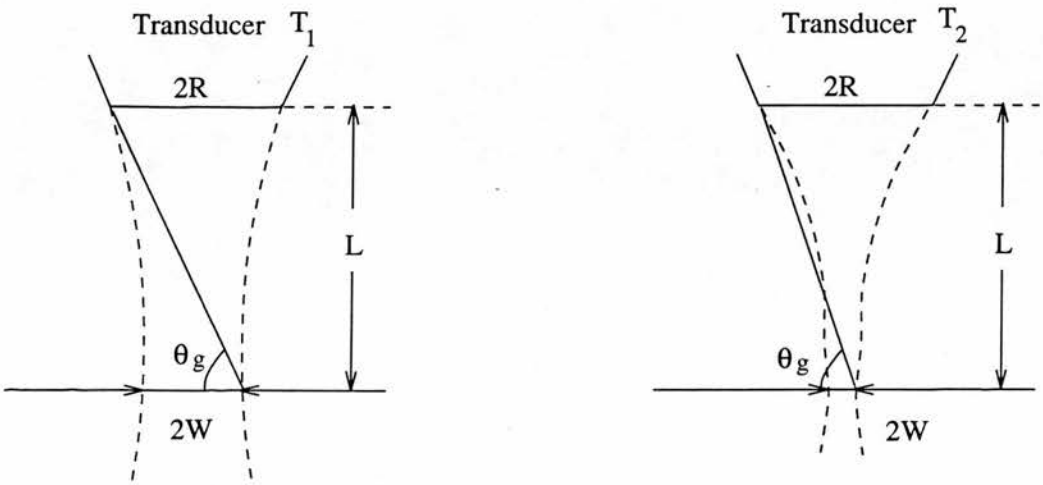


Figure 5.1: The transducer with wider beam provides wider range of Doppler angles than a transducer with a narrow beam. This produces a more significant geometrical spectral broadening but less significant transit time spectral broadening for the transducer with wider beam than the one with narrower beam.

guity" and "wave vector ambiguity" respectively. Edwards *et al.* (1971) gave a theoretical approach and suggested that these two effects are actually the same. This situation was followed by a Gedanken experiment (the details of the experiment will be described later) which suggests that the ultrasound Doppler output bandwidth can be calculated from either both the amplitude profile of the beam and the range of Doppler angles available to the transducer, or solely the range of angles available to the transducer. Based on these papers, Newhouse *et al.* (1980) suggested even in the complicated near field of an ultrasonic transducer, the transit time spectral broadening and geometrical spectral broadening are still identical. It was shown experimentally that the bandwidth of ultrasound Doppler spectra can be estimated by the extreme angles through the focused beam waist.

However, conflicts still remain. Suppose we have two transducer $T_1$ and $T_2$ with the same diameter and frequency. Transducer $T_1$ is unfocused and the $T_2$ focuses on the focal length $L$ (Figure 5.1). At the focal distance, transducer $T_1$

should produce a wider ultrasonic field than $T_2$. Consequently, the transit time for $T_1$ is larger than that for $T_2$ and the transit time spectral broadening for $T_1$ is smaller than that for $T_2$. However, if the geometrical spectral broadening is considered, the range of possible angles $180° - 2\theta_g$ for the wider beam is larger than that for narrow beam. This means for transducer $T_1$, geometrical broadening should be more significant than that for $T_2$. The result certainly conflicts with the conclusion that the transit time spectral broadening and geometrical spectral broadening are identical.

It is also found that Fish (1986) gave a theoretical calculation of the Doppler spectrum in a particular case. Assuming that the beam sensitivity along a streamline is a Gaussian function,

$$G(x) = A_g e^{-x^2/2\sigma^2} \tag{5.1}$$

it was demonstrated that the spectrum has a Gaussian shape and the width is given by

$$2\sigma_1 = V\left(\frac{2}{\sigma^2} + 32a_1^2\sigma^2\right)^{\frac{1}{2}} \tag{5.2}$$

The first term in the brackets determines the transit-time broadening and second term the wave vector spread broadening. This also indicates that the transit time and geometrical spectral broadening are not the same. Therefore, it is necessary to reconsider the Edwards' theory and the Gedanken experiment.

### 5.2.2 Transit time and geometrical spectral broadening

To understand the two spectral broadenings, it is necessary to take a close look at what happens when a particle passes through an ultrasonic field (Figure 5.2). Firstly, if the variation in wave vector orientation is negligible, *ie.* the angle between the direction of travel for the particle $\mathbf{v}$ and wave vector $\mathbf{k}$ is constant, the signal received is a single frequency signal, whose amplitude is modulated by the sensitivity pattern. So the spectrum of the signal is symmetrical about the wave frequency $\omega_0$ and has a width inversely proportional to the width of the beam for a given velocity. This broadening of the spectrum as the beam narrows is known as transit-time broadening (Newhouse *et al.*, 1976). If the beam is wide and

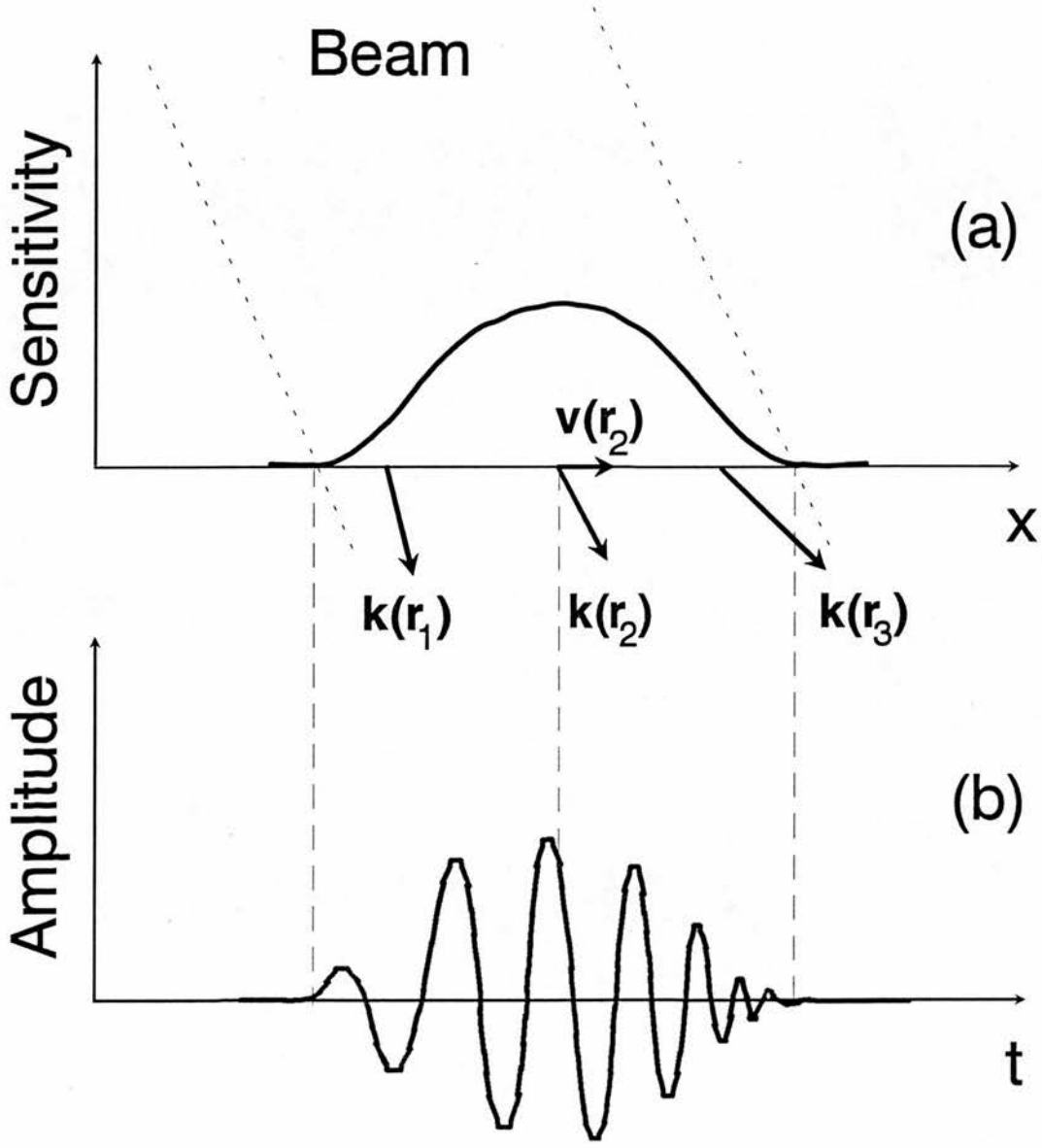


Figure 5.2: The Doppler signal obtained from a single scatterer moving along a streamline with velocity **v**. (a) Beam/scatterer geometry. The variation in the beam sensitivity and the wave vector. (b) The Doppler signal obtained from the scatterer as it passes along the streamline. Note that the amplitude of the signal is decided by the sensitivity and the frequency increases as the angle between **k** and **v** decreases.

the transit time broadening is negligible, the changes in the wave vector across the beam gives a frequency modulation of the signal. The Doppler frequency shift obtained from the scatterer changes as it passes along the streamline. The frequency increases as the angle between $\mathbf{k}$ and $\mathbf{v}$ decreases (Figure 5.2). This is known as wave vector spread or geometrical spectral broadening. It is noticed that this effect does not take the frequency spreading due to amplitude modulation into account and the spectrum is not symmetrical with respect to $\omega_0$ unless the particle travels perpendicularly to the beam axis. In practice, both the amplitude and wave vector $\mathbf{k}$ change along the path of the particle and this gives a combined effect on the spectrum.

As the following discussion is concerned about decomposition of a realistic field into a set of plane waves through Fourier transform, a brief discussion is given here about the decomposition. It must be noted that there are two kinds of decomposition of a field. The first is decomposition of the amplitude or intensity patterns by Fourier transform which is known as spatial Fourier transform. As the wave propagation direction is ignored, only the amplitude modulation of the signal is taken into account. However it must be remembered that this decomposed field is not equivalent to the original field and only their intensity patterns match to each other. Theoretically it is possible to do another decomposition which is done by decomposing the field in vector space (Miller, 1986). In this case, the decomposed field is equivalent to the original field. However, as both the amplitude modulation and wave propagation direction are taken into account, both transit time and geometrical spectral broadening are also taken into account. Therefore, the transit time and geometrical spectral broadening can not be separated by this decomposition. It must be noted that for a given field, the spatial Fourier transform will give an equivalent intensity or amplitude pattern. The full decomposition will give the same intensity pattern, as well as a wave front which is equivalent to the original field.

### 5.2.3 Edwards' approach

Edwards' *et al.* (1971) stated that they had proven that the transit time and geometrical spectral broadening were the same effect. This theoretical approach is briefly described as follows.

In a laser plane wave field, assume laser radiation of a single frequency $\omega_0$ is incident onto a set of scatterers within the fluid. The phase of the incident radiation is arbitrary and may be taken equal to zero. The field scattered onto the detector is given by summing the contributions from all scattering centres, *i.e.*,

$$E(\mathbf{K},t) = c_0 \sum_n e^{i\mathbf{K}\cdot(\hat{\mathbf{r}}_n(t)+\mathbf{L})} e^{-i\omega_0 t} P[\hat{\mathbf{r}}_n(t)+\mathbf{L}] \tag{5.3}$$

where $\mathbf{K}$ is the wave vector, the constant $c_0$ contains terms describing the average intensity of the scattered light and $\mathbf{L}$ is the distance from the photomultiplier tube to the centre of the sample volume.

It was shown by Edwards that the spectrum of the scattered field is

$$S(\mathbf{K},\omega) = \int_0^\infty R_{ii}(\mathbf{K},\tau) e^{-i\omega\tau} d\omega \tag{5.4}$$

where $R_{ii}(\mathbf{K},\tau)$ is the autocorrelation function of the scattered field which is given by

$$\begin{aligned} R_{ii}(\mathbf{K},\tau) \;=\; & c_0 \rho Re[e^{i w_0 \tau}] \int_{-\infty}^{\infty} G(\Delta\mathbf{r},\tau) e^{-i\mathbf{K}\cdot\Delta\mathbf{r}} \\ & \int_{-\infty}^{\infty} e^{-i\mathbf{K}\cdot\Delta\tau} P[\mathbf{r}(0)] \cdot \\ & P[\mathbf{r}(0)+\Delta\mathbf{r}+\mathbf{v}\tau] d\mathbf{r}(0) d\Delta\mathbf{r} \end{aligned} \tag{5.5}$$

where $G(\Delta\mathbf{r},\tau)$ is space-time correlation function which is the probability per unit volume that the scattering centre has moved $\Delta\mathbf{r}_n$ during the time interval $\tau$, P(r) is the amplitude weighting function.

Therefore, the spectrum is uniquely determined by the velocity field, the space-time correlation function $G(\Delta\mathbf{r},\tau)$, and the function that describes the intensity of the light as a function of position $P(\mathbf{r})$.

Two ways to interpret $P(\mathbf{r})$ can be found in the literature. One points out that the incident and scattered vectors are uncertain to a degree determined by the optics and this gives rise to the spectral broadening. The second concerns itself with the fact that the scattering centres spend a finite time in the sample volume. Since the positions of the particles are uncorrelated, a broadening analogous to Doppler radar ambiguity is present.

If the beam is focused, the electric field in the region of the focus of a lens can be regarded as a superposition of plane waves of differing wave vector $\mathbf{k_1}$ and relative amplitude $\Psi_1(\mathbf{k_1} - \mathbf{k_i})$.

$$E_1(\mathbf{r}) = c_1 e^{i\mathbf{k_i}\cdot\mathbf{r}} \int \Psi_1(\mathbf{k_1} - \mathbf{k_i}) e^{-i\omega_0 t} e^{i(\mathbf{k_1}-\mathbf{k_i})\cdot\mathbf{r}} d\mathbf{k_1} \qquad (5.6)$$

where $\mathbf{k_i}$ is the wave vector of incident plane wave. The function $\Psi_1(\mathbf{r})$ is completely determined by the focusing lens and the amplitude distribution of light incident on the lens.

Similarly, for the reception, we have the sensitivity field

$$E_2(\mathbf{r}) = c_2 \int \Psi_2(\mathbf{k_2} - \mathbf{k_s}) e^{-i\omega_0 t} e^{i(\mathbf{k_2}-\mathbf{k_s})\cdot\mathbf{r}} d\mathbf{k_2} \qquad (5.7)$$

The total detected electric field $P(\mathbf{r})$ is the product of $E_1(\mathbf{r})$ and $E_2(\mathbf{r})$. It can be written that,

$$\begin{aligned} P(\mathbf{r}) &= E_1(\mathbf{r}) E_2(\mathbf{r}) \\ &= c \int \Psi_1(\mathbf{k_1} - \mathbf{k_i}) e^{i(\mathbf{k_1}-\mathbf{k_i})\cdot\mathbf{r}} d\mathbf{k_1} \cdot \\ &\quad \int \Psi_2(\mathbf{k_2} - \mathbf{k_s}) e^{i(\mathbf{k_2}-\mathbf{k_s})\cdot\mathbf{r}} d\mathbf{k_2} \end{aligned} \qquad (5.8)$$

It is noted that Equation ( 5.8) is a Fourier transform. As given in equation ( 5.3), a complete specification of the optics leads to a knowledge of a function $P(\mathbf{r})$ through Fourier transforms and vice versa.

Therefore, it was concluded that the field can be decomposed into plane waves from different directions, which gives the range of Doppler angles. The range of angle gives the geometrical spectral broadening.

> Therefore the geometrical spectral broadening and transit time spectral broadening are the same. Equation ( 5.8) also indicates that the specification of $P(\mathbf{r})$ completely determines the effect of the optics on the spectrum.

Several problems are found in this theory. Firstly, the theory states that the focused field can be decomposed into a number of plane waves propagating in a range of directions and this range of angle gives geometrical spectral broadening. However, it has not been shown that the range of angles of these plane waves is the same as the range of angles related to the geometrical spectral broadening, which can be estimated by the extreme angles available for transmitting and receiving. It will be shown in section 5.2.5 that they are different. Secondly, Equation ( 5.3) is driven from a plane wave assumption which assumes there is only one direction that waves propagate. The spectrum is uniquely determined by the velocity field, $G(\Delta\mathbf{r}, \tau)$ and intensity $P(\mathbf{r})$ only because no variation of the wave propagation direction is considered. In a field which has vector variations, the equation may be more complicated. Thirdly, Equation ( 5.6), ( 5.7) and ( 5.8) are not derived with an assumption that the wave propagation direction is constant. Therefore, $P(\mathbf{r})$ can be simply put into Equation ( 5.3) to prove that the spectrum is decided for known intensity patterns.

### 5.2.4 Gedanken experiment

Edwards' theory was followed by a Gedanken experiment which stated that the ultrasound Doppler output bandwidth can be calculated either in terms of the amplitude profile of the beam and the range of angles available for the radiation backscattered to the receiver, or solely in terms of the range of angles available to the incident and backscattered radiation (Newhouse *et al.*), 1980). The experiment is as follows:

> Suppose that one of two transducers at infinity illuminates the path of a single scatterer with plane waves of frequency $f_0$ at an angle $\alpha$ (Figure 5.3). The transducer then receives backscattered plane waves

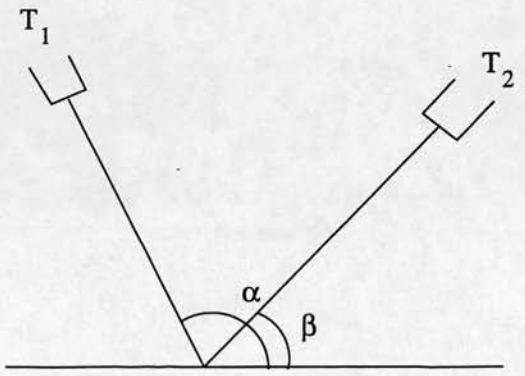


Figure 5.3: Two transducers operating at frequencies $f_0$ and $f_1$ simultaneously produce an ultrasonic field. The Doppler frequency can be calculated either from beam pattern of the field, or from the beam vessel angle $\alpha$ and $\beta$.

of frequency $f_0 - f_1$ where $f_1$ is proportional to $\cos\alpha$ and to the scatterer velocity. The first transducer is now turned off and the second transducer is set to illuminate the scatterer path at an angle $\beta$. Now a signal $f_0 - f_2$ is generated where $f_2$ is proportional to $\cos\beta$ and the scatterer velocity. When both transducers are operated simultaneously, their added output signals containing the frequencies $f_0 - f_1$, $f_0 - f_2$, and $f_0 - (f_1 + f_2)$ are received. The term $f_0 - (f_1 + f_2)$ is due to radiation emitted by one transducer and received by the other.

With the two transducers radiating simultaneously, an interference pattern is produced due to the combination of the two plane waves of incident radiation. As the particle travels through this pattern, backscattered amplitude modulated signals are radiated to the two transducers. These amplitude modulated signals when combined can be shown to consist of the same frequencies as those above. Thus there are two quite different ways of calculating the Doppler spectrum. Traditionally the spectrum bandwidth calculated from the particles'

> passage through the interference pattern has been attributed to transit time broadening; whereas the spectrum calculated from the range of angles available to the incident and backscattered radiation has been attributed to geometrical broadening. However, any beam intensity pattern can be built up from a series of plane waves. Thus the Doppler output bandwidth can either be calculated in terms of the intensity pattern traversed by the scatterer and the range of angles available to the incident and backscattered radiation, or solely in terms of the range of angles available to the incident and backscattered radiation.

The problem here is again a misunderstanding of decomposition of an ultrasonic field. It is correct that any beam intensity pattern can be built up from a set of plane waves. However, the set of plane waves which can compose the intensity pattern is not unique. If the set of plane waves only compose the intensity pattern but the wave vector spread is ignored, then this set of plane waves does not compose exactly the same field as the original field. Therefore, the Doppler frequency shifts in the two fields may be different. The so-called "geometrical spectral broadening" in the plane wave field may be different from the broadening in the original field so it can not be used to prove that the two broadenings are the same. One the other hand, if the set of plane waves forms a full decomposition, then both the transit time and geometrical broadening are considered in both the original field and the set of plane waves. Consequently the two spectral broadening are not separated and can not be compared.

### 5.2.5 Range of angle

To give evidence that the transit time and geometrical spectral broadening are different, beam amplitude patterns will be decomposed into plane waves and the range of angle for these plane waves will be calculated. This range of angle will be compared with the range of angles estimated by extreme angles from the transducer to sample volume.

Suppose a transducer produces a beam amplitude pattern $A(x)$ along the

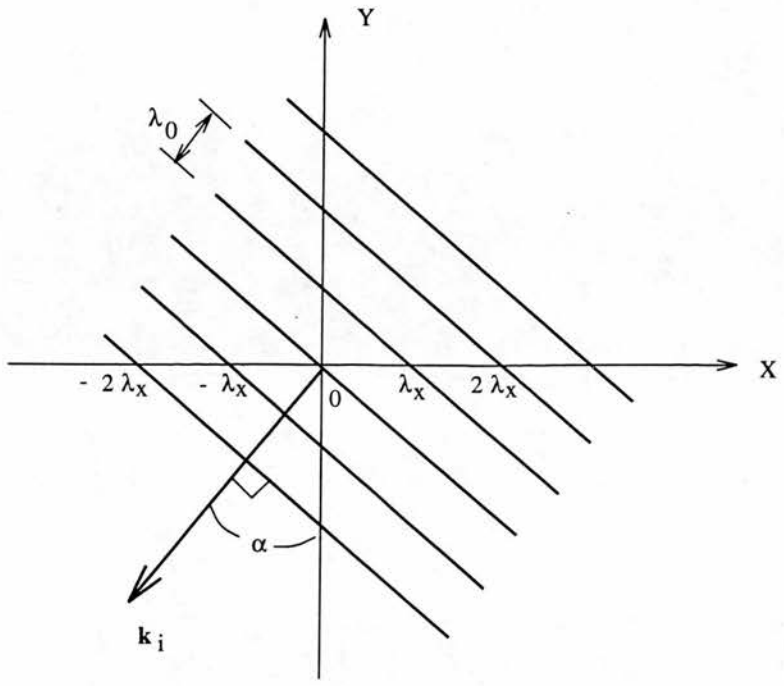


Figure 5.4: A standing wave on $x - axis$ can be composed by two cosine waves travelling at equal but opposite angles to the normal of the observation plane which is normal to Y-axis (the other cosine wave is not drawn for simplicity of the diagram). If the transmitted wavelength is known, the angle can be calculated.

$x - axis$ across a beam. This amplitude pattern can be decomposed by Fourier transform by

$$E(\nu_x) = \int_{-\infty}^{\infty} A(x) e^{-i\nu x} dx \tag{5.9}$$

where $\nu_x$ is the spatial frequency along the $x - axis$. The spatial Fourier transform decomposes the field into a series of spatial cosine functions with amplitude $E(\nu_x)$ and frequency $\nu_x$ along the $x - axis$. This function is actually a standing wave along the $x - axis$. Each cosine function is viewed as the interference pattern between two plane waves travelling at equal but opposite angles $\alpha$ to the normal of the observation plane which is normal to Y-axis (Figure 5.4). As shown in Figure 5.4, as we know the frequency of each plane waves $\lambda_0$[1], the angle between the propagation direction of each plane wave and the $x - axis$ can be calculated by

[1]A monochromatic field is assumed here

$$\sin\alpha = \frac{\lambda_x}{\lambda_0} \tag{5.10}$$

where $\lambda_x = c/\nu_x$ is the spatial wavelength of the resulting interference along the $x-axis$ and $c$ is the wave propagation speed (sound speed or light speed). For the reception field, the calculation should be the same. If the transducer transmits and receives signals using the same crystal, like most single crystal transducers in ultrasound, the transmission and reception field should be the same.

It is noticed that the spatial Fourier transform uses a set of two identical plane waves travelling at equal but opposite angles $\alpha$ to the normal of the observation plane. The wave vectors in the field always also point to the direction which is normal to the observation plane. This set of the plane waves composes a field with the same intensity pattern as the original field. However, there is no wave vector spread in this field. Therefore, by definition of the transit time spectral broadening, the plane wave field gives the same transit time spectral broadening as the original field. If the geometrical spectral broadening is the same as the transit time spectral broadening, the angle spreading in the plane wave travelling direction should be identical to the range of angle for transmission and reception of ultrasonic wave by the transducer, which can be estimated by extreme angles.

The range of angle available for transmission and reception can be calculated by the extreme angles from the transducer to the edges of the beam. Assuming the transducer is like a piston that every point on the transducer face vibrates at the same amplitude and phase, the amplitude $B(x)$ can be calculated from the integration on the transducer face by

$$B(x) = |\int \frac{1}{r} e^{(jkr-\tau_s)} ds_r| \tag{5.11}$$

where $r$ is the distance between one point on the transducer and the observation point $x$, $k = \omega_0/c$ is the wave number in the ultrasonic field and $\tau_s$ is the phase delay of ultrasonic waves from transducer for focusing. The 50% beam width $W$ then can be calculated and as shown in Figure 5.5 the extreme angle can be obtained by

$$\tan\theta_e = \frac{L}{W+R} \tag{5.12}$$

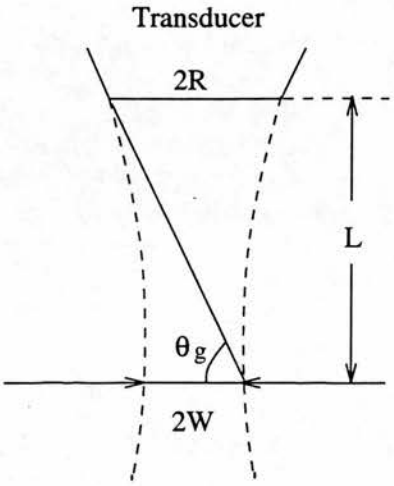


Figure 5.5: Extreme angles for the Doppler effect.

where $R$ is the radius of the transducer and $L$ is the distance between the transducer and sample volume. When the beam vessel angle is 90°, the range of angle for geometrical spectral broadening $\theta_g$ is given by

$$\theta_g = 90° - 2\theta_e \tag{5.13}$$

Therefore, the range of angle for the geometrical spectral broadening can be compared with the range of angle for the decomposed plane waves.

Figure 5.6 gives beam patterns (transmission field) of two transducers which are simulated by equation ( 5.11). The diameter of both transducers is 1.2 cm. The distances of the field planes and transducer faces are 5.0 cm and the beam vessel angle is assumed to be 90°. One transducer is unfocused while the other is strongly focused. It can be observed that the focused beam is narrower than the unfocused beam. The 50% beam-widths are 4.8 mm and 11.7 mm respectively. This gives the range of angles available for radiation as 19.1° for the focused transducer and 26.7° for the unfocused transducer. It must be noted that the range of angles available for an unfocused transducer is larger than that for a focused transducer.

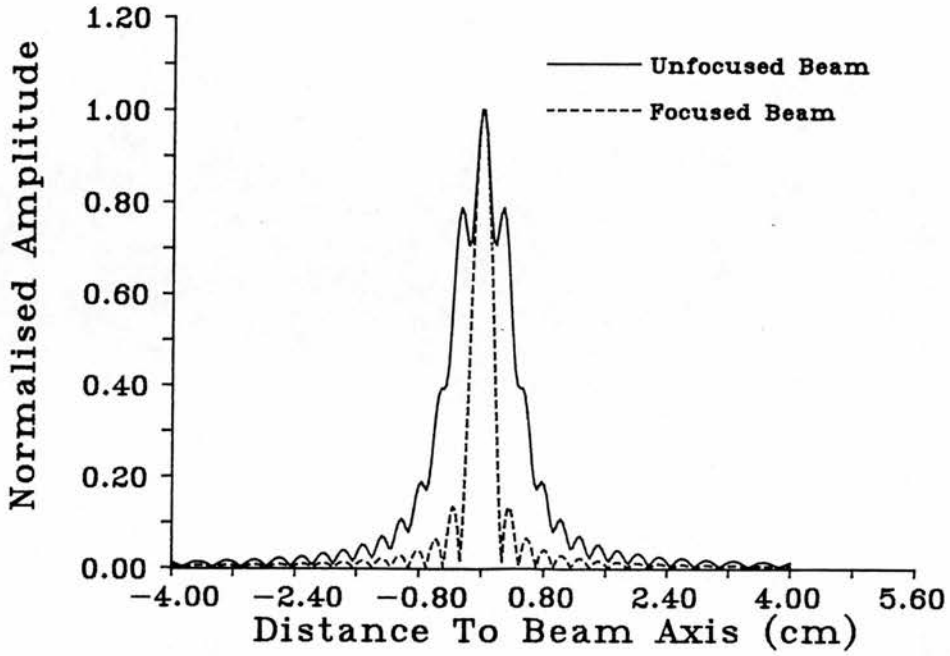


Figure 5.6: Beam patterns for a focused and an unfocused 12 mm circular transducer. It is noticed that focused beam is narrower so provides less range of angles.

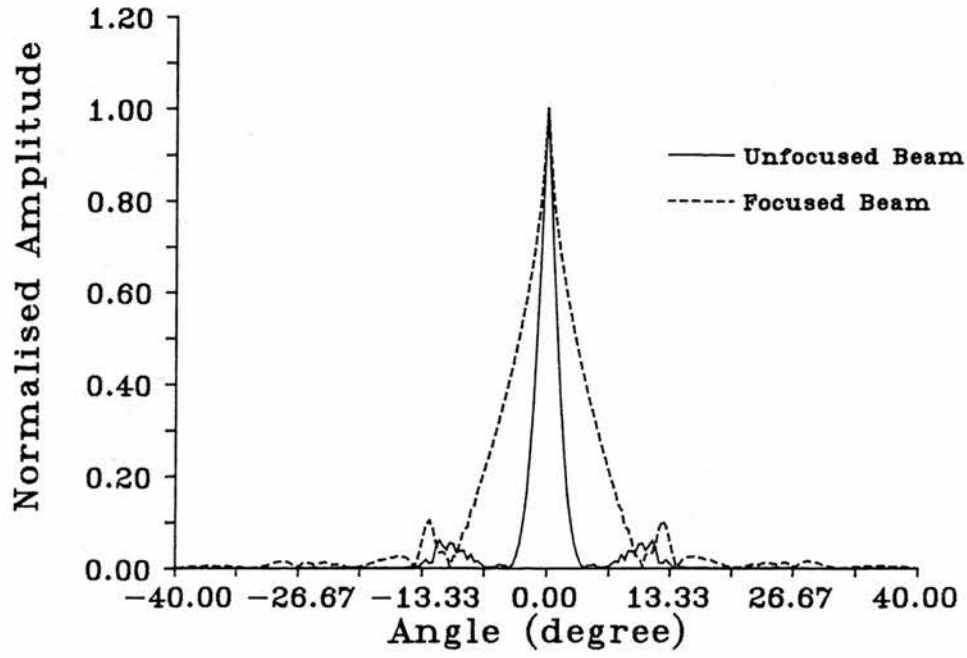


Figure 5.7: The amplitudes and propagation directions (expressed by angles) of plane waves decomposed from the beam patterns of Figure 5.6. It is noticed that focused beam has larger a range of angles. This conflicts with the results shown in Figure 5.6.

After the decomposition, the fields become a superposition of a number of plane waves. The relative amplitude and propagation direction (which is expressed by angles between propagation direction and the beam axis) are shown in Figure 5.7. The range of angles of the unfocused and focused transducer (defined as half amplitude width) are about 2.2° and 6.1° respectively. No direct relations between these angles and the angles available for radiation are observed. The focused beam has a wider range of angles than unfocused beam. As it has been shown geometrically that the range of angles for the unfocused transducer is larger than the focused transducer, this result certainly proves that the geometrical and transit time spectral broadening cannot be equivalent.

### 5.2.6 Relation between geometrical and transit time spectral broadening

As it has been proven that the geometrical and transit time spectral broadening are not identical, the relationship between them has to be reconsidered. When a particle passes through an ultrasonic beam, the amplitude of the field modulates the strength of the signal, which gives the transit time spectral broadening. Simultaneously the Doppler shift is decided by the particle/transducer geometry. Both processes together give the spectral broadening in the spectrum. So the transit time process is like a time (or spatial) window and the geometrical process is similar to a sophisticated frequency modulating (FM) system. In the time domain, the output $f(t)$ of the whole system is the multiplication of the two processes which can be described by

$$f(t) = w(t) \cdot g(t) \tag{5.14}$$

where $w(t)$ is the time window and $g(t)$ is the signal which contains frequency components resulting from the geometrical spectral broadening. The equivalent Equation ( 5.14) in the frequency domain is given by

$$F(\omega) = W(\omega) * G(\omega) \tag{5.15}$$

where $*$ denotes convolution, $W(\omega)$ is the spectrum of the window $g(t)$, $G(\omega)$ is the spectrum which describes the frequency spreading due to geometrical spectral

broadening. Therefore, the whole spectral broadening is the convolution of the geometrical spectral broadening and transit-time spectral broadening.

### 5.2.7 The magnitudes of spectral broadenings

As convolution always increases the width of the spectrum, the bandwidth of $F(\omega)$ in Equation ( 5.15) should not be smaller than the bandwidth of both $W(\omega)$ and $G(\omega)$. However, experiment (Newhouse *et al.*, 1980) has shown that the width of the spectrum can be well estimated by the extreme angles. It is also shown in Chapter 3 that the Doppler spectrum can be simulated by a theoretical model which is basically a geometrical approach. This agreement between experiment and theory seems to suggest that the transit time spectral broadening is not as significant as the geometrical spectral broadening. In some situations, the transit time broadening may be small and it may therefore be possible to ignore it.

To compare the significance of the spectral broadenings, the beams of circular transducers of diameters from 4 mm to 28 mm were simulated. All the transducers were assumed to be strongly focused. This was achieved by setting the phase delay $\tau_s$ for every point on the transducer face so that the wave from every point arrives at the centre of the sample volume in phase. In such a situation, the delay $\tau_s$ in equation ( 5.11) is given by (see section 3.4.2),

$$\tau_s = \frac{2\pi f_0}{C}(\sqrt{D^2 + X_s^2} - D) \tag{5.16}$$

where $C$ is the speed of sound, $D$ is focal length and $X_s$ is the distance of a point on the transducer face to the centre of the transducer. The strong focusing gives the maximum transit time spectral broadening and minimum geometrical broadening. All the focal lengths were 5 cm and the frequency of each transducer was 3 MHz. The amplitude across the 5 cm beam was simulated for each transducer. The beam-vessel angle was assumed to be 90°.

The decomposition was then made by Fourier transform and the range of angle for transit time spectral broadening was estimated from 50% amplitude of the amplitude-angle function. The width of each beam was estimated by the 50% amplitude and the range of angle was calculated by equation ( 5.12) and ( 5.13).

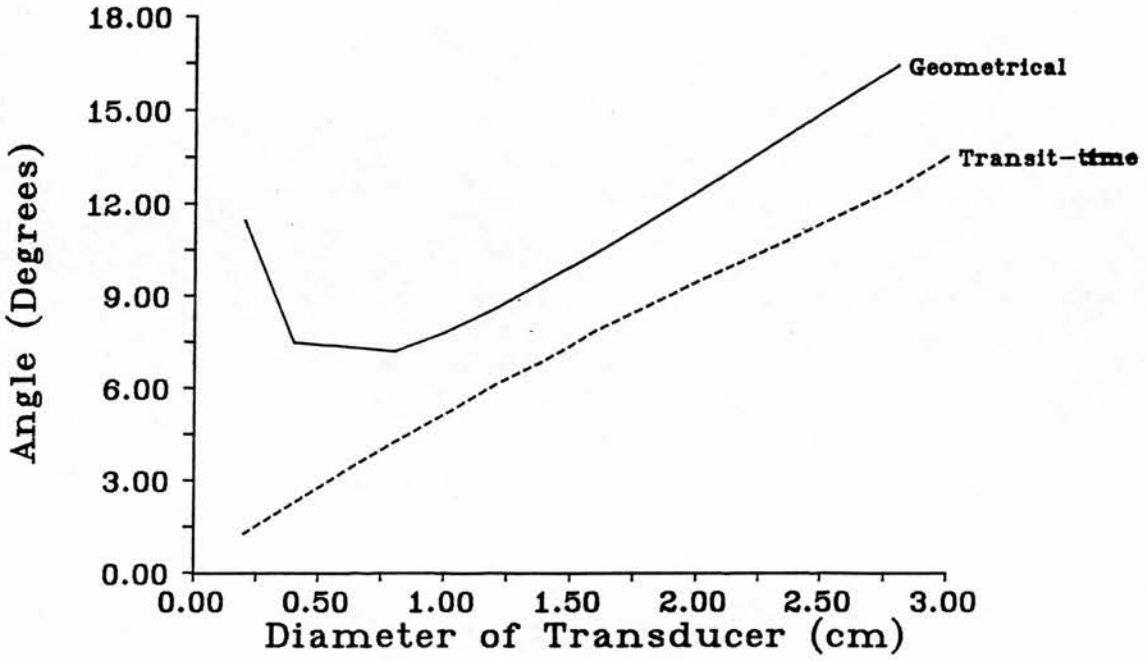


Figure 5.8: The comparison for geometrical and transit time spectral broadening against different size of circular transducers.

Figure 5.8 shows the significance of the transit time and geometrical spectral broadening for focused 3 MHz single crystal transducers. It is found that for all the transducer sizes, the transit time spectral broadening was less significant than the geometrical spectral broadening. The large geometrical spectral broadening for small transducers is due to the fact that the 3 MHz transducer can not focus well when the size is smaller than 6 mm. In practice, the transducer is never as perfectly focused and the highest velocity particles in the central stream may not pass the focal point. The beam vessel angle is usually not 90° so the effective beam width is larger. Consequently the transit time spectral broadening should be less significant and geometrical spectral broadening more significant than that illustrated in Figure 5.8. This may explain the experimental results shown by Newhouse's (Newhouse *et al.*,1980).

### 5.2.8 Summary

It has been shown that the transit time spectral broadening is not identical to geometrical spectral broadening. Equation ( 5.8) does not describe the geometrical spectral broadening and range of angles available to the scatterers. Decomposed plane waves described by Equation ( 5.8) may not physical and cannot give a real Doppler shift. It is noted that commonly used modelling techniques for producing fields from transducers use spherical waves from elements of the transducer face.

Therefore, the Doppler spectrum is not uniquely decided by the field. For a moving particle, it is necessary to know the field as well as the geometry of the particle and source of the field in the calculation of the Doppler spectrum. The geometrical spectral broadening is usually more significant than the transit time spectral broadening. In some cases the transit time spectral broadening can be ignored. However, in the region in which the beam is highly focused, especially when the aperture of the transducer is large, the transit time spectral broadening should be considered.

## 5.3 The Validity Of Using Extreme Angle To Calculate Maximum Frequency

It has been shown experimentally by Newhouse *et al.* (1980) that at the focused beam waist, the bandwidth of the Doppler signal can be calculated to a good degree of approximation using extreme angles. In Chapter 3, it was assumed that the Doppler spectrum is composed of the contribution from all the angles available for incident and backscattered radiation. However, is this method always valid ?

### 5.3.1 Theoretical consideration

The reason for asking this question is described below. Suppose there is a rectangular linear array transducer. The aperture of the transducer is large, say, 2 cm long and 1 cm wide. It is assumed that the transducer is like a rigid piston

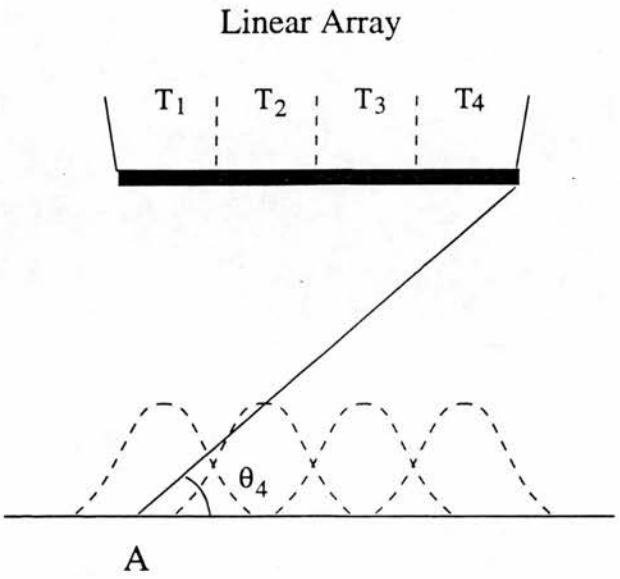


Figure 5.9: A large transducer can be subdivided into small sections so one part of the transducer may not receive signals from the field in other parts of the transducer.

so that all portions of the transducer vibrate in phase. The pressure produced at any point by such a source is the sum of the pressures that would be produced by an equivalent assembly of simple sources (Kinsler and Frey, 1962). Therefore, the transducer can be considered to be composed of four $0.5 \times 1$ cm crystals (equivalent to 4 parts of assembly of simple sources) $T1$, $T2$, $T3$ and T4 which are placed side by side and vibrate in the same phase and amplitude. Suppose the transducer is not focused. Each transducer produces a field like a Gaussian function (Figure 5.9). The field of the whole transducer is the superposition of all the fields produced by $T1$ to $T4$.

Let a particle moves at velocity v at position $A$ (Figure 5.9), which is in the field of $T1$ but only in the fringe field produced by $T4$ as the ultrasonic waves from $T4$ interfere destructively at $A$. By considering $T1$ to $T4$ separately, this particle should produce a weak signal at $T4$ while it does give a strong contribution to $T1$. As the signal received by the whole transducer is the sum of the signals from all parts of the transducer, the received signal only has a very weak frequency

component corresponding to the angle $\theta_4$. So the angle $\theta_4$ can be considered actually not available for the transmission or reception, although it is within the extreme angle for the whole field of the transducer.

Therefore, certain restrictions apply to the use of the extreme angle in considerations of geometrical spectral broadening. In the near field of a transducer, for example, the field may be subdivided into several zones, each of which are principally formed by one part of the transducer (Figure 5.9). In the simulations it is found that each zone is a Gaussian-like single peak function. The superposition of these functions gives a field with multiple peaks. As each part of the transducer produces only its corresponding transmission and reception field zone, it does not receive signals resulting from particles in zones far away from it. The extreme angle approach used in Chapter 3 should therefore not be applied in this situation. In the far field of a transducer, the field has only a single peak. It is usually impossible to subdivide this field into spatially separate zones as the fields from each part of the transducer overlap one another. The extreme angle approach can be used in this situation.

It can be concluded that in the near field of (unfocused) transducers with large aperture, in which multiple peaks can be found, the angle approach may be not valid. The maximum frequency cannot be estimated by the extreme angles available in transmission and reception. However, when the ultrasonic field has only a single peak, which occurs in the far field of the transducer, the angle approach may be used and maximum frequency can be calculated from extreme angles.

For a focused transducer, if the sample volume is at the focal point, as ultrasonic waves arrive at the sample "in phase", the beam is narrow and particles in the sample volume gives almost uniform power contribution to whole transducer surface. Therefore the angle approach can be used.

### 5.3.2 Experiment

To examine the validity of using extreme angles in estimating geometrical spectral broadening, experiments were made on the flow phantom. The transmission field of the transducer was assessed using a bilaminar hydrophone (GEC-Marconi Ltd). A theoretical estimation of the geometrical spectral broadening effect on the maximum frequency using extreme angles was made (see Appendix A). Doppler spectra were acquired during steady flow for angles from 85° to 40° in 5° steps. The depth of the tubing was set to be 5.6 cm. The maximum frequency was estimated by the 15/16 percentage method and also traced manually by the light pen system on the Doptek.

The error or overestimation of the maximum velocity is depicted in Figure 5.10. The errors were less than 6% for angles smaller than 60°. However, the errors increased sharply when the angle was greater than 70° due to geometrical spectral broadening. The solid curve is a theoretical estimation of the error at various beam-vessel angles (See Appendix A). The agreement between the curve and hand-drawn estimation is better than 3% for angles up to 80°. This shows that the overestimation in maximum frequency due to geometrical spectral broadening can be well estimated by calculation using the extreme angles.

For a wide unfocused transducer, an experiment was not performed as this situation usually does not occur in medical Doppler ultrasound and a proper transducer could not be found. However, care should be taken when a measurement is made in the near field of unfocused transducers.

## 5.4 The Use Of Linear Arrays

Linear arrays use a large proportion of the elements on the transducer face to obtain good focusing. Due to the large aperture and narrow beam, significant geometrical and transit time spectral broadening may be observed. A more serious problem is that the estimated mean and maximum frequency may change when the beam is moved across the transducer face, although on the B-mode image the

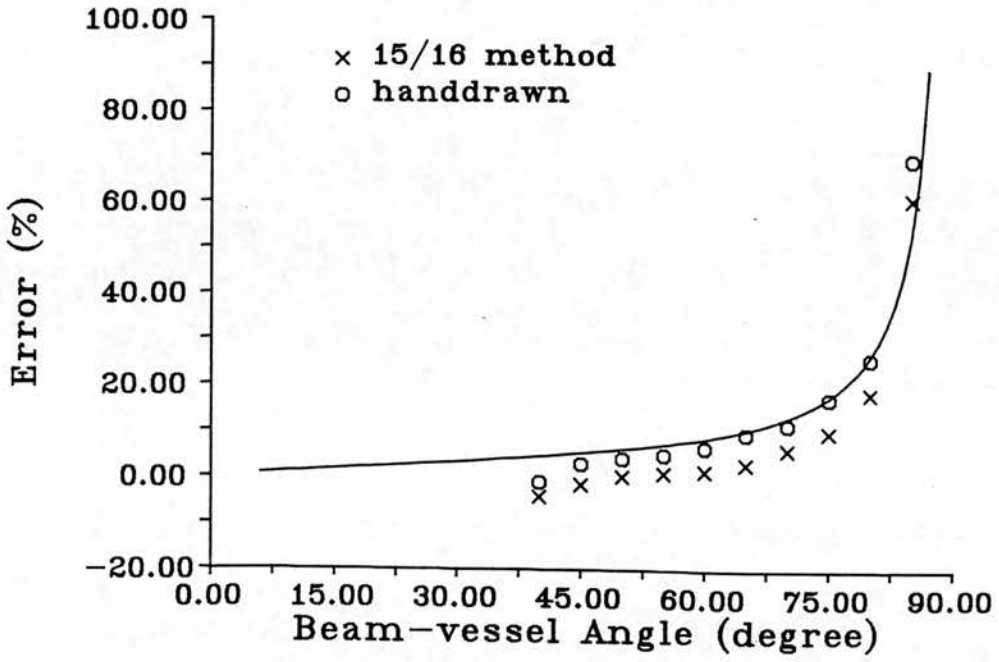


Figure 5.10: The maximum frequency can be well estimated by using the extreme angle in the calculation of Doppler shift.

Doppler angles remains the same.

Figure 5.11 illustrates some typical cases for geometrical spectral broadening in terms of aperture size. Here the aperture is wide and the beam is focused at the sample volume. As discussed before, the use of extreme angle to estimate the maximum frequency is valid in this situation. Because of the wide aperture, the angle available for transmission and reception, which is from $\theta_1$ to $\theta_2$ in Figure 5.11 (b), is very large. This gives a very large geometrical spectral broadening and causes significant overestimation of the maximum frequency.

A further problem is depicted in Figure 5.11. The beam centre can be moved across the transducer face. When the displayed axis of the beam on the screen is at one end of the transducer (Figure 5.11 (a)), as there are no elements on the left, the overestimation of the maximum velocity would be small. However, the mean velocity would be underestimated because of the elements on the right side of the displayed beam axis. When the beam moves to the right, the overestimation of the maximum velocity increases while the underestimation of the mean velocity

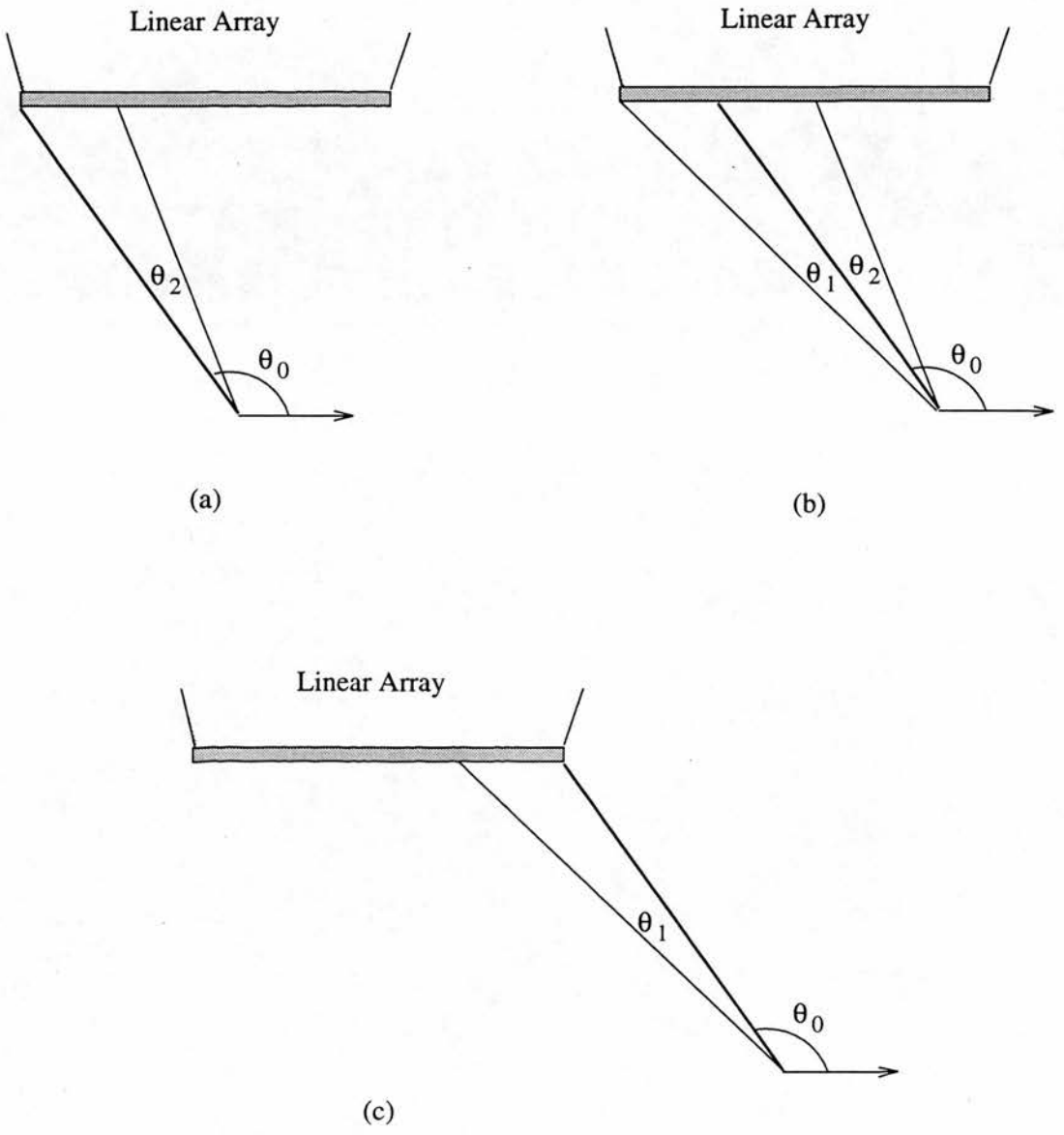


Figure 5.11: Some situations for a linear array in Doppler measurement. The solid line shows the displayed beam axis on the screen and the broken lines indicate the active elements on the transducer face and the range of angle available. (a) Beam at left edge which gives good maximum frequency estimation but underestimation in mean. (b) Beam at central part of the transducer which gives overestimation of maximum but better estimation of mean. (c) Beam at right edge which gives overestimation of both mean and maximum frequency.

decreases. The spectrum is unchanged when the numbers of elements on both left and right are equal (Figure 5.11 (b)). However, when the beam is moves further to the right and there are less activated elements on the right than left of the beam axis (Figure 5.11 (c), the mean velocity is more overestimated but the maximum frequency stays the same.

In practice, the aperture or number of elements on a linear array used for Doppler measurement differs among manufacturers. The aperture for transmission and reception can also be different. Therefore, this effect is dependent on the transducer and depth. It can be very significant for a wide aperture and less significant for a small aperture.

To illustrate this problem, experiments were made on the flow phantom. An ATL (Advanced Technology Laboratory) and an Acuson duplex scanner were used. The transducers were a 5 MHz ATL linear array and a 3.5 MHz Acuson Linear array. The widths of the transducer face were 4.5 cm and 6.0 cm respectively. A heat-shrinkable tubing of 5 mm diameter was placed at a distance about 3 cm from each transducer. The beam was then moved across the transducer face. The maximum velocity and mean velocity were estimated and compared with the true velocities measured by a stop watch and a measuring cylinder.

These experiments showed two typical situations. For the ATL 5 MHz linear array, both the mean and maximum velocity changed by a large amount when the beam was moved across the transducer face (Figure 5.12). When the beam was at the left edge of the transducer, the maximum velocity was estimated quite accurately. However, the error then increased when the beam was moved to the right and could be as high as 41.5 % at the extreme left position. The mean velocity was not well estimated because of the problems of the flow phantom discussed in Chapter 2. The relative changes of the mean velocity however were similar to the maximum velocity. The large change of the estimated velocity indicates that a wide aperture was used on the ATL scanner for Doppler measurement. The situation depicted in Figure 5.11 (c) could not be examined as the beam could not be moved to the right extreme of the transducer.

The Acuson scanner showed a different situation. Both mean and maximum

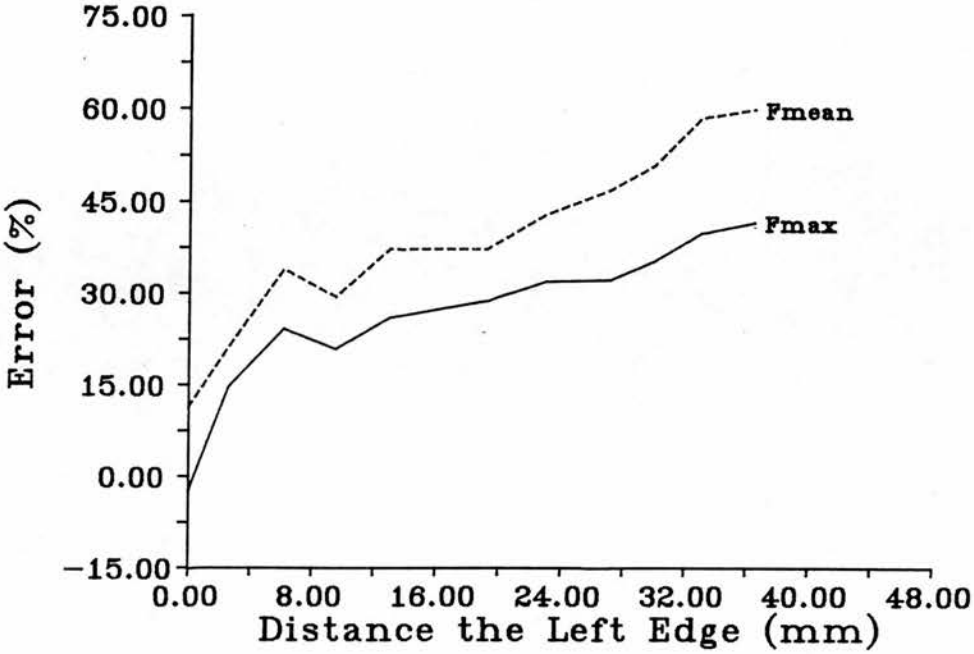


Figure 5.12: The mean and maximum frequencies using the ATL 5 MHz linear array. Large changes were observed when the beam moved across the transducer face.

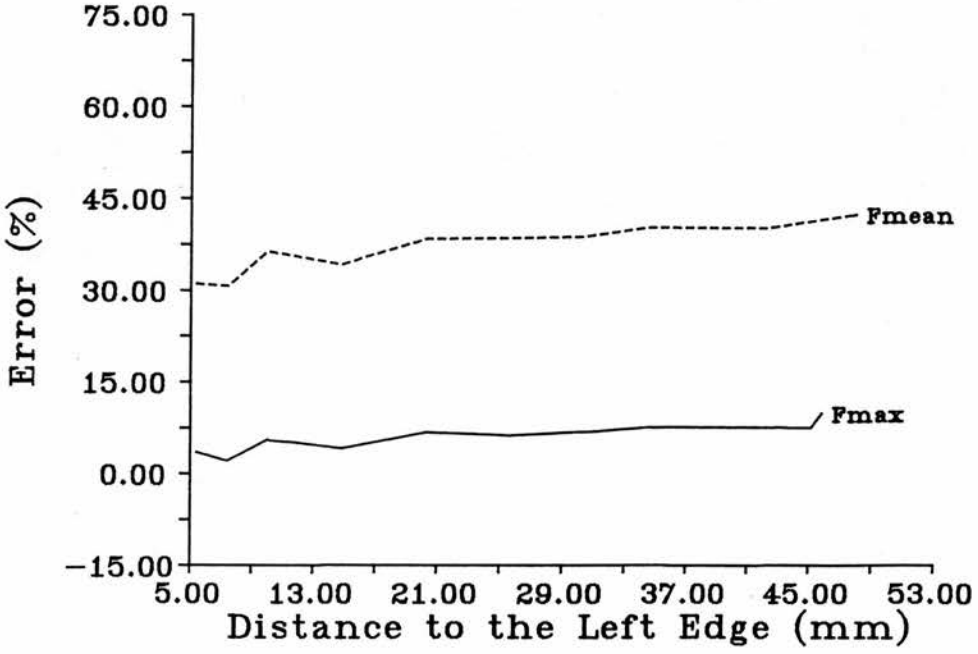


Figure 5.13: The mean and maximum frequencies using Acuson 3.5 MHz linear array. Less changes were observed when the beam moved across the transducer face.

velocity changed less significantly when the beam was moved (Figure 5.13). The errors in the maximum velocity estimation were from about 2% at left positions to about 7% at right. It was also noticed that the beam could not be move the extreme left position (Figure 5.11 (a)). This also helped to prevent large variation of errors at different positions. The smaller error on the Acuson scanner may result from a small aperture being used in Doppler measurement.

The experiment on two commercial scanners suggests that large errors in Doppler measurement could be introduced by using linear arrays. To reduce these errors, the maximum frequency should be calculated using the extreme angles of transmission and reception. To our knowledge there is at least one company (Diasonics) which does this.

## 5.5 Discussion

This chapter has discussed the identification of transit time spectral broadening and geometrical spectral broadening. The conclusion that they are different effects conflicts with commonly accepted theories. The methods used in this chapter are mainly "thought experiment" methods and look controversial. As transit time spectral broadening and geometrical spectral broadening always occur together in reality, it is difficult to separate them experimentally and no experimental evidence is given in this chapter. Therefore, further discussion and experimental proof would be beneficial to this subject.

## 5.6 Conclusion

It has been shown in this chapter that the transit time spectral broadening is not the same effect as the geometrical spectral broadening. The Doppler spectrum cannot be uniquely decided by the particle velocities and the ultrasonic intensity patterns. The geometry of the transducer and the moving particles must be considered. The transit time spectral broadening is usually less significant than geometrical spectral broadening. However, in situations where very large aperture

and strong focusing are used, both effects should be considered.

The maximum frequency can be approximately estimated by the extreme angles of transmission and reception. However, this angle approach should not be used when large transducers are used and multiple peaks are present in the ultrasonic field such as occur in the near field of unfocused transducers.

The use of a wide aperture linear array can introduce large errors in Doppler measurement. The spectrum changes considerably when the beam moves across the transducer face. In practice, the maximum frequency should be calculated by the extreme angles of transmission and reception to avoid errors.

# Chapter 6

# DIAMETER MEASUREMENT AND THE PULSE LENGTH CORRECTION

## 6.1 Introduction

In Doppler ultrasound, volume flow is generally estimated by multiplication of the cross-sectional area of the blood vessel and the mean velocity of blood cells moving in the vessel. The cross-sectional area is usually calculated from the diameter measured by ultrasound. As the area is proportional to the square of the diameter, a small error in diameter can result in a large error in the cross-sectional area and consequently in the volume flow. Therefore, the accuracy of estimation of the diameter of blood vessels is crucial to volume flow measurement using Doppler ultrasound. However, large errors in measuring diameters have been reported (Gill, 1985).

A number of methods for calculation of the diameter of blood vessels have been reported. Eik-Nes *et al.*, (1982, 1984) measured diameters on frozen images on the screen of a real-time scanner with built-in callipers. By using a time-distance recorder, diameters can be continuously measured (Lindstrum, *et al.*, 1977 and Struyk, 1985) by a digital pulsed echo tracker with phase-locked loop system. The time-motion (TM) mode of a real-time scanner was also applied to diameter

estimation by using built in callipers (Eik-Nes *et al.*, 1982; Teague *et al.* 1985) or planimetry (Rasmussen 1987). It has also been suggested that a multi-gate pulse Doppler system can be used to record the changes in artery diameter (Hoeks *et al.*, 1985). However, all these methods suffer from large errors.

A primary cause of error in diameter measurement is the limited resolution achievable using ultrasound. A particular problem is that echoes from the inner and outer surfaces of a blood vessel or even layers within the wall tend to merge together. It is generally difficult to recognise precisely the boundary of the surrounding tissue with the outer wall, or the inner wall with blood. It is believed that at best, the obtainable accuracy is of the order of a wavelength of the transmitted ultrasound pulse. Considering the wavelength of ultrasound with frequencies of 3, 5 and 10 MHz are 0.5, 0.3 and 0.15 mm respectively, the error in the area estimation, especially on the vessels of less than 5 mm diameter can be very high. For example, a 0.5 mm error in diameter measurement gives 31% error in cross-sectional area of a 3 mm vessel.

To avoid this problem, some authors have tended to measure the diameter from the outer surface of the proximal wall to the inner surface of the distal wall, and then correct for the wall thickness (Eik-Nes *et al.*, 1982; Struyk *et al.*, 1985). In practice, however, the outer surface of a blood vessel is not always observed and the thickness of the wall is generally unknown. This method is therefore not generally applicable to *in vivo* situations.

In clinical measurement, the diameter is most commonly estimated by two calliper markers placed on the inner boundaries of a vessel. However, the author surprisingly found no experimental studies in the literature of the accuracy of diameter measurement using this method. In this chapter, the cause of the error and effect of machine setting on diameter measurement will be analyzed, and a method to reduce this error will be described.

| Tube | Density ($kg/m^3$) | C ($m/s$) | Z ($kg/s/m^2$) |
|---|---|---|---|
| Heat shrinkable | 940 | 2036 | $2.94 \times 10^6$ |
| PVC | 1337 | 1714 | $2.29 \times 10^6$ |
| Silastic | 1224 | 949 | $1.16 \times 10^6$ |
| Blood Vessel | 1051 | $1513 \pm 21$ | $1.56 \pm 0.03 \times 10^6$ |
| Glycerol (10%)+Water | 1030 | 1540 | $1.59 \times 10^6$ |

Table 6.1: Some acoustic properties of tubing materials and glycerol water solution.

## 6.2 Diameter Measurement

In this section, the diameter of a number of tubes is measured using both commercial duplex scanners and a microscope. The effect of various machine setting on the diameter measurement will be considered.

### 6.2.1 Materials

In this study 4 transducers on 3 commercial duplex scanners, two Advanced Technology Laboratory, Ultramark 9 (ATL UM9) and a Diagnostic Sonar Limited, Prisma (DSL), were used. The transducers were ATL 5 MHz phased array, ATL 3 MHz phased array, ATL 5 MHz linear array and DSL 3.5 MHz convex linear array.

Artificial vessels were used since the measurement on real blood vessels are difficult. For example a blood vessel will collapse unless it is kept under pressure by the presence of flow. This would necessitate using blood vessels in a flow phantom and it would be very difficult to measure the true diameter in such a situation, whereas for the tubing this was unnecessary. For tubes three kinds of materials were used to give different reflectivity and sound speed. The materials used were transparent heat shrinkable material, silastic rubber and PVC. Some acoustic properties of these materials are listed in Table 6.1. It is shown these materials have properties which straddle those of real blood vessels. All the ultrasound measurements were made in a mixture of 10% glycerol and 90% water. This gives a sound speed of 1540 m/s at $20°C$ which corresponds to that of soft tissue. The

diameters of these tubes ranged from 1.95 mm to 11.0 mm.

### 6.2.2 Diameter measurement

#### Using microscope

In the diameter measurement, 7 heat shrinkable, 3 silastic and 2 PVC tubes were used. The real diameter and wall thickness of each tube were measured using a microscope. To compensate possible non-circularity of tubes, measurements in two orthogonal directions across each heat shrinkable tube were made and the average was taken. For silastic and PVC tubes (which are less likely to be perfectly circular), at least 6 measurements in three pairs of orthogonal directions were made.

#### Using B-mode ultrasound

The distance measurement using the built-in callipers was calibrated using steel threads. Three fine steel threads stretched in parallel were in the glycerol-water mixture. The real distance between these threads was measured by a ruler. Using each transducer, these distances were measured by cursors on frozen B-mode images and compared with the real distances to make sure that there were no significant errors.

The diameter of each tube then was measured by a pair of cursors on frozen B-mode images. Inner-to-inner, outer-to-inner and outer-to-outer diameters of each tube were examined. The same number of measurements as with the microscope were made and the average was used.

### 6.2.3 Effect of depth

The diameter of the 4.95 mm heat-shrinkable tube was measured for vessel depths ranging from 1 cm to 11 cm using the ATL 5 MHz phased array.

### 6.2.4 Effect of output power and gain

The diameter of a 4.95 mm heat shrinkable tube was measured for different B-scan gain settings using the DSL 3.5 MHz convex array. The acoustic power output was set to 18 dB and B-scan gain varied from 0 to 54 dB. Gain greater than 54 dB gave too bright an image in that the edges of tubes were not clearly observed.

For the effect of output power, the 4.95 mm heat shrink tube was measured using the ATL 3 MHz transducer with 16 output power settings from 100% to 0.56%. The B-scan gain was fixed for all of these measurements.

### 6.2.5 Effect of beam-vessel angle

A 4.95 mm heat-shrinkable tube was examined using the ATL 5 MHz linear array. The angle between the transducer face and vessel axis was varied from 0° to 41°. Hard copies were obtained using a thermal printer connected to the scanner.

## 6.3 Diameter Correction

In this section, a method of diameter correction, which can improve the accuracy of the diameter measurement is described.

### 6.3.1 Theory

In the measurement of a vessel diameter using ultrasound, a major source of error is the spatial resolution. The spatial resolution of pulse echo imaging, which may be A-mode, B-mode image or time-motion (TM) recording, is of the order of the pulse length of the transmitted pulse.

The finite length of the transmitted pulse causes the diameter to be underestimated when it is measured from the inside edges of the vessel wall echoes. As shown in Figure 6.1, the leading edge of the echo signal reflected from the

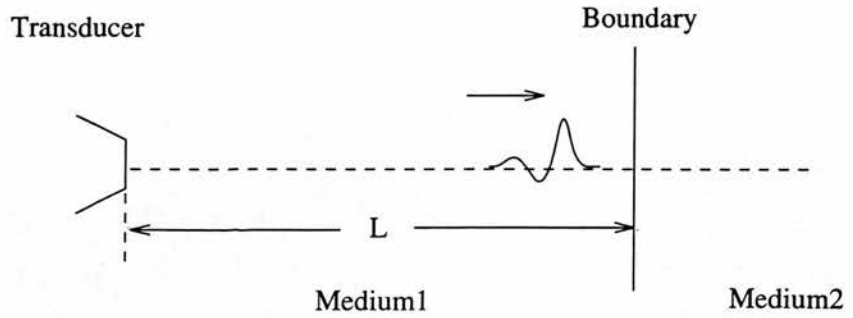


(a)

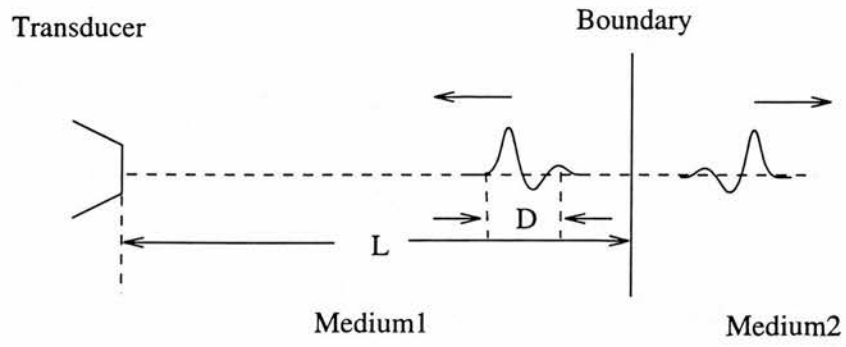


(b)

Figure 6.1: The underestimation because of pulse length: (a) when the pulse meets the boundary, it is reflected; (b) the reflection continues until the whole pulse leaves the boundary.

boundary arrives back at the transducer after time $T_1$ which is given by

$$T_1 = \frac{2L}{c} \tag{6.1}$$

where $c$ is the speed of sound, $L$ is the actual distance from the transducer to the boundary. The end of the echo signal arrives at transducer at time $T_2$ given by

$$T_2 = \frac{2L + D}{c} \tag{6.2}$$

where $D$ is the pulse length. This means that the vessel/blood boundary displayed

in a B-mode image has a depth of $\Delta d$ which can be written

$$\begin{aligned} \Delta d &= \frac{T_2 - T_1}{2} c \\ &= \frac{D}{2} \end{aligned} \tag{6.3}$$

Therefore, the inside edge of the boundary on the image extends into the vessel by $\Delta d$ and causes an underestimation of the vessel diameter by half of the pulse length. In practice, correction for this half pulse length could improve the accuracy of diameter measurement.

### 6.3.2 Pulse length measurement

The correction of the diameter using this method requires the pulse length to be known. To measure the pulse length, a 10 MHz bilaminar polyvinylidene fluoride (PVDF) membrane hydrophone (GEC-Marconi Ltd) was used. Pulse waveforms were displayed on an oscilloscope (HP 4540 A 500 MHz digital oscilloscope) connected to the preamplifier of the hydrophone. Hardcopies of the pulse waveforms were obtained from an ink jet printer interfaced to the oscilloscope.

All the commercial transducers were examined in a measuring tank filled with water. Measurements were carried out using the M-mode; in this mode signals were continuously recorded from one scan line. The hydrophone was rigidly fixed on a holder under water and the distance between the transducer and hydrophone was set to 5 cm. Acoustic pulse waveforms were displayed on the oscilloscope and the time intervals $\Delta t$ between the first and last peak, in which the peak pressures were larger than 10% of the maximum, were measured using the oscilloscope measuring system. Hard copy of each waveform was printed.

As the diameter measurements were carried out in a glycerol-water solution with sound speed of 1540 m/s which corresponds to that of soft tissue, the half pulse length $\Delta d$, which is the correction of the diameter, was given by

$$\Delta d = \frac{1}{2} 1540 \Delta t \tag{6.4}$$

| Transducer | T1 | T2 | T3 | T4 |
|---|---|---|---|---|
| Pulse length (ns) | 454 | 588 | 506 | 962 |
| Correction (mm) | 0.35 | 0.45 | 0.39 | 0.74 |

Table 6.2: Pulse length of each transducer where T1 : ATL 5 MHz Phased Array; T2 : ATL 3 MHz Phased Array; T3 : ATL 5 MHz Linear Array; T4 : DSL 3.5 MHz Linear Array.

### 6.3.3 The diameter correction

The diameter of the vessel from each ultrasonic image was corrected by adding the half pulse length $\Delta d$ as described in section 6.3.1 and 6.3.2. Diameters before and after the correction were then compared with the real diameter which is measured by a microscope, and the percentage errors were calculated.

## 6.4 Results And Discussion

### 6.4.1 Pulse length measurement

A typical example of pulse length measurement is shown in Figure 6.2. As the built-in measuring system of the oscilloscope was very accurate ($\pm$ 1 ns), the error in pulse length is small and can be ignored. The pulse length and the correction of diameter for 4 transducers are listed in Table 6.2. It should be noted that the pulse length differs among machines and among transducers. For example, the pulse length correction of DSL 3.5 MHz linear array is significantly larger than the other transducers and consequently, the corrections for the inner diameter are also different.

### 6.4.2 Inner diameter measurement and its correction

Table 6.3 and gives results of inner diameter measurement using the ATL 5 MHz linear array. The absolute error in diameter and percentage error in area before and after the pulse length correction using all 4 transducers are also shown

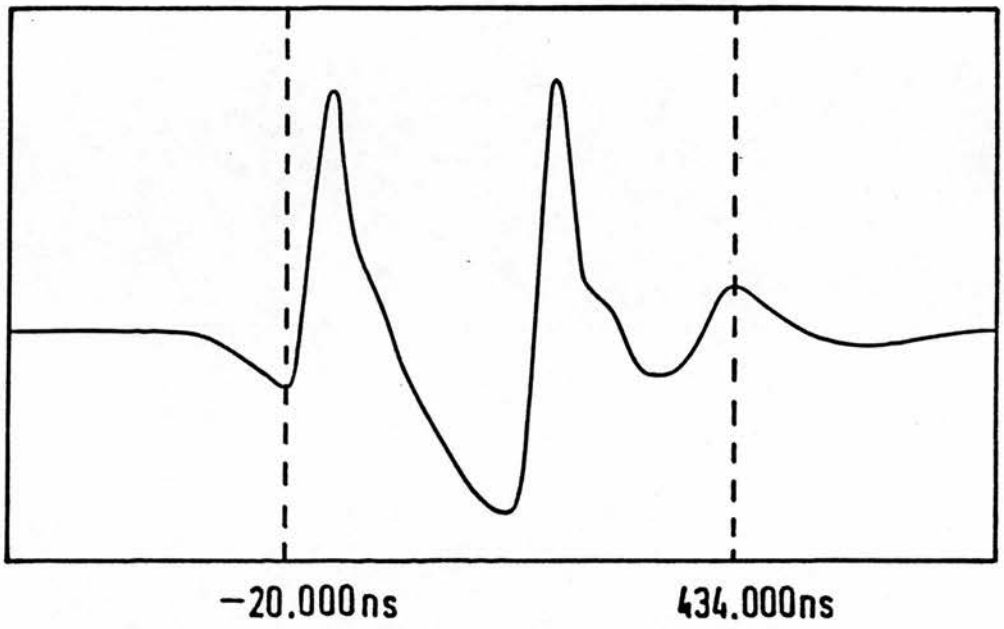


Figure 6.2: The pulse length measurement of the ATL 5 MHz phased array.

in Figure 6.3 and Figure 6.4. Tables of the details can also be found in the Appendix B. No relationship are observed between the absolute error and either the size of vessel or the material of vessel wall.

After the correction, errors in diameter are significantly reduced. The diameter correction is found to be independent to the machine, vessel size, wall thickness and materials. Although the pulse length is significantly different between transducers, especially between the DSL transducer and ATL transducers, the errors in corrected diameters are found to be independent of transducer. This shows that the error in diameter measurement is due to underestimation by the pulse length factor. It is also noted that the error after correction is typically about 0.1 mm to 0.2 mm which smaller than the wavelength of the ultrasonic pulses.

The cross-sectional areas calculated from measured diameters have large errors ranging from about 7% to 56% in tubes of different sizes used in this study. After the pulse length correction, the error was greatly reduced to from 0% to 10%.

It is also found that after the pulse length correction, there is still a small

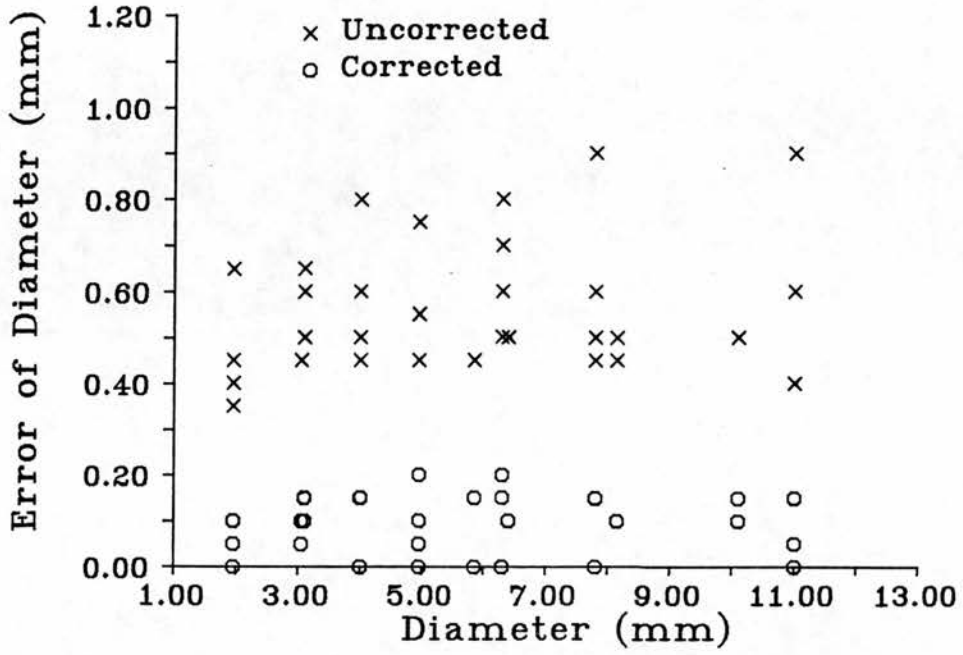


Figure 6.3: The absolute error of diameter measurement before and after the pulse length correction

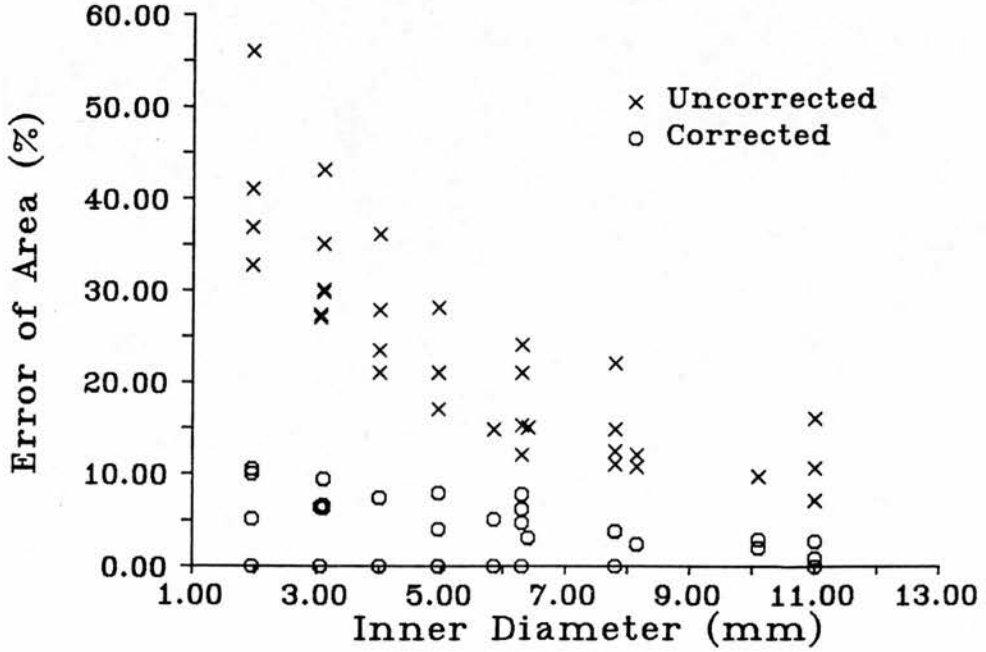


Figure 6.4: The percentage error of area before and after the pulse length correction.

| Tube | Heat shrinkable | | | | | | | Silastic | | | PVC | |
|---|---|---|---|---|---|---|---|---|---|---|---|---|
| $ID_{rea}$ | 1.95 | 3.1 | 4.0 | 4.95 | 6.3 | 7.8 | 11.0 | 3.05 | 6.4 | 10.1 | 5.85 | 8.15 |
| $ID_{mea}$ | 1.5 | 2.6 | 3.55 | 4.5 | 5.9 | 7.35 | 10.6 | 2.6 | 5.9 | 9.6 | 5.4 | 7.65 |
| $ID_{err}$ | -0.45 | -0.5 | -0.45 | -0.45 | -0.6 | -0.45 | -0.4 | -0.45 | -0.5 | -0.5 | -0.45 | -0.5 |
| $E_{are}$(%) | 41 | 30 | 21 | 17 | 12 | 11 | 7.1 | 27 | 15 | 9.7 | 14.8 | 12 |
| $ID_{cor}$ | 0.06 | -0.1 | 0.06 | 0.06 | -0.2 | 0.06 | 0.01 | 0.06 | -0.1 | -0.1 | 0.06 | -0.1 |
| $E_{are}$(%) | 6.1 | 6.3 | 3.0 | 2.4 | 6.2 | 1.5 | 0.2 | 3.9 | 3.1 | 2.0 | 2.0 | 2.4 |

Table 6.3: The inner-to-inner diameters measured with ATL 5 MHz convex linear array and diameters after the pulse length correction. The correction of the diameter=0.35 mm. In the table, $ID_{rea}$ and $ID_{mea}$ are the diameter measured by microscope and ultrasound, $OID_{err}$ and $OID_{cor}$ is the absolute error of diameters before and after the pulse length correction, $E_{are}$ is the percentage error in area.

underestimation in the inner diameter. This may be because only the transmitted pulse length was corrected for. However, when the pulse is received by the transducer, the transducer may produce another cycle or so in the received signal and consequently increase the error due to the pulse length. In practice, if the received pulse length can be corrected, the accuracy could be further improved.

The vessel material used in this study had speeds of sound both larger and smaller than the speed of sound in tissue. After the pulse length correction, the inner diameter is independent of the materials. This indicates the speed of sound has no effect on the accuracy of diameter measurement. For all the three materials, the back-scattered signal was still stronger than that with patients. In practice, the reflected signal from the boundary may be slightly weaker. However, from observations on umbilical veins *in vivo*, the boundary between the vessel wall and blood was still clear as long as a near 90° beam-vessel angle could be obtained.

### 6.4.3 Effect of depth

There is no significant change in diameters observed at depth ranging from 1 cm to 11 cm (for details please see the Appendix B).

| Tube | Heat shrinkable | | | | | | | | | |
|---|---|---|---|---|---|---|---|---|---|---|
| $Gain(dB)$ | 0 | 6 | 12 | 18 | 24 | 30 | 36 | 42 | 48 | 54 |
| $ID_{mea}$ | 4.5 | 4.3 | 4.3 | 4.1 | 4.3 | 4.1 | 4.3 | 4.1 | 4.1 | 4.3 |
| $OID_{mea}$ | 5.4 | 5.3 | 5.4 | 5.4 | 5.3 | 5.3 | 5.3 | 5.3 | 5.3 | 5.3 |
| $OD_{mea}$ | 6.0 | 6.0 | 6.2 | 6.2 | 6.2 | 6.2 | 6.4 | 6.2 | 6.4 | 6.4 |

Table 6.4: Diameters measured with different gains while Output = 18 dB $ID_{rea}$ = 4.95 mm; $ID_{rea}$ = 5.6 mm; $ID_{rea}$ = 5.9 mm. DSL 3.5 MHz convex array was used.

### 6.4.4 Effect of output power and gain

Table 6.4 and Table 6.5 gives the measured diameters at different B-scan gains and output powers respectively. Apart from very low or high gain and output power, there was no significant change in measured diameter when the gain or output power changed, as long as the edge of vessel was clear. It was impossible to measure diameters when the gain was higher than 54 dB in because the images were too bright.

Both linear array and phased array transducers were used in this study. It was found easier to use the linear arrays than the phased arrays. This is because in the experimental arrangement in which tubes were straight, a long and clear vessel image could be observed with a linear array. However using a phased array, only a short piece of the vessel could be observed.

The image of a tube often shows a blurred band which is due to reflection from the side of the vessel wall and a bright band corresponding to the echo from the bottom of the vessel. The cursor should be placed at the interface of these two bands in the measurement. Usually it is easier to recognize the interface with linear arrays. Therefore, for linear arrays the set up of the B-scan gain and output power were not as critical as for phased arrays.

| *Output* (%) | 100 | 71 | 50 | 35 | 25 | 18 | 13 | 8.9 |
|---|---|---|---|---|---|---|---|---|
| $ID_{mea}$ | 4.4 | 4.5 | 4.4 | 4.45 | 4.5 | 4.5 | 4.5 | 4.45 |
| *Output* (%) | 6.3 | 4.5 | 3.2 | 2.2 | 1.6 | 1.1 | 0.79 | 0.56 |
| $ID_{mea}$ | 4.5 | 4.45 | 4.45 | 4.6 | 4.6 | 4.7 | 4.65 | 4.6 |

Table 6.5: Inner-to-inner diameter measured by 3 MHz ATL phased array at output from 100% to 0.56%. Gain was fixed when output power was changed. The measured diameters did not change significantly unless the output was very low.

| Tube | Heat shrinkable | | | | | | | | |
|---|---|---|---|---|---|---|---|---|---|
| *Angle* | 0 | 6 | 10 | 11 | 13 | 16 | 26.5 | 38 | 41 |
| $ID_{mea}$ | 4.5 | 4.5 | 4.4 | 4.5 | 4.1 | 4.3 | 3.9 | 4.5 | 3.9 |

Table 6.6: Inner diameter measured at different angles by ATL UM9 5 MHz linear array.

### 6.4.5 Effect of beam-vessel angle

It was found that the quality of the vessel images reduce sharply when the beam-vessel angle increases. Consequently the diameter measurement became difficult because of the uncertainty of the vessel edges on the screen. When the beam-vessel angle is bigger than 10°, the diameter measurement can have large errors (Table 6.6). It is therefore recommended that the diameter measurement should be made when the beam-vessel angle is within $90° \pm 10°$.

When the beam-vessel angle differs from the 90°, theoretically, the pulse length should be corrected and become $\Delta d/\cos\theta$. However, in the experiment, it was found that the quality of image deteriorates when the angle was larger than 10° and was not suitable for the measurement. In theory, at 10° the angle correction is only 15% larger of that at 90°. For the 5 MHz ATL linear array, which was used in the experiment, this increase in the pulse length correction is 0.05 mm. This is much smaller than the random error (about 0.4 mm) at that angle due to the uncertainty of the vessel edges. This means the angle correction of the pulse length is in general not necessary when 2D imaging is used.

| Transducer | T1 | T2 | T3 | T4 |
|---|---|---|---|---|
| $ID_{err} \pm \sigma$ | -0.475±0.045 | -0.571±0.107 | -0.475±0.05 | -0.779±0.104 |
| $ID_{cor} \pm \sigma$ | -0.125±0.045 | -0.221±0.107 | -0.025±0.05 | -0.0386±0.104 |

Table 6.7: The summary of the errors of inner diameter measured from all the tubes and all the transducers. $ID_{err}$ and $ID_{cor}$ are the inner diameters errors before and after pulse length correction, $\sigma$ is the standard deviation.

### 6.4.6 Random errors

The diameter measurement is often associated with big random error. Taking more measurements and using the average (Eik-Nes, 1982) usually can improve the accuracy. A summary of the systematic error and random error of inner diameter measurement on all tubes and by all 4 transducers before and after the pulse length correction is listed in Table 6.7.

## 6.5 Conclusion

It was found the inner diameter of vessel was underestimated due to the length of the transmitted ultrasonic pulse. After correcting this effect, the accuracy of the inner diameter estimation can be significantly improved from up to 0.9 mm before the correction to less than 0.2 mm, which is smaller than the wavelength of the ultrasonic pulses, after the correction. The corrected diameter was found to be independent of machine, transducer, material of vessel, B-scan gain, and output acoustic power. Accurate measurement can be difficult to make when the beam-vessel angle is outside $90° \pm 10°$.

# Chapter 7

# NON-LINEAR PROPAGATION IN DOPPLER ULTRASOUND

## 7.1 Introduction

It is usually acceptable in biomedical applications of ultrasound to consider that acoustic propagation is a linear process. However, the propagation of acoustic waves is in fact a non-linear process (Blackstock, *et al.*, 1965; Bakhvalov, *et al.*, 1978). Inevitably, this results in pulse waveform distortion, harmonic generation and shock formation.

Evidence has accumulated to indicate that the linear treatment may not always be appropriate in medical ultrasound. Muir and Carstensen (1980) investigated a variety of effects resulting from the non-linear propagation of finite-amplitude ultrasound and experimentally demonstrated non-linear acoustic phenomena in water. It was suggested that the harmonics generated could enlarge the beamwidth and hence degrade the lateral resolution of instruments. A theoretical model of the non-linear propagation of pulsed focused acoustic beams was developed to estimate the degree of distortion (Bacon, 1984). It has also been shown that for pulsed diagnostic beams shock formation in water was not only possible but common among commercial machines (Duck and Starritt,1984; Duck *et al.* 1985). The significance of the values of the parameter B/A, which shows the degree of

non-linearity, for tissues and biological fluids also indicated that it is important to consider the non-linear propagation of ultrasound in diagnosis and tissue characterisation (Law *et al.* 1985). Shock formation in tissue is possible where the beam has high intensity, high frequency and high focal gain.

The emphasis in the above papers is on wave propagation, the possible importance of harmonic generation, attenuative losses and their relevance for studies of biological effects and physiotherapy. Since non-linear propagation results in changes in the ultrasonic field and generation of harmonics, a transmitted pulse may be distorted when it arrives at the blood vessel. Therefore, the scatterers (blood cells) may be excited by a distorted wave. The Doppler spectrum may be changed consequently. However, to date, there have been no studies on the influence of non-linear propagation on Doppler measurements.

In this chapter, the non-linear propagation of ultrasonic waves will be demonstrated when the Doppler mode is used on two commercial scanners. The influence of non-linear propagation on Doppler measurement will be investigated.

## 7.2 Non-linear Propagation

The simplified approach commonly used in medical ultrasonics to describe wave propagation assumes that changes in pressure and density in the propagating medium are linearly related. If the density of the medium increases, a proportional increase in pressure is expected. However, this approach is correct only for waves of infinitesimally small amplitude and is not always appropriate in medical ultrasonic applications.

A more accurate pressure-density relationship of this is the series expansion (Duck *et al.*, 1984),

$$p = c_0^2 \rho + \frac{1}{2} \frac{c_0^2}{\rho_0} \left( \frac{B}{A} \right) \rho^2 + \cdots \tag{7.1}$$

where $c_0$ is the sound speed for waves of infinitesimal amplitude, $\rho_0$ is the static density, and $B/A$ is the second order parameter of nonlinearity for the medium. Retention of the first term gives the standard linear relationship. For water at

30°C $B/A$ has a value of 5.2. Most of the soft tissues of the body have higher values of $B/A$ (Law *et al.*, 1985).

The parameter of non-linearity, $B/A$, also occurs in the relationship between phase velocity, $V(x)$ and particle velocity, $U(x)$,

$$V(x) = c_0 + \left(1 + \frac{1}{2}\frac{B}{A}\right) U(x) \tag{7.2}$$

Therefore the phase velocity not only depends on the infinitesimal sound speed constant, but also on the local particle velocity via $B/A$. In the compressional phase of a pulse waveform, $U(x)$ is positive and $V(x)$ becomes greater than $c_0$ while $V(x)$ is lower than $c_0$ in the rarefaction phase. Hence, the positive half-cycles of the waveform propagate faster than the negative half-cycles and consequently catch up with the negative half-cycles. This results in distortion of the waveform. At increasing depth the distortion increases and a shock wave may then appear.

## 7.3 Non-linear Propagation And Doppler Ultrasound

The result of the nonlinearity of the speed of sound is the cumulative distortion in the propagating pulse waveforms. This generates new frequency components and these components are harmonically related. If an ultrasonic pulse is transmitted, by the time the pulse reaches the target of interest, it may have been distorted by non-linear propagation and new harmonics are generated. Therefore particles are insonated by a pulse which has a wider bandwidth so the backscattered signals received by the transducer have a wider bandwidth. This may result in changes in the Doppler spectrum.

A Doppler system is a narrow-band system. The bandwidth of the transducer and receiving system is usually smaller than the frequency of the high harmonics. Therefore, the high frequency harmonics may be filtered out by the Doppler system and have little effect on the Doppler spectrum. However, the amplitude of the fundamental frequency decreases when the amplitude of higher harmonics increases (Muir and Carstensen, 1980). In addition since a transmitted pulse

wave has a spectrum of different amplitudes over a range of frequency, different decreases in amplitude can result in the frequency components within the detection range of the Doppler instrument. Finally, the distortion due to non-linear propagation is not uniformly distributed in the sample volume. At centre of the beam, where the pressure amplitude is usually the largest, the distortion is more severe. Therefore compared to other regions, there are more energy losses in the fundamental harmonic because of the stronger high harmonics generated in this region. This may change the effective beam intensity profile in the sample volume and therefore the Doppler spectrum. However, the scale of these effects on the Doppler spectrum is unknown.

As can be seen from the above, the process of distortion due to non-linear propagation is very complex. It is therefore expedient to investigate experimentally the significance of this effect on the Doppler spectrum. In this study, non-linear propagation was demonstrated using Doppler transducers on two commercial duplex machines, and the effect of non-linear propagation on the Doppler spectrum was examined.

## 7.4 Methods

### 7.4.1 Equipment

To measure the beam waveforms, a bilaminar polyvinylidene fluoride (PVDF) membrane hydrophone was used (GEC-Marconi Ltd). The hydrophone is made from a membrane stretched over an annular frame and has an active element of 0.5 mm diameter in the centre. The thin membrane introduces little acoustic perturbation and so senses the free field acoustic pressure at the element. The bandwidth of the hydrophone was calibrated to be 10 MHz by its manufacturer. Waveforms were displayed on an oscilloscope (HP 4540 A 500 MHz digital oscilloscope) connected to the preamplifier of the hydrophone. Hardcopy was obtained from an ink jet printer interfaced to the oscilloscope.

Two transducers on two commercial duplex scanners were used in the demon-

| Machine | DSL | ATL UM9 |
|---|---|---|
| Type | Single Crystal | Phased array |
| Shape | Circular | Square |
| Size | 10 mm | 11 × 11 mm |
| Frequency | 2.5 MHz | 5 MHz |
| Focus | 6-8 cm | 4-5 cm |
| Gate length | 10 mm | 10 mm |

Table 7.1: Some characteristics of the two transducers used in this study.

stration of non-linear phenomena and for the Doppler spectrum study. The details of the two machines and transducers are listed in Table 7.1. In all cases the hydrophone-transducer distance was 5.5 cm for the ATL UM9 (Advanced Technology Laboratory, Ultramark 9) 5 MHz probe, and 8.5 cm for the DSL (Diagnostic Sonar Limited, Prisma) 2.5 MHz probe. These points corresponded to the site of greatest pulse waveform non-linear distortion in water.

Both a flow phantom and a string phantom were used in this study. The flow phantom has the advantage that it is similar to the physiological situation. The string phantom test provides a line of scatterers with the same velocity passing through the centre of the beam. As the distortion is most severe at the centre of the beam, it would be expected that the effect of non-linearity would be observed more easily with the string phantom than with the flow phantom.

The flow phantom used has been described in Chapter 2. The artificial blood was a suspension of sephadex G25 superfine particles in a mixture of 42% glycerol to 58% water. This gives a viscosity of $0.004 kgm^{-1}s^{-1}$ at $20°C$ which corresponds to that of blood at $37°C$ (McDicken, 1986). The spectra from blood and Sephadex are very similar in terms of their first and second order statistical properties (Hoskins *et al.*, 1990b).

The string phantom (BBS Medical Electronic AB, Sweden) contains a DC-motor, drivebelt, three pulleys and a string loop all mounted on a frame. The frame can be adjusted to give a suitable beam-string angle and height in the water tank. A loop of surgical nylon thread was used as the string.

For both the string and flow phantom studies the transducer-target distances

were 5.5 cm for the ATL 5 MHz probe and 8.5 cm for the DSL 2.5 MHz probe. These were identical to the transducer-hydrophone distances.

### 7.4.2 Demonstration of non-linear phenomena using a hydrophone

The transmitted ultrasonic pulse shape was observed at a fixed depth in water using a hydrophone and an oscilloscope to demonstrate the non-linear phenomena. The effect of output power and position in the beam on the pulse waveforms were investigated.

The ultrasonic pulses from both of the commercial transducers were examined in a measuring tank. The transducers were mounted on a platform which could be moved in two orthogonal directions above the water tank. The hydrophone was rigidly fixed on a holder under water and the distance between the transducer and hydrophone could be adjusted.

In the flow phantom experiments described in Section 7.4.3 the effect of non-linearity on the Doppler spectrum was investigated. It is known that the heat shrink tubing used has a higher attenuation than human blood vessels, and that differences in acoustic impedance between the heat shrink tubing and the surrounding material lead to refraction and reflection of the ultrasound beam. In this case it is important to establish that the pulse waveforms insonating the artificial blood are not adversely affected by the tubing, in terms of the degree of non-linear distortion present. Pulse waveforms were collected in this experiment with the same hydrophone-transducer arrangement as above, but with one half of a longitudinally cut heat-shrink tube placed over the active element of the hydrophone. The half tubing was oriented at 60° with respect to the axis of the beam.

#### The effect of increasing output power on pulse waveforms at the centre of the beam

For the DSL 2.5 MHz single crystal probe, pulse waveforms were obtained using a Doppler output power setting of +18 dB, +12 dB, +6 dB and 0 dB. For the 5 MHz phased array on the ATL UM9 scanner, pulse waveforms were obtained using Doppler output powers of 100%, 71%, 50%, 35%, 25%, 18% and 13% of the maximum Doppler output.

#### The pulse waveforms across the beam

Pulse waveforms from both the 5 MHz ATL probe and the 2.5 MHz DSL probe were measured across the beam at intervals of 0.5 mm.

### 7.4.3 Effect of non-linear propagation on the Doppler spectrum

As indicated above, non-linear propagation may distort the Doppler spectrum and increase the maximum Doppler frequency shift. In this section, the effects of non-linearity on both the maximum Doppler frequency shift and spectrum were investigated using the flow phantom and the string phantom.

#### Flow phantom measurements

A steady flow of maximum velocity 1 m/s was set on the flow phantom in a vessel of 5 mm inner diameter. Doppler signals were recorded on an audio cassette for both the ATL probe and the DSL probe. In each case the beam-vessel angle was 60°. The gate length was adjusted to cover the whole vessel. This gave a gate length of 10 mm for each machine. The output power was set to +18 dB. The recorded Doppler signals were replayed through a Doptek spectrum analyzer for analysis of the maximum frequency. The average value of the maximum frequency was extracted. The entire Doppler sonogram of 240 lines was transferred to a

computer for further analysis. On the computer, the average spectral profile of 240 lines of the sonogram was calculated.

#### String phantom measurement

For the string phantom test, the DSL machine was used. A constant string velocity of 1 m/s was used with a beam-string angle of 60°. The gate length was 10 mm. Doppler signals were again acquired onto audio cassette for power outputs of 0 dB, +6 dB, +12 dB and +18 dB. Further analysis was again performed using the Doptek spectrum analyzer and the computer.

## 7.5 Results

### 7.5.1 The pulse waveforms measured by the hydrophone

The pulse waveforms recorded for outputs of 0 dB, +6 dB, +12 dB, +18 dB from the 2.5 MHz DSL single crystal transducer are shown in Figure 7.1 The distortion due to the non-linear propagation became more severe as the output power was increased. The pulse waveform with 0 dB output was similar to a sine wave. However, the shock formation was clearly observed when the output increased to +18 dB. The compressional cycles showed a clear steepening on its leading edge with a sharp peak. There was an asymmetry in the magnitude of the compression and rarefaction cycles. The peak pressure of compressional and rarefactional cycles were 1.49 MPa and 0.74 MPa respectively. Similar results were also obtained from the 5 MHz ATL phased array.

The waveforms behind the half tubing are illustrated in Figure 7.2. Comparing the waveforms to those without the half tubing (Figure 7.1), the amplitudes of the peak pressure are reduced. In the waveform with +18 dB output, the compression peak pressure reduces from 1.49 MPa to 0.62 MPa. However, the distortion of the waveform is still significant.

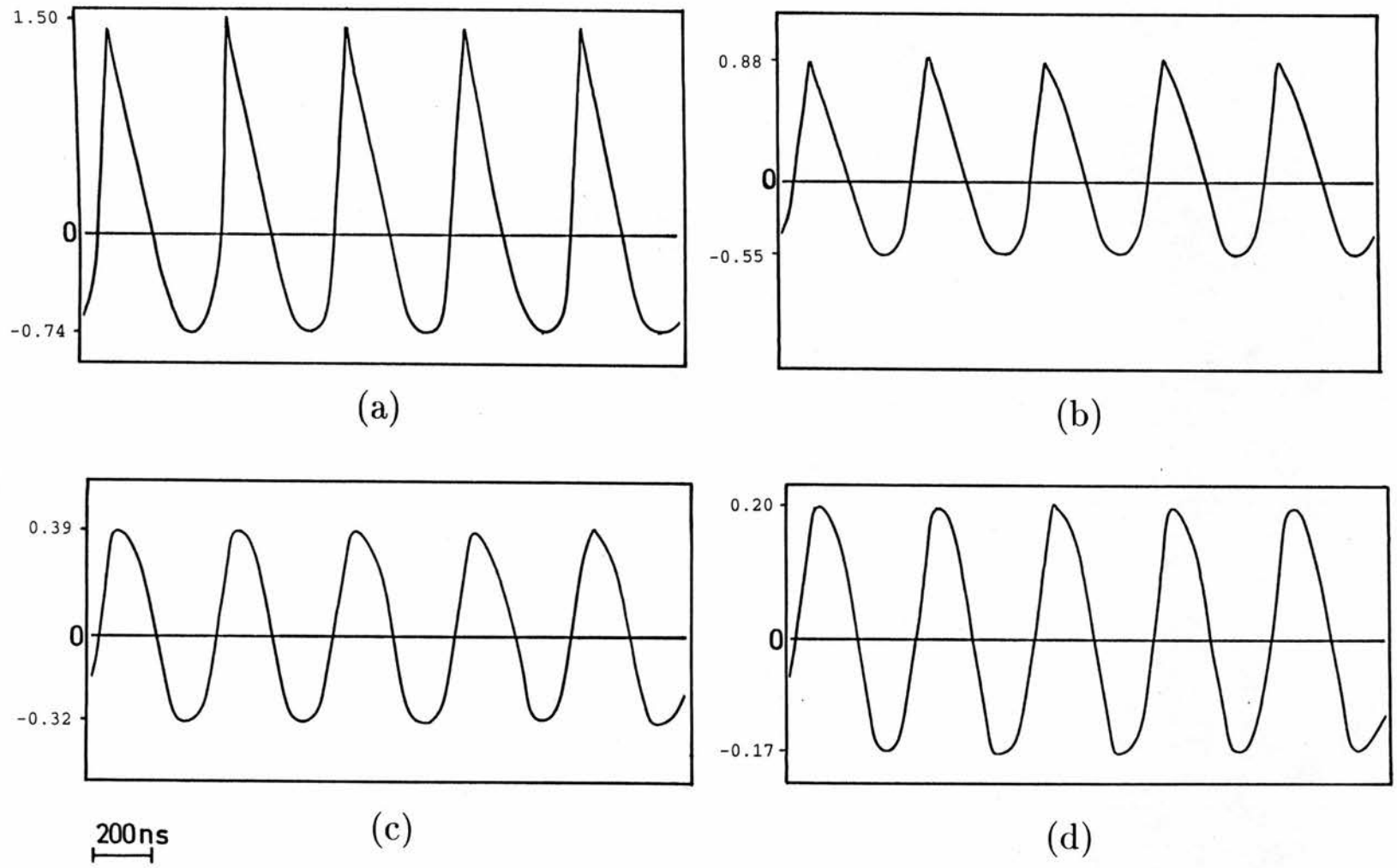


Figure 7.1 Pulse waveforms from the 2.5 MHz single crystal transducer observed at a distance of 8.5 cm, with Doppler output power a) +18db (-0.74 to 1.5 MPa). b) +12db (-0.55 to 0.88 MPa). c) +6db (-0.32 to 0.39 MPa). d) 0db (-0.17 to 0.20 MPa).

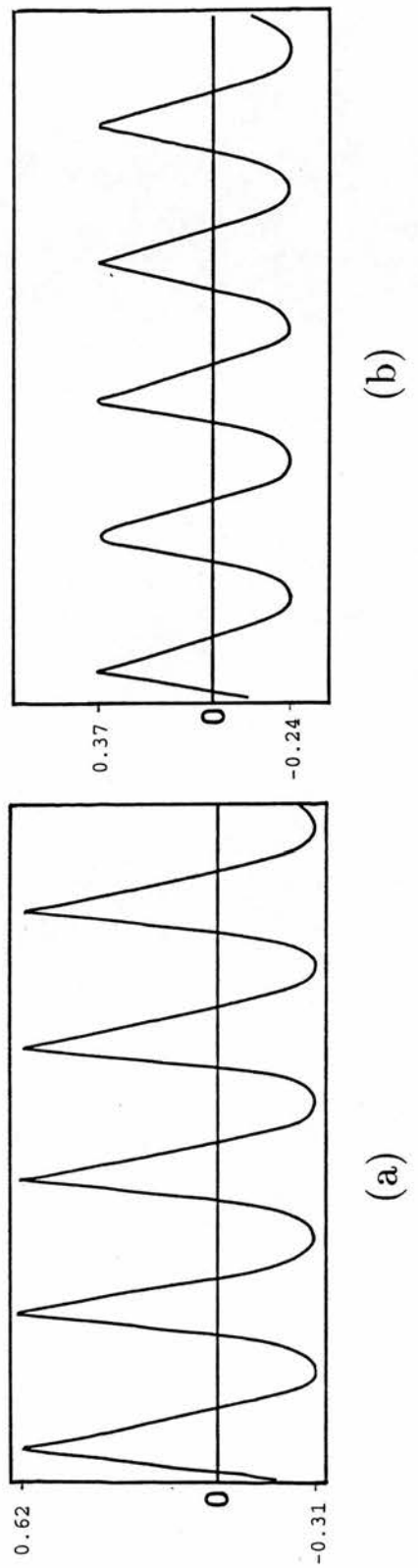


Figure 7.2 Pulse waveforms from the 2.5 MHz single crystal transducer observed behind a half tube with output power a) +18db (-0.31 to 0.62 MPa). b) +12db (-0.24 to 0.37 MPa). c) +6db (-0.13 to 0.17 MPa). d) 0db (-0.083 to 0.091 MPa).

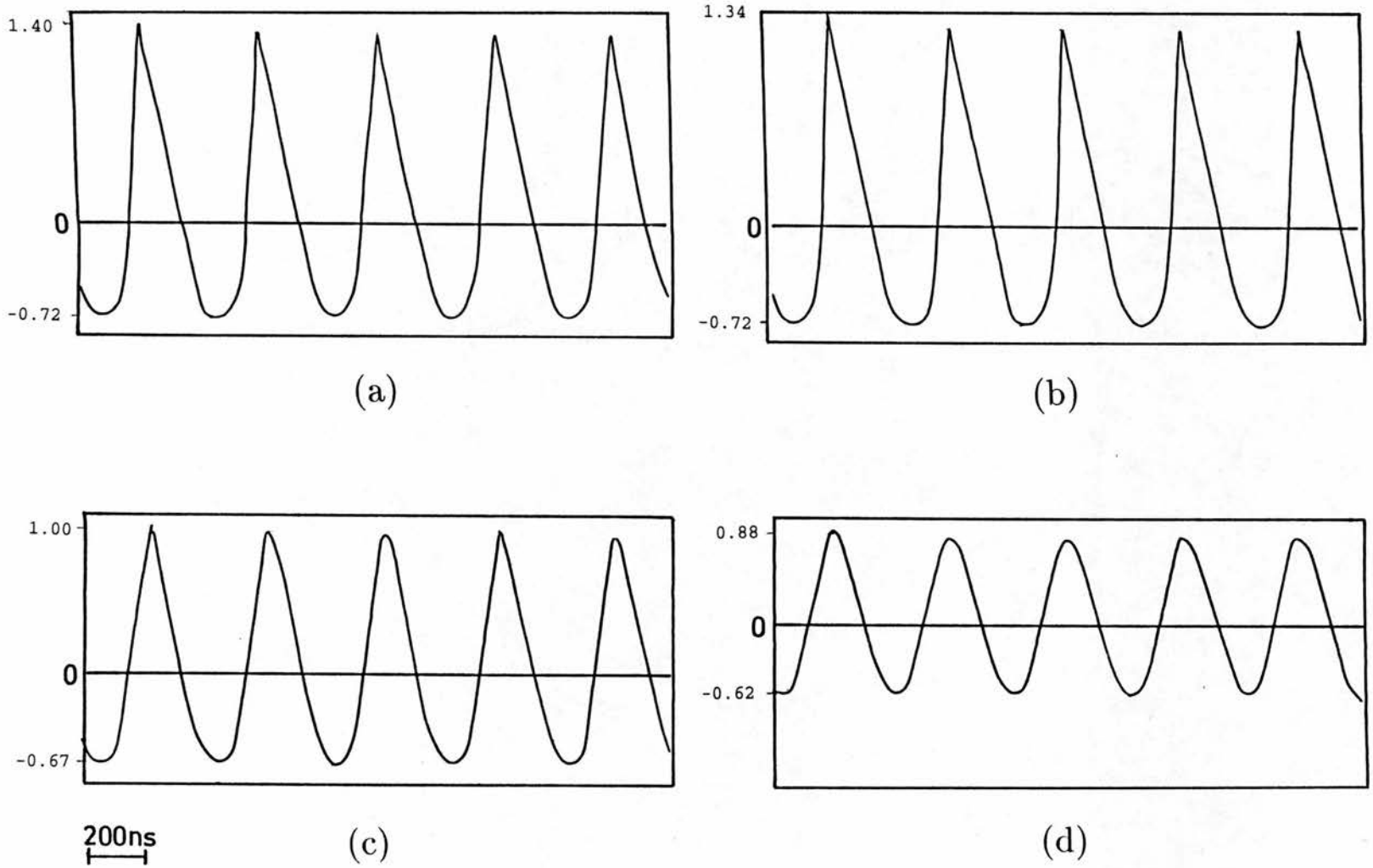


Figure 7.3 Pulse waveforms from the 2.5 MHz transducer observed with +18db Doppler output power at a) beam centre (-0.72 to 1.4 MPa). b) 1.0 mm from the centre (-0.72 to 1.34 MPa). c) 2.0 mm from the centre (-0.67 to 1.0 MPa). d) 3.0 mm from the centre (-0.62 to 0.88 MPa).

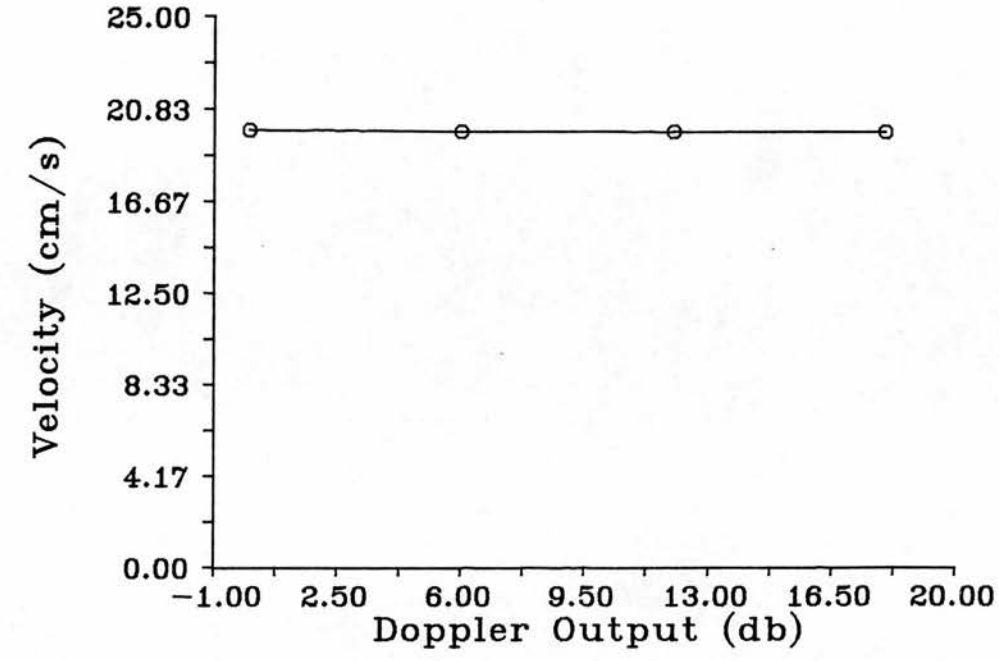


(a)

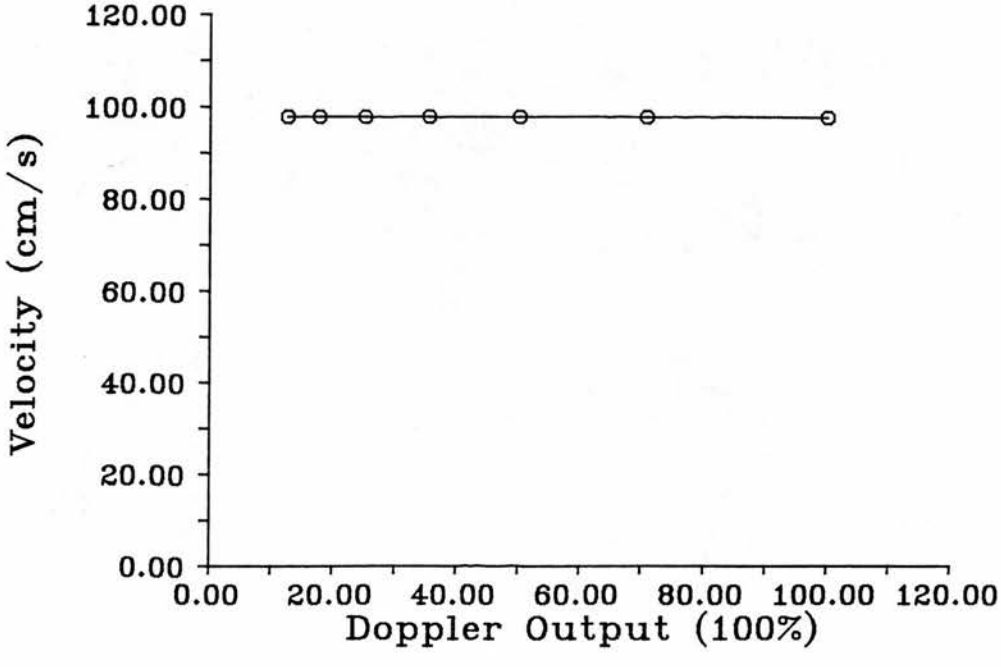


(b)

Figure 7.4: The measured maximum frequencies with different Doppler outputs (a) 2.5 MHz single crystal transducer; (b) 5.0 MHz phased array transducer.

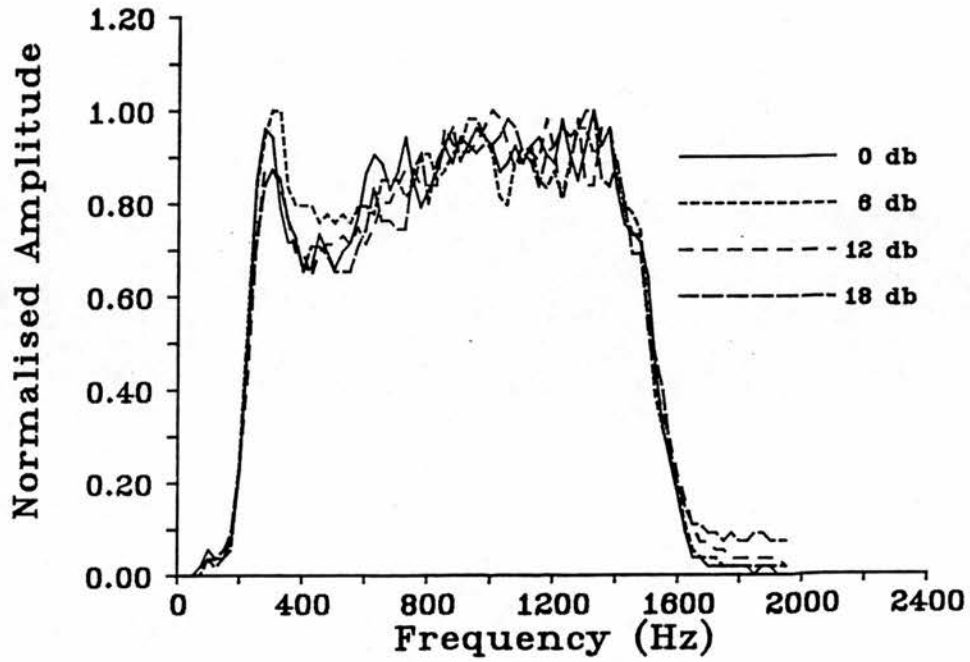


Figure 7.5: Doppler spectra received by the 2.5 MHz transducer using the flow phantom with Doppler output power 0dB, +6dB, +12dB and +18dB. No significant differences were observed.

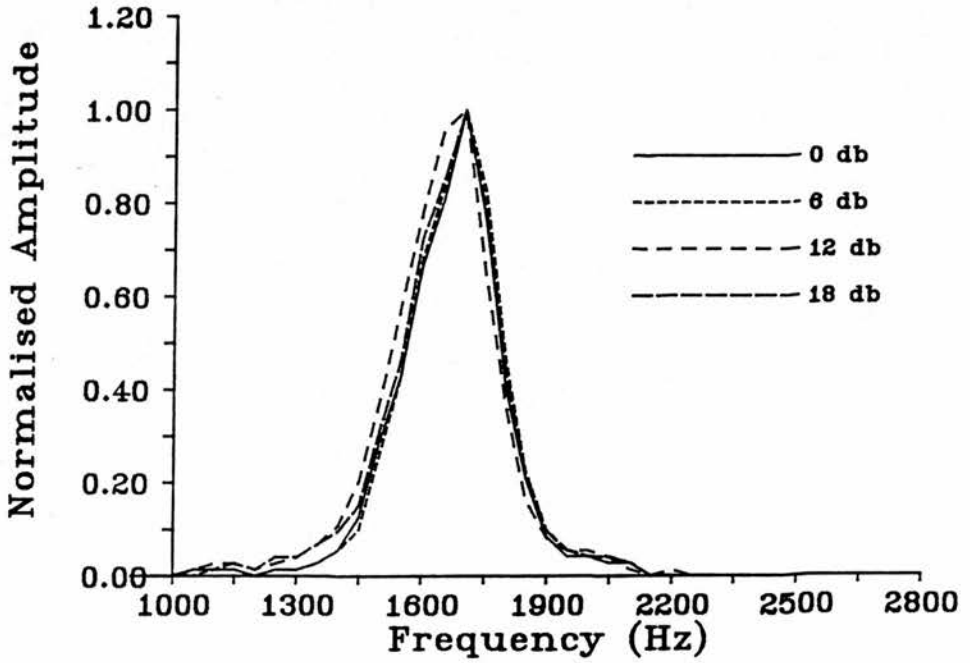


Figure 7.6: Doppler spectra received by the 2.5 MHz transducer using the string phantom with Doppler output power 0dB, +6dB, +12dB and +18dB. No significant differences were observed.

Figure 7.4 shows the maximum frequency from the flow phantom for both transducers with different output powers. There is no significant change in maximum frequency even though the corresponding pulse waveforms have clearly different degrees of non-linear distortion.

Figure 7.5 shows the averaged spectral profiles of data acquired from the flow phantom using the DSL 2.5 MHz probe with different output powers. Although the distortion of the pulse waveforms are obvious (Figure 7.3), there are again no significant differences between the Doppler spectral profiles. Figure 7.6 shows the averaged spectral profiles of data acquired from the string phantom using the DSL 2.5 MHz probe with different output powers. Again no significant difference among these profiles are observed.

## 7.6 Discussion

Although the pulse waveforms showed clearly different degrees of non-linear distortion, the flow and string phantom experiments indicate that the non-linearity does not affect the Doppler spectrum both in terms of the maximum frequency and the Doppler spectral profile.

There are several possible factors which can lead to such a result. The limited bandwidth of transducers and electronic processes such as demodulation, filtering, sampling *etc.* may cut off the high frequency harmonics. In the experiments, it was also found that only at the centre of the beam was the distortion due to non-linear propagation significant (Figure 7.3). In other parts of the beam, the waveforms were near to sine waves. Thus only a small part of the scatterers, which were in the sample for the flow phantom and along the string on the string phantom, were excited by the distorted waveform while most of the particles were not. Therefore, the influence of the non-linear propagation should be small. It is also interesting to notice that as most of the high harmonics are filtered out, the received backscattered signals from the central region of the beam should lose some energy due to the non-linear distortion. So if the beam centre is placed at the centre of the vessel, the maximum frequency should decrease rather than

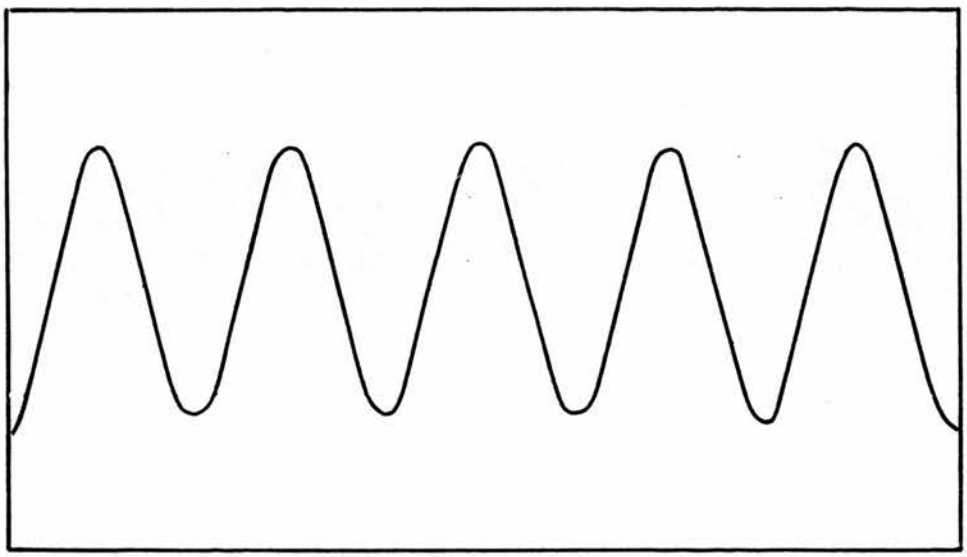

Figure 7.7: The pulse received by a transducer placed face to face with the DSL 2.5 MHz transducer.

increase. Although in the experiment a decrease was observed, it was small (only 0.5%) and not considered significant.

To verify that the limited bandwidth of the transducer and the distribution of the distortion can lead to a less distorted pulse received by the transducer, one more experiment was made. A single crystal 2.5 MHz transducer, which is very similar to the DSL 2.5 MHz transducer was used. This transducer was placed under water face with face to the DSL transducer. The distance between the two transducers was 5.5 cm which is identical to the previous hydrophone measurement. The pulse waveforms received by the new transducer were recorded by the oscilloscope and the printer. Using a Doppler output +18dB, which gave the most distorted waveform in Figure 7.1 (a), the received pulse was as shown in Figure 7.7. The waveform is very near to a sine wave and hardly distorted. This indicates that the limitation in bandwidth of the transducer and of area where the distortion is severe can significantly reduce the distortion in the signals received by the transducer.

In practice intrinsic spectral broadening also occurs (Newhouse *et al.*, 1980; Censor *et al.*, 1988). Each moving target subtends a range of angles so that the energy from each target will be spread into a range of Doppler frequencies. This leads to blurring of the Doppler spectral profile. The maximum Doppler frequency will arise from the largest transducer-target angle for targets within the beam. This target angle will not be for the centrally placed portion of the vessel or the string, but rather for a portion in an area not affected by the non-linearity. The relevant portion of the Doppler spectrum to look at for the effects of non-linearity will be near but not at the maximum frequency of spectra from the flow phantom, and at the centroid frequency of the string phantom spectra. In each case there was no significant effect. This indicates that spectral broadening may have acted to mask any effect which may be present.

In some clinical measurements, because the attenuation in soft tissue reduces the power of the ultrasound, as well as the fact that the high frequency components will be attenuated more than the lower frequency components, the distortion of the pulse waveforms will be less significant than in our experimental set up. Therefore, in practice non-linear propagation will give even less significant change in the Doppler spectrum than that in water. In situations where the ultrasonic pulse travels through liquid paths, for example the full bladder, amniotic fluid or a water-bath, non-linear distortion may be present but it will not offset the Doppler measurements.

## 7.7 Conclusion

Non-linear propagation of the pulse waveforms from commercially available duplex scanners operated in the Doppler mode can be observed. However, the non-linear propagation has no significant effect on the Doppler frequency shift measurement.

# Chapter 8

# PULSATILE FLOW

## 8.1 Introduction

In previous chapters, Doppler measurements from flow with a parabolic velocity profile has been discussed. To establish a parabolic flow profile, a long straight, non-branching tubing with a constant diameter and a steady flow rate are required. However, flow rates in most of human arteries are pulsatile and blood vessels curve and branch. Curvatures, branches and sometimes stenoses cause flow profiles to be skewed or even turbulent (Nichols and FO'Rourke, 1990). In this chapter, some preliminary work on the measurement of flow will be considered when the velocity profile is not parabolic.

The mean velocity measured from the mean frequency is usually not reliable (Chapter 4). An alternative approach is to estimate mean velocity using the maximum frequency envelope of the Doppler waveform. This has the advantage that the maximum is less sensitive to most of the factors discussed in Chapter 4. Maximum frequency methods usually assume that the velocity profile is flat (Light and Cross, 1972; Fisher *et al.*, 1983) or parabolic at all points during the cardiac cycle. For a flat profile, the maximum velocity simply equals the mean velocity. For parabolic flow, mean velocity $V_{mean}(t)$ is a half of the maximum. In general, however, this approach is not valid as the velocity profile in arteries usually falls somewhere between parabolic and flat (McDonald, 1974).

A theoretical study by Evans, D.H. (1985) suggested that under certain conditions, where there is not necessarily plug or parabolic flow, the time averaged mean velocity $\overline{V_{mean}}$ of a pulsatile flow is equal to half of the time averaged maximum velocity when calculated over an integral number of cardiac cycles. This relationship was derived for ideal conditions where the vessel is long and straight, the diameter is constant, and the flow is unidirectional and laminar. It should be noted that the relationship between the time averaged maximum and mean velocities as suggested by Evans, D.H. (1985) for pulsatile flow is the same as the relationship for steady and parabolic flow if the assumption is made of parabolic flow at all points during the cardiac cycle. Using this approach the mean velocity averaged over a number of cardiac cycles $\overline{V_{mean}}$ can be estimated by

$$\overline{V_{mean}} = \left( \frac{c}{4F_0 \cos\theta} \right) \overline{(F_d)_{max}} \tag{8.1}$$

where $c$ is the sound speed, $\theta$ is the beam-vessel angle and $\overline{(F_d)_{max}}$ is the maximum frequency averaged over a number of cardiac cycles.

To date there has been no experimental data presented to support the use of Equation ( 8.1). It is the intention of this chapter to examine the accuracy of this theory over a range of beam-vessel angles, flow rates and waveform pulsatility.

It is noticed that this theory is derived under some conditions. The the vessel must be long and straight so that the flow in the vessel is laminar. No large flow reversal should be present so that the maximum velocity always occurs at the centre of the vessel. However, in the body, many blood vessels branch and curve and flow reversal can be found in many arteries. When flow enters a curved section, the centrifugal force tends to skew the parabolic profile towards the outside wall and secondary spiral flow patterns may occur (Evans, D.H. *et al.*, 1989a). Stonebridge and Brophy (1991) suggested that the spiral flow may be physiological and universally in blood vessels, even they are relatively straight. In this chapter, Evans' theory will also be examined in a region of curvature and where there is flow reversal.

## 8.2 Method

### 8.2.1 Materials

To collect data in *vitro*, the physiological flow phantom (Chapter 2) was used. The artificial blood was a suspension of sephadex G 25 superfine particles in a mixture of 42% glycerol to 58% water. This has a viscosity of 0.004 $kg/ms$ at $20°C$ which corresponds to that of blood at $37°C$.

A Doptek 4 MHz continuous wave unit was used for waveform acquisition. All the spectra were recorded on magnetic tapes. Simultaneous measurements of absolute flow were made using a measuring cylinder and a stop watch.

Two kinds of tubing were made. The straight tubes, which were used in all the experiments except those concerning spiral flow, were made from heat-shrinkable material. Tubes with diameters of 5.0 mm and 8.0 mm were used. To create spiral flow, three spiral tubes were also constructed. Each tubing was coiled around a metal support rod in the form of a helix. The diameters of the tubes were 3.87 mm, 5.0 mm and 6.5 mm. The pitches, or the distance between each spiral, of the tubes were 6 cm, 11 cm and 11 cm respectively.

The flow waveforms used in this study included steady flow as well as unidirectional and bidirectional flow of different pulsatility. Four typical waveforms are illustrated in Figure 8.1. The peak velocity of all waveforms was about 1 m/s which is similar to the physiological value in many vessels of interest.

### 8.2.2 Effect of pulsatility

Waveforms of different pulsatility and shapes were acquired. Tubing of internal diameter of 5.0 mm and 8.0 mm were used. 13 waveforms of pulsatility index ranging from 0 to 12.53 were used with the 5.0 mm tube. 18 waveforms of pulsatility index ranging from 0 to 12.07 were examined on the 8.0 mm tubing for a more detailed study. The distance between transducer face to the centre of each

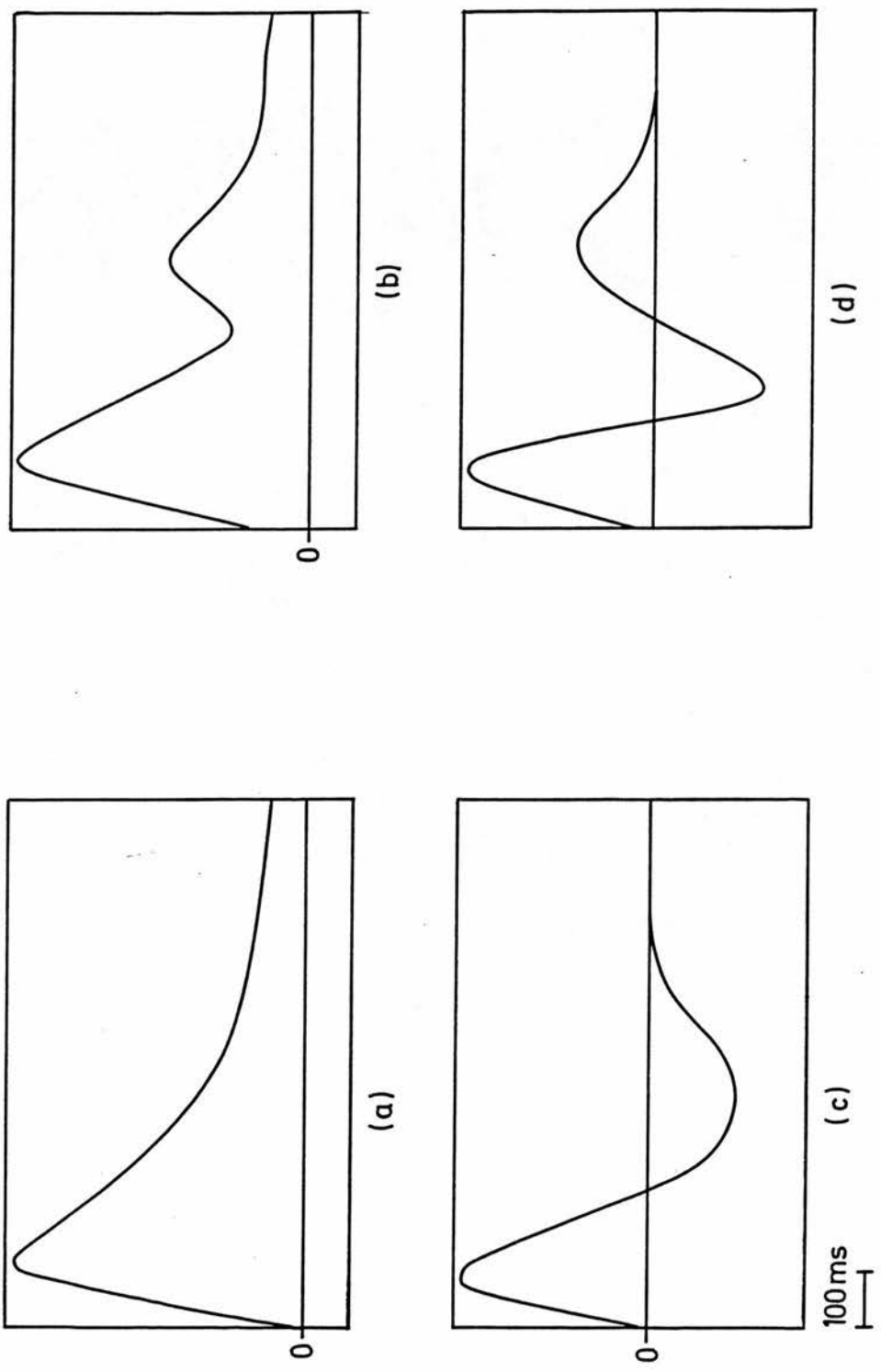


Figure 8.1: Typical waveforms used in this study. (a) single-phase unidirectional flow; (b) biphasic unidirectional flow; (c) biphasic bidirectional flow; (d) triphasic bidirectional flow.

tube was 5.0 cm.

### 8.2.3 Effect of beam-vessel angle

Four waveforms of different pulsatility and shape including steady flow, unidirectional flow and bidirectional flow were acquired for angles from 85° to 35° in 5° steps. The depth of the tubing was set to be 5.6 cm. The experimental results were also compared with the theoretical estimation described in Chapter 7 and Appendix A.

### 8.2.4 Flow rates

Two waveforms (see Figure 8.1 (b) and (d)) with unidirectional flow and bidirectional flow were examined using 5.0 mm tubing. Twelve different flow rates were used. The peak velocities were from 48.9 cm/s to 244 cm/s corresponding to Reynolds number from 672 to 3358. This enabled some momentary turbulence, which was observed as irregular high frequency spikes on spectra, to occur at the higher velocities. The diameter of the tubing was 5.0 mm and the distance between transducer and vessel was 5.0 cm.

### 8.2.5 Stenosis

To find out how stenosis and turbulence affect the estimation of mean velocity, a 75% artificial stenosis with an internal diameter of 2.5 mm was fixed in the 5.0 mm heat-shrinkable tubing. Three waveforms were acquired from 9 different sites both distal and proximal to the stenosis. The distance between the transducer face and the centre of the beam was 5.0 cm.

### 8.2.6 Spiral tubing

Black ink was injected into each spiral tubing with a syringe and a fine needle at about 1 cm to the spiral. Observation of the spiral shape of the flow was made.

For maximum velocity measurement, two experiments were performed. First the 3.87 mm spiral tubing and steady flow were used. The flow rate ranged from about 150 ml/min to 410 ml/min (maximum velocity from about 24 cm/s to 61 cm/s). This range is similar to that in the umbilical vein. As it is difficult to define the beam-vessel angle for the spiral part of the tubing, Doppler spectra were acquired from the straight part of the tubing. Fourteen positions ranged from 0 cm to 16 cm from the end of the spiral were examined.

For the 5.0 cm spiral tubing, both pulsatile and steady flow were used. Two velocities were of about 90 cm/s and 50 cm/s were selected. Six waveforms including steady flow, unidirectional pulsatile and bidirectional pulsatile flow were used. The measurements were made at 11 positions from 2 cm to 40 cm from the end of the spiral. The same experiment was repeated using the 6.5 cm tubing using three waveforms, which also included steady, unidirectional and bidirectional flow. Measurements were made at 12 positions from 1.0 cm and 20.0 cm to the end of the spiral.

### 8.2.7 Data analysis

The spectra recorded on tapes were transferred to the Doptek unit for calculation of the maximum frequency envelope. The envelope of each waveform was traced manually using the Doptek light pen system, and automatically using the 15/16 percentile method. In the percentile method the total value T of pixel values (voltage amplitude) of a single spectral line is calculated. The maximum frequency is then calculated as the point where the sum of pixel values below that frequency just exceeds a specified percentage of T. In this case this is 15/16 expressed in percentage terms.

The estimated mean velocity $\overline{V_{mean}}$ was calculated using Equation ( 8.1). The

true mean velocity was calculated from timed collection of flow using Equation ( 8.2)

$$\overline{V_{real}} = \frac{Volume\ in\ measuring\ cylinder}{Time\ of\ collecting} \cdot \frac{1}{\pi r^2} \tag{8.2}$$

where $r$ is the internal radius of the tubing.

The difference between the Doppler estimated mean velocity and true mean velocity was expressed as the error $E$ by

$$E = \frac{\overline{V_{real}} - \overline{V_{mean}}}{\overline{V_{real}}} \tag{8.3}$$

The measured mean velocity $\overline{V_{mean}}$ is in general lower when calculated from the envelope obtained using the 15/16 percentile method than calculated from the envelope obtained by hand-drawing. This is a direct result of the fact that in the 15/16 percentile method 1/16 of the spectral power lies above the maximum frequency, whereas in the manual method the operator is able to assess the highest frequency present. By using both hand-drawing and 15/16 percentile methods, we hope we can obtain a better understanding of the error in mean velocity measurement.

## 8.3 Results

### 8.3.1 Effect of pulsatility

Figure 8.2 (a) illustrates the ratio $E$ of waveforms with different pulsatility index values in 5.0 mm diameter tubing. The broken line represents $E = 1.054$ which is the average of the ratios. The results showed a reasonably good agreement with the theory of Evans, D.H. (1985). Little difference between waveforms of different pulsatility and shape were shown at this diameter. The systematic error of about 5% can be explained by the geometrical spectral broadening. It must be noted that even those waveforms with large flow reversal obey the theory reasonably well.

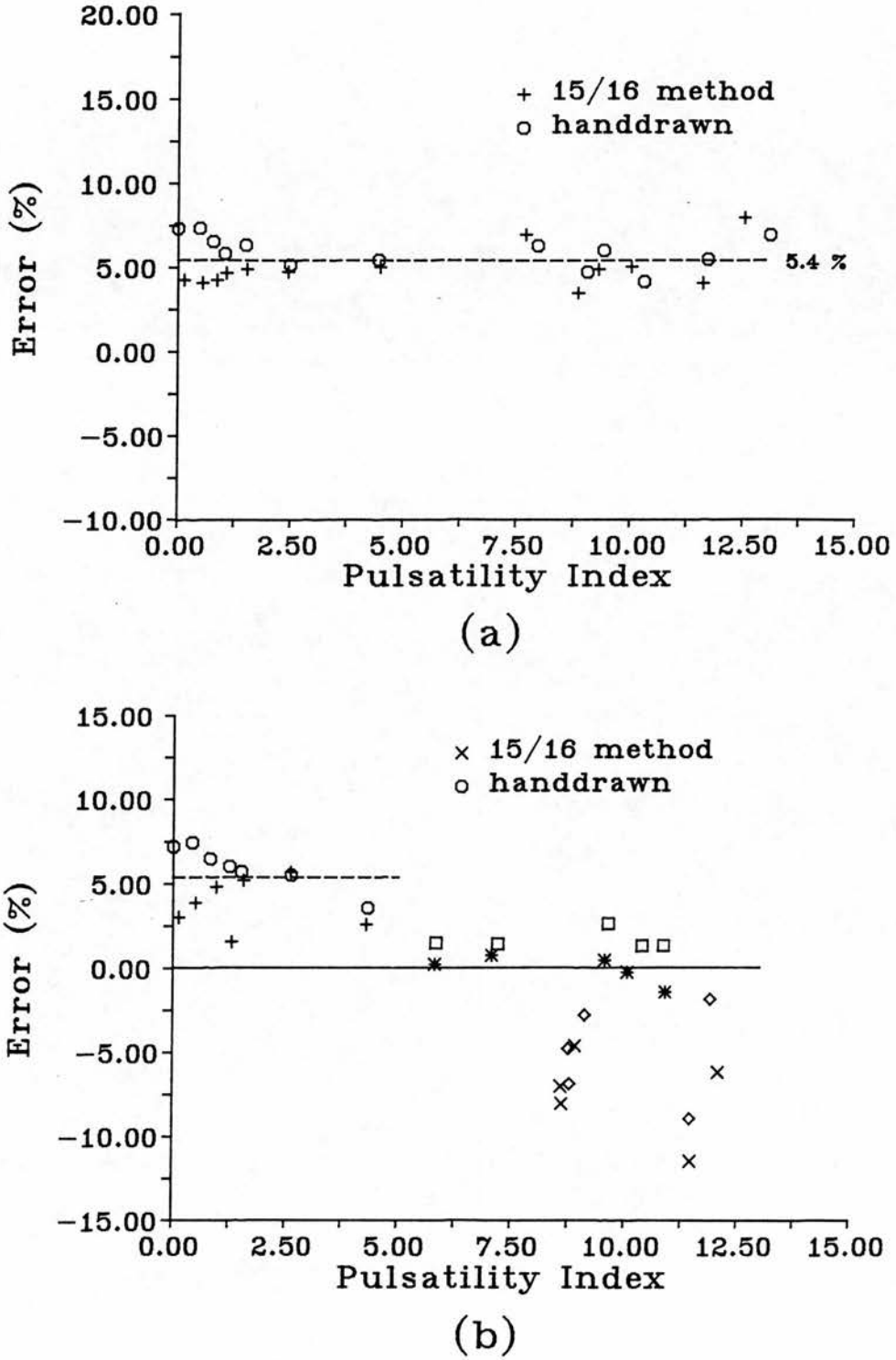


Figure 8.2: Effect of pulsatility. In (a) 5 mm tubing was used. ◯ and + denote results from hand-drawing and 15/16th method respectively. In (b) 8 mm tubing was used. ◯ and + denote the results from unidirectional waveforms; □ and ∗ symbolise the bidirectional and biphasic flow and ◇ and × indicate bidirectional and triphasic flow.

For the larger tubing of 8.0 mm diameter, it was shown that the ratio E was more dependent on pulsatility (Figure 8.2 (b)). The waveforms in this test can be classified in to three categories. The first group was unidirectional flow denoted by $\bigcirc$ and $+$. Similar results to those of the 5.0 mm tubing were obtained in that a consistent overestimation of mean velocity by about 5% was made. The second were symbolised as $\square$ and $*$. The waveforms in this group were bidirectional and biphasic. The errors were near 0 which shows about 5% drop compared with the first group. Symbols $\diamond$ and $\times$ indicate the waveforms which have three phases. There was more variation of $E$ for this group and on average there is a 7% or 8% fall in $E$ compared to the second group. The changes may be due to two causes. Firstly, large flow reversal can cause a considerable difference in velocity between layers in the tube and therefore vortices may form. A second cause may be distortion of the tube when large flow reversal occurs.

### 8.3.2 Effect of beam-vessel angle

The ratio $E$ of four waveforms including steady flow, unidirectional and bidirectional flow (See Figure 8.1) measured at angles from 40° to 85° are illustrated in Figure 8.3. The errors were less than 6% for angles smaller than 60°. However, the errors increased sharply when the angle was greater than 70° due to intrinsic spectral broadening. It was impossible to measure the velocity beyond the angle of 40° because the critical angle effect sharply diminished the intensity of the Doppler signal. Again little difference between waveforms was shown.

To see if the error caused by geometrical spectral broadening could be corrected, a theoretical estimation of the ratio $E$ at various beam-vessel angles was made (See Appendix A). The agreement between the curve of estimated error and hand-drawn estimation is better than 3% for angles up to 80° (Figure 8.3).

### 8.3.3 Effect of flow rate

The ratio $E$ of the measured mean velocity against real mean velocity is plotted in Figure 8.4. No obvious changes were observed for different flow rates. As

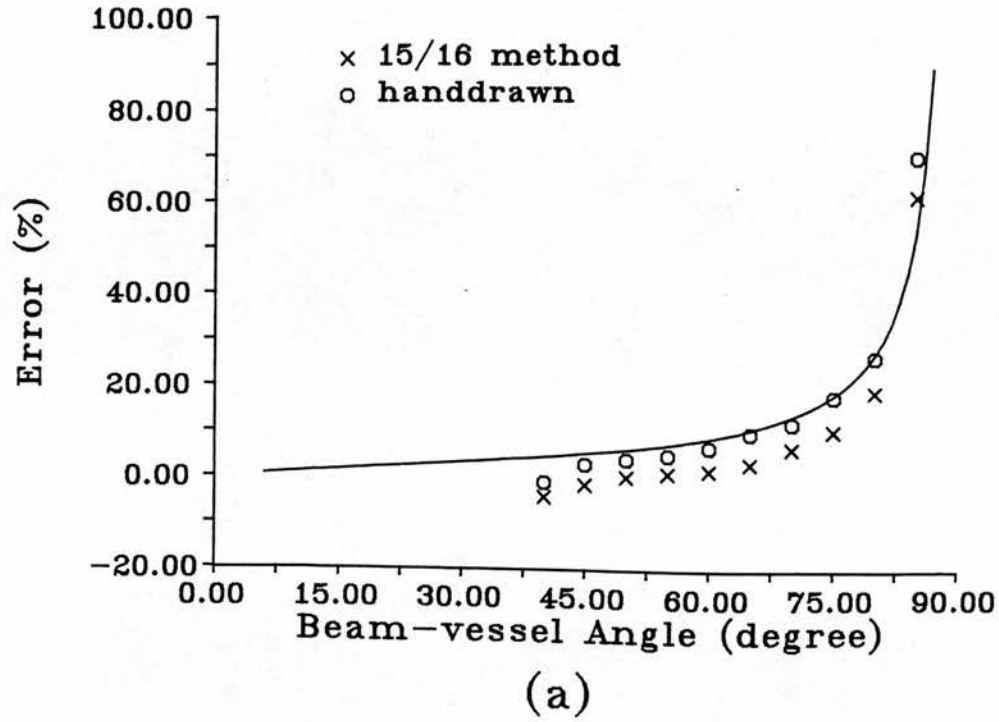


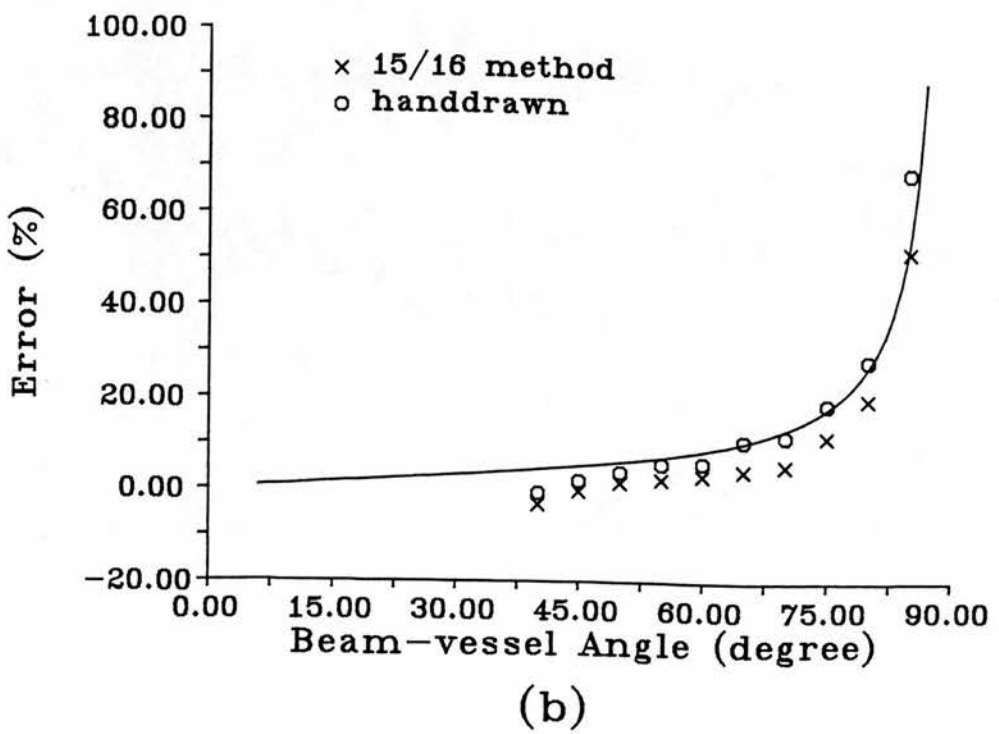


Figure 8.3: (a) and (b)

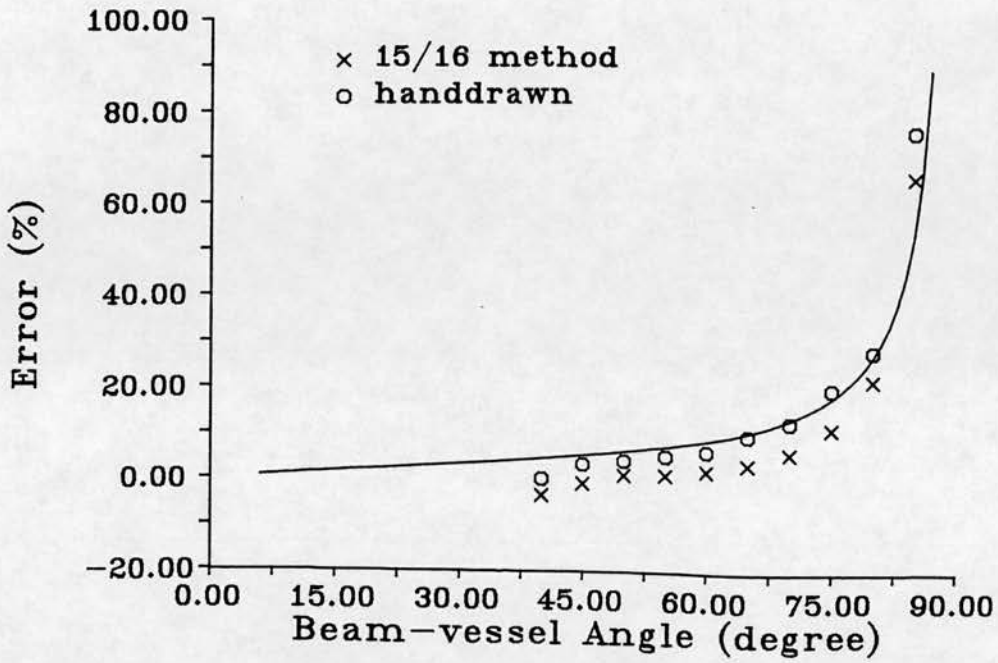


(c)

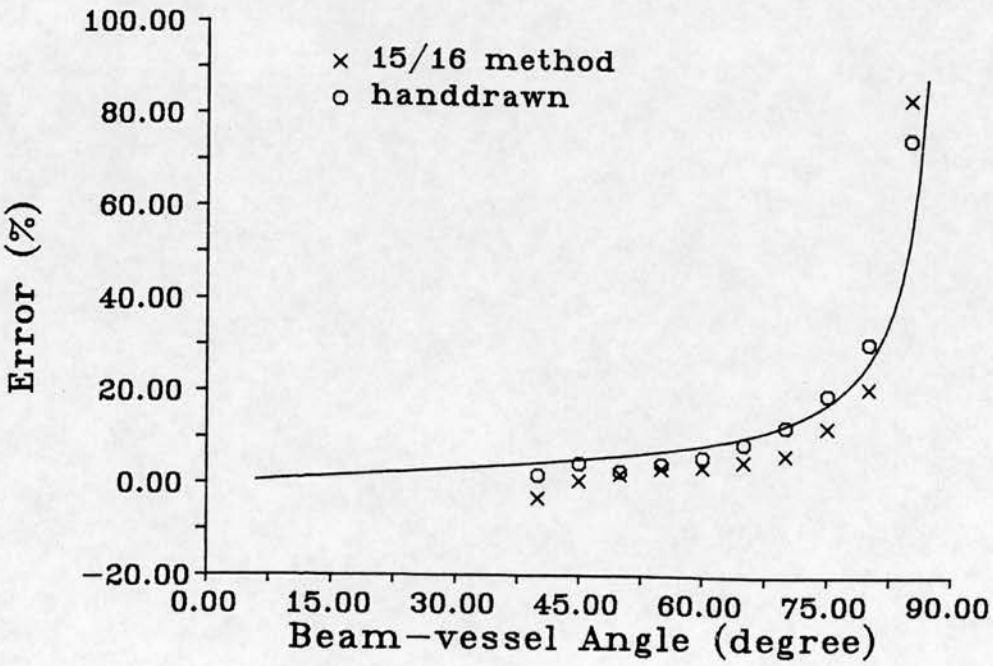


(d)

Figure 8.3: Effect of angle with (a) steady flow; (b) unidirectional flow; (c) biphasic flow with flow reversal; (d) triphasic flow with flow reversal. The solid curves are the estimated values with the consideration of geometrical spectral broadening (See Appendix A).

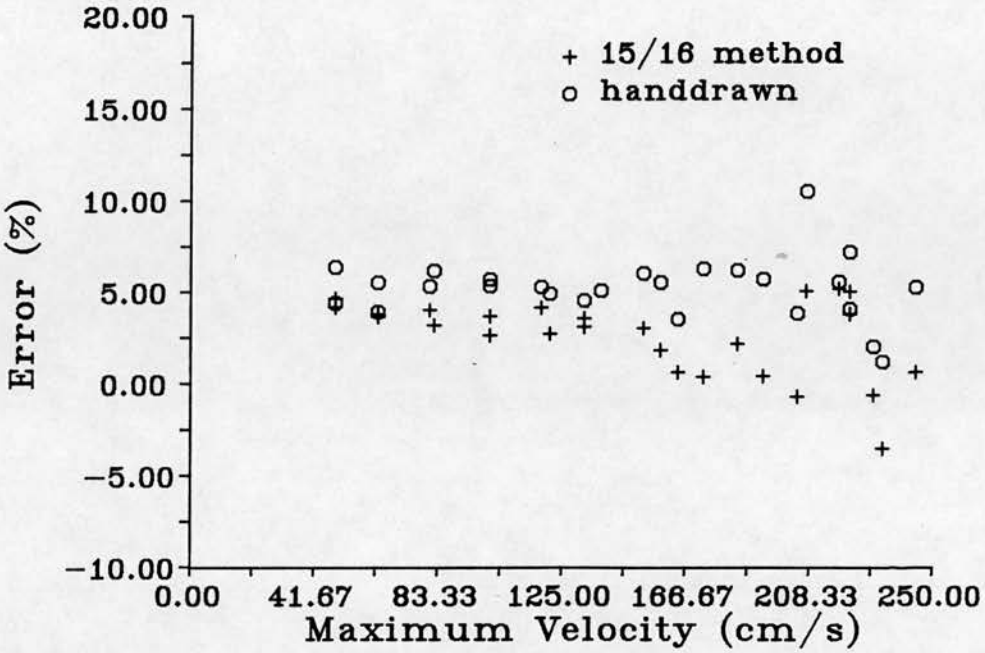


Figure 8.4: Effect of flow rate. No significant changes were observed for different flow rates

expected, the errors at small flow rates were quite low. At high velocity, momentary turbulence was observed as irregular high frequency spikes. It was also found that when the pulsatility of the waveform was higher, the turbulence appeared at higher flow rates.

### 8.3.4 Effect of stenosis

Large changes in the ratio $E$ were observed with maximum values of $E$ of about 3.0 in the region of the stenosis (Figure 8.5). At the distal side of the stenosis, the ratio E changed considerably for each of the waveforms used. The ratio E tended to the pre-stenotic value at a distance of about 13 cm distal to the stenosis. At the proximal side, the errors are small for steady (Figure 8.5 (a)) and unidirectional (Figure 8.5 (b)) flow. For the bidirectional flow, during reverse flow the turbulent region is on the proximal side of the stenosis and will manifest itself on the reverse flow component of the pre-stenotic waveforms. This explains the large drop in E observed in Figure 8.5 (c).

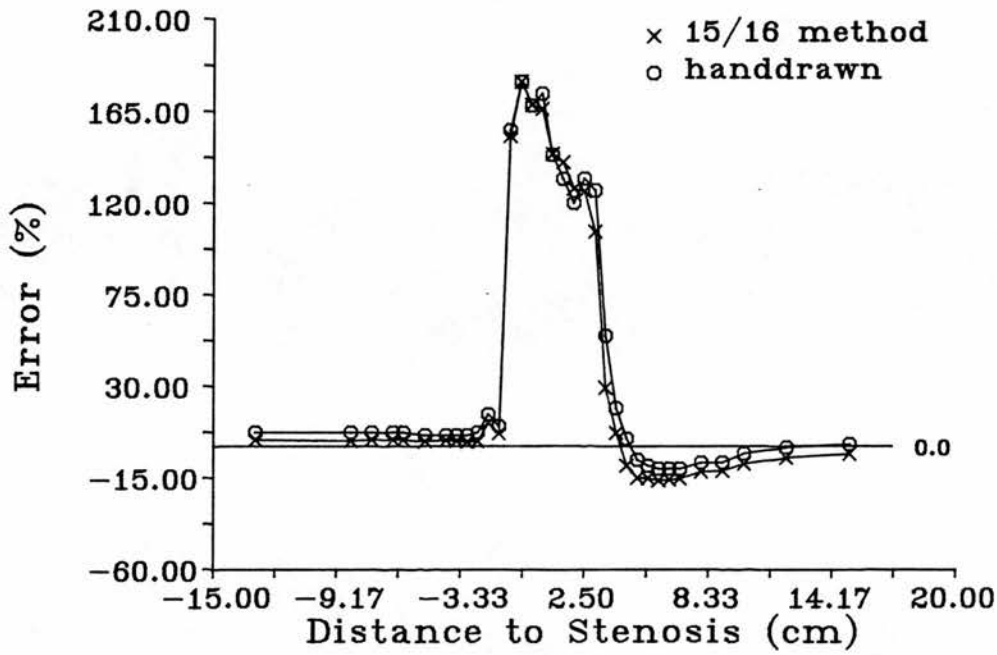


(a)

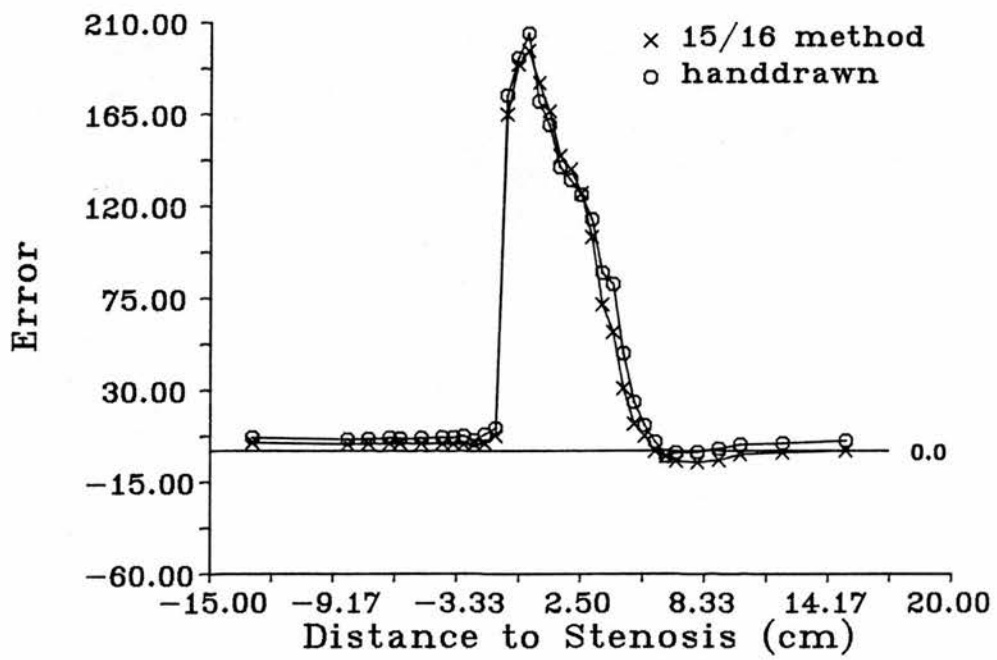


(b)

Figure 8.5: (a) and (b)

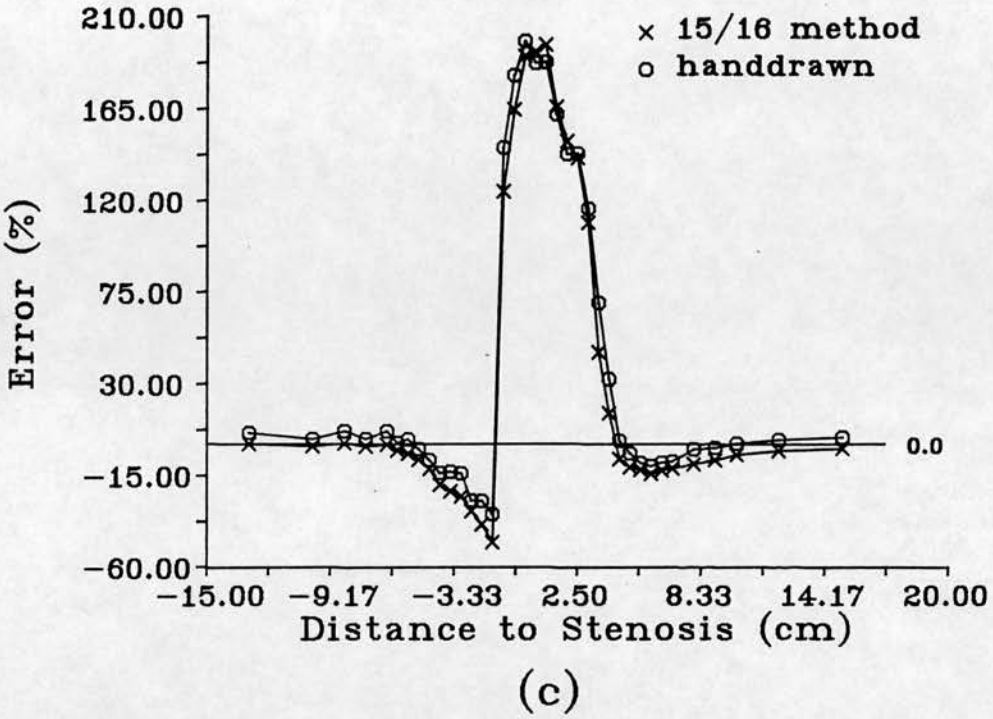


(c)

Figure 8.5: Effect of stenosis with (a) steady flow; (b) unidirectional flow. (c) triphasic flow with flow reversal. Negative distance is proximal to the stenosis and positive is distal.

### 8.3.5 Effect of spiral flow

For a steady flow, the error in the velocity estimation decreased when the sampling site was away from the end of the spiral (Figure 8.6). This is expected as the spiral secondary flow, which is the flow in the plane normal to the vessel axis, diminishes gradually with the distance. It is also found that errors in the velocity estimation are dependent on the flow rate. Smaller flow rates give relatively small errors. The highest error is about 15%. For a distance over about 4 cm to the spiral, most errors drop to under 10%.

The experiment using pulsatile flow showed some quite different results. For the 6.5 mm tubing, the steady flow at the end of the spiral has an error just over 5% (Figure 8.7). The error increases with the distance from the end of the spiral and is maximum at a distance 8 cm from the spiral, and then decreases for larger distance. This is different from the results for 3.87 mm spiral tube, indicating that the error is dependent on the diameter of the tubing and flow rate. For

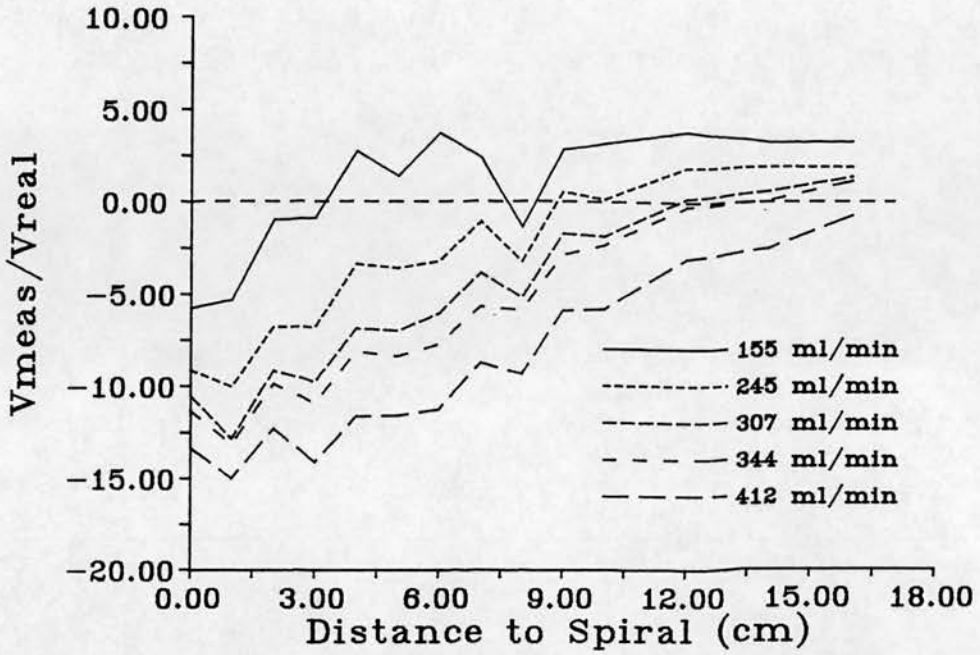


Figure 8.6: Steady flow on the 3.87 spiral tubing. The errors in mean velocity estimation decreased when the distance to the spiral is increased and the flow rate is decreased.

bidirectional flow the error is higher than 10%. However, it is interesting that the unidirectional flow gave small errors under 4% in all the measurements. This suggests that unidirectional flow may cancel some effects of spiral flow profile.

A more detailed study therefore was made on the 5.0 mm spiral tubing. The results are shown in Figure 8.8. The steady flow gives very similar results to 3.87 tubing (Figure 8.6). For unidirectional flow, three waveforms which had different pulsatility indices of 0.5, 1.5 and 2.4 respectively were used. The results indicate that all three waveforms have errors less than about 9% in the mean velocity estimation. These errors are smaller than for steady and bidirectional flow and decrease faster with distance. Waveforms with higher pulsatility result in smaller errors which tend to be more constant over a range of distance. The bidirectional flow again caused a large underestimation of the mean velocity and changed significantly with the distance.

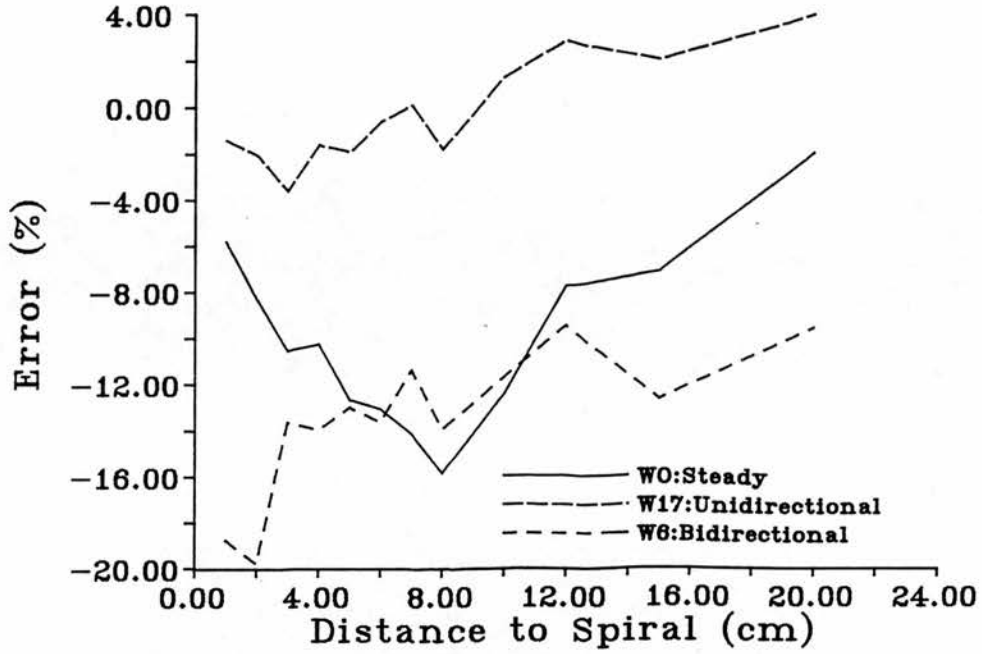


Figure 8.7: Pulsatile flow on 6.5 mm spiral tubing. Steady flow and bidirectional flow gave large errors in the mean velocity estimation. However, unidirectional flow caused small errors.

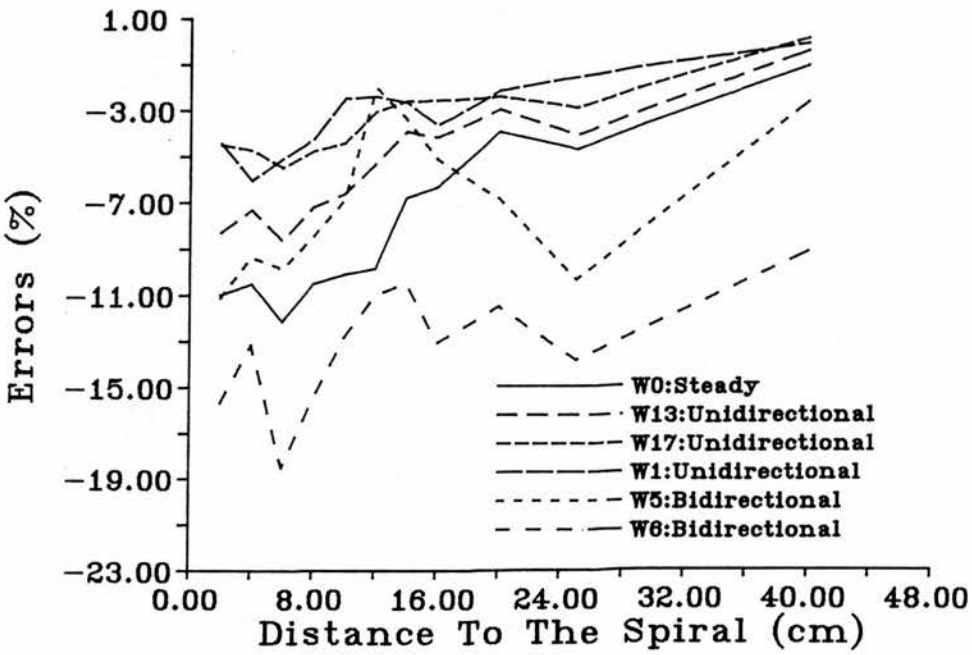


Figure 8.8: Pulsatile flow on 5.0 mm spiral tubing. The higher pulsatility in unidirectional flow results in lower errors.

## 8.4 Discussion

This study has shown that for a large range of physical conditions, the theory of Evans, D.H. for estimation of the mean velocity from the maximum velocity agrees reasonably well with the experimental results. This theory assumes that the maximum velocity is centrally located in the vessel, which is true for unidirectional flow in a long straight, non-branching tube. The results of this study suggest that there is only a small difference in estimation of mean velocity when there is flow reversal and a relatively small vessel is used. This may imply that in practice the maximum velocity is still located in the centre of the vessel, or it is not necessary to assume that the maximum velocity is always located in the centre of vessel.

In practice, because of the finite size of the transducer and sample volume, geometrical spectral broadening occurs (see Chapter 5). This leads to overestimation of the maximum frequency using Equation ( 8.1), particularly at large beam-vessel angles. The agreement between the theoretically estimated curves and experimental data (Figure 8.3) suggests this effect may be corrected.

One important assumption concerns the flow pattern in the vessel. The assumption of a long straight non-branching tube implies that the flow is laminar. If the sampled site is located near stenoses or large curvatures, the theory can not be assumed to be valid. Measurement in these locations should be avoided. A second possible cause of error is the change in diameter. The diameter of a vessel increases in systole and decreases in diastole and therefore changes the flow profile. This effect is most noticeable in the aorta and large arteries. These factors may modify the application of this method of mean velocity estimation in practice (Eik-Nes, *et al.*, 1982, 1984; Marsal, *et al.* 1984; Teague, *et al.*, 1985; Struyk, *et al.*, 1985).

The experiments with the spiral tubes also showed that the unidirectional pulsatile flow gives smaller errors in the mean velocity estimation than those with steady and bidirectional flow. Higher pulsatility results in lower error. This suggests that the pulsatility of the flow can to some extent cancel the effect of spiral flow. Therefore, more accurate mean velocity estimations can be obtained

with unidirectional pulsatile flow than steady or bidirectional flow.

A Doptek continuous wave Doppler unit was used in this study. In practice, pulsed wave Doppler is most often used in Duplex scanners. Pulsed Doppler units may be roughly classified into two groups; those that use long gate times sufficient to interrogate the entire vessel, and those that use very short gates so that the flow in only a small part of the vessel is interrogated. For volume flow measurement, long gate time PW operation is most commonly used. As a long pulse has a narrow frequency bandwidth and this results in little spectral broadening, the spectrum measured is actually very similar to those measured by CW operation. For short pulses, as the bandwidth of the spectrum of the transmitted pulse is of order of inverse of the pulse length, spectral broadening will happen. Therefore the mean velocity measured by the method discussed in this paper may be overestimated.

## 8.5 Conclusion

In this study, it has been shown that under ideal conditions, the mean velocity is generally estimated to within about 5 % from the maximum frequency envelope of the Doppler waveforms over a large range of waveform pulsatility values and flow rates. This error increases as the beam-vessel angle increases due to intrinsic spectral broadening. The mathematical model for the maximum frequency estimation using extreme angles shows that the error in estimation of the mean velocity could be reduced to less than 3%. The presence of turbulence, for example in the region of a stenosis, can cause considerably large errors. For unidirectional flow the errors are less than 9% in the region immediately beyond the spiral tubing. For steady and bidirectional flow the errors are larger. This suggests a more accurate estimation may be obtained in pulsatile flow than steady flow in clinical practice.

# Chapter 9

# CONCLUSION AND FUTURE WORK

## 9.1 Summary And Conclusion

A detailed study in the accuracy of volume flow measurement has been performed both theoretically and experimentally in this thesis. Two computer models were developed to simulate the Doppler spectrum in various measuring conditions such as different transducer-vessel geometry, transducer type and focusing, *etc.*. Good agreement was obtained between the simulations and experimental studies a on computer controlled flow phantom. The effect of a number of factor on the volumetric flow measurement was investigated. These factors were transducer type and size, distance between the transducer and the vessel, focusing, misalignment of the beam and the vessel, size of the vessel, beam-vessel angle, reflection and refraction at the vessel wall, velocity profile and geometrical spectral broadening.

Theoretical and experimental studies were also made of other factors which may affect the volume flow measurement. These factors include the non-linear propagation of ultrasonic waves, intrinsic spectral broadening, cross-sectional area measurement, pulsatility of flow, curvature of vessel and stenosis. The significance of the effect of each factor on flow measurement was analyzed.

Possible improvements of the accuracy of volumetric flow measurement were

also sought during these studies. It was found that a half pulse length correction in the diameter measurement could significantly improve the accuracy of the cross-sectional area estimation. A new maximum frequency extraction method which is not sensitive to most of the measuring conditions including geometrical spectral broadening was suggested and analyzed. In typical situations, the systematic error of such an estimation is less than 2%. However, one must bear in mind that the random errors caused by the stochastic properties of the Doppler spectrum is much higher. Further work needs to be done before this new method can be used in practice.

The effect of each factor which may affect the volume flow measurement is briefly summarized below.

- **Insonation.** This group of factors changes the insonation of the vessel. The factors include type, size and focusing of the transducer, depth and size of the vessel, misalignment between the vessel and transducer, reflection and refraction at the vessel wall. The mean frequency is particularly sensitive to these factors. The maximum frequency is less sensitive. The maximum frequency, which was extracted independent of geometrical spectral broadening, gives a good estimation which is within 2% of the true maximum. In clinical situations, the effect of reflection and refraction can be ignored.

- **Cross-sectional area.** The inaccuracy of measurement of cross-sectional area is one of the major sources of error in flow measurement. The absolute error is machine and transducer dependent. It was found that a half pulse length correction can greatly improve the accuracy of such a measurement and reduce the absolute error in the diameter measurement to less than about 0.2 mm with different transducers operating at from 3.0 MHz to 5.0 MHz.

- **Flow disturbance.** It was proven experimentally that the mean velocity of pulsatile flow can be estimated by half of the maximum velocity averaged over an integral number of cardiac cycles. In the region of stenosis, about 300% overestimation of the mean velocity can be observed. The curvature of the vessel cause up to 15% error in the mean velocity estimation. It was also

found that in the region of curvature of the vessel, a unidirectional pulsatile flow waveform can give a better estimation of the mean velocity than steady or bidirectional pulsatile flow.

- **Intrinsic spectral broadening.** Intrinsic spectral broadening includes geometrical and transit time spectral broadening. Geometrical spectral broadening causes up to 70% overestimation of the maximum velocity. To obtain a good estimation of the maximum velocity, the maximum frequency estimation, independent of geometrical spectral broadening, can be used. For other maximum velocity estimations, the extreme Doppler angle should be used, especially when a linear array is employed. It was suggested that the geometrical and transit time spectral broadening are not the same effect as generally believed. The geometrical spectral broadening is usually more significant than the transit time spectral broadening.

- **Non-linear propagation.** Non-linear propagation has no significant effect on the Doppler frequency shift measurement.

## 9.2 Future Work

### 9.2.1 Flow phantom

It has been shown in this thesis that the flow phantom results in large errors in the mean velocity measurement. The major types of distortion in the Doppler spectrum are from reflection, sedimentation and refraction. However, these effects may be reduced by changing the materials and arrangement of the phantom.

Reflection is the major source of distortion of the Doppler spectrum. The significance of reflection is mainly because of the total reflection occurring at the boundary. If the speed of sound in the wall materials is near or slightly smaller than that in fluids both outside and inside the tubing, this error can be greatly reduced. The matching of the speeds of sound can be done by two methods. One is to find a material of tube that is relative stiff (so the diameter may not change significantly) and has similar speed of sound to water. The second

method is to change the composition of the fluids to match the speed of sound in the wall material. Refraction also can be reduced by the same way. Another possible method to reduce the reflection and refraction is to choose very thin wall tubing, such as the tubing made from a polythene bags. As the wall thickness is much smaller than a wavelength, ultrasonic waves can penetrate the wall without reflection and refraction. Sedimentation can be diminished by using a vertical tube or by the use of particles that have similar density to the artificial blood.

### 9.2.2 Geometrical spectral broadening independent maximum frequency

It has been shown in Chapter 4 that the geometrical spectral broadening independent maximum frequency has good characteristics for Doppler measurement. it is not sensitive to most of the factors considered in Chapter 4 and gives small errors in the maximum velocity estimation. However, it is necessary that further investigations, especially experimental investigations under different measuring conditions are performed. For practical use of this method, a particular problem is that the maximum amplitude has to be measured. For a steady flow, the amplitude can be obtained from the time averaged spectrum. However, if the flow is pulsatile, the time average cannot be made. The stochastic fluctuation of the spectrum and spectral estimation technique may prevent an accurate maximum amplitude from being estimated. The use of filtering techniques (Hoskins *et al.*, 1991) which use image processing methods to reduce speckle in Doppler spectra may solve this problem.

### 9.2.3 Pulsatile flow

It was verified that the mean velocity can be estimated from the time averaged maximum envelope over an integral number of cardiac cycles. The conditions for the use of this method are that a long straight vessel can be found and that its diameter is constant. It was also found that the presence of pulsatile flow can reduce errors due to curvature of the vessel. This may be due to the factor that

the velocity components which are not parallel to the vessel axis may cancel out. Since in the human body the diameter of vessels usually changes during a cardiac cycle, it would be interesting to know the relationship between the mean velocity and maximum frequency envelope in an elastic tube with pulsatile diameter.

### 9.2.4 In *vivo* measurement

The techniques described in this thesis for the reduction of errors in ultrasonic Doppler blood flow measurement should be tested in animal preparations.

# BIBLIOGRAPHY


Avasthi, P.S.; Greene, E.R.; Voyles, W.F. and Eldridge, M.W. (1984) A comparison of echo-Doppler and electromagnetic renal blood flow measurements. J. Ultrasound Med. 3:213-218.

Bacon, D.R. (1984) Finite amplitude distortion of the pulsed fields used in diagnostic ultrasound. Ultrasound in Med. & Biol. 10:189-195.

Baker, D.W.; Johnson, S.L. and Strandness, D.E. (1974) Prospects for quantisation of transcutaneous pulsed Doppler techniques in cardiology and peripheral vascular disease. Cardiovascular Applications of Ultrasound (Edited by Reneman, R.S.) pp 108-124. North-Holland, Amsterdam.

Bakhvalov, N.S.; Zhileikin, Y.M.; Zabolotskaya, E.A. and Khokhlov, R.V. (1978) Focused high-amplitude sound beams. Sov. Phys. Acoust. 24:10-15.

Bascom, P.A.J.; Cobbold, R.S.C. and Roelofs, B.H.M. (1986) Influence of spectral broadening on continuous wave Doppler ultrasound spectra: a geometric approach. Ultrasound in Med. & Biol. 12:387-395.

Bascom, P.A.J. and Cobbold, R.S.C. (1990) Effects of transducer beam geometry and flow velocity profile on the Doppler power spectrum: a theoretical study. Ultrasound in Med. & Biol. 16:279-295.

Barendsen, G.J. Plethysmography. In : Verstraete M (ed.) (1980) Methods in Angiology: A Physical-Technical Introduction. Martinus Nijhoff, The Hague, pp 38-92.

Blackstock, D.T. (1965) Connection between the Fay and Fubini solutions for plane sound waves of finite amplitude. J. Acoust. Soc. of Am. 39:1019-1026.

Borodzinski, K; Filipezynski, I; Nowiki, A. and Powalowski,T. (1976) Quantitative transcutaneous measurements of blood flow in carotid artery by means of pulse and continuous wave Doppler methods. Ultrasound in Med. & Biol. 2:189-193.

Carstensen, E.L.; Law, W.K. and McKay, N.D. (1980) Demonstration of nonlinear acoustical effects at biomedical frequencies and intensities. Ultrasound in Med. & Biol. 6:359-368.

Censor, D.; Newhouse, V.L.; Vontz, T. and Ortega, H.V. (1988) Theory of ultrasound Doppler-spectra velocimetry for arbitrary beam and flow configurations. IEEE Trans. Bio. Eng. BME:35:740-751.

Cobbold, R.S.C. (1974) Transducers for biomedical measurement: principles and applications. Wiley, New York.

Cobbold, R.S.C.; Veltink, P.H. and Johnston, K.W. (1983) Influence of beam profile and degree of insonation on the CW Doppler ultrasound spectrum and mean velocity. IEEE Trans. on Sonics and Ultrason. SU-30:364-370.

D'Alessio, T. (1985) 'Objective' algorithm for maximum frequency estimation in Doppler spectral analysers. Med. Biol. Engng. and Comput. 23:63-68.

Douville, Y.; Johnston, K.W.; Kassam, M.; Zuech, P; Cobbold, R.S.C. and Jares, A. (1983) An in vitro model and its application for the study of carotid Doppler spectral broadening. Ultrasound in Med. & Biol. 9:347-356.

Duck, F.A. and Starritt, H.C. (1984) Acoustic shock generation by ultrasonic imaging equipment. Br. J. Radiol. 57:231-240.

Duck, F.A.; Starritt, H.C.; Perkins, M.A. and Hawkins, A.J. (1985) The output of pulse-echo ultrasound equipment: A survey of powers, pressures and intensities. Br. J. Radiol. 58:989-1001.

Edwards, R.V.; Angus, J.C.; French, M.J. and Dunning, J.W, Jr (1971) Spectral analysis of the signal from the laser Doppler flowmeter: time-independent systems. J. Appl. Phys. 24:837-850.

Eik-Nes, S.H.; Marsal, K.; Brubakk, A.O.; Kristofferson, K. and Ulstein, M. (1982) Ultrasonic measurement of human fetal blood flow. J. Biomed. Engng. 4:28-36.

Eik-Nes, S.H. (1984) Methodology and basic problems related to blood flow studies in the human fetus. Ultrasound in Med. & Biol. 10:329-337.

Evans, D.H. and Parton, L. (1980) The directional characteristics of some ultrasonic Doppler blood-flow probes. Ultrasound in Med. & Biol. 7:51-62.

Evans, D.H. (1982) Some aspects of the relationship between instantaneous volumetric blood flow and continuous wave Doppler ultrasound recordings. I. Ultrasound Med Biol. 8:605-609.

Evans, D.H. (1985) On the measurement of the mean velocity of blood flow over the cardiac cycle using Doppler ultrasound. Ultrasound in Med. & Biol. 11:735-741.

Evans, D.H. (1986) Can ultrasonic Duplex scanners really measure volumetric flow ? In: Physics in medical ultrasound (Ed. J.A. Evans), Chapter 19, 145-154, IPSM, 47 Belgrave Square, London.

Evans, D.H.; Schlindwein, F.S. and Levene, M.I. (1989a) The relationship between time averaged intensity weighted mean velocity, and time averaged maximum velocity in neonatal cerebral arteries. Ultrasound in Med. & Biol. 15:429-435.

Evans, D.H.; McDicken, W.N.; Skidmore, R. and Woodcock, J.P. (1989b) Doppler ultrasound: physics, instrumentation, and clinical applications. John Wiley & Sons Ltd, Chichester.

Evans, J.M.; Skidmore, R.; Luckman, N.P. and Wells, P.N.T. (1986a) A new approach to the noninvasive measurement of cardiac output using an annular array Doppler technique - I. Theoretical considerations and ultrasonic fields. Ultrasound in Med. & Biol. 15:169-178.

Evans, J.M.; Skidmore, R.; Luckman, N.P. and Wells, P.N.T. (1986b) A new approach to the noninvasive measurement of cardiac output using an annular array Doppler technique - II. practical implementation and results. Ultrasound in Med. & Biol. 15:179-187.

Fish, P.J. (1986) Doppler methods. in Physical Principles of medical ultrasonics. (editor Hill, C.R.) :339-376.

Fisher, D.C.; Sahn, D.J.; Friedman, M.J.; Larson, D.; Valdes-Cruz, L.M.; Horowitz, S.; Goldberg, S.J. and Allen, H.D. (1983) The mitral valve orifice method for noninvasive two-dimensional echo Doppler determinations of cardiac output. Circulation 67:872-877.

Gill, R.W. (1978) Quantitative blood flow measurements in deep-lying vessels using pulsed Doppler with the Octoson. In Ultrasound in Medicine 4:341-348. (Edited by White, D.N. and Lyons, E.A.). Plenum Press, New York.

Gill, R.W. (1979) Pulsed Doppler with B-mode imaging for quantitative blood flow measurement. Ultrasound in Med. & Biol. 5:223-235.

Gill, R.W.; Kossoff, G.; Warren, P.S. and Garrett, W.J. (1984) Umbilical venous flow in normal and complicated pregnancy. Ultrasound in Med. & Biol. 10:349-363.

Gill, R.W. (1985) Measurement of blood flow by ultrasound: accuracy and sources of error. Ultrasound in Med. & Biol. 11:625-641.

Griffith, J.M.; Brody, W.R. and Goodman, L. (1976) Resolution performance of Doppler ultrasound flowmeters. J. Acoust. Soc. of Am. 60:607-610.

Hill, C.R. (1986) Physical principles of medical ultrasonics. Ellis Horwood Limited, Chichester, England.

Hoeks, A.P.G.; Reneman, R.S. and Peronneau, P.A. (1981) A multi-gate pulsed Doppler system with serial data processing. IEEE Trans. on Sonics and Ultrason. SU-28:242-247.

Hoeks, A.P.G.; Ruissen, C.J.; Hick, P. and reneman, R.S. (1985) Transcutaneous detection of relative changes in artery diameter. Ultrasound in Med. & Biol. 11:51-59.

Hoskins, P.R.; Anderson, T.A. and McDicken, W.N. (1989) A computer controlled flow phantom for generation of physiological Doppler waveforms. Phys. Med. Biol. 34:1709-1717.

Hoskins, P.R.; Loupas, T. and McDicken, W.N. (1990a) A comparison of three different filters for speckle reduction of Doppler spectra. Ultrasound Med.& Biol. 16:375-389.

Hoskins, P.R. (1990b) A comparison of the Doppler spectra from human blood and artificial blood used in a flow phantom. Ultrasound in Med. & Biol. 16:141-147.

Hoskins, P.R. (1991a) An investigation of simulated umbilical artery Doppler waveforms I. The effect of 3 physical parameters on the maximum frequency envelope and on pulsatility index. Ultrasound in Med. & Biol. 17:7-21.

Hoskins, P.R. (1991b) An investigation of simulated umbilical artery Doppler waveforms II. A comparison of 3 Doppler waveform quality indices. Ultrasound in Med. & Biol. 7:7-21.

Hoskins, P.R.; Li, S.F. and McDicken, W.N. (1992) Velocity estimation using Duplex scanners (letter). Ultrasound in Med. & Biol. 17:195-199.

Hottinger, C.F. and Meindl, J.D. (1979) Blood flow measurement using the attenuation-compensated volume flowmeter. Ultrasonic Imaging 1:1-15.

Huntsman, L.; Stewart, D.K.; Barnes, S.R.; Franklin, S.B; Colocousis, J.S. and Hessel, E.A. (1983) Noninvasive Doppler determination of cardiac output in man: Clinical validation. Circulation 67:593-602.

Issartier, P.; Siooufi, M. and Pelissier, R. (1978) Simulation of blood flow by a hydrodynamic generator. Med. prog. Technol. 6:39-40.

Johnston, K.W.; Maruzzo, B.C. and Cobbold, R.S.C. (1978) Doppler methods for quantitative measurement and localization of peripheral arterial occlusive

disease by analysis of the blood flow velocity waveform. Ultrasound in Med. & Biol. 4:209-223.

Jouppila, P. and Kirkinen, P. (1984) The role of fetal blood flow measurements in obstetrics. In Measurements of Fetal Blood Flow (Edited by A. Kurjak) C.I.C., Rome.

Kinsler, L.E. and Frey, A.R. (1962) Fundamentals of acoustics. Johhn Wiley & Sons, Inc. USA.

Kiyose, T.A.; Kusaba, M; Kamori,M.; Inokuci, Y.; Takamatsu, Y. and Takahara, H. (1977) Development of a pump system for experimental model simulation of blood flow in peripheral artery. Fucuota Acta Med. 68:86-91.

Kremkau, F.W. (1990) Doppler angle error due to refraction. Ultrasound Med. Biol. 16:523-524.

Law, W.K.; Frizzell, L.A. and Dunn, F. (1985) Determination of the nonlinearity parameter B/A of biological media. Ultrasound in Med. & Biol. 11:307-318.

Law, Y.F.; Cobbold, R.S.C.; Johnston, K.W. and Bascom, P.A.J. (1987) Computer-controlled pulsatile pump system for physiological flow simulation. Med. & Biol. Eng. & Comput. 25:590-595.

Lewis, P.; Psaila, J.V.; Davies, W.T.; McCarty, K. and Woodcock, J.P (1986) Measurement of volume flow in the human common femoral artery using a duplex ultrasound system. Ultrasound in Med. & Biol. 12:777-784.

Li, S.; McDicken, W.N. and Hoskins, P.R. (1993) Refraction in Doppler ultrasound (letter). Ultrasound in Med. & Biol. 19:593-594.

Light, L.H. (1970) Transcutaneous observation of the blood velocity in the ascending aorta in man. In Ballistocardiography and Cardiovascular Therapy. 26:214-221.

Light, H. and Cross, G. (1972) Cardiovascular data by transcutaneous aortovelography. In:Blood flow measurement (Ed. Roberts, V.C.), Chapter 11 pp 60-63, Sector, London.

Lindstrom, K.; Marsal, K.; Gennser, G.; Bengtsson, L.; Benthin, M. and Daho, P. (1977) Device for measurement of fetal breathing movements-I. Ultrasound in Med. & Biol. 3:143-151.

Lynn, P.A. and Fuerst, W (1990) Introductory digital signal processing with computer applications. pp 141-144, John Wiley & Sons Ltd, Chicheser.

Marsal, K.; Lindbland, A. and Lingman, G. (1984) Blood flow in the fetal descending aorta; intrinsic factors affecting fetal blood flow, i.e. fetal breathing movements and cardiac arrhythmia. Ultrasound in Med & Biol. 10:339-348.

Mathie, R.T. (ed.) (1882) Blood flow measurement in Man. Castle House Publication, Turbridge Wells.

McDicken, W.N. (1986) A versatile test-object for the calibration of ultrasonic Doppler flow instruments. Ultrasound in Med. & Biol. 12:245-249.

McDicken, W.N. (1991) Diagnostic ultrasonics : Principles and use of instruments. Churchill Livingstone, Edinburgh, U.K.

McDonald, D.A. (1974) Blood flow in arteries. Edward Arnold, London. pp 137.

Mo, L.Y.L.; Yun, L.C.M. and Cobbold, R.S.C. (1988) Comparison of four digital maximum frequency estimators for Doppler ultrasound. Ultrasound in Med. & Biol. 14:355-363.

Mo, L.Y.L. and Cobbold, R.S.C. (1992) A unified approach to modelling the backscattered Doppler ultrasound from blood. IEEE Trans. Bio. Eng. BME-39:450-461.

Morse, P.M. and Ingard, K.U. (1968) Theoretical Acoustics. McGraw-Hill, New York.

Muir, T.G. and Carstensen, E.L. (1980) Prediction of nonlinear acoustic effects at biomedical frequencies and intensities. Ultrasound in Med. & Biol. 6:345-357.

Najib, N.; Mansour, A.R. and Amidon, C.L. (1985) Gastrointestinal transit-time - An in vitro analysis of the various parameters controlling the critical flow

velocity of particles in a horizontal tube. Drug Development and Industrial pharmacy. 11:635-652.

Nakamura, T.; Moriyasu, F.; Nobuyuki, B.; Nishida, O.; Tamada, T.; Kawasaki, T.; Masahiko, S. and Uchino, H. (1989) Quantitative measurement of abdominal arterial blood flow using image-directed Doppler ultrasonography: superior mesenteric, splenic, and common hepatic arterial blood flow in normal adults. J Clin Ultrasound 17:261-268.

Newhouse, V.L.; Varner, L.W. and Bendick, P.J. (1977) Geometrical spectrum broadening in ultrasonic Doppler systems. IEEE Trans. Bio. Eng. BME-24:478-480.

Newhouse, V.L.; Furgason, E.S.; Johnson, G.F. and Wolf, D.A. (1980) The dependence of ultrasound Doppler bandwidth on beam geometry. IEEE Trans. on Sonics and Ultrason. SU-27:50-59.

Nichols, W.W. and FO'Rourke, M. (1990) McDonald's Blood Flow in Arteries: theoretical , experimental and clinical principles. Edward Arnold, , London.

Nowicki, A.; Karlowicz, P.; Piechocki, M. and Secomski, W. (1985) Method for the measurement of the maximum Doppler frequency. Ultrasound in Med. & Biol. 11:479-486.

Oates, C.P. (1989) The Doppler shift & speed of sound in blood. Ultrasound in Med. & Biol. 15:75.

Papoulis, A. (1958) Probability, Random Variables, and Stochastic Processes. McGraw-Hill, New York.

Qamar, M.I.; Read, A.E.; Skidmore, R.; Evans, J.M. and Williamson, R.C.N. (1985) Transcutaneous Doppler ultrasound measurement of coeliac axis blood flow in Man. Br. J. Surg. 72:391-393.

Rasmussen, K. (1987) Precision and accuracy of Doppler flow measurements. In *vitro* and *in vivo* study of the applicability of the method in human fetuses. Scand. J. Clin. Lab. Invest. 47:311-318.

Sainz, A; Roberts, V.C. and Pinardi, G. (1976) Phase-locked loop techniques applied to ultrasonic Doppler signal processing. Ultrasonics 14:128-132.

Shercliff, J.A. (1962) The theory of electromagnetic Flow-measurement. Cambridge university Press, Cambridge, UK.

Shung, K.K.; Sigelmann, R.A. and Reid, J.M. (1977) Angular dependence of scattering of ultrasound from blood. IEEE Trans. Bio. Eng. BME-24:325-331.

Shung, K.K.; Cloutier, G. and Lim, C.C. (1992) The effects of hematocrit, shear rate, and turbulence on ultrasonic Doppler spectrum from blood. IEEE Trans. Bio. Eng. BME-39:462-469.

Skidmore, R. and Follett, D.H. (1978) Maximum frequency follower from the processing of ultrasonic Doppler shift signals. Ultrasound in Med. & Biol. 4:145-147.

Stonebridge, P.A. and Brophy, C.M. (1991) Spiral laminar flow in arteries ? The Lancet 338:1360-1361.

Struyk, P.C.; Pijpers, L.; Wlandimiroff, J.W.; Lotgering, F.K.; Tonge, M. and Bom, N. (1985) The time-distance recorder as a means of improving the accuracy of fetal blood flow measurements. Ultrasound in Med. & Biol. 11:71-77.

Tarnoczy, T. (1965) Sound focusing lenses and waveguides. Ultrasonics 3:115-127.

Teague, M.J.; Willson, K.; Battye, C.K.; Taylor, M.G.; Griffin, D.R.; Campbell, S. and Roberts, V.C. (1985) A combined ultrasonic linear array scanner and pulsed Doppler velocimeter for the estimation of blood flow in the foetus and adult abdomen-I: Technical aspects. Ultrasound in Med. & Biol. 11:27-36.

Terry, H.J. (1972) The electromagnetic measurement of blood flow during arterial surgery. Biomed. Eng. 7:466-472.

Thompson, R.S.; Aldis, G.K. and Linnett, I.W. (1990) Doppler ultrasound spectral power density distribution : measurement artefacts in steady flow. Med. & Biol.Eng. & Comput. 28:60-66.

Varner, L.W.; Newhouse, V.L. and Bendick, P.J. (1975) Application of transit time effects to the independent measurement of blood velocity and angle. Proc. 28th ACEMB, pp 76.

Whitney, R.J. (1953) the measurement of volume changes in human limbs. J.Physiol. (London) 121: 1-27.

Wijngaard, J.A.G.W.V.D.; Groenenberg, I.A.L.; Wlandimiroff, J.W. and Hop, W.C.J. (1989) Cerebral Doppler ultrasound of the human fetus. British Journal of Obstetrics and Gynaecology. 96:845-849.

Wlandimiroff, J.W.; Tonge, H.M. and Stewart, P.A. (1986) Doppler ultrasound assessment of cerebral blood flow in the human fetus. British Journal of Obstetrics and Gynaecology. 93:471-475.

Woodcock J.P. (1975) Theory and practice of blood flow measurement. Butterworth, London.

Woodcock J.P. (ed.) (1976) Clinical Blood flow measurement. Sector, London.

Wyatt D.G. (1971) Electromagnetic flood-flow measurements. In: Watson B W (ed.) 1971 IEE medical Electronics Monographs 1-6, Peter Peregrinus, London, pp 181-243.

# Appendix A

# AN ESTIMATION OF THE EFFECT OF GEOMETRICAL SPECTRAL BROADENING USING EXTREME ANGLES

The geometry for an unfocussed transducer can be illustrated simply in Figure A.1. Region I is the near field and region II is the far field where the beam diverges and it has an approximate constant divergent angle $\mu$.

A CW transducer is usually composed of two half-disc crystals. One acts as transmitter and the other receiver. Two crystal axes are orientated at a convergence angle of $\delta$ in front of the transducer. The beam can be depicted in Figure A.1. The maximum Doppler shift can be calculated by using the two extreme rays of the beam

$$(F_d)_{sp} = \frac{VF_0}{C}(\cos\theta_1 + \cos\theta_2) \tag{A.1}$$

where $V$ is the velocity of the scatterer, $C$ is the speed of ultrasound and $F_0$ is the transmitted frequency.

It can be calculated that the distance between the beam edge and beam centre at distance $MO$ (Figure 0) is given by

$$OE = OA\frac{\cos\mu}{\sin(\theta+\delta-\mu)} - MO\frac{\sin\delta}{\sin(\delta+\theta)} \tag{A.2}$$

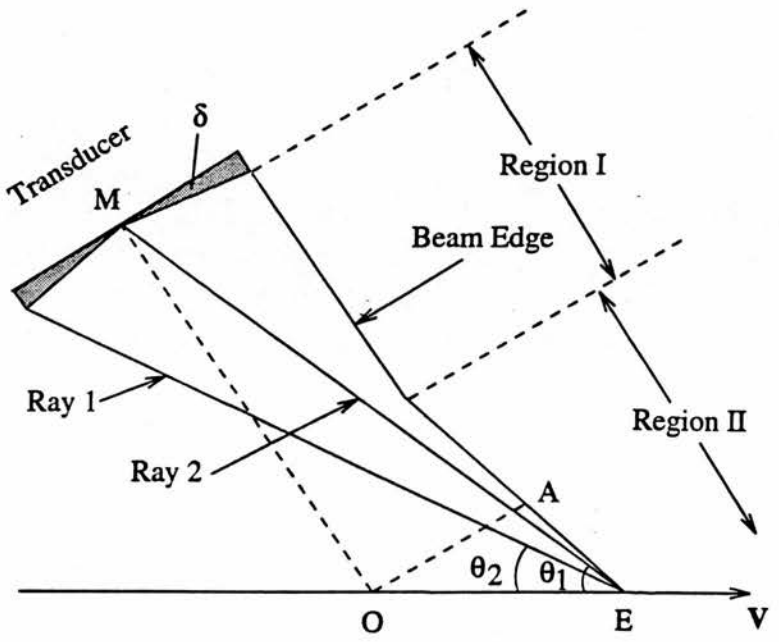


Figure A.1: The idealised beam field for a transducer.

where $\theta$ is the beam-vessel angle and $OA$ is the beam width at distance $OM$. Therefore, for ray1,

$$D_{x_1} = -OM\cos\theta - OE - r\sin(\theta - \delta) \quad \text{(A.3)}$$

$$D_{y_1} = OM\sin\theta - r\cos(\theta - \delta) \quad \text{(A.4)}$$

where $r$ is the radius of the transducer, $D_{x_1}$ and $D_{x_1}$ are projections of ray1 on $x - axis$ and $y - axis$ respectively. Therefore we obtain

$$\cos\theta_1 = -\frac{D_{x_1}}{(D_{x_1}^2 + D_{y_1}^2)^{\frac{1}{2}}} \quad \text{(A.5)}$$

Similarly, for ray 2 , we have

$$D_{x_2} = -OM\cos\theta - OE \quad \text{(A.6)}$$

$$D_{y_2} = OM\sin(\theta + \delta) \quad \text{(A.7)}$$

and

$$\cos\theta_2 = -\frac{D_{x_2}}{(D_{x_2}^2 + D_{y_2}^2)^{\frac{1}{2}}} \quad \text{(A.8)}$$

The Doppler shift with geometrical spectral broadening can be therefore calculated by equation ( A.1).

The error E then is estimated by

$$\begin{aligned} E &= \frac{V_{mean} - V_{real}}{V_{real}} \\ &= \frac{(F_d)_{sp} - F_d}{F_d} \\ &= \frac{\cos\theta_1 + \cos\theta_2 - 2\cos\theta}{2\cos\theta} \end{aligned} \tag{A.9}$$

where $F_d$ is the Doppler frequency shift for ideal conditions.

The CW transducer we used in the experiment had diameter of 8.0 mm. The angle between two crystals was 168°. The beam width was measured at 50% of the maximum pressure amplitude, *i.e.*, FWHM (pressure), at distance 5.6 cm was 6.5 mm and the divergent angle was 5.7 degrees. The transducer had a transmitting frequency of 4 MHz and its length of near zone was 17.3 mm.

# Appendix B

# EXPERIMENTAL DATA OF THE DIAMETER MEASUREMENT AND MEASUREMENT AND CORRECTION

All the diameters in tables are in millimeters.

## Acoustic properties of tube materials and blood vessels

| Tube | Density ($kg/m^3$) | C ($m/s$) | Z ($kg/s/m^2$) |
|---|---|---|---|
| Heat-shrinkable | 940 | 1850 | $1.74 \times 10^6$ |
| PVC | 1337 | 1714 | $2.29 \times 10^6$ |
| Silastic | 1224 | 949 | $1.16 \times 10^6$ |
| Blood Vessel | | $1513 \pm 21$ | $1.56 \pm 0.03 \times 10^6$ |

## Pulse length of transducers

| Transducer | T1 | T2 | T3 | T4 |
|---|---|---|---|---|
| Pulse length (ns) | 454 | 588 | 506 | 962 |
| Correction (mm) | 0.35 | 0.45 | 0.39 | 0.74 |

T1 : ATL 5MHz Phased Array

T2 : ATL 3MHz Phased Array

T3 : ATL 5MHz Linear Array

T4 : DSL 3.5MHz Linear Array

# Diameter measurement using the ATL's 5 MHz phased array

## Inner diameter

| Tube | Heat shrinkable | | | | | | | Silastic | | | PVC | |
|---|---|---|---|---|---|---|---|---|---|---|---|---|
| $ID_{rea}$ | 1.95 | 3.1 | 4.0 | 4.95 | 6.3 | 7.8 | 11.0 | 3.05 | 6.4 | 10.1 | 5.85 | 8.15 |
| $ID_{mea}$ | 1.55 | 2.6 | 3.5 | 4.4 | 5.8 | 7.3 | 10.6 | 2.6 | 5.9 | 9.6 | 5.4 | 7.7 |
| $ID_{err}$ | -0.4 | -0.5 | -0.5 | -0.55 | -0.5 | -0.5 | -0.4 | -0.45 | -0.5 | -0.5 | -0.45 | -0.45 |
| $E_{are}(\%)$ | 36.8 | 29.7 | 23.4 | 21.0 | 15.2 | 12.4 | 7.1 | 27.3 | 15.0 | 9.7 | 14.8 | 10.7 |
| $ID_{Cor}$ | 0.05 | -0.15 | -0.15 | -0.2 | -0.15 | -0.15 | 0.05 | -0.1 | -0.1 | -0.15 | -0.15 | -0.1 |
| $E_{cor}(\%)$ | 5.1 | 9.4 | 7.4 | 7.9 | 4.7 | 3.8 | 0.9 | 6.4 | 3.1 | 2.9 | 5.1 | 2.4 |

Correction of the diameter=0.35 mm

## Outer-to-inner diameter

| Tube | Heat shrinkable | | | | | | | Silastic | | | PVC | |
|---|---|---|---|---|---|---|---|---|---|---|---|---|
| $OID_{rea}$ | 2.4 | 3.5 | 4.35 | 5.5 | 6.8 | 8.25 | 11.7 | 3.75 | 7.9 | 12.0 | 7.4 | 9.65 |
| $OID_{mea}$ | 2.1 | 3.3 | 4.25 | 5.15 | 6.65 | 7.95 | 11.4 | 4.0 | 8.5 | 12.9 | 6.9 | 9.15 |
| $OID_{err}$ | -0.3 | -0.2 | -0.1 | -0.35 | -0.25 | -0.3 | -0.3 | 0.25 | 0.6 | 0.9 | -0.5 | -0.5 |

## Inner diameter calculated using outer-to-inner diameter

| Tube | Heat shrinkable | | | | | | | Silastic | | | PVC | |
|---|---|---|---|---|---|---|---|---|---|---|---|---|
| $ID_{rea}$ | 1.95 | 3.1 | 4.0 | 4.95 | 6.3 | 7.8 | 11.0 | 3.05 | 6.4 | 10.1 | 5.85 | 8.15 |
| $Wall$ | 0.45 | 0.4 | 0.35 | 0.55 | 0.5 | 0.45 | 0.7 | 0.7 | 1.5 | 1.9 | 1.55 | 1.5 |
| $ID_{est}$ | 1.75 | 2.95 | 3.95 | 4.7 | 6.25 | 7.6 | 10.8 | 2.85 | 6.1 | 9.8 | 5.5 | 7.8 |
| $ID_{err}$ | -0.2 | -0.15 | -0.05 | -0.25 | -0.05 | -0.2 | -0.2 | -0.2 | -0.3 | -0.3 | -0.35 | -0.35 |

## Outer diameter

| Tube | Heat shrinkable | | | | | | | Silastic | | | PVC | |
|---|---|---|---|---|---|---|---|---|---|---|---|---|
| $OD_{rea}$ | 2.9 | 3.85 | 4.7 | 5.9 | 7.3 | 8.7 | 12.35 | 4.4 | 9.4 | 14.0 | 9.0 | 11.15 |
| $OD_{mea}$ | 2.8 | 3.95 | 5.0 | 5.8 | 7.3 | 8.5 | 12.2 | 5.5 | 11.1 | 16.2 | 8.5 | 10.6 |
| $OD_{err}$ | 0.1 | -0.1 | -0.3 | 0.1 | 0.0 | 0.2 | 0.15 | -1.1 | -1.7 | -2.2 | 0.5 | 0.55 |

## Diameters measured in various depth

| Tube | Heat shrinkable | | | | | | | | | | |
|---|---|---|---|---|---|---|---|---|---|---|---|
| Depth (cm) | 1.0 | 2.0 | 3.0 | 4.0 | 5.0 | 6.0 | 7.0 | 8.0 | 9.0 | 10.0 | 11.0 |
| $ID_{mea}$ | 4.3 | 4.3 | 4.3 | 4.3 | 4.5 | 4.3 | 4.3 | 4.3 | 4.5 | 4.5 | 4.3 |
| $OID_{mea}$ | 6.0 | 6.1 | 6.1 | 6.1 | 5.9 | 5.9 | 5.9 | 6.2 | 6.0 | 6.0 | 6.0 |
| $OD_{mea}$ | 5.2 | 5.3 | 5.4 | 5.4 | 5.4 | 5.3 | 5.2 | 5.3 | 5.2 | 5.2 | 5.2 |

Real diameter = 4.95

# Diameter measurement using ATL's 3 MHz phased array

## Inner diameter

| Tube | Heat shrinkable | | | | | | |
|---|---|---|---|---|---|---|---|
| $ID_{rea}$ | 1.95 | 3.1 | 4.0 | 4.95 | 6.3 | 7.8 | 11.0 |
| $ID_{mea}$ | 1.6 | 2.5 | 3.4 | 4.4 | 5.6 | 7.2 | 10.4 |
| $ID_{err}$ | -0.35 | -0.6 | -0.6 | -0.55 | -0.7 | -0.6 | -0.6 |
| $E_{are}(\%)$ | 32.7 | 35.0 | 27.8 | 21.0 | 21.0 | 14.8 | 10.6 |
| $ID_{cor}$ | 0.1 | -0.15 | -0.15 | -0.1 | -0.25 | -0.15 | -0.15 |
| $E_{cor}(\%)$ | 10.5 | 9.4 | 7.4 | 4.0 | 7.8 | 3.8 | 2.7 |

Correction of the diameter=0.45 mm

## Outer-to-inner diameter

| Tube | Heat shrinkable | | | | | | |
|---|---|---|---|---|---|---|---|
| $OID_{rea}$ | 2.4 | 3.5 | 4.35 | 5.6 | 6.8 | 8.25 | 11.7 |
| $OID_{mea}$ | 2.4 | 3.4 | 4.2 | 5.2 | 6.5 | 8.0 | 11.2 |
| $OID_{err}$ | -0.0 | -0.1 | -0.15 | -0.4 | -0.3 | -0.25 | -0.5 |

## Inner diameter calculated using outer-to-inner diameter

| Tube | Heat shrinkable | | | | | | |
|---|---|---|---|---|---|---|---|
| $ID_{rea}$ | 1.95 | 3.1 | 4.0 | 4.95 | 6.3 | 7.8 | 11.0 |
| $ID_{est}$ | 2.0 | 3.05 | 3.9 | 4.75 | 6.1 | 7.6 | 10.6 |
| $Wall$ | 0.45 | 0.4 | 0.35 | 0.55 | 0.5 | 0.45 | 0.7 |
| $ID_{err}$ | 0.05 | -0.05 | -0.1 | -0.2 | -0.2 | -0.2 | -0.4 |

## Outer diameter

| Tube | Heat shrinkable | | | | | | |
|---|---|---|---|---|---|---|---|
| $OD_{rea}$ | 2.9 | 3.85 | 4.7 | 5.9 | 7.3 | 8.7 | 12.35 |
| $OD_{mea}$ | 3.3 | 4.3 | 5.0 | 6.0 | 7.4 | 8.8 | 12.2 |
| $OD_{err}$ | -0.4 | -0.55 | -0.3 | -0.1 | -0.1 | -0.1 | 0.15 |

## Output power

| *Output* (%) | 100 | 71 | 50 | 35 | 25 | 18 | 13 | 8.9 |
|---|---|---|---|---|---|---|---|---|
| $ID_{mea}$ | 4.4 | 4.5 | 4.4 | 4.45 | 4.5 | 4.5 | 4.5 | 4.45 |
| *Output* (%) | 6.3 | 4.5 | 3.2 | 2.2 | 1.6 | 1.1 | 0.79 | 0.56 |
| $ID_{mea}$ | 4.5 | 4.45 | 4.45 | 4.6 | 4.6 | 4.7 | 4.65 | 4.6 |

2D gain is fixed when output power is changed.

# Diameter measurement using the ATL's 5 MHz linear array

## Inner diameter

| Tube | Heat shrinkable | | | | | | | Silastic | | | PVC | |
|---|---|---|---|---|---|---|---|---|---|---|---|---|
| $ID_{rea}$ | 1.95 | 3.1 | 4.0 | 4.95 | 6.3 | 7.8 | 11.0 | 3.05 | 6.4 | 10.1 | 5.85 | 8.15 |
| $ID_{mea}$ | 1.5 | 2.6 | 3.55 | 4.5 | 5.9 | 7.35 | 10.6 | 2.6 | 5.9 | 9.6 | 5.4 | 7.65 |
| $ID_{err}$ | -0.45 | -0.5 | -0.45 | -0.45 | -0.6 | -0.45 | -0.4 | -0.45 | -0.5 | -0.5 | -0.45 | -0.5 |
| $E_{are}$ (%) | 41 | 30 | 21 | 17 | 12 | 11 | 7.1 | 27 | 15 | 9.7 | 14.8 | 12 |
| $ID_{cor}$ | 0.06 | -0.1 | 0.06 | 0.06 | -0.2 | 0.06 | 0.01 | 0.06 | -0.1 | -0.1 | 0.06 | -0.1 |
| $E_{cor}$ (%) | 6.1 | 6.3 | 3.0 | 2.4 | 6.2 | 1.5 | 0.2 | 3.9 | 3.1 | 2.0 | 2.0 | 2.4 |

Correction of the diameter=0.39 mm

## Outer-to-inner diameter

| Tube | Heat shrinkable | | | | | | | Silastic | | | PVC | |
|---|---|---|---|---|---|---|---|---|---|---|---|---|
| $OID_{rea}$ | 2.4 | 3.5 | 4.35 | 5.6 | 6.65 | 8.25 | 11.7 | 3.75 | 7.9 | 12.0 | 7.4 | 9.65 |
| $OID_{mea}$ | 2.35 | 3.4 | 4.3 | 5.3 | 6.45 | 8.05 | 11.4 | 4.1 | 8.6 | 13.0 | 7.1 | 9.35 |
| $OID_{err}$ | <-0.1 | -0.1 | <-0.1 | -0.3 | -0.2 | -0.2 | -0.3 | 0.35 | 0.7 | 1.0 | -0.3 | -0.3 |

## Inner diameter calculated using outer-to-inner diameter

| Tube | Heat shrinkable | | | | | | | Silastic | | | PVC | |
|---|---|---|---|---|---|---|---|---|---|---|---|---|
| $ID_{rea}$ | 1.95 | 3.1 | 4.0 | 4.95 | 6.3 | 7.8 | 11.0 | 3.05 | 6.4 | 10.1 | 5.85 | 8.15 |
| $ID_{est}$ | 2.0 | 3.05 | 4.0 | 4.85 | 6.05 | 7.7 | 10.8 | 2.95 | 6.1 | 9.9 | 5.7 | 8.0 |
| $Wall$ | 0.45 | 0.4 | 0.35 | 0.55 | 0.5 | 0.45 | 0.7 | 0.7 | 1.5 | 1.9 | 1.55 | 1.5 |
| $ID_{err}$ | 0.05 | -0.05 | 0.0 | -0.1 | -0.25 | 0.1 | -0.2 | -0.1 | -0.3 | -0.2 | -0.15 | -0.15 |

## Outer diameter

| Tube | Heat shrinkable | | | | | | | Silastic | | | PVC | |
|---|---|---|---|---|---|---|---|---|---|---|---|---|
| $OD_{rea}$ | 2.9 | 3.85 | 4.7 | 5.9 | 7.3 | 8.7 | 12.35 | 4.4 | 9.4 | 14.0 | 9.0 | 11.15 |
| $OD_{mea}$ | 3.15 | 4.1 | 5.1 | 5.8 | 7.2 | 8.75 | 12.25 | 5.5 | 11.4 | 16.25 | 8.7 | 10.8 |
| $OD_{err}$ | -0.75 | -0.25 | -0.4 | 0.1 | 0.1 | -0.05 | 0.1 | -1.1 | -2.0 | -2.25 | 0.3 | 0.35 |

## Beam-vessel angle

| Tube | Heat shrinkable | | | | | | | | |
|---|---|---|---|---|---|---|---|---|---|
| $Angle$ | 0 | 6 | 10 | 11 | 13 | 16 | 26.5 | 38 | 41 |
| $ID_{mea}$ | 4.5 | 4.5 | 4.4 | 4.5 | 4.1 | 4.3 | 3.9 | 4.5 | 3.9 |

# Diameter measurement using DSL's 3.5 MHz convex array

## Inner diameter

| Tube | Heat shrinkable | | | | | | |
|---|---|---|---|---|---|---|---|
| $ID_{rea}$ | 1.95 | 3.1 | 4.0 | 4.95 | 6.3 | 7.8 | 11.0 |
| $ID_{mea}$ | 1.3 | 2.35 | 3.2 | 4.2 | 5.5 | 6.9 | 10.1 |
| $ID_{err}$ | -0.65 | -0.65 | -0.8 | -0.75 | -0.8 | -0.9 | -0.9 |
| $E_{are}$ (%) | 56 | 43 | 36 | 28 | 24 | 22 | 16 |
| $ID_{cor}$ | 0.1 | 0.1 | 0.06 | 0.0 | 0.06 | -0.15 | -0.15 |
| $E_{cor}$ (%) | 10 | 6.6 | 3.0 | 0.0 | 1.9 | 3.8 | 2.7 |

The correction of the diameter=0.74 mm

## Outer-to-inner diameter

| Tube | Heat shrinkable | | | | | | |
|---|---|---|---|---|---|---|---|
| $OD_{rea}$ | 2.4 | 3.5 | 4.35 | 5.5 | 6.65 | 8.25 | 11.7 |
| $OD_{mea}$ | 2.6 | 3.5 | 4.3 | 5.4 | 6.7 | 8.2 | 11.5 |
| $OD_{err}$ | 0.2 | 0.0 | -0.05 | -0.1 | 0.05 | -0.05 | -0.2 |

## Inner diameter calculated using outer-to-inner diameter

| Tube | Heat shrinkable | | | | | | |
|---|---|---|---|---|---|---|---|
| $ID_{rea}$ | 1.95 | 3.1 | 4.0 | 4.95 | 6.3 | 7.8 | 11.0 |
| $ID_{est}$ | 2.2 | 3.15 | 4.0 | 4.95 | 6.3 | 7.8 | 10.9 |
| $Wall$ | 0.45 | 0.4 | 0.35 | 0.55 | 0.5 | 0.45 | 0.7 |
| $ID_{err}$ | 0.25 | 0.05 | 0.0 | 0.0 | 0.0 | 0.0 | -0.1 |

## Outer diameter

| Tube | Heat shrinkable | | | | | | |
|---|---|---|---|---|---|---|---|
| $OD_{rea}$ | 2.9 | 3.85 | 4.7 | 5.9 | 7.3 | 8.7 | 12.35 |
| $OD_{mea}$ | 3.5 | 3.85 | 5.3 | 6.4 | 7.6 | 9.2 | 12.7 |
| $OD_{err}$ | -0.6 | -0.45 | -0.6 | -0.5 | -0.3 | -0.5 | -0.35 |

## Diameter at various gains

| Tube | Heat shrinkable | | | | | | | | | |
|---|---|---|---|---|---|---|---|---|---|---|
| $Gain(db)$ | 0 | 6 | 12 | 18 | 24 | 30 | 36 | 42 | 48 | 54 |
| $ID_{mea}$ | 4.5 | 4.3 | 4.3 | 4.1 | 4.3 | 4.1 | 4.3 | 4.1 | 4.1 | 4.3 |
| $OID_{mea}$ | 5.4 | 5.3 | 5.4 | 5.4 | 5.3 | 5.3 | 5.3 | 5.3 | 5.3 | 5.3 |
| $OD_{mea}$ | 6.0 | 6.0 | 6.2 | 6.2 | 6.2 | 6.2 | 6.4 | 6.2 | 6.4 | 6.4 |

Output = 18 db

$ID_{rea}$ = 4.95 mm; $OID_{rea}$ = 5.6 mm; $OD_{mea}$ = 5.9 mm;

## Diameter at various outputs

| Tube | Heat shrinkable | | | | |
|---|---|---|---|---|---|
| $Output(db)$ | 0 | 6 | 12 | 18 | 24 |
| $ID_{mea}$ | 4.1 | 4.1 | 4.3 | 4.3 | 4.1 |
| $OID_{mea}$ | 5.3 | 5.3 | 5.3 | 5.3 | 5.3 |
| $OD_{mea}$ | 6.4 | 6.2 | 6.2 | 6.2 | 6.2 |

Set the gain to get clear image.

$ID_{rea}$ = 4.95 mm; $OID$ = 5.6$mm$; $OD$ = 5.9 mm;

# Summary

| Transducer | T1 | T2 | T3 | T4 |
|---|---|---|---|---|
| $ID_{mea}$ | -0.475±0.045 | -0.571±0.107 | -0.475±0.05 | -0.779±0.104 |
| $ID_{cor}$ | -0.125±0.045 | -0.221±0.107 | -0.025±0.05 | -0.0386±0.104 |

# Appendix C

# PUBLISHED PAPERS AND LETTERS

1. Hoskins P R, Li S and McDicken W N, 1991 "Velocity estimation using duplex scanners" *Ultrasound in Med & Biol* 17, 195-198.

2. Li S, Hoskins P R, Anderson T and McDicken W N "Measurement of mean velocity during pulsatile flow using time averaged maximum frequency of Doppler ultrasound waveforms" *Ultrasound in Med & Biol* 19:105-113, 1993.

3. Li S, McDicken W N and Hoskins P R "Blood vessel diameter measurement by ultrasound" *Physiological Measurement* 14:291-297, 1993.

4. Li S, McDicken W N and Hoskins P R "Non-linear propagation in Doppler ultrasound" *Ultrasound in Med & Biol.* 19:359-364,1993.

5. Li S, McDicken W N and Hoskins P R "The refraction in Doppler ultrasound" *Ultrasound in Med & Biol.* 19:593-594, 1993.

*Ultrasound in Med. & Biol.* Vol. 17, No. 2, pp. 195–199, 1991
Printed in the U.S.A.

0301-5629/91 $3.00 + .00


# LETTERS TO THE EDITOR

## VELOCITY ESTIMATION USING DUPLEX SCANNERS

Sir,

Tessler et al (1990) reported recently a study of the accuracy and variability of peak velocity assessed using duplex Doppler systems. True velocity was assessed using a flow phantom and compared with the measured peak velocity after angle correction, and it was observed that there was overestimation of the true velocity by 25% in some cases. In their study Tessler et al did not attempt to study the causes of this overestimate related to instrumentation. Recently we have become involved with a Doppler quality control programme including the assessment of velocity measurement by duplex systems.

One test phantom used was a commercial string phantom (BBS Medical Electronic, Hagersten, Sweden). The string moves at a single velocity however this may give rise to a very large range of Doppler frequencies (figure 1). This is almost certainly due to intrinsic spectral broadening (Newhouse et al 1980, Censor et al 1988) and the large degree of spectral broadening of figure 1 is a reflection of the use of a focused beam from a large linear array. The measured velocity was taken from the centre of the spectral trace. This was compared with the true string velocity measured automatically by the string phantom. The degree of intrinsic spectral broadening was quantitated by calculating the ratio of the total bandwidth $\delta B$ of the spectrum to the measured centre velocity V.

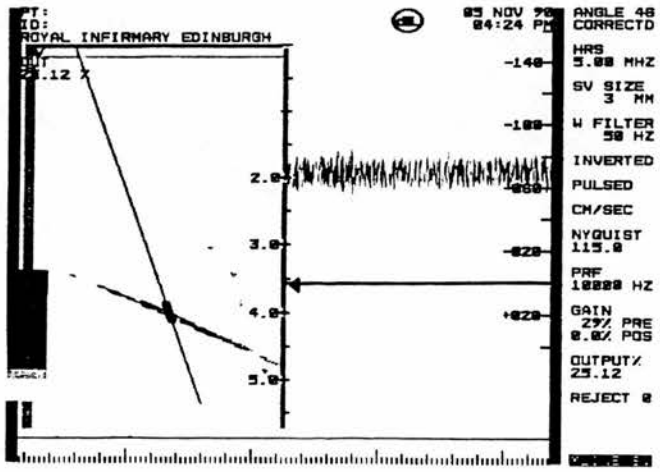


Figure 1 B-scan and Doppler waveforms taken using a string phantom.

A flow phantom was also used with steady flow (Hoskins et al 1989). The true maximum velocity was assessed from the measured volume flow and the known vessel cross sectional area, assuming a parabolic velocity profile. The volume flow was measured by timed collection of the fluid. The true maximum velocity was compared with the maximum velocity estimated using the duplex system after angle correction.

| | | Flow $\frac{V(meas)}{V(true)}$ | String $\frac{V(meas)}{V(true)}$ | String $\frac{\delta B}{2V(meas)}$ |
|---|---|---|---|---|
| Acuson 128 | (LA) | 1.23 | 0.96 | 0.34 |
| ATL UM9 | (LA) | 1.14 | 1.03 | 0.15 |
| Diasonics DRF-1000 | (LA + OD) | 1.01 | 1.02 | 0.05 |

Table 1 Results for velocity calibration for the flow and string phantom. The ratio of the measured velocity, v(meas), to the true velocity, v(true) is given. The last column shows the degree of spectral broadening assessed using the string phantom. LA = linear array, OD = offset Doppler.

Our preliminary results are presented in table 1. In all cases the measured and true velocities agree to less than 5% for the string phantom. For the flow phantom 2 of the 3 machines gave large overestimation of the true peak velocity and in both cases the degree of spectral broadening is of the same order of size as the degree of velocity overestimation. In both of these machines the Doppler beam was formed using a linear array. For the third machine there is an offset Doppler probe and this gave low spectral broadening and also close agreement between the measured and true velocities for both the string and flow phantom.

The results suggest that the overestimate of peak velocity noticed by us and in the paper of Tessler et al (1990) is due to intrinsic spectral broadening. The dependence of estimated peak velocity on machine settings was further investigated using the flow phantom and an ATL UM9 system with a 5 MHz linear array.

On the ATL UM9 the position of the Doppler aperture can be adjusted across the linear array. The effect of aperture position on estimated peak velocity was investigated for a true peak velocity of 72 cm/s, a transducer-vessel depth of 3.5 cm and a beam-vessel angle of $60^{o}$. Figure 2 shows a reduction in estimated velocity for aperture positions near to the end of the array. In all there was a change of 38% in estimated peak velocity. It was also noticed that the detected Doppler signal strength was smaller for aperture positions near to the end of the array. Both of these effects are consistent with the use of a smaller aperture for positions near to the end of the array.

The degree of spectral broadening is known to be angle dependent (Censor et al 1988), and the effect in practice of angle on peak velocity was investigated for a true peak velocity of 73 cm/s, a transducer - vessel distance of 3.5 cm, and a centrally placed aperture. Figure 3 shows that there is a reduction in the estimated peak velocity for smaller angles. For the range of angles used the total change in estimated peak velocity was 29%.

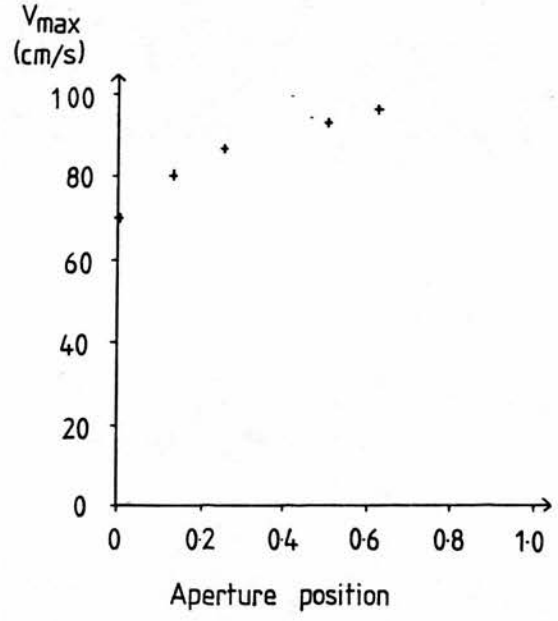


**Figure 2** Dependence of duplex measured velocity on aperture position. The full width of the linear array is normalised to 1.0 and distances are given with respect to one end of the array.

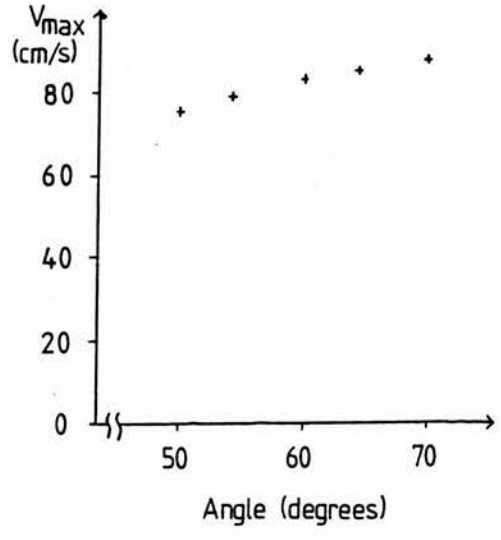


**Figure 3** Dependence of duplex measured velocity on angle.

The dependence of spectral broadening and hence estimated peak velocity on machine parameters such as beam-vessel angle and aperture position may well contribute to the variability of peak velocity measurements in studies such as that performed by Tessler et al (1990).

Accurate assessment of velocity is very desirable in clinical practice. The degree of inaccuracy of velocity estimation which arises as a result of intrinsic spectral broadening has not been appreciated by many people including ourselves. Reduction in spectral broadening could be produced by reducing the aperture width however this would be done at the expense of reduced sensitivity. An alternative approach, which at least one manufacturer is now performing, is to perform velocity calibration for the smallest beam-vessel angle which the aperture gives.

Yours faithfully

P.R. Hoskins, S.F.Li and W.N. McDicken
Department of Medical Physics, Royal Infirmary, Edinburgh.

REFERENCES

Censor, D., Newhouse, V.L., Vantz, T. and Ortega, H.V. Theory of ultrasound Doppler spectra velocimetry for arbitrary beam and flow configuration. IEEE Trans. Biomed. Eng. BME 35, 740-751, 1988.

Hoskins, P.R., Anderson, T. and McDicken, W.N. A computer controlled flow phantom for generation of physiological Doppler waveforms. Phys. Med. Biol. 11, 1709-1717, 1989.

Newhouse, V.L., Furgason, E.S., Johnston, G.F. and Wolf, D.A. The dependence of ultrasound Doppler bandwith on beam geometry. IEEE Trans. Sonics. Ultrason. SU 27, 50-59, 1980.

Tessler, F.N., Kimme-Smith, C., Sutherland, M.L., Schiller, V.L., Penella, R.R. and Grant E.G. Inter- and intra-observer variability of Doppler peak velocity measurements: an in-vitro study. Ultrasound Med. Biol. 16: 653-657, 1990.

'rasound in Med. & Biol. Vol. 19, No. 2, pp. 105–113, 1993
nted in the USA

0301-5629/93 $6.00 + .00


*Original Contribution*

# MEASUREMENT OF MEAN VELOCITY DURING PULSATILE FLOW USING TIME-AVERAGED MAXIMUM FREQUENCY OF DOPPLER ULTRASOUND WAVEFORMS

S. LI, P. R. HOSKINS, T. ANDERSON and W. N. MCDICKEN
Department of Medical Physics and Medical Engineering, Royal Infirmary of Edinburgh, Edinburgh EH3 9YW, UK

(*Received* 6 *August* 1992; *in final form* 14 *September* 1992)

**Abstract—It has been suggested that mean velocity of flow could be estimated by the time-averaged maximum frequency over an integral number of cardiac cycles (Gill 1985). The present study verified this theory experimentally with a computer-controlled flow phantom. The effects of some parameters on the relationship between mean velocity and time-averaged maximum frequency were also studied. Parameters investigated included beam-vessel angle, diameter of tubing, pulsatility, flow rate and stenosis. The velocities measured by the Doppler system were compared with the actual velocities. A simple theoretical model was also developed to compare with the experimental results. The results showed that, in a long straight tube, the mean velocity can be estimated to within about 5% from the time-averaged maximum Doppler shift at various flow rates and pulsatilities. The error due to geometrical spectral broadening, especially for large beam-vessel angles, can be estimated to within 3% and therefore corrected.**

*Key Words:* **Ultrasound, Pulsatile flow, Maximum frequency, Mean velocity.**

## INTRODUCTION

uantitative measurements of blood flow in a num-r of vessels have been reported, such as the com-on femoral artery (Lewis et al. 1986), umbilical in (Gill et al. 1984) and the superior mesenteric tery (Qamar et al. 1984, 1986). In order to measure w, estimates are needed of the mean velocity and e vessel cross-sectional area. Using a duplex scan-r, the vessel cross-sectional area is estimated using scan, and the mean velocity is estimated from the ppler waveform.

The mean velocity can be estimated from the ne-averaged, intensity-weighted mean frequency aker 1970; Brody and Meindl 1974; Gill 1979), or m the time-averaged maximum frequency over an egral number of cardiac cycles.

The intensity-weighted mean frequency enve-e is affected by a number of physical parameters. nuniform insonation may severely distort the ape of the Doppler spectrum and consequently use errors in the intensity-weighted mean frequency envelope (Cobbold et al. 1983; Evans 1982). The envelope can also be distorted by misalignment of the beam and vessel, system frequency response, filtering and noise, etc. In clinical measurements, it can be further affected by attenuation of the beam by both tissue and blood.

An alternative approach is to estimate mean velocity using the maximum frequency envelope of the Doppler waveform. Maximum frequency methods usually assume that the velocity profile is flat (Evans et al. 1989; Fisher et al. 1983) or parabolic at all points during the cardiac cycle. For a flat profile, the maximum velocity simply equals the mean velocity. For parabolic flow, mean velocity $V_{mean}(t)$ is a half of the maximum. In general, however, this approach is not valid as the velocity profile in arteries usually falls somewhere between parabolic and flat (McDonald 1974).

A theoretical study by Evans (1985) suggested that under certain conditions, where there is not necessarily plug or parabolic flow, the time-averaged mean velocity $\overline{V}_{mean}$ of a pulsatile flow is equal to half of the time-averaged maximum velocity when calculated over an integral number of cardiac cycles. This rela-

Address correspondence to: S. Li.

tionship was derived for ideal conditions where the vessel is long and straight, the diameter is constant, and the flow is unidirectional and laminar. It should be noted that the relationship between the time-averaged maximum and mean velocities as suggested by Evans for pulsatile flow is the same as the relationship for steady and parabolic flow if the assumption is made of parabolic flow at all points during the cardiac cycle. Using this approach, the mean velocity averaged over a number of cardiac cycles $\overline{V_{mean}}$ can be estimated by

$$\overline{V_{mean}} = \left(\frac{c}{4F_0 \cos\theta}\right)\overline{(F_d)_{max}} \qquad (1)$$

where $c$ is the sound speed, $F_0$ is the transmitted ultrasonic frequency, $\theta$ is the beam-vessel angle and $\overline{(F_d)_{max}}$ is the maximum frequency averaged over a number of cardiac cycles.

To date, there has been no experimental data presented to support the use of eqn (1). In this study, the accuracy of estimation of volume flow using eqn (1) was investigated for a range of beam-vessel angles, of flow rates, of waveform pulsatility, and in the region of a stenosis.

## METHOD

*Materials*

To collect data *in vitro,* a physiological flow phantom was used. A detailed description of the phantom was given in a previous publication by Hoskins et al. (1989). The phantom was composed of 3 parts: a large tank with holders for the tubing and the transducer; a gear pump driven by a computer-controlled stepping motor; and a Doptek spectrum analyser. The probe holder had an arm which could keep the sampling site and the distance between transducer and sampling site unchanged when the angle was altered. The speed of the motor was controlled by a microcomputer and therefore enabled waveforms of different shapes and velocities to be produced. The artificial blood was a suspension of Sephadex G 25 superfine particles in a mixture of 42% glycerol to 58% water. This has a viscosity of 0.004 kg/ms at 20°C which corresponds to that of blood at 37°C. The spectra from blood and Sephadex are very similar in terms of their first- and second-order statistical properties (Hoskins et al. 1990).

The vessels were constructed from heat-shrinkable material which was moulded around rods of known diameter (McDicken 1986). The accuracy of construction of the vessel diameter was found to be better than 0.05 mm using a microscope. Angle measurement is better than ±1° with the experimental setup. The critical angle for the total reflection of heat-shrinkable tubing in water is 37°. A Doptek 4 MHz continuous-wave (CW) unit was used for waveform acquisition. All the spectra were recorded on magnetic tapes. Simultaneous measurements of absolute flow were made using a measuring cylinder and a stop watch.

The flow waveforms used in this study included steady flow, unidirectional and bidirectional flow of different pulsatility. Four typical waveforms are illustrated in Fig. 1. The peak velocity of all waveforms was about 1 m/s which is similar to the physiological value in many vessels of interest.

*Effect of pulsatility*

Waveforms of different pulsatilities and shapes were acquired. Tubing of internal diameters of 5.0 mm and 8.0 mm were used. Thirteen waveforms of pulsatility index ranging from 0 to 12.53 were used with the 5.0 mm tube. Eighteen waveforms of pulsatility index ranging from 0 to 12.07 were examined on the 8.0 mm tubing for a more detailed study. The distance between transducer face to the centre of each tube was 5.0 cm.

*Effect of beam-vessel angle*

Four waveforms of different pulsatilities and shapes including steady flow, unidirectional flow and bidirectional flow were acquired for angles from 85° to 35° in 5° steps. The depth of the tubing was set to be 5.6 cm.

The transmission field of the transducer was assessed using a bilaminar hydrophone (GEC-Marconi Ltd, Essex, UK). A theoretical estimation of the geometrical spectral broadening effect on the maximum frequency was made (see Appendix).

*Flow rates*

Two waveforms (see Figs. 1b and 1d) with unidirectional flow and bidirectional flow were examined. Twelve different flow rates were used. The peak velocities were from 48.9 cm/s to 244 cm/s corresponding to Reynolds numbers from 672 to 3358. This enabled some momentary turbulence, which was observed as irregular high-frequency spikes on spectra, to occur at the higher velocities. The diameter of the tubing was 5.0 mm and the distance between transducer and vessel was 5.0 cm.

*Stenosis*

To find out how stenosis and turbulence affect the estimation of mean velocity, a 75% artificial steno-

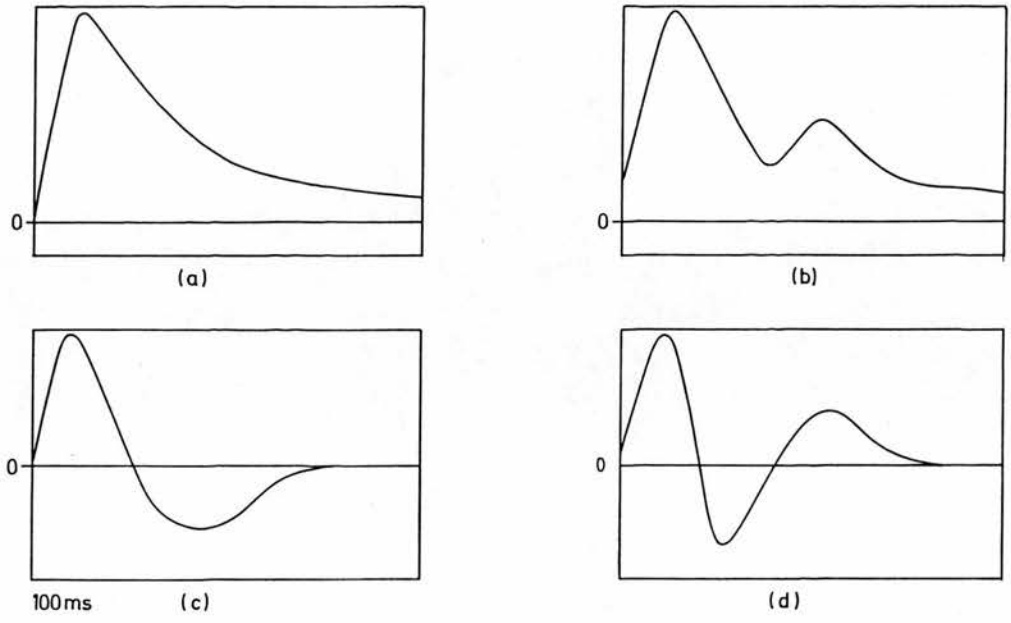


Fig. 1. Typical waveforms used in this study. (a) single-phase unidirectional flow; (b) biphasic unidirectional flow; (c) biphasic bidirectional flow; (d) triphasic bidirectional flow.

with an internal diameter of 2.5 mm was fixed in 5.0 mm heat-shrinkable tubing. Three waveforms re acquired from 9 different sites both distal and ximal to the stenosis. The distance between transer face and centre of the beam was 5.0 cm.

*Data analysis*

The spectra recorded on tapes were transferred to the Doptek unit for calculation of the maximum frequency envelope. The envelope of each waveform was traced manually using the Doptek light pen sys-

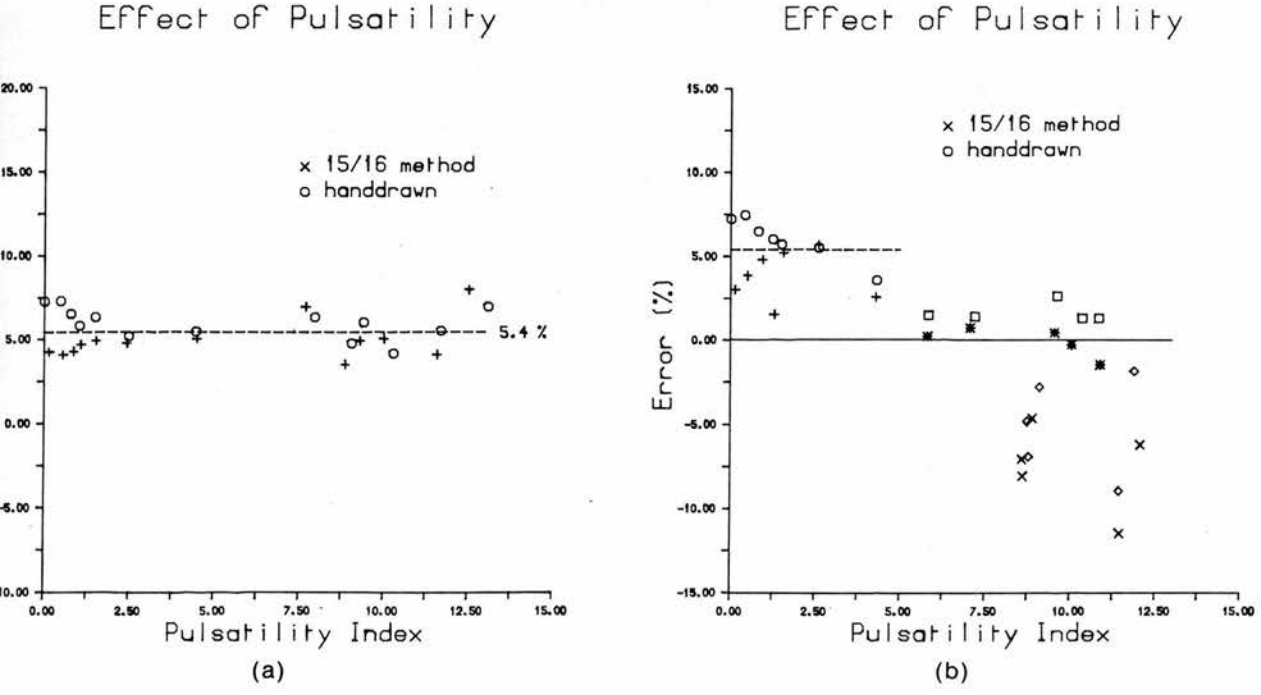


Fig. 2. Effect of pulsatility. In (a) 5 mm tubing was used. O and + denote results from hand-drawing and the $\frac{15}{16}$th method, respectively. In (b) 8 mm tubing was used. O and + denote the results from unidirectional waveforms; □ and ∗ symbolise the bidirectional and biphasic flow; and ◇ and × indicate bidirectional and triphasic flow.

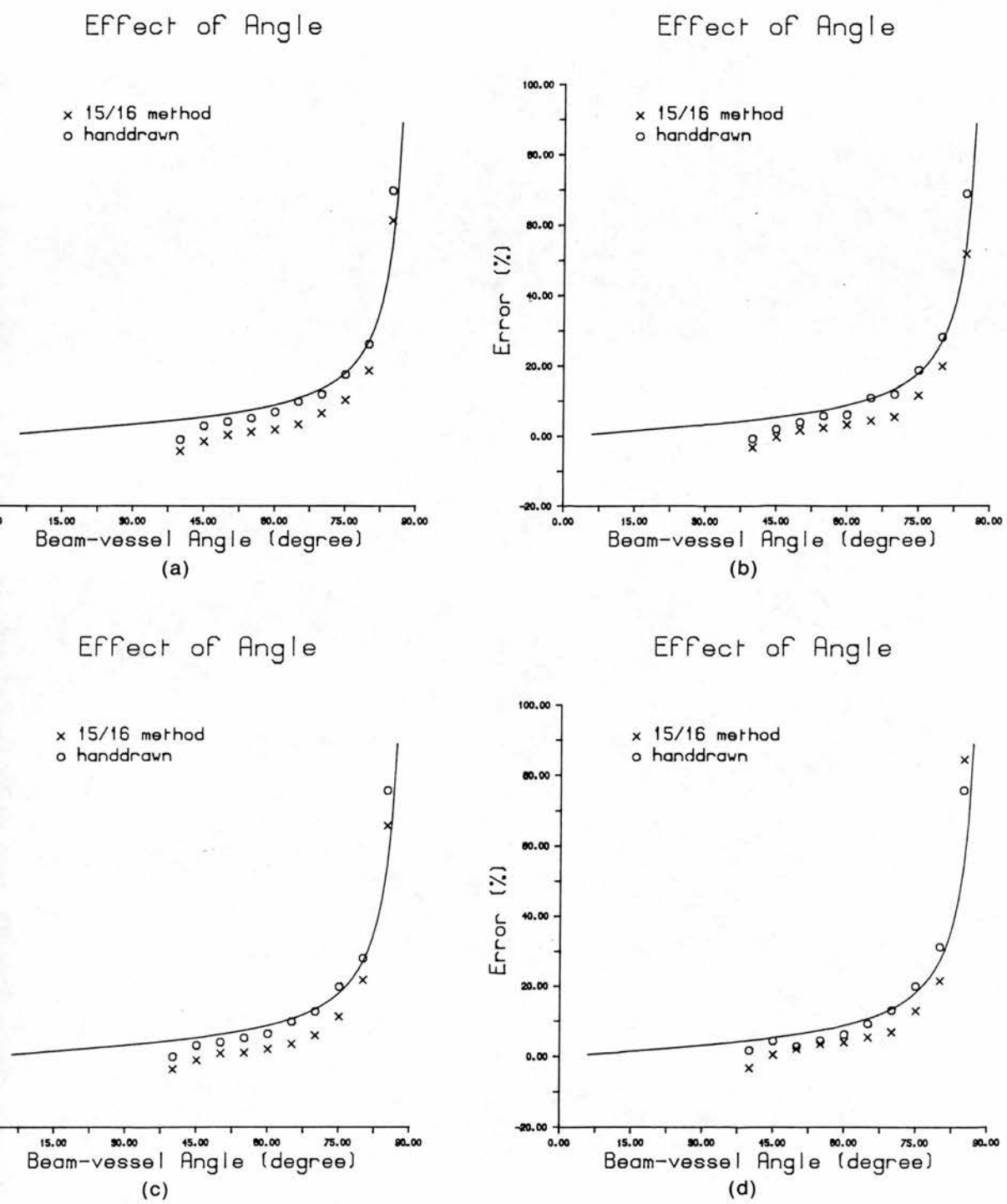


3. Effect of angle with (a) steady flow; (b) unidirectional flow; (c) biphasic flow with flow reversal; (d) asic flow with flow reversal. The solid curves are the estimated values with the consideration of geometrical spectral broadening (see Appendix).

d automatically using the $\frac{15}{16}$ percentile n the percentile method, the total value $T$ of ues (voltage amplitude) of a single spectral lculated. The maximum frequency is then calculated as the point where the sum of pixel values below that frequency just exceeds a specified percentage of $T$. In this case, this is $\frac{15}{16}$ expressed in percentage terms.

The estimated mean velocity $\overline{V_{mean}}$ was calcu-ed using eqn (1). The true mean velocity was cal-ated from timed collection of flow using eqn (2) ow:

$$\overline{V_{real}} = \frac{\text{Volume in measuring cylinder}}{\text{Time of collecting}} \cdot \frac{1}{\pi r^2} \quad (2)$$

ere $r$ is the internal radius of the tubing.

The difference between the Doppler-estimated an velocity and true mean velocity was expressed he error $E$ by

$$E = \frac{\overline{V_{real}} - \overline{V_{mean}}}{\overline{V_{real}}}. \quad (3)$$

## RESULTS

The ratio $E$ of measured to true mean velocities n general lower when calculated from the envelope ained using the $\frac{15}{16}$ percentile method compared to values of $E$ calculated from the envelope obtained nand-drawing. This is a direct result of the fact that he $\frac{15}{16}$ percentile method $\frac{1}{16}$ of the spectral power lies ve the maximum frequency, whereas in the man- method the operator is able to assess the highest quency present.

*ect of pulsatility*

Fig. 2a illustrates the ratio $E$ of waveforms with erent pulsatility index values in a 5.0 mm diame-ubing. The broken line represents $E = 5.4\%$ which ne average of the ratios. The results showed a rea-ably good agreement with the theory of Evans 85). Little difference between waveforms of differ- pulsatilities and shapes was shown at this diame- The systematic error of about 5% can be explained he geometrical spectral broadening which is dis-sed later. It must be noted that even those wave-ns with large flow reversal obey the theory reason- well.

For the larger tubing of 8.0 mm diameter, it was wn that the ratio $E$ was more dependent on pulsa-y (Fig. 2b). The waveforms in this test can be clas-d into three categories. The first group was unidi-ional flow denoted by ○ and +. Similar results to 5.0 mm tubing's were obtained in that a consistent restimation of mean velocity by about 5% was de. The second group was symbolised as □ and ∗. waveforms in this group were bidirectional and nasic. The errors were near 0 which shows about drop compared with the first group. Symbols ◇ × indicate the waveforms which have three phases. There was more variation of $E$ for this group, and on average there is a 7% or 8% fall in $E$ compared to the second group. The changes may be due to two causes. Firstly, large flow reversal can cause a considerable difference in velocity between layers in the tube and therefore vortices may form. A second cause may be distortion of the tube when large flow reversal occurs.

*Effect of angle*

The ratio $E$ of four waveforms including steady flow, unidirectional and bidirectional flow measured at angles from 40° to 85° are illustrated in Fig. 3. The errors were less than 6% for angles smaller than 60°. However, the errors increased sharply when the angle was greater than 70° due to intrinsic spectral broadening. It was impossible to measure the velocity beyond the angle of 40° because the critical angle effect sharply diminished the intensity of the Doppler signal. Again, little difference between waveforms was shown.

To study if the error caused by geometrical spectral broadening could be corrected, a theoretical estimation of the ratio $E$ at various beam-vessel angles was made (see Appendix). The agreement between the curve of estimated error and hand-drawn estimation is better than 3% for angles up to 80°.

*Effect of flow rate*

The ratio $E$ of the measured mean velocity against real mean velocity is plotted in Fig. 4. No obvi-

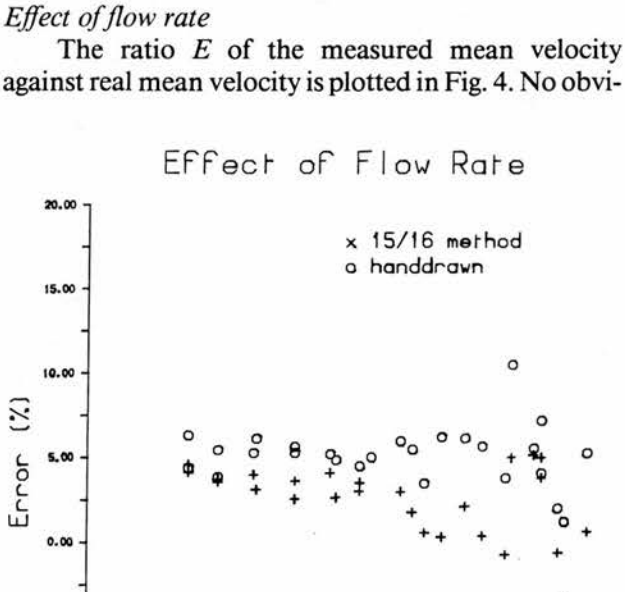


Fig. 4. Effect of flow rate.

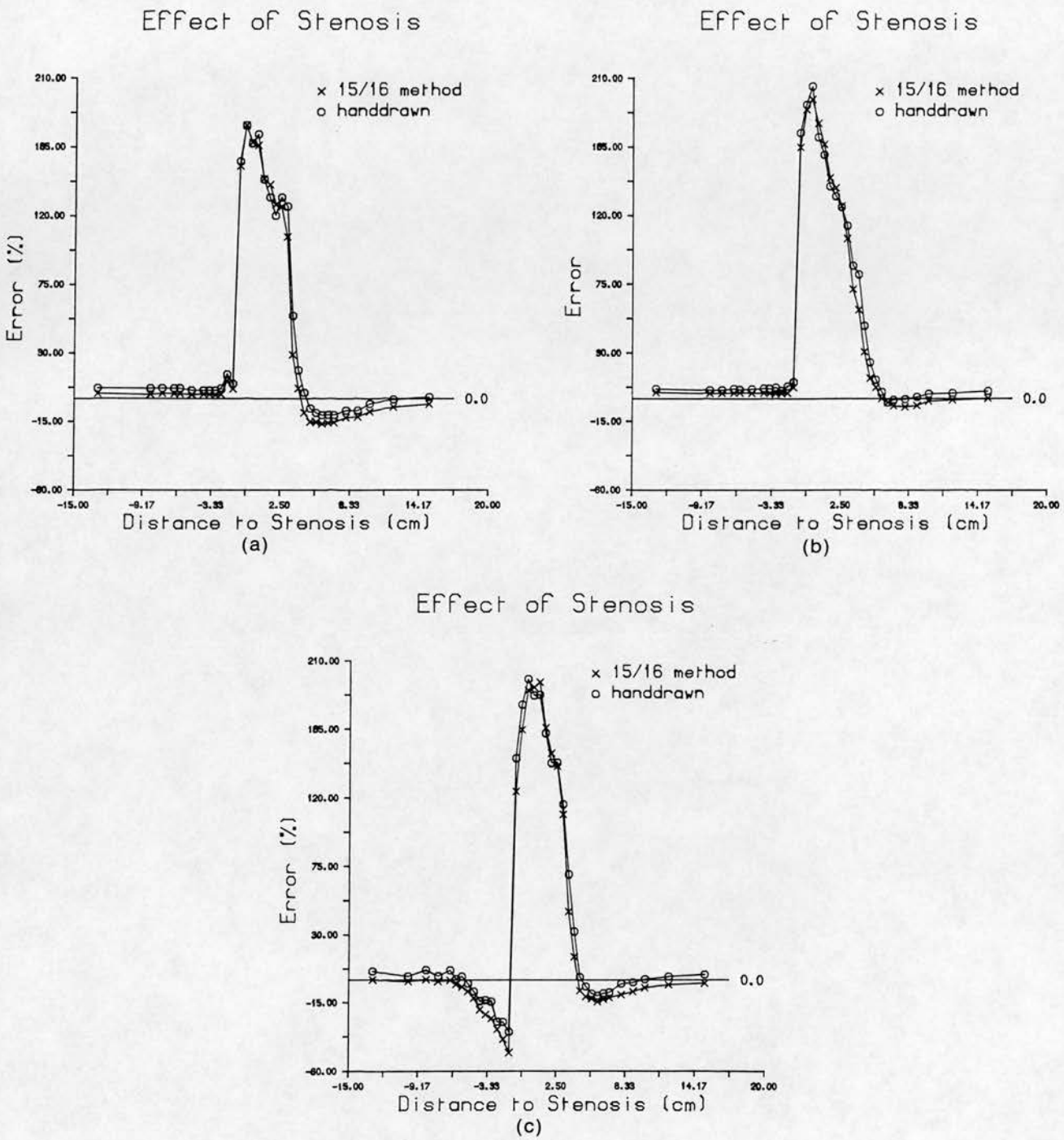


Fig. 5. Effect of stenosis with (a) steady flow; (b) unidirectional flow; (c) triphasic flow with flow reversal. Negative distance is proximal to the stenosis and positive is distal.

ous changes were observed among different flow rates. As expected, the errors at small flow rates were quite low. At high velocity, momentary turbulence was observed as irregular high frequent spikes. It was also found that when the pulsatility of the waveform was higher, the turbulence appeared at higher flow rates.

*Effect of stenosis*

Large changes in the ratio $E$ were observed with maximum values of $E$ of about 200% in the region of the stenosis (Fig. 5). At the distal side of the stenosis, the ratio $E$ changed considerably for each of the waveforms used. The ratio $E$ tended to the prestenotic value at a distance of about 13 cm distal to the steno-

is. At the proximal side, the errors are small for teady (Fig. 5a) and unidirectional (Fig. 5b) flow. For he bidirectional flow, during reverse flow the turbuent region will be on the proximal side of the stenosis nd will manifest itself on the reverse flow component f the prestenotic waveforms. This explains the large rop in $E$ observed in Fig. 5c.

## DISCUSSION

This study has shown that for a large range of hysical conditions, the theory of Evans for estimaion of the mean velocity from the maximum velocity grees reasonably well with the experimental results. his theory assumes that the maximum velocity is entrally located in the vessel, which is true for unidiectional flow in a long, straight, nonbranching tube. he results of this study suggest that there is only a mall difference in estimation of mean velocity when here is flow reversal. This may imply that in practice t is not necessary to assume that the maximum velocty is always located in the centre of the vessel.

In practice, because of the finite size of the transducer and sample volume, geometrical spectral roadening occurs (Bascom et al. 1986; Newhouse et l. 1977, 1980, 1987). This leads to overestimation of he maximum frequency using of eqn (1), particularly at large beam-vessel angles. The agreement beween the theoretically estimated curves and experimental data (Fig. 3) suggests this effect may be orrected.

One important assumption concerns the flow attern in the vessel. The assumption of a long, traight, nonbranching tube implies that the flow is aminar. If the sampled site is located near stenoses or arge curvatures, the theory cannot be assumed to be alid. Measurement in these locations should be voided. A second possible cause of error is the hange in diameter. The diameter of a vessel increases n systole and decreases in diastole and therefore hanges the flow profile. This effect is most noticeable n the aorta and large arteries. These factors may mody the application of this method of mean velocity stimation in practice (Eik-Nes et al. 1982, 1984; Maršál et al. 1984; Struyk et al. 1985; Teague et al. 985).

A Doptek CW Doppler unit was used in this tudy. In practice, pulsed-wave (PW) Doppler is most ften used in duplex scanners. Pulsed Doppler units nay be roughly classified into two groups: those that se long gate times sufficient to interrogate an entire essel, and those that use very short gates so that the ow in only a small part of the vessel is interrogated. or volume flow measurement, a PW operation with long gate times is most commonly used and it is actually very similar to a CW operation. For short pulse, as the bandwidth of the spectrum of the transmitted pulse is of order of the pulse length, spectral broadening may happen. Therefore, the theory discussed in this paper may need a slight modification in that case.

## CONCLUSION

In this study, it has been shown that under ideal conditions, the mean velocity is generally estimated to within about 5% from the maximum frequency envelope of the Doppler waveforms over a large range of waveform pulsatility values and flow rates. This error increases as the beam-vessel angle increases due to intrinsic spectral broadening. The mathematical model developed in this paper shows that the error in estimation of the mean velocity could be reduced to less than 3%. The presence of turbulence, for example in the region of a stenosis, can cause considerably large errors.

## REFERENCES


Baker, D. W. Pulsed ultrasonic Doppler blood flow sensing. IEEE Trans. Sonics Ultrason. SU-17:170–185; 1970.

Bascom, P. A. J.; Cobbold, R. S. C.; Roelofs, B. H. M. Influence of spectral broadening on continuous wave Doppler ultrasound spectra: A geometric approach. Ultrasound Med. Biol. 12:387–395; 1986.

Brody, W. R.; Meindl, J. L. Theoretical analysis of the CW Doppler ultrasonic flowmeter. IEEE Trans. Biomed. Eng. BME-21:183–192; 1974.

Cobbold, R. S. C.; Veltink, P. H.; Johnston, K. W. Influence of beam profile and degree of insonation on the CW Doppler ultrasound spectrum and mean velocity. IEEE Trans. Sonics Ultrason. SU-30:364–370; 1983.

Eik-Nes, S. H.; Maršál, K.; Brubakk, A. O.; Kristoffersen, K.; Ulstein, M. Ultrasonic measurement of human fetal blood flow. J. Biomed. Eng. 4:28–36; 1982.

Eik-Nes, S. H.; Maršál, K.; Kristoffersen, K. Methodology and basic problems related to blood flow studies in the human fetus. Ultrasound Med. Biol. 10:329–337; 1984.

Evans, D. H. Some aspects of the relationship between instantaneous volumetric blood flow and continuous wave Doppler ultrasound recordings—I. Ultrasound Med. Biol. 8:605–609; 1982.

Evans, D. H. On the measurement of the mean velocity of blood flow over the cardiac cycle using Doppler ultrasound. Ultrasound Med. Biol. 11:735–741; 1985.

Evans, D. H.; Schlindwein, F. S.; Levene, I. M. The relationship between time averaged intensity weighted mean velocity, and time averaged maximum velocity in neonatal cerebral arteries. Ultrasound Med. Biol. 15:429–435; 1989.

Fisher, D. C.; Sahn, D. J.; Friedman, M. J.; Larson, D.; Valdes-Cruz, L. M.; Horowitz, S.; Goldberg, S. J.; Allen, H. D. The mitral valve orifice method for noninvasive two-dimensional echo Doppler determinations of cardiac output. Circulation 67:872–877; 1983.

Gill, R. W. Performance of the mean frequency Doppler modulator. Ultrasound Med. Biol. 5:237–247; 1979.

Gill, R. W.; Kossoff, G.; Warren, P. S.; Garrett, W. J. Umbilical venous flow in normal and complicated pregnancy. Ultrasound Med. Biol. 10:349–363; 1984.

Gill, R. W. Measurement of blood flow by ultrasound: Accuracy and sources of error. Ultrasound Med. Biol. 11:625–641; 1985.
Hoskins, P. R.; Anderson, T.; McDicken, W. N. A computer controlled flow phantom for generation of physiological Doppler waveforms. Phys. Med. Biol. 34:1709–1717; 1989.
Hoskins, P. R.; Loupas, T.; McDicken, W. N. A comparison of the Doppler spectra from human blood and artificial blood used in a flow phantom. Ultrasound Med. Biol. 16:141–147; 1990.
Lewis, P.; Psaila, J. V.; Davies, W. T.; McCarty, K.; Woodcock, J. P. Measurement of volume flow in the human common femoral artery using duplex ultrasound system. Ultrasound Med. Biol. 12:777–784; 1986.
Maršál, K.; Lindblad, A.; Lingman, G.; Eik-Nes, S. H. Blood flow in the fetal descending aorta; intrinsic factors affecting fetal blood flow, *i.e.* fetal breathing movements and cardiac arrythmia. Ultrasound Med. Biol. 10:339–348; 1984.
McDicken, W. N. A versatile test-object for the assessment of the performance of Doppler flow instruments. Ultrasound Med. Biol. 12:245–249; 1986.
McDonald, D. A. Blood flow in arteries. London: Edward Arnold; 1974:64–69.
Newhouse, V. L.; Varner, L. W.; Bendick, P. J. Geometrical spectrum broadening in ultrasonic Doppler systems. IEEE Trans. Biomed. Eng. BME-24:478–480; 1977.
Newhouse, V. L.; Furgason, E. S.; Johnson, G. F.; Wolf, D. A. The dependence of ultrasound Doppler bandwidth on beam geometry. IEEE Trans. Sonics Ultrason. SU-27:50–59; 1980.
Newhouse, V. L.; Censor, D.; Vontz, T.; Cisneros, J. A.; Goldberg, B. Ultrasound Doppler probing of flows transverse with respect to beam axis. IEEE Trans. Biomed. Eng. BME-34:779–789; 1987.
Qamar, M. I.; Read, A. E.; Skidmore, R.; Evans, J. M.; Wells, P. N. T. Noninvasive assessment of the superior mesenteric artery blood flow in man. Gut 25:A546–547; 1984.
Qamar, M. I.; Read, A. E.; Skidmore, R.; Evans, J. M.; Wells, P. N. T. Transcutaneous Doppler ultrasound measurement of superior mesenteric artery blood flow in man. Gut 27:100–105; 1986.
Struyk, P. C.; Pijpers, L.; Wladimiroff, W.; Lotgering, F. K.; Tonge, M.; Bom, N. The time-distance recorder as a means of improving the accuracy of fetal blood flow measurements. Ultrasound Med. Biol. 11:71–77; 1985.
Teague, M. J.; Willson, C. K.; Battye, C. K.; Taylor, M. G.; Griffin, D. R.; Campbell, S.; Roberts, V. C. A combined ultrasonic linear array scanner and pulsed Doppler velocimeter for the estimation of blood flow in the foetus and adult abdomen—I: Technical aspects. Ultrasound Med. Biol. 11:27–36; 1985.

## APPENDIX

*An estimation of the effect of geometrical spectral broadening on flow measurement*

The geometry for an unfocused transducer can be simply illustrated in Fig. A1. Region I is the near field and region II is the far field where the beam diverges and it has an approximate constant divergent angle $\mu$.

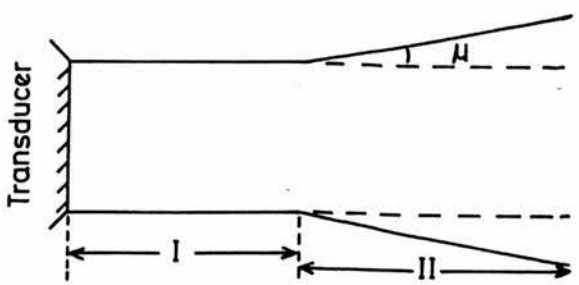


Fig. A1. Idealised field shape of unfocused beam of a circular transducer.

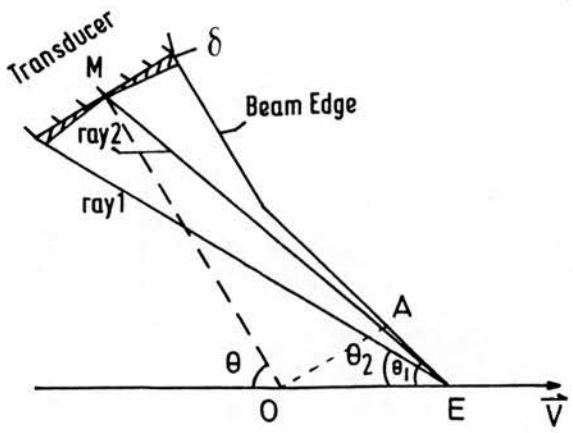


Fig. A2. Geometry used in calculating maximum frequency in the far field of a 2D shaped transducer.

A CW transducer is usually composed of two half-disc crystals. One acts as transmitter and the other as receiver. Two crystal axes are oriented at a convergence angle of $\delta$ in front of the transducer. The beam can be depicted in Fig. A2. The maximum Doppler shift can be calculated by using the two extreme rays of the beam

$$(F_d)_{sp} = \frac{VF_0}{C}(\cos\theta_1 + \cos\theta_2) \qquad \text{(A1)}$$

where $V$ is the velocity of the scatterer, $C$ is the speed of ultrasound and $F_0$ is the transmitted frequency.

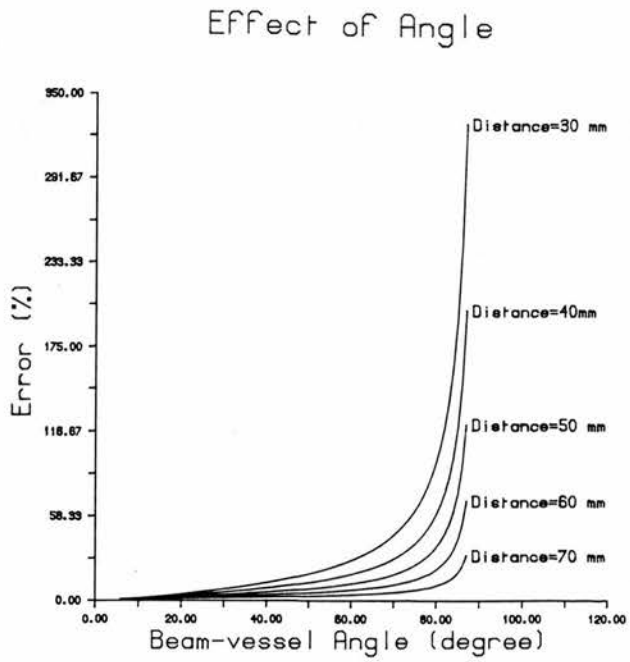


Fig. A3. Estimation of the error for various transducer-vessel distances and beam-vessel angles.

It can be calculated that the distance between the beam edge nd beam centre at distance $MO$ (Fig. A2) is given by

$$OE = OA\frac{\cos\mu}{\sin(\theta+\delta-\mu)} - MO\frac{\sin\delta}{\sin(\delta+\theta)} \tag{A2}$$

here $\theta$ is the beam-vessel angle and $OA$ is the beam width at distance $OM$. Therefore, for ray 1,

$$D_{x_1} = -OM\cos\theta - OE - r\sin(\theta-\delta) \tag{A3}$$

$$D_{y_1} = OM\sin\theta - r\cos(\theta-\delta) \tag{A4}$$

here $r$ is the radius of the transducer, $D_{x_1}$ and $D_{x_1}$ are projections f ray 1 on $x$-axis and $y$-axis, respectively. Therefore, we obtain

$$\cos\theta_1 = -\frac{D_{x_1}}{(D_{x_1}^2 + D_{y_1}^2)^{1/2}}. \tag{A5}$$

Similarly, for ray 2, we have

$$D_{x_2} = -OM\cos\theta - OE \tag{A6}$$

$$D_{y_2} = OM\sin\theta \tag{A7}$$

and

$$\cos\theta_2 = -\frac{D_{x_2}}{(D_{x_2}^2 + D_{y_2}^2)^{1/2}}. \tag{A8}$$

The Doppler shift with geometrical spectral broadening can be therefore calculated by eqn (A1).

The ratio $E$ then is estimated by

$$E = \frac{V_{\text{real}} - V_{\text{mean}}}{V_{\text{real}}} = \frac{F_d - (F_d)_{sp}}{F_d} = \frac{2\cos\theta - \cos\theta_1 - \cos\theta_2}{2\cos\theta} \tag{A9}$$

where $F_d$ is the Doppler frequency shift in ideal conditions.

The CW transducer we used in the experiment had a diameter of 8.0 mm. The angle between two crystals was 168°. The beam width was measured at 50% of the maximum pressure amplitude (*i.e.*, FWHM, pressure, at distance 5.6 cm was 6.5 mm and the divergent angle was 5.7 degrees). The transducer had a transmitting frequency of 4 MHz and its length of near zone was 17.3 mm. Some estimated results in a different distance are illustrated in Fig. A3. The comparison with the experimental data is given in Fig. 3.

Physiol. Meas. **14** (1993) 291–297. Printed in the UK

# Blood vessel diameter measurement by ultrasound

S Li, W N McDicken and P R Hoskins

Department of Medical Physics and Medical Engineering, Royal Infirmary of Edinburgh, Edinburgh, UK

Received 22 June 1992, in final form 16 February 1993

**Abstract.** Blood vessel diameter measurement is crucial to volume flow measurement in medical ultrasound. The accuracy of the measurement is examined in this study. Experiments were made on three kinds of tube using four transducers on three commercial duplex ultrasound scanners. The accuracy of the inner diameter measurement is affected by ultrasonic pulse length. By correcting this effect, it has been shown that the accuracy of the measurement can be increased significantly over a range of conditions.

## 1. Introduction

The accuracy of estimation of the cross-sectional area of vessels is crucial to volume flow measurement using ultrasound Doppler techniques. The cross-sectional area is usually calculated from the diameter measured by ultrasound. However, large errors in such measurements have been reported (Gill 1985).

One of the primary errors in diameter measurement is due to the limited resolution achievable using ultrasound. At its best, the obtainable accuracy is of the order of one wavelength of the transmitted ultrasound. Considering that the wavelengths of ultrasound of frequencies 3 MHz, 5 MHz and 10 MHz are 0.5 mm, 0.3 mm and 0.15 mm respectively, the error in the area estimation, especially on small vessels of a few millimetres diameter, can be very high.

As the echoes from the inner and outer surfaces of a blood vessel tend to merge together, it is considered that only the first echo is reliable. Therefore, some authors have measured from the outer surface of the proximal wall to inner surface of the distal wall and corrected for the wall thickness (Eik-Nes *et al* 1982, 1984, Struyk *et al* 1985). In practice, however, the outer surface of the blood vessel is not always observed and the thickness of the wall is generally unknown. This method is not generally applicable to the *in vivo* situation.

In clinical measurement, the diameter is most commonly estimated by two callipers placed on the inner boundaries of a vessel image. Surprisingly there are no reported experimental studies of the accuracy of this method. In this paper, the accuracy of the inner diameter measurement is examined and a method to improve the inner diameter measurement is described.

## 2. Method

In this study, four transducers on three commercial duplex scanners, two from Advanced Technology Laboratory, Ultramark 9 (ATL UM9), and one from Diagnostic Sonar Limited,

0967-3334/93/030291+07$07.50 

Prisma (DSL), were used. The transducer types are ATL 5 MHz phased array, ATL 3 MHz phased array, ATL 5 MHz linear array and DSL 3.5 MHz convex linear array.

For the tubes three kinds of material were used to give different reflectivity and sound speed. The materials used were transparent heat-shrinkable plastic, silastic rubber and PVC. Some acoustic properties of these materials and blood vessels are listed in table 1. It is shown these materials have properties which straddle those of real blood vessels (Goss *et al* 1978). Artificial vessels were used since measurements on real blood vessels are difficult. For example a blood vessel will collapse unless it is kept under pressure by the presence of flow. This would necessitate using a flow phantom during measurements on blood vessels and it would be very difficult to measure the true diameter, whereas for the tubing this was unnecessary. The diameters of the tubes ranged from 1.95 mm to 11.0 mm. All the ultrasound measurements were made with the tubes immersed in a mixture of 10% glycerol and 90% water. This mixture has a sound speed of 1540 m $s^{-1}$at 20 °C which corresponds to that of soft tissue.

**Table 1.** Acoustic properties of tubing materials and blood vessels.

| Tube | Density (kg $m^{-3}$) | C (m $s^{-1}$) | Z (kg $s^{-1}$ $m^{-2}$) |
|---|---|---|---|
| Heat shrinkable | 960 | 1979 | $1.90 \times 10^6$ |
| PVC | 1337 | 1714 | $2.29 \times 10^6$ |
| Silastic | 1224 | 949 | $1.16 \times 10^6$ |
| Blood Vessel | — | $1513 \pm 21$ | $1.56 \pm 0.03 \times 10^6$ |

Three fine steel threads were stretched in parallel in the glycerol–water mixture. The distances between threads were accurately known. Using each transducer, the calibration was performed by placing the callipers on the leading edge of the echoes from the steel threads.

For the diameter measurement, seven heat-shrinkable, three silastic and two PVC tubes were used. The diameter of each tube was measured using a microscope. The inner diameter of each tube was then measured with cursors on the B-mode image.

The effects of gain, output power, incident angle and depth on the diameter measurement were also investigated. A heat-shrinkable tube of diameter 4.95 mm was used. For the effect of gain, the DSL 3.5 MHz convex array was used. The output power was set to be 18 dB and gain varied from 0 to 54 dB. A gain larger than 54 dB gave too bright an image in which the edge of the tube was not clearly observed. The same tube was then measured using the ATL 3 MHz transducer with 16 output power settings from 100% to 0.56%. The gain was fixed in these measurements. For the effect of incident angle, the diameter of the tube was measured while the angle between the transducer face and vessel axis varied from 0° to 41°. For the effect of depth, the tube was examined at depths ranging from 1 cm to 11 cm in steps of 1 cm using the ATL 5 MHz phased array.

## 3. Correction of the pulse length

The finite length of the transmitted pulse causes the diameter to be underestimated when it is measured from the inside edges of the vessel wall echoes. As shown in figure 1, the leading edge of the echo signal reflected from the boundary arrives back at the transducer after time $T_1$ which is given by

$$T_1 = 2L/c \tag{1}$$

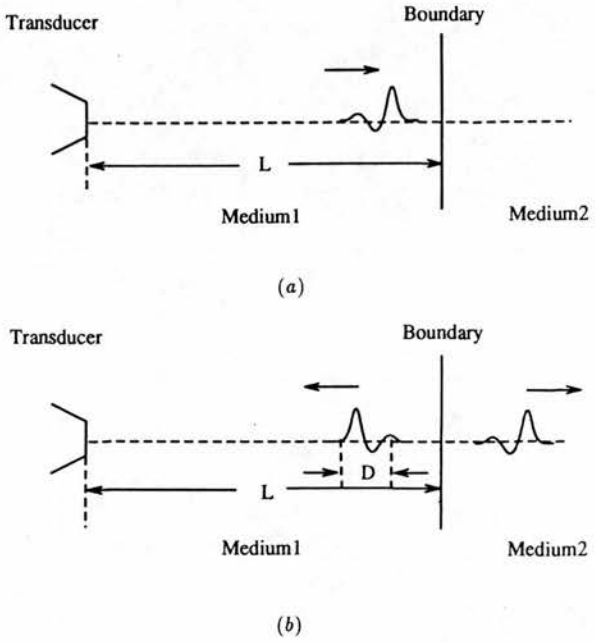


**Figure 1.** The underestimation because of pulse length: (*a*) when the pulse meets the boundary, it is reflected; (*b*) the reflection continues until the whole pulse leaves the boundary.

where $c$ is the speed of sound and $L$ is the actual distance from the transducer to the boundary. The end of the echo signal arrives at transducer at time $T_2$, given by

$$T_2 = (2L + D)/c \tag{2}$$

where $D$ is the pulse length. This means that the vessel/blood boundary displayed in a B-mode image has a depth of $\Delta d$ which can be written as

$$\Delta d = \tfrac{1}{2}(T_2 - T_1)c = \tfrac{1}{2}D. \tag{3}$$

Therefore, the inside edge of the boundary on the image extends into the vessel by $\Delta d$ and causes an underestimation of the vessel diameter by half of the pulse length. In practice, correction for this half pulse length could improve the accuracy of diameter measurement.

To measure the pulse length, a bilaminar polyvinylidene fluoride (PVDF) membrane hydrophone (GEC–Marconi Ltd) was used. Pulse waveforms were displayed and measured on an oscilloscope (HP 4540 A 500 MHz digital oscilloscope) connected to the preamplifier of the hydrophone.

All the commercial transducers were examined in a measuring tank filled with water. M-mode was used to stop the scanning. The hydrophone was rigidly fixed on a holder under water and the distance between the transducer and hydrophone was 5 cm. Pulse waveforms were displayed on the oscilloscope and the time interval $\Delta t$ was measured as the time between the first and last peaks in which the peak pressures were larger than 10% of the maximum.

Each of the pulse lengths was then calculated. As the diameter measurement was carried out in the solution with sound speed of 1540 m $s^{-1}$ which corresponds to that of soft tissue, the half pulse length $\Delta d$, which is the diameter correction, was estimated by

$$\Delta d = \tfrac{1}{2}(1540\Delta t). \tag{4}$$

Each of the measured inner diameters was corrected by subtracting $\Delta d$ from the cursor result. All the results were compared with the true diameter and measured diameter before the correction.

## 4. Results

A typical example of pulse length measurement is shown in figure 2. As the built-in measuring system of the oscilloscope was very accurate ($\pm 1$ ns), the error in pulse length is small and can be ignored. The pulse lengths and the diameter corrections for the four transducers are listed in table 2. The pulse length differs among machines and transducers; consequently, the corrections for the diameter are different.

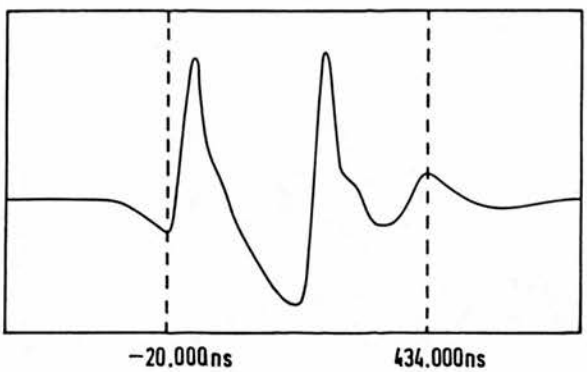


**Figure 2.** The pulse length measurement of the ATL 5 MHz phased array.

**Table 2.** The pulse lengths of transducers measured by the hydrophone and the corresponding corrections of diameter measurement. Transducers are T1: ATL 5 MHz phased array, T2: ATL 3 MHz phased array, T3: ATL 5 MHz linear array and T4: DSL 3.5 MHz linear array.

| Transducer | T1 | T2 | T3 | T4 |
|---|---|---|---|---|
| Pulse length (ns) | 454 | 588 | 506 | 962 |
| Correction (mm) | 0.35 | 0.45 | 0.39 | 0.74 |

Figure 3 gives the results of diameter measurement. The absolute errors were dependent on transducers because of different pulse lengths among transducers. After the correction, errors in diameter are greatly reduced. The error after the correction is typically about 0.1–0.2 mm. Consequently, the errors in the cross-sectional area were significantly reduced, especially for small vessels (figure 4). There was no difference among the tubes made from three kinds of material. This suggests that the reflectivity of the boundary has no significant effect on the blood vessel diameter measurement. The absolute error in diameter was very similar among all sizes of tube in the study.

No significant changes in diameter measurement were found when the depth, gain and output power were altered.

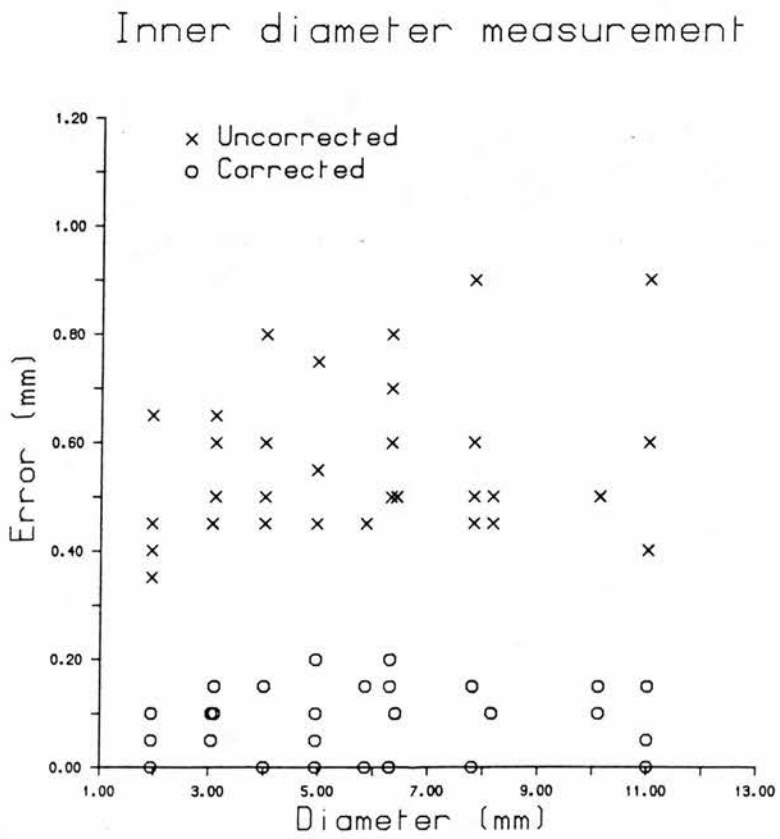


**Figure 3.** The absolute error of diameter measurement before and after the pulse length correction.

For the effect of incident angle, it is found that the quality of the vessel images reduced sharply when the angle increased. Consequently the diameter measurement became difficult because of the uncertainty in identifying the vessel edges on the screen. When the angle between the beam axis and the perpendicular to the vessel axis was greater than 10°, the measurement error became large (table 3). Similar difficulties are encountered with real blood vessels.

**Table 3.** Inner diameter measured at different beam–vessel angles with a heat-shrinkable tube. Pulse length corrections have been made. Angles in the table are the angle between the beam and the normal of the vessel axis. The true diameter is 4.95 mm.

| Angle (°) | 0 | 6 | 10 | 11 | 13 | 16 | 26.5 | 38 | 41 |
|---|---|---|---|---|---|---|---|---|---|
| $ID_{meas}$ | 4.9 | 4.9 | 4.8 | 4.9 | 4.5 | 4.7 | 4.3 | 4.9 | 4.3 |

## 5. Discussion

The cross-sectional areas calculated using the imaged diameter have a large error ranging from about 7% to 56% for the tubes of different size used in this study. After the pulse

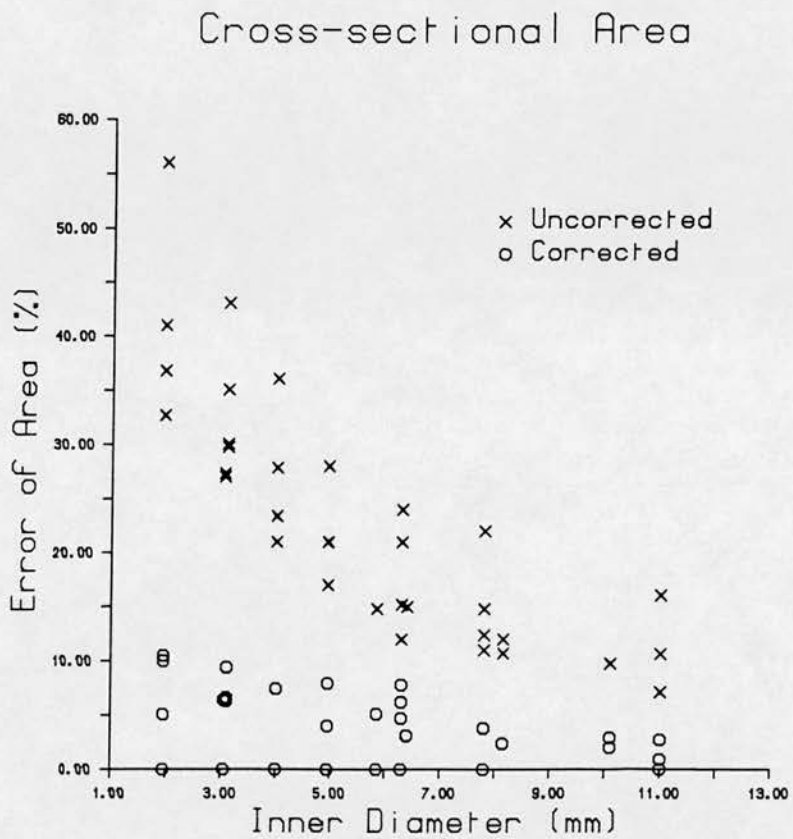


**Figure 4.** The percentage error of area before and after the pulse length correction.

length correction, this range was reduced to 0–10.5%. The error in diameter is about 0.1–0.2 mm which is about a typical pixel size in an image. It is noted that this error is smaller than the wavelength. Furthermore, the corrected diameter shows no relationships with transducers, machines, tube materials or size.

Because of the correction of the pulse length, only the boundary of the innermost layer of the vessel wall and blood is considered. Theoretically this avoids the influence of the finite vessel wall thickness (consisting of several layers) which leads to many problems in locating the point of the proximal vessel wall. In practice, the edge of the innermost layer of the vessel and blood may not be very clear on some B-mode images. Therefore, experience in locating the boundary may be needed.

As sound speed in blood is about 1570 m $s^{-1}$ rather than 1540 m $s^{-1}$ set on machines, the correction for this effect may also improve the accuracy of the diameter measurement by 2%.

## 6. Conclusion

The diameter of a vessel, measured by the distance of separation of inner edges on ultrasound images, is underestimated due to the pulse length. By correcting this effect, the accuracy of this measurement can be significantly improved over a range of physical and instrument

conditions. Accurate measurement can be difficult when the beam–vessel angle is smaller than 80°.

## References

Eik-Nes S H, Marsal K, Brubakk A O, Kristofferson K and Ulstein M 1982 Ultrasonic measurement of human fetal blood flow *J. Biomed. Eng.* **4** 28–36

Eik-Nes S H, Marsal K and Kristoffersen K 1984 Methodology and basic problems related to blood flow studies in the human fetus *Ultrasound Med. Biol.* **10** 329–37

Gill W R 1985 Measurement of blood flow by ultrasound: accuracy and source of error *Ultrasound Med. Biol.* **11** 625–41

Goss S A, Johnson R L and Dunn F 1978 Comprehensive compilation of empirical ultrasonic properties of mammalian tissues *J. Acoust. Soc. Am.* **64** 423–57

Struyk P C, Pijpers L, Wladimiroff J W, Lotgering F K, Tonge M and Bom N 1985 The time-distance recorder as a means of improving the accuracy of fetal blood flow meausrements *Ultrasound Med. Biol.* **11** 71–7

*Ultrasound in Med. & Biol.* Vol. 19, No. 5, pp. 359–364, 1993
Printed in the USA

0301-5629/93 $6.00 + .00


●*Original Contribution*

# NONLINEAR PROPAGATION IN DOPPLER ULTRASOUND

S. Li, W. N. McDicken and P. R. Hoskins
Department of Medical Physics and Medical Engineering, University of Edinburgh, Royal Infirmary, Edinburgh, EH3 9YW, UK

(*Received* 23 *January* 1992; *in final form* 19 *January* 1993)

**Abstract—The nonlinear propagation of ultrasound was demonstrated using Doppler transducers on two commercial duplex machines. The influence of nonlinear propagation on Doppler measurements was studied on both a flow phantom and a string phantom. It was found that although the pulse waveforms showed clearly different degrees of nonlinear distortion, no effect due to the nonlinearity could be detected on the received Doppler spectrum both in terms of the maximum frequency or underlying Doppler spectral profile.**

***Key Words:*** **Nonlinear propagation, Doppler, Spectrum.**

## INTRODUCTION

It is usually acceptable in biomedical applications of ultrasound to consider that acoustic propagation is a linear process. However, the propagation of acoustic waves is in fact a nonlinear process (Bakhvalov et al. 1978; Blackstock 1965). Inevitably, this results in pulse waveform distortion, harmonic generation and shock formation.

Evidence has accumulated to indicate that the linear treatment may not always be appropriate in medical ultrasound. Muir and Carstensen (1980) investigated a variety of effects resulting from the nonlinear propagation of finite-amplitude ultrasound and experimentally demonstrated nonlinear acoustic phenomena in water. It was suggested that the harmonics generated could enlarge the beamwidth and hence degrade the lateral resolution of instruments. A theoretical model of the nonlinear propagation of pulsed focused acoustic beams was developed to estimate the degree of distortion (Bacon 1984). It has also been shown that for pulsed diagnostic beams shock formation was not only possible but common among commercial machines (Duck and Starritt 1984; Duck et al. 1985). Values of the nonlinear parameter B/A for tissues and biological fluids also indicated the importance of nonlinearity in diagnosis and tissue characterisation (Law et al. 1985).

The emphasis in these papers is on wave propagation, the possible importance of harmonic generation, attenuative losses and their relevance for studies of biological effects and physiotherapy. However, to date, there have been no studies on the influence of nonlinear propagation on Doppler measurements.

Since nonlinear propagation results in changes in the ultrasonic field and generation of harmonics, a transmitted pulse may be distorted when it arrives at the blood vessel. Therefore, the scatterers (blood cells) may be excited by a distorted wave. The Doppler spectrum may be changed consequently.

A Doppler system is a narrow-band system. However, the amplitude of the fundamental frequency decreases when the amplitude of higher harmonics increases (Muir and Carstensen 1980). In addition, since a transmitted pulse wave has a spectrum of different amplitudes over a range of frequency, different decreases can result in those harmonics within the detection range of the Doppler instrument. Finally, the distortion due to nonlinear propagation is not uniformly distributed in the sample volume. At the centre of the beam, where the pressure amplitude is usually the largest, the distortion is more severe. This may change the beam intensity profile in the sample volume and therefore the Doppler spectrum. However, the scale of these effects on the Doppler spectrum is unknown.

As can be seen from the above, the process of distortion due to nonlinear propagation is very complex. It is therefore expedient to investigate experimentally the significance of this effect on the Doppler spectrum. In this study, nonlinear propagation was demonstrated using Doppler transducers on two

Address correspondence to: S. Li.

commercial duplex machines, and the effect of nonlinear propagation on the Doppler spectrum was examined.

## METHODS

*Equipment*

To measure the beam waveforms, a bilaminar polyvinylidene fluoride (PVDF) membrane hydrophone was used (GEC-Marconi Ltd, Essex, England). The hydrophone was made from a membrane stretched over an annular frame and has an active element of 0.5 mm diameter in the centre. The thin membrane introduces little acoustic perturbation and so senses the free field acoustic pressure at the element. The bandwidth of the hydrophone was calibrated to be 10 MHz. Waveforms were displayed on an oscilloscope (HP 4540 A 500 MHz digital oscilloscope) connected to the preamplifier of the hydrophone. Hardcopy was obtained from an ink jet printer interfaced to the oscilloscope.

Two transducers on two commercial duplex scanners were used in the demonstration of nonlinear phenomena and for the Doppler spectrum study. The details of the two machines and transducers are listed in Table 1. In all cases, the hydrophone-transducer distance was 5.5 cm for the ATL UM9 (Advanced Technology Laboratory, Ultramark 9) 5 MHz probe, and 8.5 cm for the DSL (Diagnostic Sonar Limited, Prisma) 2.5 MHz probe. These points corresponded to the site of greatest pulse waveform nonlinear distortion in water.

Both a flow phantom and a string phantom were used in this study. The flow phantom has the advantage that it is similar to the physiological situation. The string phantom test provides a line of scatterers with the same velocity passing through the centre of the beam. As the distortion is most severe at the centre of the beam, it would be expected that the effect of nonlinearity would be observed more easily with the string phantom than with the flow phantom.

A detailed description of the flow phantom used in this study has been given in a previous publication by Hoskins et al. (1989). The phantom was composed of a large tank with tubing supported in it, a probe holder and a gear pump driven by a computer-controlled DC motor. The speed of the motor was controlled by a microcomputer which enabled stable and repeatable velocities to be produced. For the tubing, transparent heat-shrinkable material was used. This was moulded around rods of known diameter. The artificial blood was a suspension of Sephadex G25 superfine particles in a mixture of 42% glycerol to 58% water. This gives a viscosity of 0.004 kg $m^{-1}$ $s^{-1}$ at 20°C which corresponds to that of blood at 37°C (McDicken 1986). The spectra from blood and Sephadex are very similar in terms of their first- and second-order statistical properties (Hoskins et al. 1990).

Table 1. Some characteristics of the two transducers used in this study.

| Machine | DSL | ATL UM9 |
|---|---|---|
| Type | Single crystal | Phased array |
| Shape | Circular | Square |
| Size | 10 mm | 11 × 11 mm |
| Frequency | 2.5 MHz | 5 MHz |
| Focus | 6–8 cm | 4–5 cm |
| Gate length | 10 mm | 10 mm |

A string phantom (BBS Medical Electronic AB) was also used to examine the effect of nonlinear propagation on the Doppler spectrum. It contains a DC-motor, drivebelt, three pulleys and a string loop all mounted on a frame. The frame can be adjusted to give a suitable beam-string angle and height in the water tank. A loop of surgical nylon thread was used as the string.

For both the string and flow phantom studies, the transducer-target distances were 5.5 cm for the ATL 5 MHz probe and 8.5 cm for the DSL 2.5 MHz probe. These are identical to the transducer-hydrophone distances.

*Experimental measurements*

The transmitted pulse shape was observed at a fixed depth in water using a hydrophone and an oscilloscope to demonstrate the nonlinear phenomenon. The effects of output power and position in the beam on the pulse waveforms were investigated.

The ultrasonic pulses from both of the commercial transducers were examined in a measuring tank. The transducers were mounted on a platform which could be moved in two orthogonal directions above the water tank. The hydrophone was rigidly fixed on a holder under water, and the distance between the transducer and hydrophone could be adjusted.

In the flow phantom experiments described below, the effect of nonlinearity on the Doppler spectrum is investigated. It is known that the heat shrink tubing used has a higher attenuation than human blood vessels, and that differences in acoustic impedance between the heat shrink tubing and the surrounding material lead to refraction and reflection of the ultrasound beam. In this case, it is important to establish that the pulse waveforms insonating the artificial blood are not adversely affected by the tubing, in terms of the degree of nonlinear distortion present. Pulse waveforms were collected in this experiment with the same hydrophone-transducer arrangement

as above, but with one half of a longitudinally cut heat-shrink tube placed over the active element of the hydrophone. The half tubing was oriented at 60° with respect to the axis of the beam.

For the DSL 2.5 MHz single crystal probe, pulse waveforms were obtained using a Doppler output power setting of 0 dB, + 6 dB, +12 dB and +18 dB. For the 5 MHz phased array on the ATL UM9 scanner, pulse waveforms were obtained using Doppler output powers of 100%, 80%, 50%, 35%, 25%, 18% and 13% of the maximum Doppler output.

Pulse waveforms from both the 5 MHz ATL probe and the 2.5 MHz DSL probe were also measured across the beam at intervals of 0.5 mm.

In this study, the effects of nonlinearity on both the maximum Doppler frequency shift and spectrum were investigated using a flow phantom and a string phantom.

For the flow phantom test, a steady flow of maximum velocity of 1 m/s was set on the flow phantom in a vessel of 5 mm inner diameter. Doppler signals were recorded on an audio cassette for both the ATL probe and the DSL probe. In each case, the beam-vessel angle was 60°. The gate length was adjusted to cover the whole vessel. This gave a gate length of 10 mm for each machine. The recorded Doppler signals were replayed through a Doptek spectrum analyser for analysis of the maximum frequency. The average value of maximum frequency was extracted. The entire Doppler sonogram of 240 lines was transferred to a computer for further analysis. On the computer, the average spectral profile of 240 lines of the sonogram was calculated.

For the string phantom test, the DSL machine was used. A constant string velocity of 1 m/s was used with a beam-string angle of 60°. The gate length was 10 mm. Doppler signals were again acquired onto audio cassette for power outputs of +18 dB, +12 dB, +6 dB and 0 dB. Further analysis was again performed using the Doptek spectrum analyser and the computer.

## RESULTS

*The pulse waveforms measured by the hydrophone*

The pulse waveforms of outputs of +18 dB, +12 dB, +6 dB and 0 dB from the 2.5 MHz DSL single crystal transducer are shown in Fig. 1. The distortion due to the nonlinear propagation became more serious as the output power was increased. The pulse waveform with 0 dB output was similar to a sine wave. However, the shock formation was clearly observed when the output increased to +18 dB. The compressional cycles showed a clear steepening on its leading edge with a sharp peak. There was an asymmetry in the magnitude of the compression and rarefaction cycles. The peak pressures of compressional

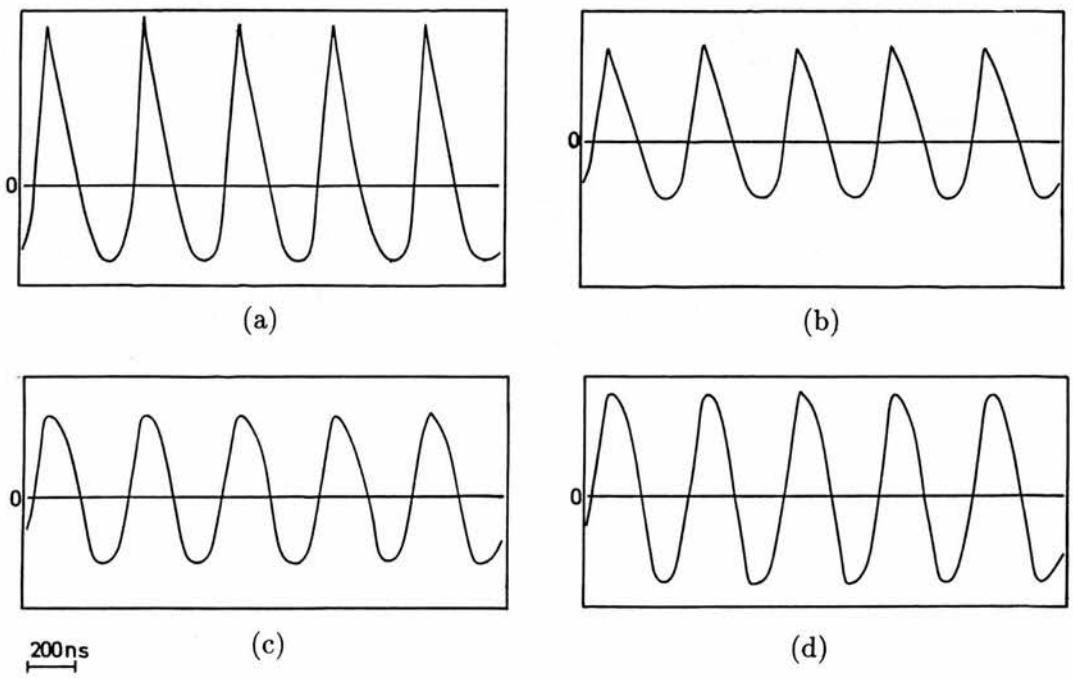


Fig. 1. Pulse waveforms from the 2.5 MHz single transducer observed at the distance of 8.5 cm. (a) The power output was +18 dB (−0.74–1.5 MPa). (b) The power output was +12 dB (−0.55–0.88 MPa). (c) The power output was +6 dB (−0.32–0.39 MPa). (d) The power output was 0 dB (−0.17–0.20 MPa).

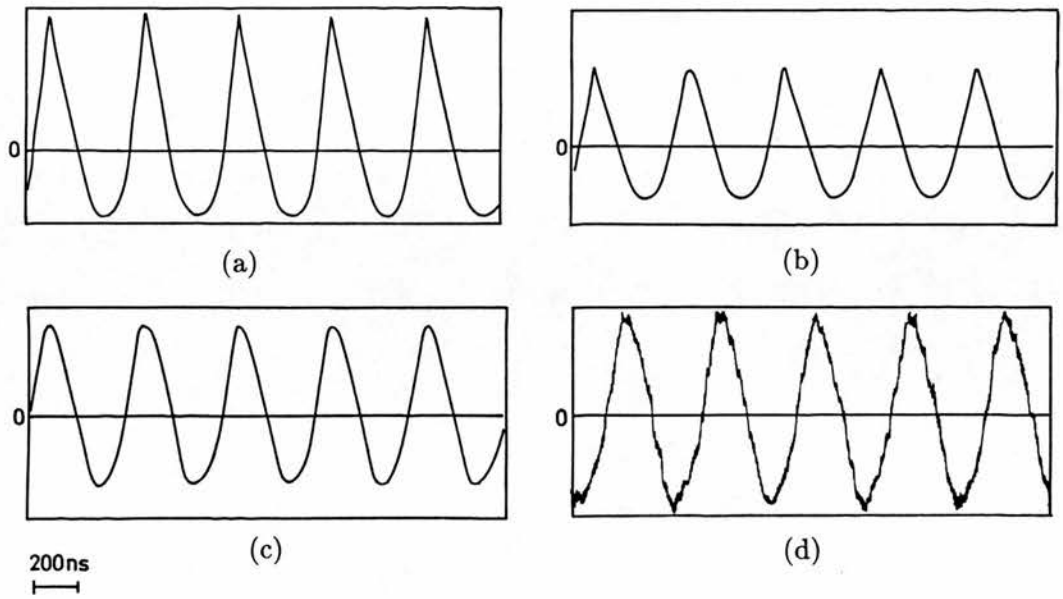


Fig. 2. Pulse waveforms from the 2.5 MHz single transducer observed behind a half tubing. (a) The power output was +18 dB (−0.31–0.62 MPa). (b) The power output was +12 dB (−0.24–0.37 MPa). (c) The power output was +6 dB (−0.13–0.17 MPa). (d) The power output was 0 dB (−0.083–0.091 MPa).

and rarefactional cycles were 1.49 MPa and 0.74 MPa, respectively. Similar results were also obtained from the 5 MHz ATL phased array.

The waveforms behind the half tubing are illustrated in Fig. 2. Comparing the waveforms to those without the half tubing (Fig. 1), the amplitudes of the peak pressure were reduced. In the waveform with +18 dB output, the compression peak pressure reduced from 1.49 MPa to 0.62 MPa. However, the distortion of the waveform was still quite significant.

Figure 3 illustrates the spatial distribution of the distortion of pulse waveforms within the beam of the

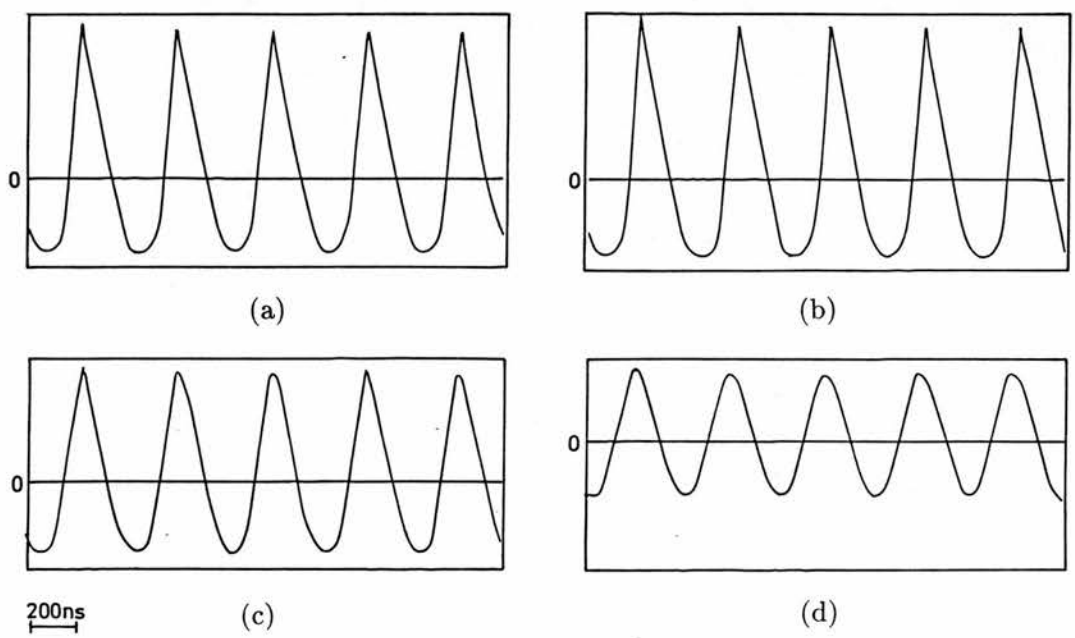


Fig. 3. Pulse waveforms from the 2.5 MHz transducer observed with +18 dB Doppler output power. (a) Waveforms at the beam centre (−0.72–1.4 MPa). (b) Waveforms at 1.0 mm from the centre (−0.72–1.34 MPa). (c) Waveforms at 2.0 mm from the centre (−0.67–1.0 MPa). (d) Waveforms at 3.0 mm from the centre (−0.62–0.88 MPa).

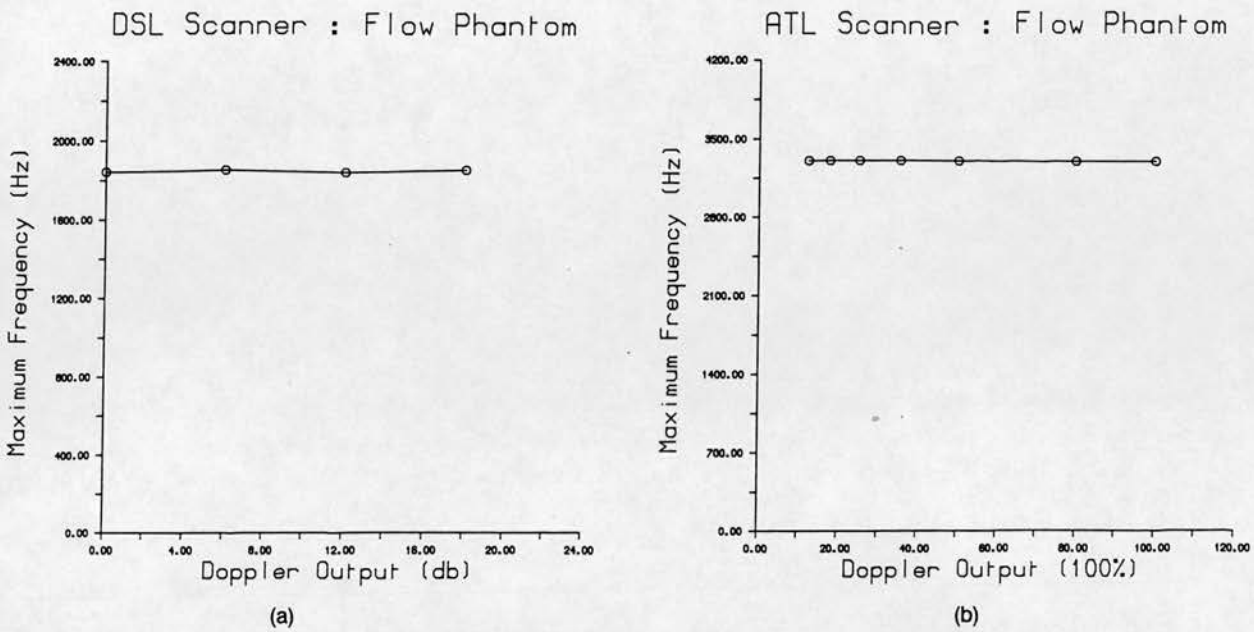


Fig. 4. The measured maximum frequencies with different Doppler outputs. (a) 2.5 MHz single crystal transducer. (b) 5.0 MHz phased array.

DSL single crystal transducer. It is shown that only within 1 mm from the beam centre were the waveforms highly distorted. The distortion decreased away from the beam centre. At about 2.0 mm from the centre, the waveform is already quite near to a sine wave. However, the amplitude, at the same distance, did not drop very significantly (peak positive pressure from 1.44 MPa at the centre to 1.03 MPa at 2 mm from the centre).

*Doppler measurements*

Figure 4 gives the maximum frequency from the flow phantom for both transducers with different output powers. There was no significant change in maximum frequency even though the corresponding pulse waveforms have clearly different degrees of nonlinear distortion.

Figure 5 shows the averaged spectral profiles of data acquired from the flow phantom using the DSL 2.5 MHz probe with different output powers. Although the distortion of the pulse waveforms is obvious (Fig. 2), there are again no significant differences among the Doppler spectral profiles. Figure 6 shows the averaged spectral profiles of data acquired from the string phantom using the DSL 2.5 MHz probe with different output powers. Again, no significant differences among these profiles were observed.

## DISCUSSION

Although the pulse waveforms showed clearly different degrees of nonlinear distortion, the flow and string phantom experiments indicate that the nonlinearity does not affect the Doppler spectrum both in terms of the maximum frequency or the Doppler spectral profile.

There are several possible factors which can produce such a result. First of all, the harmonic frequencies generated are high and mainly outside the detec-

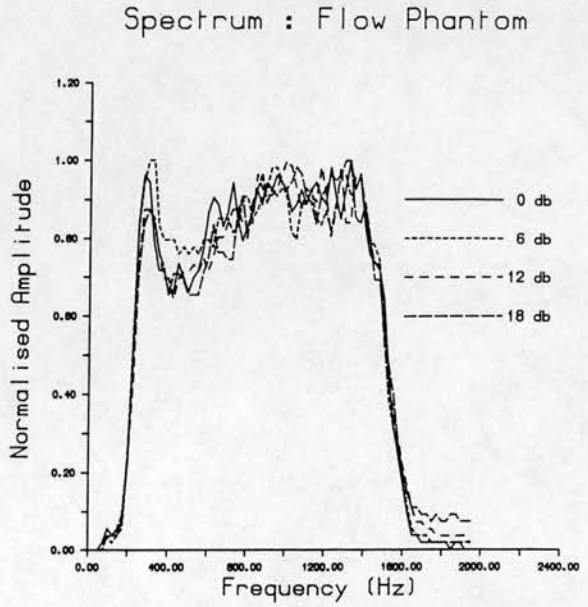


Fig. 5. Doppler spectra received by the 2.5 MHz transducer using the flow phantom with Doppler output power 0 dB, + 6 dB, + 12 dB and 18 dB. No significant differences were observed.

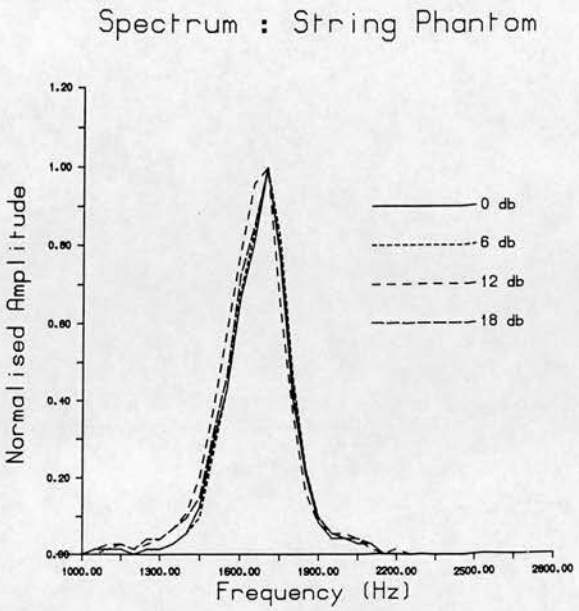


Fig. 6. Doppler spectra received by the 2.5 MHz transducer using the string phantom with Doppler output power 0 dB, + 6 dB, + 12 dB and 18 dB. No significant differences were observed.

tion range of the receiver. Therefore, the effective spectrum of the insonation signal remains similar. Secondly, in the experiments, it was found that only at the centre of the beam was the distortion due to nonlinear propagation obvious (Fig. 3). In other parts of the beam, the waveforms were near to sine waves. Thus, only a small part of the scatterers, which were in the sample volume for the flow phantom and along the string for the string phantom, were excited by the distorted waveform while most of the particles were not.

In practice, intrinsic broadening also occurs (Censor et al. 1988; Newhouse et al. 1980, 1987). Each moving target subtends a range of angles so that the energy from each target will be spread into a range of Doppler frequencies. This leads to general blurring of the Doppler spectral profile. The maximum Doppler frequency will arise from the largest transducer-target angle for targets within the beam. This target angle will not be for the centrally placed portion of the vessel or the string, but rather for a portion in an area not affected by the nonlinearity. The relevant portion of the Doppler spectrum to look at for the effects of nonlinearity will be near but not at the maximum frequency for the spectra from the flow phantom, and at the centroid frequency for the string phantom spectra. In each case, there was no significant effect. This may indicate that spectral broadening has acted to mask any effect which possibly was present.

In many clinical measurements, because the attenuation in soft tissue reduces the power of the ultrasound, as well as the fact that the high frequency components will be attenuated more than the lower frequency components, the distortion of the pulse waveforms will be less significant than in our experimental setup. Therefore, nonlinear propagation will give even less change in the Doppler spectrum. In situations where the ultrasonic pulse travels through liquid paths, for example the full bladder, amniotic fluid or a water bath, nonlinear distortion may be present but it will not upset the Doppler measurements.

## CONCLUSION

Nonlinear propagation of the pulse waveforms from duplex scanners operated in the Doppler mode can be observed. However, the nonlinear propagation gives no significant effect on the Doppler frequency shift measurement.

## REFERENCES

Bacon, D. R. Finite amplitude distortion of the pulsed fields used in diagnostic ultrasound. Ultrasound Med. Biol. 10:189–195; 1984.

Bakhvalov, N. S.; Zhileikin, Y. M.; Zabolotskaya, E. A.; Khokhlov, R. V. Focused high-amplitude sound beams. Sov. Phys. Acoust. 24:10–15; 1978.

Blackstock, D. T. Connection between the Fay and Fubini solutions for plane sound waves of finite amplitude. J. Acoust. Soc. Am. 39:1019–1026; 1965.

Censor, D.; Newhouse, V. L.; Vontz, T.; Ortega, H. V. Theory of ultrasound Doppler-spectra velocimetry for arbitrary beam and flow configurations. IEEE Trans. Biomed. Eng. 35:740–751; 1988.

Duck, F. A.; Starritt, H. C. Acoustic shock generation by ultrasonic imaging equipment. Br. J. Radiol. 57:231–240; 1984.

Duck, F. A.; Starritt, H. C.; Perkins, M. A.; Hawkins, A. J. The output of pulse-echo ultrasound equipment: A survey of powers, pressures and intensities. Br. J. Radiol. 58:989–1001; 1985.

Hoskins, P. R; Anderson, T.; McDicken, W. N. A computer controlled flow phantom for generation of physiological Doppler waveforms. Phys. Med. Biol. 34:1709–1717; 1989.

Hoskins, P. R.; Loupas, T.; McDicken, W. N. A comparison of the Doppler spectra from human blood and artificial blood used in a flow phantom. Ultrasound Med. Biol. 16:141–147; 1990.

Law, W. K.; Frizzell, L. A.; Dunn, F. Determination of the nonlinearity parameter B/A of biological media. Ultrasound Med. Biol. 11:307–318; 1985.

McDicken, W. N. A versatile test-object for the assessment of the performance of Doppler flow instruments. Ultrasound Med. Biol. 12:245–249; 1986.

Muir, T. G.; Carstensen, E. L. Prediction of nonlinear acoustic effects at biomedical frequencies and intensities. Ultrasound Med. Biol. 6:345–357; 1980.

Newhouse, V. J.; Furgason, E. S.; Johnson, G. F.; Wolf, D. A. The dependence of ultrasound Doppler bandwidth on beam geometry. IEEE Trans. Sonics Ultrason. SU-27:50–59; 1980.

Newhouse, V. J.; Censor, D.; Vontz, T.; Cisneros, J. A.; Goldberg, B. B. Ultrasound Doppler probing of flows transverse with respect to beam axis. IEEE Trans. Biomed. Eng. BME-34:779–789; 1987.

*Ultrasound in Med. & Biol.* Vol. 19, No. 7, pp. 593–594, 1993
Printed in the USA

0301-5629/93 $6.00 + .00


# ●*Letter to the Editor-in-Chief*

## REFRACTION IN DOPPLER ULTRASOUND

**To the Editor-in-Chief:**

In Oates' (1989) letter, it was suggested that as the speed of sound in blood is 1570 m/s rather than 1540 m/s, the Doppler estimated velocity may be underestimated by about 2%. Kremkau (1990) also claimed that because of refraction at the vessel-wall/blood boundary, the Doppler angle will change, thus causing the Doppler estimated velocity to be overestimated by up to 7%. We think these two effects should not be treated separately.

In Fig. 1, the beam–vessel angle is labeled $\theta'_1$ and the angle between the beam and the perpendicular to the vessel is labelled $\theta_1$. Because of refraction, the Doppler angle in the blood vessel is $\theta'_2$ and the angle between the refracted beam and the perpendicular to the vessel is $\theta_2$. It is known that

$$\frac{c_{\text{tissue}}}{c_{\text{blood}}} = \frac{\sin\theta_1}{\sin\theta_2} \tag{1}$$

where $c_{\text{tissue}}$ and $c_{\text{blood}}$ are the speed of sound in tissue and blood, respectively. Therefore, the Doppler shift $f_d$ is given by

$$f_d = \frac{2vf_0}{c_{\text{blood}}}\cos\theta'_2. \tag{2}$$

Substitute eqn (1) into eqn (2) and considering that

$$\sin\theta = \cos(90° - \theta), \tag{3}$$

we obtain

$$\begin{aligned} f_d &= 2vf_0\frac{\sin\theta_2}{c_{\text{blood}}} \\ &= 2vf_0\frac{\sin\theta_1}{c_{\text{tissue}}} \\ &= 2vf_0\frac{\cos\theta'_1}{c_{\text{tissue}}}. \end{aligned} \tag{4}$$

t is noted that this is the usual Doppler equation. The speed of sound in the above equation is $c_{\text{tissue}}$ and the beam–vessel angle is $\theta'_1$. This means that no error is introduced in using a speed of sound in tissue of 1540 m/s and $\theta'_1$ as the beam–vessel angle in the standard Doppler formula for velocity estimation. We think the authors of the two letters noticed the change in either speed of sound or Doppler angle but did not consider both of them together.

An extension of the above discussion is that no matter how many parallel layers of medium separate tissue and blood, we can always use the beam–vessel angle and speed of sound in tissue to calculate the Doppler frequency shift. This is because for each layer, it is always true that

$$\frac{\sin\theta_1}{c_1} = \frac{\sin\theta_2}{c_2} = \frac{\sin\theta_3}{c_3} = \ldots. \tag{5}$$

Therefore, refraction occurring between a number of parallel boundary layers which have different speeds of sound cannot influence the Doppler estimated velocity.

To verify the above discussion, experiments were made on a flow phantom (Hoskins et al. 1989). Heat-shrinkable tubing of diameter 5 mm was fixed in a water-bath. Both water and a mixture of 42% glycerol to 58% water were used as artificial blood. The speed of sound in water is 1480 m/s while that in the mixture is 1690 m/s, a difference of 14%. Water gave little refraction as the speed of sound was the same inside and outside the tubing. When the glycerol–water mixture was used, the speed of sound in the mixture inside the vessel was significantly higher than that of the surrounding water, giving rise to considerable refraction.

A Doptek 4 MHz continuous wave (CW) unit was used for acquisition of Doppler spectra. Doppler spectra were acquired at beam–vessel angles ranging from 40° to 85° in 5° steps. The maximum frequency was extracted using the 15/16 percentage method which calculates the maximum frequency as the point where the sum of pixel values (voltage amplitude) below that frequency just exceeds 15/16 of the total. Simultaneous measurements of absolute flow were made using a measuring cylinder and a

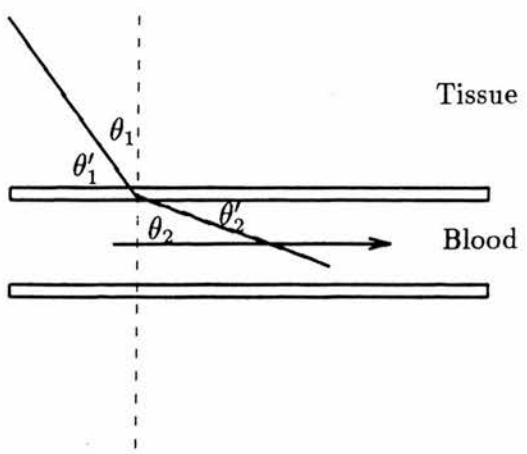


Fig. 1. The geometry of the refraction.

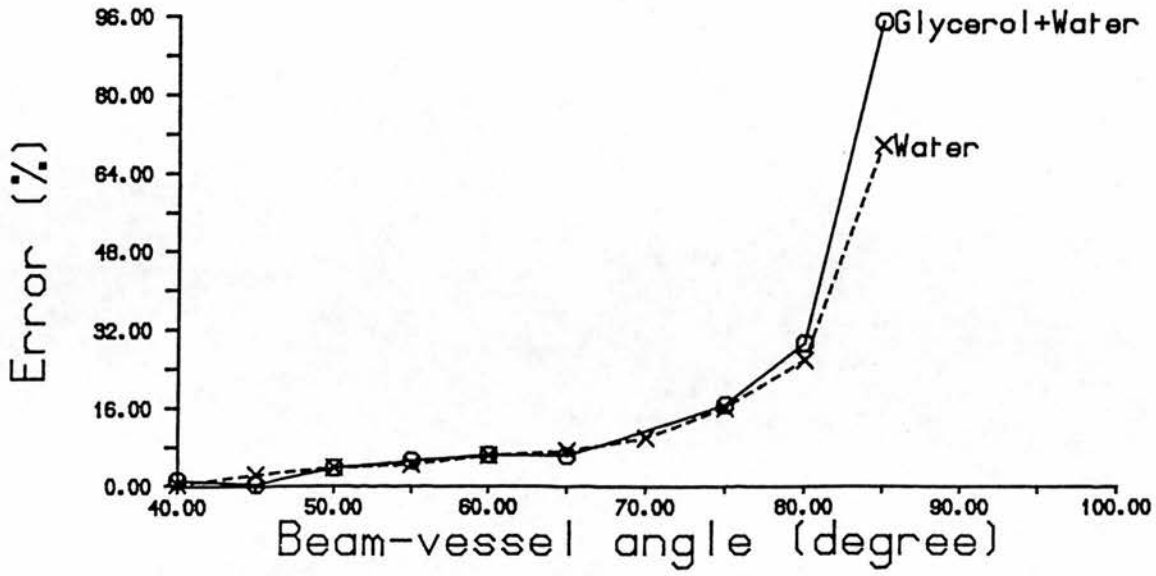


Fig. 2. A comparison between the Doppler measurements in water and the mixture of glycerol and water. Error figures are calculated by comparison between the Doppler estimated flow rates and measured absolute flow rates.

stop watch. The true maximum velocity then was estimated assuming a parabolic flow profile.

Figure 2 gives the errors in estimation of maximum velocity from both water and the glycerol–water mixtures at different beam–vessel angles. It is shown that, although the speed of sound and consequently the refraction is different for the two media, there is no significant difference between these two solutions. The errors in the estimation at large beam–vessel angles are higher mainly because of geometrical spectral broadening. The experimental error in angle measurement was $\pm 0.5°$, giving a maximum percentage error of $\pm 10\%$ at 80°. At smaller angles, this error is much lower.

Therefore, we conclude that in the calculation of Doppler estimated velocity, the speed of sound in tissue and beam–vessel angle should always be used and this gives no error in the velocity estimation.

S. Li
W. N. McDicken
P. R. Hoskins

*Department of Medical Physics and Medical Engineering*
*Royal Infirmary*
*Edinburgh EH3 9YW, UK*

## REFERENCES

Hoskins, P. R.; Anderson, T.; McDicken, W. N. A computer controlled flow phantom for generation of physiological Doppler waveforms. Phys. Med. Biol. 34:1709–1717; 1989.

Kremkau, F. W. Doppler angle error due to refraction. Ultrasound Med. Biol. 16:523–524; 1990.

Oates, C. P. The Doppler shift & speed of sound in blood. Ultrasound Med. Biol. 15:75; 1989.

*Received* 14 *April* 1993